A Study on the Synthesis of Phytochemical Incorporated Biopolymer-based Materials for Evaluating Therapeutic Potentials

Thesis submitted to

Jadavpur University

By

Sanghita Das

In partial fulfilment of the requirements for the degree of

Doctor of Philosophy (Ph.D) in Science

Department of Physics

Jadavpur University

Kolkata-700032

July 2024

যাদবপুর বিশ্ববিদ্যালয়
কলকাতা-৭০০০৩২, ভারত

JADAVPUR UNIVERSITY
KOLKATA-700 032, INDIA

FACULTY OF SCIENCE : DEPARTMENT OF PHYSICS

CERTIFICATE FROM THE SUPERVISOR(S)

This is to certify that the thesis entitled *"A Study on the Synthesis of Phytochemical Incorporated Biopolymer-based Materials for Evaluating Therapeutic Potentials"* submitted by Mrs. Sanghita Das who got her name registered on 16/03/2022 (Index no.: 93/22/Phys./27) for the award of Ph.D. (Science) Degree of Jadavpur University, is absolutely based upon her own work under the supervision of Prof. Sukhen Das and Dr. Anindita Dey and that neither this thesis nor any part of it has been submitted for either any degree/diploma or any other academic award anywhere before.

Sukhen Das

Prof. Sukhen Das 12/07/2024

Professor

Department of Physics

Jadavpur University

Kolkata-700032

Prof. Sukhen Das
Department of Physics,
Jadavpur University
Kolkata - 700 032

Anindita Dey 12/07/24

Dr. Anindita Dey

Assistant professor

Department of Botany

Asutosh College

Kolkata- 700026

Dr. Anindita Dey
Assistant Professor
Department of Botany
Asutosh College, Kol-26

যাদবপুর বিশ্ববিদ্যালয়
কলকাতা-৭০০০৩২, ভারত

JADAVPUR UNIVERSITY
KOLKATA-700032, INDIA

FACULTY OF SCIENCE : DEPARTMENT OF PHYSICS

CERTIFICATE OF SIMILARITY CHECK

This is to certify that the plagiarism checking for this thesis entitled ***"A Study on the Synthesis of Phytochemical Incorporated Biopolymer-based Materials for Evaluating Therapeutic Potentials"*** authored by Mrs. Sanghita Das has been performed using professional plagiarism prevention software iThenticate. According to the report generated after plagiarism checking there is a 9% similarity in this thesis, which is in the category "Level 0" (minor similarities) as per the "Promotion of Academic Integrity and Prevention of Plagiarism in Higher Education Institutions Regulations, 2018" of the University Grand Commission (UGC) of India. The common knowledge or coincidental terms up to 10 (ten) consecutive words (as prescribed in the above said UGC Regulation up to 14 (fourteen) terms for such common knowledge or coincidental terms can be excluded) and own works of the candidate published in various peer-reviewed journals (those are attached in the thesis) are excluded from the similarity checking. It is certified that the present thesis submitted by Mrs. Sanghita Das is plagiarism-free and has followed standard norms of academic integrity and scientific ethics.

Sukhen Das 12/07/2024

Prof. Sukhen Das
Professor
Department of Physics
Jadavpur University
Kolkata-700032

Prof. Sukhen Das
Department of Physics,
Jadavpur University
Kolkata - 700 032

Anindita Dey 12/07/24

Dr. Anindita Dey
Assistant professor
Department of Botany
Asutosh College
Kolkata- 700026

Dr. Anindita Dey
Assistant Professor
Department of Botany
Asutosh College, Kol-26

Dedicated to

My Parents

Abstract

THESIS TITLE: A Study on the Synthesis of Phytochemical Incorporated Biopolymer-based Materials for Evaluating Therapeutic Potentials

Submitted by: Sanghita Das

Index no.: 93/22/Phys./27

Multifunctional biomaterials have been very popular in revolutionizing the areas of biomedical applications. The promising pharmacological potentials of phytochemical incorporated biopolymeric nanomaterials have led researchers to explore their *in vitro* biological potentials and preliminary *in vivo* efficacy. These biocomposites can be extensively used in drug delivery because of their wide range of versatility, nontoxicity, stability, high drug loading capacities, sustained drug release properties, biocompatibility compared to other synthetic or inorganic materials. The therapeutic properties of these biocomposites are introduced by incorporating phytochemicals i.e. piperine and thymoquinone over conventional antibiotics to overcome the problem of bacterial resistance.

To understand the plausible effect of fabricated biocomposites we have used naturally abundant, biodegradable biopolymers like guar gum, sodium alginate, carboxymethyl cellulose, chitosan and psyllium husk mucilage. Our study involves nanonization of bio active hydrophobic phytochemicals encapsulating efficient drug delivery vehicle which will overcome the problem of instability in therapeutic applications. The sustained release behaviour of phytochemicals from polymeric vehicles makes these biocomposites useful for prolonged persistence at the site of infection during drug administration.

In the study we have reported the synthesis of some biocomposites such as thymoquinone and piperine encapsulated guar gum delivery-vehicle; thymoquinone incorporated chitosan-sodium alginate and chitosan- psyllium husk mucilage composite films; piperine encapsulated guar gum-psyllium husk mucilage nanocomposites and guar gum-carboxymethyl cellulose nanocomposites. The physical characterizations of these biocomposites have performed by techniques such as X-Ray Diffraction (XRD), Fourier-Transform Infrared Spectroscopy (FTIR), Thermogravimetric Analysis (TGA), Dynamic Light Scattering (DLS) study, Ultraviolet-Visible Spectroscopy (UV-Vis), Field Emission Scanning Electron Microscopy

(FESEM), Transmission Electron Microscopy (TEM), Atomic Force Microscopy (AFM) etc. *In vitro* biological characterizations establish the efficacy of these functionalized biomaterials which involve estimation of minimum inhibitory concentration (MIC), minimum bactericidal concentration (MBC), estimation of intracellular reactive oxygen species (ROS) generation etc. in different pathogenic bacterial strains. We have observed the pH dependent release behaviour of phytochemicals from the biopolymer-based drug delivery system and evaluated the biocompatibility in normal human cell line. We have also measured cytotoxicity, intracellular ROS, GSH and NADPH levels, mitochondrial membrane potential, nuclear damage to evaluate anticancer potentials. We have observed the hepatoprotective effect of piperine in acute liver injury in mice model by measuring intracellular ROS generation in hepatocytes, serum levels of alanine aminotransferase (ALT) and aspartate aminotransferase (AST) and histopathological study etc.

Moreover, our synthesised phytochemical incorporated biopolymer-based materials possess commendable ameliorative attributes that could be effectively used against diverse pathological conditions and these may bring back cost effective, biocompatible natural phyto-components in further usage.

Acknowledgment

First and foremost, I am deeply indebted to my esteemed Ph.D. supervisor, ***Prof. (Dr.) Sukhen Das*** *for his valuable mentorship, unwavering guidance, unfailing support, and insightful feedback which have been instrumental in shaping my research. His dedication to my academic pursuits has been a constant source of inspiration.*

I extend my earnest appreciation to ***Dr. Anindita Dey*** *for her remarkable contributions, encouragement, and valuable insights throughout my research. Her expertise has been a guiding light, and I am grateful for her continuous assistance.*

I would take the opportunity to express my thanks to ***Prof. Papiya Nandy, Dr Ruma Basu, Prof. Parimal Karmakar*** *and* ***Dr. Soumyaditya Sutradhar*** *for their valuable guidance.*

I would like to express my truthful gratitude to ***Prof Tarakdas Basu,*** *a paragon of knowledge for his impactful advice and support in my research journey.*

I am thankful to all my teachers for their contributions and positive influences throughout my educational journey.

Special thanks go to my lab partner ***Dr. Debbethi Bera*** *and* ***Manisha Kundu.*** *Without your continuous assistance and support my doctoral journey would have remained incomplete. Whenever I need any type of assistance regarding my research and other problems, you two always stand with me.*

I extend my heartfelt gratitude to ***Dr. Biplab Kumar Paul*** *for his invaluable guidance and support in my Ph.D. journey.*

Next, I am extremely thankful to ***Satarupa Bhattacharya*** *for her assistance and support which give a new direction in my research work.*

I am also grateful to ***Dr. Dheeraj Mondal, Dr. Munmun Bardhan, Dr. Debopriya Battacharya*** *for their valuable suggestions and support.*

I am extremely thankful to ***Dr. Santanu Das, Dr. Debopriya Ghosal, Dr. Somtirtha Banerjee, Dr. Navonil Bose, Dr. Nur Amin Hoque, Dr. Madhuchanda Sarkar, Dr. Bidisha Ghosh, Dr. Shubham Roy, Dr. Shilpa Maity, Dr. Souravi Bardhan, Dr. Anandalal Gayen, Dr. Tanumoy Debnath,*** *for their valuable guidance and support.*

I would like to express my gratitude to those who have supported me in this PhD journey, my lab mates ***Souvik, Md. Minarul Saikh, Saheli, Dhananjoy, Somen da, Neelanjana, Namrata, Tanmoy, Jhilik, Indrajit, Piyali, Anuja, Monisha, Suman, Sumana, Shriparna, Anwesha, Aliva, Shubojit.***

A special thanks goes to ***Debmalya Sarkar*** *for your support during the hardest time of my doctoral journey.*

I want to extend my thanks to the ***Department of Biotechnology, Jadavpur University*** *and* ***Department of Biochemistry & Biophysics, University of Kalyani*** *for the infrastructural support and instrumental facility provided throughout my doctoral period.*

I would like to take the opportunity to convey my heartfelt gratitude to ***the employees of the Departmental Office of Physics*** *for their unwavering assistance whenever needed.*

A special thanks to my dearest friend ***Bidisha Chakraborty*** *for your presence and immense support.*

Finally, I would like to express my love to ***my father (Mr. Soumen das) and my mother (Mrs. Sulata Das)*** *for the trust. Their unconditional love, care, and blessings always encouraged me and gave me the strength in every step of my life.*

A special thanks goes to my brother ***Shubhamay Das*** *for his love and invaluable assistance. You are always there to help me from the very beginning.*

Also, this journey would never be completed without the love and support of my husband ***Debapriya Hazra*** *who sacrificed his time for me and always motivated me towards excellence. I am truly blessed to have you as my partner.*

I would like to express my special love to my son, ***Jyotishka*** *whose presence made me stronger and more fulfilled than I could have ever imagined.*

I want to add special thanks to my other family members whose blessings and supports helped me to complete this doctoral journey. Thanks to all those whose presence and contribution enriched my research and made this journey a memorable one. I am truly indebted to each one of them.

Sanghita Das

Sanghita Das

List of Publications

Journal Publication

Published

1. **Sanghita Das,** Debbethi Bera, Debojyoti De, Dheeraj Mondal, Parimal Karmakar, Sukhen Das, Anindita Dey**;** 2022. Thymoquinone incorporated chitosan-sodium alginate/psyllium husk derived biopolymeric composite films: A comparative antibacterial and anticancer profile. ***European Polymer Journal***, *180*, p.111608.
2. **Sanghita Das,** Debbethi Bera, Kunal Pal, Dheeraj Mondal, Parimal Karmakar, Sukhen Das, Anindita Dey; 2020. Guar gum micro-vehicle mediated delivery strategy and synergistic activity of thymoquinone and piperine: An in vitro study on bacterial and hepatocellular carcinoma cells. ***Journal of Drug Delivery Science and Technology***, *60*, p.101994.
3. **Sanghita Das,** Anindita Dey, Sukhen Das, Papiya Nandy; 2020. An Overview on Cancer-Fighting Phytochemicals from Selected Medicinal Plants in Bengal. ***Mathews Journal of Pharmaceutical Science***, *4*(2), pp.1-16.
4. Souravi Bardhan, Shubham Roy, **Sanghita Das**, Ishita Saha, Dhananjoy Mondal, Jhilik Roy, Dipak Kr. Chanda, Solanky Das, Parimal Karmakar, Sukhen Das ;2022. Real-time sensitive detection of Cr (VI) in industrial wastewater and living cells using carbon dot decorated natural kyanite nanoparticles**.** ***Spectrochimica Acta Part A: Molecular and Biomolecular Spectroscopy***, *273*, p.121061.

Under Review

1. **Sanghita Das**, Debojyoti De, Debbethi Bera, Parimal Karmakar, Sukhen Das, Anindita Dey; Oxidative stress- generated antibacterial and anticancer activities of piperine incorporated guar gum and psyllium husk derived biopolymeric nanocomposite. *Material today communications*.
2. **Sanghita Das**, Soumajit Chakrabarty, Manisha kundu, Susmita Nandi, Debbethi Bera, Tarakdas Basu, Sukhen Das, Anindita Dey; Guar gum and carboxymethyl cellulose nanocomposite loaded with piperine: a multipurpose nanoparticle with potential antibacterial and anticancer properties. *Polymer*.

3. Debbethi Bera, **Sanghita Das,** Manisha Kundu, Santanu Das, Suman Bhandary, Sukhen das, Papiya Nandy, 2024. Synthesis and characterization of biocompatible Gadolinium-capped silver functionalized ZnS nanocomposite with antibacterial potentials. *The Journal of Materials Science: Materials in Engineering*.

Book Chapter

1. Anindita Dey, Sumanta Dey, **Sanghita Das**, Madhumita Majumder, Papiya Nandy, and Ashesh Nandy; Combating the vectors and management of vector-borne diseases with essential oil nanoemulsions; 'Natural Products in Vector-Borne Disease Management' Edited by Nagendra Singh Chauhan and Durgesh Nandini Chauhan; Academic Press, **Elsevier**; pp. 81-113. https://doi.org/10.1016/B978-0-323-91942-5.00006-9.
2. Anindita Dey, **Sanghita Das**, Papiya Nandy; Nano-fertilizer: A distinctive entreaty of nanomaterials to crop field, **LAP LAPBART** Academic Publishing; "Modern Trends in Material Science Research" edited by Dr. Ujjal Kumar Sur, ISBN: 978-620-7-47260-4, p 3-26

List of Conferences Attended

1. Oral representation in "**Young Scientists Conference**" on 22nd – 25th December 2020 as a part of India International Science Festival 2020 organized by Ministry of Science and Technology; Ministry of Earth Science; Ministry of Health and Family Welfare, Govt. of India in collaboration with VIBHA and CSIR.

2. Oral representation in "**Strategies for Improving Agricultural Productivity and Farmer's Income in the Context of Climate Change**" on 16th -18th December 2023 organized by The Agricultural Society of India & Institute of Agriculture Science, University of Calcutta.

3. Oral representation in "**6th Annual Congress on Plant Science and Biology**" on 9th – 10th November 2020 organized by EuroSciCon and the Editors of Journal of Single cell Biology.

4. Oral representation in "**Commemoration of Centenary Birth anniversary of Prof. Shyamal Sengupta**" on 7th February 2024 organized by Condensed Matter Physics Research Centre & Department of Physics, Jadavpur University.

5. Participated in "The Challenges and Scientific Advances of SARS-COV 2" on 27th August 2020 organized by Department of Microbiology, Assam University in collaboration with Springer Nature and Society for Environmental Sustainability.

6. Participated in "Artificial Intelligence in Drug Discovery" on 1st September 2020 organized by CSIR-North East Institute of Science & Technology, Jorhat.

7. Participated in "Unique Marine Fauna Webinar (04) Series on "Marine Ornamental Aquaculture: Measure towards Conservation of Biodiversity" on 24th August 2020 organized by Zoological Survey of India.

8. Participated in "Aquatic Faunal Diversity of Arunachal Pradesh" on 20th August 2020 organized by Zoological Survey of India.

9. Participated in "Science Biology and the World's Future" on 25th August 2020 organized by Department of Botany and IQAC, Dinabandhu Andrews College.

Contents

Abbreviations

AFM	*Atomic Force Microscope*
AL	*Alginate*
ALP	*Alkaline Phosphate*
ALT	*Alanine Transaminase*
AST	*Aspartate Transaminase*
ATP	*Adenosine triphosphate*
A549	*Adenocarcinomic human alveolar basal epithelial cell*
B. subtilis	*Bacillus subtilis*
BW	*Body weight*
CAT	*Catalase*
CFU	*Colony-forming unit*
CH	*Chitosan*
CLD	*Chronic liver disease*
CMC	*Carboxymethyl cellulose*
CMCNa	*Sodium Carboxymethyl cellulose*
CPCSEA	*Committee for the Purpose of Control and Supervision of Experiments on Animals*
DCF	*Dichlorofluorescein*
$DCFH_2$-DA	*2, 7 -dichlorodihydrofluorescein diacetate*
DDS	*Drug Delivery System*
DLC	*Drug Loading Content*
DLE	*Drug Loading Efficiency*
DLS	*Dynamic Light Scattering*
DMEM	*Dulbecco's modified eagle's medium*
DMSO	*Dimethyl Sulfoxide*
DNA	*Deoxyribonucleic acid*
DTA	*Differential Thermal Analyzer*

E. coli	*Escherichia coli*
EDTA	*Ethylenediamine tetra acetic acid*
E. faecalis	*Enterococcus faecalis*
FTIR	*Fourier Transform Infrared spectroscopy*
FESEM	*Field Emission Scanning Electron Microscope*
GG	*Guar Gum*
GSH	*Glutathione*
Hb	*Haemoglobin*
HepG2	*Hepatoblastoma cell line*
H_2O_2	*Hydrogen Peroxide*
HT-29	*Human colorectal adenocarcinoma cell line*
IC_{50}	*Half-maximal Inhibitory Concentration*
IPN	*Inter Penetrating Network*
IMTECH	*Microbial Type Culture Collection*
ISO	*International Organization for Standardization*
IUPAC	*International Union of Pure and Applied Chemistry*
JCPDS	*Joint Commission of Powder Diffraction Standards*
LD_{50}	*Median Lethal Dose*
LFT	*Liver Function Test*
MBC	*Minimum Bactericidal Concentration*
MDA	*Malondialdehyde*
MIC	*Minimum Inhibitory Concentration*
MMP	*Mitochondrial Membrane Potential*
MTCC	*Microbial Type Culture Collection*
MTT	*3-(4, 5- dimethylthiazol-2-yl)- 2, 5-diphenyltetrazolium bromide*
NADPH	*Nicotinamide Adenine Dinucleotide Phosphate*
NAPQI	*N-acetyl-p-benzoquinone imine*
NOAEL	*No observed adverse effect level*
OD	*Optical Density*

P. aeruginosa	*Pseudomonas aeruginosa*
PH	*Psyllium Husk*
PBS	*Phosphate Buffer Saline*
PC3	*Human prostate adenocarcinomic cell line*
PDI	*Polydispersity index*
PIP	*Piperine*
RBC	*Red Blood Corpuscle*
RIPA	*Radioimmunoprecipitation Assay*
RNA	*Ribonucleic acid*
ROS	*Reactive Oxygen Species*
S. aureus	*Staphylococcus aureus*
SD	*Standard Deviation*
SE	*Standard Error*
SGOT	*Serum Glutamic Oxaloacetic Transaminase*
SGPT	*Serum Glutamic Pyruvic Transaminase*
SOD	*Superoxide dismutase*
S. pneumoniae	*Streptococcus pneumoniae*
TEM	*Transmission Electron Microscopy*
TGA	*Thermal Gravimetric Analysis*
TiO_2–Ag	*Silver-titanium dioxide*
TQ	*Thymoquinone*
UV	*Ultra Violet*
V. cholera	*Vibrio cholera*
WBC	*White Blood Corpuscle*
WHO	*World Health Organization*
WI38	*Human fetal lung fibroblast cell line*
XRD	*X-Ray diffraction*

List of Figures

List of Tables

Chapter 1

Introduction

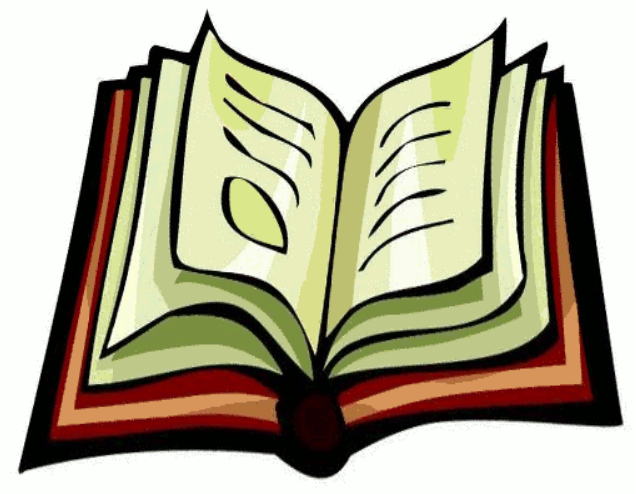

1.1 Motivation

The global health crisis can be avoided thanks to recent advancements in drug delivery systems that use diverse gene pools of ethnobotanically relevant plant species instead of conventional therapeutics.[1,2] Despite incredible progression in modern medication, the effectivity of conventional antibiotics is faded away by the emergence of different resistance mechanisms. Resistance against frontline antibiotics is established in bacteria by engaging mobile genetic elements (such as transposons plasmids, insertion sequences), changing cell permeability, mutation, production of a new range of enzymes, alteration in efflux pumps, etc.[3-5] Almost similar concerns in cancer treatment regarding in search of more effective chemopreventive alternatives with lesser side effects are desirable to improve the treatment. Since the advent of modern pharmaceutical science, formulation of efficient drug delivery systems based on plant-derived materials such as biopolymers and phytochemicals is a broad field of research on developing novel carrier systems.[6-8] According to an estimation by the World Health Organization, 80 % of the rural population rely chiefly on medicinal herbs and traditional medicine as a primary healthcare system.[9] It has been reported that approximately 50% of all modern pharmaceutics in clinical use are plant-derived.[10] Many of these bioactive compounds such as flavonoids, terpenoids, and alkaloids have received considerable attention for their antimicrobial, antiapoptotic, antimutagenic, hepatoprotective, anti-malignant, antineoplastic, and potential chemo preventive properties.[11,12] Despite all these encouraging biomedical possessions, the implementation of natural therapeutics is arrested due to several difficulties. Hydrophobic phytochemicals cause hindrances in the effective formulation and may lead to unstable end products restricting their therapeutic and biomedical applications.[13-15] To keep these drawbacks in mind, researchers focus on developing novel biopolymer-based, biocompatible, environment-friendly nanomaterials for drug delivery that could be implemented to combat the lethal consequences of chemically synthesized conventional drugs.[16,17] Considering the unique medicinal properties of phytoconstituents that attribute curative effects, analytical procedures for their identification, isolation, characterization, nanonization, and dose standardization are required for successful implementation.[18,19]

This thesis focuses on formulating biopolymeric composite materials to deliver natural therapeutics to evaluate their antibacterial, anti-cancer, and hepatoprotective potential.

1.2 Biopolymers as excipients in drug delivery

The introduction of polymer science in the field of pharmaceuticals opens a promising route toward designing versatile drug delivery systems (DDS). The main approach of drug delivery includes maintaining a proper formulation technique, transporting and delivering therapeutic components in the target site of a biological system to attain the desired healing effect.[22-22] Biopolymers are natural polymers derived from various living organisms like plants, animals, fungi and microorganisms which include silk, wool, cellulose, chitin, protein, DNA, etc. The advancement of derivatives of biopolymers have become popular in the development of novel drug-delivery devices. For several reasons, considerable interests are generated in the development of new plant-derived excipients over synthetic ones. Water-solubility, biodegradability, and biocompatibility of biopolymeric excipients such as gums and mucilages offer promising characteristics to develop drugs/therapeutic materials with improved release characteristics (figure 1.1).[23,24]

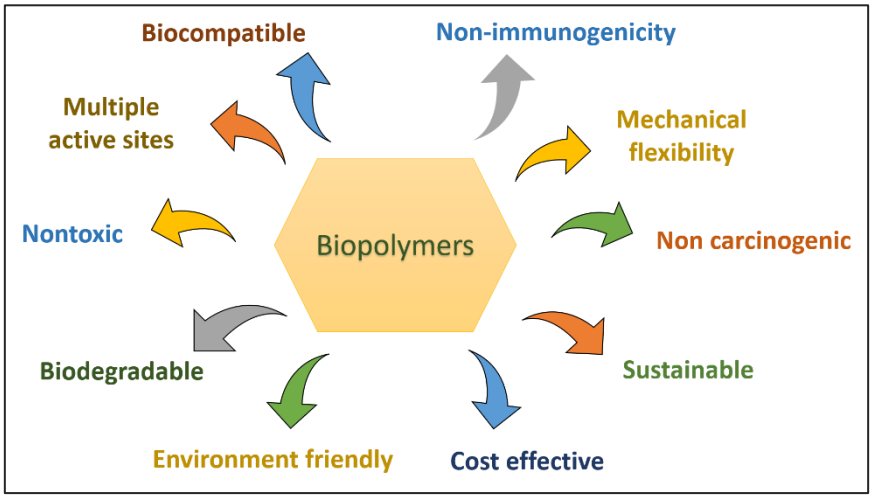

Figure 1.1: *Schematic representation of advantages of biopolymers.*

1.2.1 Advantages of biopolymer-based nanocomposite

The development of biopolymer-based nanocomposites with added functionalities has revolutionized the production qualities required to meet the demands of contemporary technology. The exceptional mechanical and functional features of biopolymeric nanostructures make them unique in terms of their potential sustainability, biocompatibility, low toxicity, and environmentally friendly production and processing..[25] This array of exclusive properties offers opportunities to develop robust functional drug delivery systems that are not only strong, economic, and non-toxic but also multifunctional.[26] For biological

applications, the biopolymers with bioactive compounds like proteins, lipids, and drugs collectively develop scaffolds, hydrogels, nanofibers, nanoparticles, nanocomposites, etc. to achieve targeted delivery, sustained drug release, and biocompatibility.[27]

1.2.1.1 Functional advantages

- Among all the polymers available to be used as excipients in drug delivery systems, plant-derived polymers are highly suggested because of their compatibility with bioactive therapeutics.[28]
- Biopolymers are the building blocks for therapeutic formulations because their biodegradable nature triggers easy removal of this carrier after the release of the therapeutics in the biological system.[29,30]
- New drug delivery systems for oral administration require new excipients to overcome the inconvenience of multiple regular injections.[31]
- Biopolymer-based nanocomposite offers diverse chemical modifications like crosslinking, etc.[32]
- Biopolymeric nanocomposites are less prone to rapid enzymatic degradation which allows them to maintain the concentration of therapeutics in systemic circulation over a long time period compared to the bulk therapeutics.[33]
- Sustained and controlled drug release patterns can be achieved by biopolymeric nanocomposites which offer prolonged release and less frequent doses of drugs.[34]

1.2.1.2 Structural advantages

- Biopolymers can be categorized into polynucleotides, polypeptides, and polysaccharides. Polysaccharides are long chains of monosaccharide units attached by glycosidic linkages.[35] These polysaccharides are comprised of flexible and semi-flexible primary structures.[36] Required mechanical and functional properties can be introduced by inducing complementary weak intra- and intermolecular bonding and folding into these primary structures.[37]
- Polymeric materials with preferred properties can be achieved by blending i.e simple mixing of polymers without chemical reactions. Expensive investment or critical synthesis procedures are not required to achieve proper blending compared to other polymerization techniques.[38,39]

- Structural enhancement of polymeric material can be attained by introducing different techniques of crosslinking which links functional groups of a polymer to another one through covalent bonding, ionic bonding, hydrogen bonding, etc. It has been reported that cross-linking of polymer chains can modify the release dynamics of the incorporated active agents, reduce antigenicity and modulate tensile strength, stiffness, cell-matrix interactions, resistance to enzymatic actions, and chemical degradation.[40-42]
- Some biopolymers bear a resemblance to the structural organizations of the extracellular environment. The chemical structures of biopolymeric materials are similar to the macromolecules native to the extracellular matrix of biological systems which make them compatible. These compatibilities enhance their functional attributes within the host body.[43,44]

1.2.1.3 Environmental benefits

- The backbone of biopolymer consists of carbon, oxygen, and nitrogen atoms which make them completely biodegradable.[45] As biopolymeric composites are derived from natural plant sources such as flax, psyllium husk, gum, etc., microorganisms easily consume these materials and eventually degrade to organic matter.[46]
- One of the primary benefits of biopolymeric materials is reduced environmental footprint.[47] Biopolymeric materials can lessen the emissions of CO_2 and hazardous waste products as they are readily degraded into their constituent organic residues.[48]
- Biopolymers are non-toxic to living organisms including humans and most importantly environmentally safe for agricultural uses.[45]
- Biopolymers are chosen over synthetic alternatives due to their non-toxicity, compatibility, non-immunogenicity and abundance in diverse biological systems.[49,50]

1.2.2 Future scope of biopolymers

Biopolymers gain profound attention among the scientific community considering the natures and features of these natural resources.[51] Biopolymers are produced by living organisms and have the potential to replace synthetic polymers to be used efficiently in different material synthesis, biomedical and therapeutic applications, food and packaging industry, water purification etc.[52-54] As per reports 300 million tons of synthetic plastics are produced annually and the application of biopolymeric materials are roughly less than 1% compared to the usage of petroleum-derived synthetic plastics.[55] Some sustainability challenges that influence the

demand for biopolymers are the availability of sources, competition with existing synthetic polymers, large-scale production issues, etc have to be considered.[55,56] Factors contributing the rising demand of biopolymers are the global interest in using natural materials compared to synthetic one, the unpredictable price of fossil fuels, the greenhouse effect, concern on waste management etc.[57] Driven by all these aspects, various biopolymer-based industries are expected to flourish. Considering these issues, to make biopolymers viable for various fields, it needs to work on some factors like modified manufacturing routes for higher yield, find out better strains of algae and plant species that can effectively produce sufficient amount of biopolymers, proper downstream process method to lower the production cost.[58,59] Considering the demands and need of sustainability standards authorities like ISO have issued methods and procedures for material testing for biopolymer production and extraction.[60] Therefore, it can be said that biopolymer-based industries have an encouraging future, driven by the functional, structural, environmental, and economic advantages of biopolymers in production of biomaterials.

1.3 Strategies for drug delivery

1.3.1 Stimuli-responsive strategy

Effective drug delivery is achievable through stimuli-responsive strategy that identifies the microenvironment of the target site and reacts dynamically.[61] The concept of stimuli-responsive drug delivery was first proposed by introducing thermosensitive liposomes for the localised release of drugs through hyperthermia in the 1970s.[62] Since then, stimuli-responsive drug delivery strategies have been widely exploited. Stimuli-responsive drug delivery devices can be sensitive to endogenous stimuli as well as exogenous stimuli.[63] Endogenous stimuli include variation of pH, redox potential, and increased or decreased concentration of certain enzymes or compounds.[63,64] Exogenous stimuli-responsive drug delivery depends on externally applied stimuli such as temperature variation, ultrasounds, X-rays, magnetic, light, and electric fields, etc.[64] Recently multi-stimuli responsive drug strategies are used to achieve an on-demand drug release where more than one stimulus is employed to improve drug delivery.

1.3.2 Co-delivery strategy

The development of nanocarrier-based drug delivery strategies offers an advanced co-delivery system in drug administration with the ability to incorporate therapeutics. Compared to the direct delivery of free drugs, encapsulation of drugs in a proper vehicle offers distinct

advantages such as improved solubility of the drug, sustained drug release behaviour, better pharmacodynamic properties, extended circulation, and less side effects.[65-67] Co-delivery systems include drug/gene co-delivery which overcomes the resistance of membrane transport protein-related efflux pump, which carries profound interest in the multidrug resistance mechanism.[68] Example includes the study of Sun et al. which demonstrated co-delivery of all-trans-retinoic acid and chemotherapeutic drug doxorubicin for cancer treatment which includes synergetic suppression of tumour cell as well as inhibition of cancer stem cells.[69]

1.3.3 Biomimetic delivery strategy

Biomimetic drug delivery strategies are novel strategies that focus on mimicking the unique structural configurations, functional mechanisms, and biosynthetic pathways of any living system. Such strategies maximize the functionality of the drug delivery system by mimicking the structural composition of biological membranes, and the budding mechanism of exosomes.[70,71] Biomimetic drug delivery strategies involve direct interaction with the biological system as it has the advantages of excellent biocompatibility, negligible immunogenicity, prolonged systematic circulation, etc.[72,73] Examples include the application of red blood cell-derived immunomodulatory signals or direct usage of erythrocyte membrane as a surface coating material.[74] Such systems are mainly based on advancing membrane-camouflaged compounds, extracellular vesicles, lipoprotein-coated excipients, etc. for their significant biomimetic properties. Kuai et al. developed high-density lipoprotein mimicking nano-discs for neoantigens-based personalized immunotherapy which can induce adaptive immunity with inhibitory potential on tumour growth.[75]

1.3.4 Ligand-modified targeted drug delivery

The movement toward ligand-mediated targeted drug delivery has been ushered in by a better insight into the exclusive biological interactions.[76,77] Ligand-mediated drug delivery has been widely exploited for biomedical applications that focused on enhanced penetration and permeation across biological barriers, internalization by target cells or specific subcellular sites, etc.[78,79] Generally this type of delivery systems include targeting moieties that are distributed on the surface of delivery vehicles. But only a small part of this system can participate in the interaction with target cells leads to controlled recognition capacity.[80] Inside the systemic circulation, ligands interact with specific plasma macromolecular moiety and stimulate ligand-derived modification of surface properties which are considered to be the main initiating signal to enter into the cells.[81] For ligand-modified delivery riboflavin, folate, carbohydrates like

simple sugar, glycan; cell-penetrating peptides, lipoproteins, and transferrin are used in transportation and targeting to specific locations.[82] Nanoparticles functionalized on gangliosides (lipid-anchored glycan) can detect and bind with toxins including cholera toxin of *Vibrio cholera*.[83] Such gangliosides are also known to interact with other pathogenic strains like *S. pneumoniae* which suggests that ganglioside-functionalized vehicles have effectiveness for targeted antibacterial applications.[84]

1.4 Literature Review on biopolymer-based drug delivery system

The thesis showcases biopolymers, including polysaccharides like guar gum, chitosan, alginate, carboxymethyl cellulose, and psyllium husk mucilage to develop biopolymeric vehicles and film.

1.4.1 Guar gum

Guar gum is a non-ionic polysaccharide extracted from endosperms of *Cyamopsis tetragonolobus* of the Leguminosae family. This natural gum consists of polysaccharides with high molecular weight which predominantly contains galactomannans with a linear chain of (1→4)-β-d-mannopyranosyl units with α-d-galactopyranosyl units attached by (1→6) linkages (average molecular weight of 220 kDa).[85] Guar gum swells to dissolve in polar solvent by forming strong hydrogen bonds and is utilized as a novel food additive, binder, emulsifier, disintegrant, stabilizer, and thickener. Guar gum is degraded by *Clostridium butyricum*, a human commensal bacterium in the large intestine, and prevents constipation, and obesity, maintains bowel regularity, controls diabetes, and facilitates mineral absorption.[86,87] Guar gum can be widely used in drug delivery due to its high viscosity, water solubility, biocompatibility, and commercial availability.[88] The derivatives of guar gum such as hydroxypropyl guar gum, synthesized by reacting the hydroxyl groups with other chemicals, displayed improved properties.[89] Guar gum and its derivatives are employed to develop different coatings, matrix tablets, hydrogels, nanocomposite, and nano or microparticles that can be used as a vehicle for sustained and targeted drug delivery.[90] The gel-forming property and enzymatic degradation of guar gum in the colon have been investigated by many researchers which enhances its prospect in pharmaceuticals for colon-targeted drug delivery.[91,92]Altaf et al. assessed the potential of guar gum as a sustained release system of diltiazem as a model drug which revealed that guar gum derived tablets could be a very efficient alternative for sustained release of diltiazem.[93] In another study, Al-Saidan et al. established that guar gum-based matrix tablets showed sustained oral delivery of metoprolol tartrate.[94] Baweja et al. formulate a hydrophilic matrix of guar gum

and methylated guar gum to study the controlled release of chlorpheniramine maleate which exhibited that the rate of drug release was increased with the degree of methylation of guar gum due to the reduced viscosity of the methylated guar gum.[95]

1.4.2 Chitosan

Chitosan is a promising hydrophilic cationic polyelectrolyte obtained by alkaline *N*-deacetylation of chitin, a structural component of the exoskeleton of crustaceans such as shrimps, crabs, lobsters, etc.[96] The structure of chitosan is composed of a linear binary heteropolysaccharide of β-1,4-linked glucosamine with N-acetylation of glucosamine residues.[97] The sources and synthesis procedure usually determine the molecular weight of chitosan which vary between 300 to 1000 kD with a degree of deacetylation from 30% to 95%.[98] Chitosan is widely utilized in tablet formulation as a diluent, packaging, textile, and cosmetics industries and has the potential to act as a binder, lubricant, or disintegrating agent.[99] The mucoadhesive properties of chitosan enhance the prospect as a suitable material for the localized delivery of drugs in the oral cavity.[100] Recently chitosan has been studied and employed in pharmaceutical sectors for its outstanding properties such as biodegradability, biocompatibility, antimicrobial activity, and ecological friendliness, etc.[101] Vasudev et al. studied the synthesis of chitosan/polyethylene vinyl acetate co-matrix which showed sustained release of aspirin-heparin to prevent cardiovascular thrombosis.[102] Sahasathian et al. formulate sustained-release tablets of amoxicillin by using chitosan as a drug carrier which revealed that chitosan with particle size less than 75 microns showed a significant sustained release profile of amoxicillin.[103] Bao et al. developed chitosan-functionalized graphene oxide as a nano carrier for an anti-cancer drug, camptothecin which showed 17.5% drug release in 72 hrs.[104] Xie et al. studied chitosan and dextran-modified graphene oxide nanocomposite as a vehicle for anticancer drug doxorubicin. Results showed that the nanocomposite was efficiently internalized in MCF-7 cells and strong cytotoxicity was observed in MCF-7 cell lines.[105] Reddy et al. developed Cefadroxil incorporated cross-linked chitosan-guar gum semi-interpenetrating network (IPN) microspheres where encapsulation efficiency was between 69% to 78%. Cefadroxil was found to be released in a sustained and controlled way from the semi-IPN microspheres up to 10 hrs.[106]

1.4.3 Alginate

Alginate or alginic acids are linear, unbranched, hydrophilic, anionic polysaccharides isolated from the cell wall of brown seaweed and marine algae such as *Macrocystis pyrifera*,

Ascophyllum nodosum, and *Laminaria hyperborea.*[107] Sodium alginate is the sodium salt of alginate consisting of alternating blocks of D-mannuronic acid and L-guluronic acid residues linked in α- or β-1,4 glycosidic bonds.[107] It is used as a thickener in the preparation of creams. The molecular weight of alginate is between 20 to 600 kDa.[108] It has been evaluated and investigated as a suspending agent, emulsion stabilizer, and binder of tablets and utilized in the synthesis of microspheres, beads, liposomes, tablets, buccal films, etc.[109] Alginates with microbial origin have a huge possibility as industrial polymers because of their structural diversity in chemical composition and their capability to sol-gel transition.[109] Different modifications of alginate have been done to formulate alginate-based drug delivery systems. Miyazaki et al. studied the release behaviour of bio-adhesive tablets of ketoprofen from the prepared mixture of chitosan and sodium alginate (1:4 ratio of chitosan and alginate) and oral sustained release tablets of ketoprofen.[110] Liew et al. evaluate the release behaviour of drug from a formulation of sodium alginate and observed that sodium alginate-based matrices showed sustained drug release up to 8 hrs.[108] Goel et al. studied fast disintegrating tablets of ondansetron HCl using interpolymer chitosan-alginate (1:1) complex and proposed that this complex swelled up imbibing water which led to rupture of tablet matrix within seconds.[111] Anirudhan et al. developed pH-sensitive bioactive silica–alginate/folic acid conjugated o-carboxymethyl chitosan-gelatin nanocomposite for the loading of 5-fluorouracil and Bisdemethoxycurcumin which showed a sustained release profile and anticancer effect on colon cancer cell line.[112]

1.4.4 Psyllium Husk

Psyllium husk (Ispaghula) is the seed husk of *Plantago ovata* and *Plantago psyllium* of Plantaginaceae family, which is known as a dietary fibre supplement to promote the regulation of bowel function and also effective in both constipation and diarrhoea, two opposite gut conditions.[113,114] Hydrocolloids extracted from psyllium husk contain a complex heteropolysaccharide, arabinoxylan.[113] Psyllium husk mucilage is found to prevent high cholesterol levels, ulcerative colitis, and irritable bowel syndrome; and reduce glucose in the post-prandial period.[114] Psyllium husk contains numerous active components i.e. 4-O-methyl glucuronic acid, arabinoxylan, campesterol, linoleic acid, oleic acid, palmitic acid, L-cystine, L-asparagine, sterol, β-sitosterol, etc.[115] Psyllium husk mucilage is used commercially as sustaining agent, binder, lubricant, demulcent, emulsifying and suspending agent.[116] It is a vital constituent of commercially available laxative materials i.e. metamucil.[117] Several researches have been performed on clinical usefulness of husk in the pharmaceutical sector.

Previous studies showed the *in vitro* release profile of some model drugs i.e. tetracycline hydrochloride, insulin, and tyrosine from psyllium mucilage and acrylic acid-derived hydrogels for colon-specific drug delivery. Experimental outcomes revealed that the release kinetics of drugs from the composite hydrogels follows the non-Fickian mechanism in distilled water as well as in pH 7.4 buffer. It has also been observed that the polymer chain relaxation rate of hydrogel and the drug diffusion rate are interrelated.[118] Rosu and co-researchers demonstrated controlled release of aspirin from psyllium-derived composites comprising titanium dioxide nanoparticles as nanomaterial matrix. The result suggested a slowest delay in the release of aspirin from the composite nanomaterial.[119] Kumar et al. developed pH-sensitive grafted cross-linked psyllium by using ceric ammonium nitrate as a redox initiator and quercetin as a model drug for colon-targeted drug delivery. Results demonstrated 93% quercetin release at pH 7.4 (pH of intestinal fluid) and showed significant anticancer activity compared to bulk quercetin.[120] Patil et al. fabricated psyllium seed husk polysaccharide-based wound dressing films complexed with povidone-iodine and were assessed for antibacterial activity against a broad range of bacterial strains as well as wound healing potential in albino rats.[121]

1.4.5 Carboxymethyl cellulose

Carboxymethyl cellulose is a cellulose-derived hydrophilic, polysaccharide possessing both carboxylate and hydroxyl groups with high chemical stability, pH sensitivity, non-toxicity, and gel-forming properties.[122] Carboxymethyl cellulose is a biocompatible macromolecule that has the potential to develop drug delivery systems with the aim of sustained and controlled drug release.[123] It is reported that CMC has several biomedical applications such as wound healing, bioimaging, tissue engineering, and drug delivery.[124] Cellulose derivatives, especially carboxymethyl cellulose sodium salt have been utilized as stabilizing or reducing agents in numerous applications in a variety of fields such as textile, chemical, food, cosmetics, and pharmaceutical industries, etc.[125,126] Ng et al. carried out a study on lyophilized wafers containing antimicrobial agents using two different cellulose derivatives, sodium carboxymethyl cellulose and methylcellulose. Sodium carboxymethyl cellulose-neomycin tri sulphate salt hydrate showed a better flux of drug release as well as greater inhibition of both Gram-positive and Gram-negative bacterial strains.[127] In another study Sarkar et al. have demonstrated multiple applications like drug carrier, osteogenic activity, and bio-imaging of synthesized carbon dots conjugated carboxymethyl cellulose hydroxyapatite nanocomposite. Chemotherapeutic drugs like doxorubicin incorporated nanocomposite showed good anticancer properties.[128] Carboxymethyl cellulose was utilized as an emulsifying agent for

curcumin to synthesize curcumin-activated carboxymethyl cellulose-clay nanocomposite. The result demonstrated enhanced release of curcumin in water (pH 5.4) which is over 60% within 2 hrs and 30 mins.[129] Another study reported antioxidant and antimicrobial properties of TiO_2–Ag incorporated carboxymethyl cellulose-gelatin nanoparticle. They developed an antioxidant film having antibacterial activity of nanoparticles against *Escherichia coli* and *Staphylococcus aureus* bacteria.[130]

1.5 Phytochemicals

Plants are a rich source of phyto-active chemicals or bio-nutrients. It is well-established that plants develop these chemical components to protect themselves, whereas modern researches revealed that most of these phytochemicals have ameliorative effects against different diseases of humans.[131] In the Ayurveda, several plants with therapeutic possessions are recognized in various texts but it need advanced guidelines for proper standardization, manufacture, and quality control. It has been stated that approximately 50% of all modern pharmaceutics in clinical use are plant-derived.[132] Phytochemicals have a promising biological role in preventing numerous chronic diseases such as cancer, diabetes, coronary heart disease, etc., and are known to possess hepatoprotective, antidiabetic, anti-inflammatory, antimutagenic, antimetastatic, anti-asthmatic, antifungal activity, antineoplastic, chemopreventive and neuroprotective properties.[132,133] Phytochemicals are secondary metabolites with antioxidants, pro-oxidant, immunity-potentiating, and detoxifying properties and are taxonomically extremely diverse. These phytocomponents are the major reservoir of potential precursors of newer drugs based on their chemical nature and pharmacological actions.[131,134] These bioactive compounds consist of a wide range of chemicals (alkaloids, flavonoids, terpenoids, polyphenols, organosulfur, etc) with differing potency.[135] However, Indian medicinal plants-derived phytochemicals with multi-functional potentials have received considerable attention for further systematic study for evaluating their potential against a broad range of diseases.

1.5.1 Phytochemicals and disease prevention

Since the earliest times, plant chemicals have been recognized to exert health benefits and heal infectious diseases due to their content of secondary metabolites. According to previous reports, medicinal plants containing active components i.e. vitamins, carotene, polysaccharides, polyphenols, flavonoids, alkaloids, lignin, xanthones, etc. have significant antibacterial, anticarcinogenic, tumor-suppressive, and antimetastatic activities.[136] Though the conventional therapeutic options have indisputably boosted survival rates, metastasized cancer

remains fatal.[137] Besides this other health issues like antibacterial resistance, jaundice, and chronic diseases like diabetes are found to be treatable with these bioactive compounds.[135] Hence, constant searching for more effective chemo-preventive approaches is urgently desirable for advanced treatment. According to a survey by the World Health Organization, 80 % of the rural population depends primarily on medicinal herbs and traditional remedies as a primary healthcare option.[138] Thus, the various combinations of the phytochemicals extracted from these plants may undergo further assessment for their numerous medicinal properties. According to chemical constituents, phytochemicals can be differentiated into different classes i.e alkaloids, polyphenols sulfur-containing phytochemicals, and terpenoids, etc.[135]

- ***Alkaloids:*** Alkaloid compounds (sanguinarine, berberine, piperine) have excellent antibacterial efficacy and can be used in the treatment of many bacterial diseases.[139] Alkaloids like taxols, camptothecin, harringtonine, acronycine, thalicarpine, ellipticine, and matrines are generating research interest in the antineoplastic activity due to their potential to target the DNA and protein of cancerous cells.[140]

- ***Polyphenols***: Polyphenols classified as flavonoids and non-flavonoids, exert good antibacterial activity against a broad range of bacterial strains due to their ability to inhibit bacterial energy metabolism as well as cell membrane function.[141] flavonoids like galangin, kaempferol, quercetin, myricetin, apigenin, luteolin, catechin, epicatechin, naringenin, hesperetin, cyanidin, and malvidin have been reported for their inhibitory activity against different bacterial strains.[142] The non-flavonoid polyphenols include phenolic acids (ferulic acid and coumaric acid, gallic acid, chlorogenic acid, cinnamic acid), quinones (derived from benzoquinone, naphthoquinone, or anthraquinone), tannins and stilbenes, also have received increasing attention due to their antimicrobial potentials.[142] Phenolic acids have been shown to have significant antibacterial activity against Gram-positive bacteria than Gram-negative bacteria as Gram-negative bacteria have an outer hydrophobic layer that can exclude certain hydrophilic molecules like phenols.[143] Quinones (emodin, thymoquinone, chrysophanol, and rhein) have shown noticeable antibacterial as well as antineoplastic activity.[144]

- ***Organosulfur compounds:*** Organosulfur compounds such as allicin, ajoene, and isothiocyanates have been found to possess anticancer properties, antibacterial activity against both Gram-positive and Gram-negative bacteria as well as powerful antioxidant activity.[145]

- ***Terpenoid compounds***: Terpenoid compounds (myrcene, geraniol, cymene, and carvacrol) have been studied extensively and several researches have shown their ability to inhibit the growth of many bacteria.[146]

1.6 Literature review on thymoquinone and piperine

1.6.1 Thymoquinone

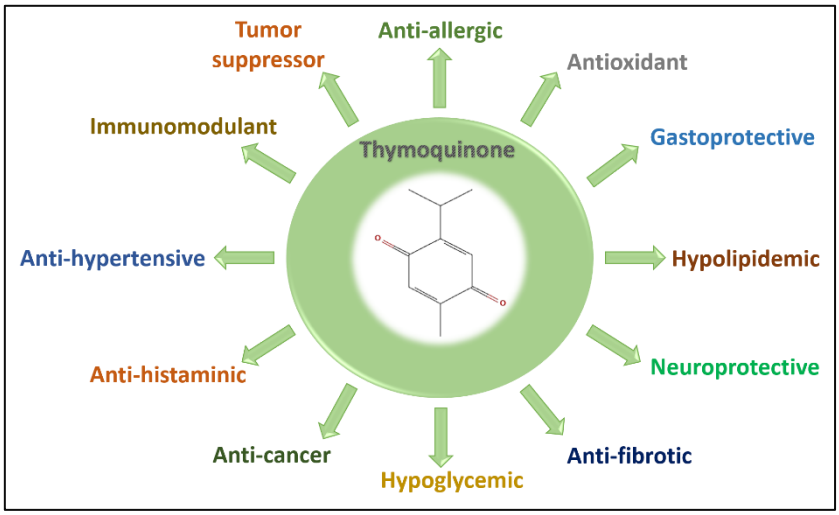

Figure 1.2: *Schematic representation of medicinal properties of thymoquinone.*

Thymoquinone (2-isopropyl-5-methyl-1,4-benzoquinone) a phyto-active dietary compound of *Nigella sativa*, is a traditionally used natural medicine that exerts extensive biomedical activities like anti-inflammatory, antioxidant, hepatoprotective, antimicrobial, antiparasitic, anticancer, antihypertensive, and anti-asthmatic properties (figure 1.2).[147] Evidence so far indicated the effectiveness of thymoquinone against various kinds of microorganisms and this bioactive compound was known to inhibit the growth of certain pathogenic bacterial strains. Thymoquinone also reduces the MIC values of conventional antibiotics in case of co-administration. This phytochemical also confirmed a prominent antifungal activity against *Candida albicans*, *Aspergillus fumigatus*, etc.[148] Thymoquinone possesses a significant bactericidal property against the Gram-positive *Staphylococcus aureus* and *Staphylococcus epidermidis* strains (MICs values ranged from 8 to 32 μg/mL).[149] For the wound healing application, thymoquinone containing polymeric films and hydrogels exhibited *in vitro* skin permeation and potential antibacterial activity against *S. aureus*.[150] In several studies thymoquinone was reported to induce apoptosis via p53-dependent as well as p53-independent pathway.[151] It also exerts anticancer activities via inducing apoptosis by regulating pro- as well as anti-apoptotic genes in different human cancers such as breast, cervical, liver, pancreatic,

oral, bone, prostate, blood, head, neck, and lung.[152] In a study reported by Liu and his coworkers, thymoquinone was shown to induce apoptosis by regulating Bcl-2 and Bax genes in ovarian cancer cell lines.[153] Another research reported cytotoxic activity of thymoquinone-incorporated nanostructured lipid carriers which decreased Hep3B growth, activated cell cycle arrest, and apoptosis. The study also revealed the antioxidant properties of lipid carriers with decreasing ROS levels.[154]

1.6.2 Piperine

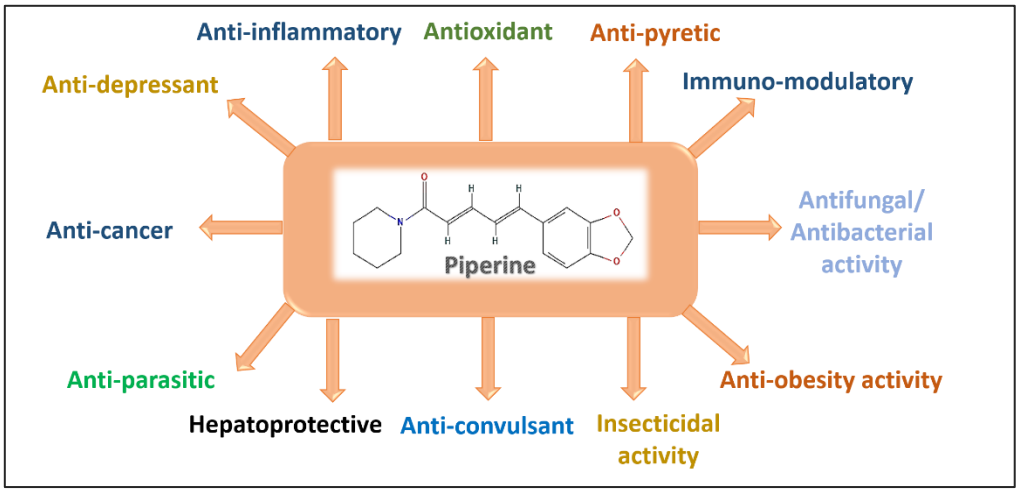

Figure 1.3: *Schematic representation of medicinal properties of piperine.*

Piperine is a natural alkaloid extracted from the seeds of *Piper longum* that possess excellent antioxidant, anticonvulsant, antimicrobial, neuroprotective, larvicidal, antiparasitic, anticancer properties, and other pharmacological activities (figure 1.3).[155] Hikal et al. reported antimicrobial growth inhibition of piperine against *S. aureus*, *B. subtilis*, *Salmonella sp.* and *E. coli* by employing the agar well diffusion method.[156] Ameliorative effects of piperine on liver disease have been investigated in several studies based on different hepatic health biomarkers which have exerted the lowering of serum ALT, AST, and ALP levels of cholesterol-fed Swiss albino mice.[157,158] Piperine has been extensively studied for its inhibiting role in carcinogenesis as well as chemo-preventive properties.[159] Recent studies reported that piperine as a sole agent and in the case of co-treatment with other drugs effectively reduces tumorigenesis as well as carcinogenesis. Ding et al. reported that co-administration of piperine with docetaxel exerted synergistic cytotoxic activity in HepG2 cell lines compared to docetaxel alone.[160] In a study conducted by Sehgal and coworkers, piperine in combination with curcumin has promising antigenotoxic potentials against a carcinogenic agent (benzo[a]pyrene) induced toxicity in Swiss albino mice. The experimental outcome showed reduced lipid peroxidation, and

enhanced levels of endogenous antioxidants like SOD, catalase, and glutathione peroxidase in the liver.[161] Studies showed that piperine inhibits concentration-dependent human melanoma cell growth rate by inducing apoptosis via the suppression of tumorigenesis.[162] A Study conducted by Rad & Hoskin illustrated that piperine-incorporated nanoparticles induce apoptosis and repress the growth of triple-negative breast cancer cells. Interestingly no such cytotoxic activities were observed in normal fibroblast cells.[163] Yaffe et al. showed that piperine, (dose of 75–150 μM) suppresses the proliferation of various colon cancer cells with little effect on normal fibroblasts and epithelial cell lines. Piperine has been shown to prevent the growth of HT-29 colon carcinoma cells by arresting the cell cycle at the G1 phase.[164] Piperine has emerged as a potential autophagy-regulating anticancer therapeutic against various cancers *in vivo* and could be an efficient alternative for antitumor therapy.[165]

1.7 Materials and Methods

1.7.1 Bacteria, Cells and Animal

Test bacterial strains i.e. Gram-positive *Enterococcus faecalis* 441, *Staphylococcus aureus* 740, and Gram-negative *Escherichia coli* 443, *Pseudomonas aeruginosa* 1688 were purchased from Microbial Type Culture Collection, IMTECH (Chandigarh, India). HepG2, A549, PC3, and WI38 Cell lines were procured from the National Centre for Cell Science (Pune, India).C6 glioma cells were collected from Dr. Suvendra Nath Bhattacharya, IICB, Kolkata.

The *in vivo* experiments were performed on Swiss albino mice obtained from a CPCSEA-approved animal house (Registration No. 50/CPCSEA/1999).

1.7.2 Media, Reagents and Dyes

PIP, TQ, CMCNa (viscosity 400–1000 mPa.s, average Mw ~250,000, degree of substitution 1.2), Na-AL with viscosity (25ºC): 5–40 cps, were purchased from Sigma-Aldrich (Switzerland). GG was obtained from Hi-Media chemicals. CH $(C_6H_{11}NO_4)n$ (molecular weight: 100–300 kDa) was purchased from Acros organics. PH was obtained from a market of Kolkata, India. All other reagents of analytical grade including fluorescence stains, paracetamol, and silymarin were supplied by Merck ltd, HiMedia Pvt. Lt., and SRL Pvt. Lt. (India). All experimental procedures were performed by using deionized water of 18 MΩ-cm. For biological experiments, all therapeutics-loaded vehicles were sterilized under UV radiation.

1.7.3 Characterization Tools

To establish the characteristic nature of the synthesized nanomaterials and nanofilms we have used various characterization tools. Data provided by these tools determine the chemical structure, thermal stability, size, shape, and morphology of the nanomaterials which contribute significant effects to the research work.

Brief descriptions of the instrumental methods are discussed below:

1.7.3.1 Fourier Transform Infrared (FTIR) Spectrometer

In our studies, Fourier Transform Infrared (FTIR) Spectroscopy was conducted using FTIR-8400S; Shimadzu, Japan in the absorbance spectra range from 400 cm^{-1} to 4000 cm^{-1} with high scan speed. For preparing the nanocomposites for FTIR spectroscopy, it was ground into fine powder and mixed with potassium bromide to form a pellet.

The quantitative analysis of FTIR spectroscopy was done by using the Lambert-Beer Law. When infrared radiation passes through a sample, specific wavelengths are absorbed by the molecules of the sample. The intensity of this absorption is measured and recorded as an absorption spectrum. According to the Lambert-Beer Law, the absorbance (A) at a given wavelength is as follows.

$$A = \varepsilon . c . l \quad \text{.....(1.1)}$$

where ε is the molar absorptivity, c is the concentration of the sample, and l is the path length of the light through the sample. This relationship allows FTIR spectroscopy to not only identify the molecular structure based on the absorption peaks but also to quantify the concentration of specific compounds within the sample by analyzing the absorbance values. Using FTIR spectra the composition of the biocompatible nanocomposites can be identified and their interaction patterns can be studied.[165]

1.7.3.2 X-ray Diffraction (XRD)

The structural properties of synthesized nanomaterials and films have been examined by X-ray diffractometer (XRD; Model-D8, Bruker AXS Inc., Madison, WI). For Cu Kα (target operating at 40 kV voltage and 35 mA current with Wavelength-1.5406 Å and scan speed 1s/step) radiation, Germanium (002) monochromator has been used. A small amount of sample was taken for grinding to a fine and uniform powder with the help of a mortar pestle which improves sharp peak and accuracy.

The working principle of X-ray diffraction can be explained using the equation known as Bragg's law. Bragg's law describes the relationship between the scattering angle (θ), the wavelength of X-rays (λ), and the spacing between crystal lattice planes (d). The equation is used to calculate the lattice spacing of the sample from measured diffraction angles.

$$n\lambda = 2dSin\theta \quad \text{.....(1.2)}$$

According to Bragg's Law, X-rays are diffracted by striking crystal planes at a specific angle that satisfies the condition for constructive interference. Constructive interference occurs when the path difference between the scattered waves from adjacent crystal planes is an integrated multiple of the X-rays' wavelength (nλ). This leads to the formation of diffraction peaks in the XRD pattern. By measuring the angle at which the diffraction peaks occur and knowing the wavelength of the X-ray, the spacing between the crystal lattice parameters and the presence of specific crystalline phases can be obtained. The obtained diffraction patterns are utilized to study the structural properties of the synthesized samples.[166]

1.7.3.3 Thermal Gravimetric Analysis (TGA)

To estimate the thermal stability, purity, moisture content, and decomposition mechanism of samples we used thermal gravimetric analysis (TGA). In addition, to determine the evaporation rates of any mixture and temperature-dependent mass loss of the samples, TGA has been performed by using the TGA/SDTA851e, Mettler Toledo AG instrument.

Approximately, 5mg fine powder of the sample was kept in an aluminum or platinum holder to scan for TGA.TGA is a method where a change in mass of the material is recorded with the change in temperature in an inert atmosphere when the initial mass is known.[167]

1.7.3.4 Ultra Violet-Visible (UV- Vis) Spectrophotometer

UV-Vis spectroscopy is an analytical technique used to measure the absorbance of ultraviolet light by a sample, providing valuable information about its structure. In this study, we have used an Epoch microplate reader, from BioTek, USA.

At first, reference was set with the solvent of the diluted sample and then scan was taken 200 to 800 nm. The spectrum plots absorbance against wavelength, displaying peaks at wavelengths where absorption occurs. According to the Lambert-Beer Law, the absorbance at each peak is proportional to the concentration of the molecules and the length of the light through the sample. This leads to qualitative analyses by identifying compounds based on their absorption patterns and by determining the concentration of these compounds. In the case of the

determination of bacterial growth with time at different concentrations of the nanomaterials, a UV scan was recorded at 600nm.[168]

1.7.3.5 Field Emission Scanning Electron Microscope (FESEM)

A field emission scanning electron microscope (FESEM) has been used to observe the surface morphology of synthesized materials and nanocomposites. The morphological surface images were captured by using FESEM; INSPECT F50, Netherlands. By using a Q150T Turbo Pumped Sputter Coater the surface of the sample was gold coated and then with the help of a holder sample was placed under the FESEM.

The working principle is similar to the conventional scanning microscopes. An electron beam is focused by electromagnetic lenses and scans the surface of the sample, where the reflected electrons create an image of the surface by generating many low-energy secondary electrons. FESEM micrographs provide information about the shape as well as the size of the sample whether it is in the micro-scale or nano-scale range.[169]

1.7.3.6 Transmission Electron Microscope (TEM)

To investigate the fine structure of materials at high resolutions, down to the atomic level we have used TEM (JEOL JEM F200). To prepare the sample, A pinch of material was diluted with acetone and drop cast on a TEM grid kept overnight for drying. The next day the grid was observed under TEM.

In TEM, an electron gun emits a beam of high-energy electrons that travel through the vacuum tube to create the required images. As the electrons interact with the sample, they are either scattered or transmitted depending on the density and composition of the sample. The contrast in the TEM image is created by differences in electron density and the scattering properties of various regions within the sample, providing insights into the morphology of the sample.[170]

1.7.3.7 Atomic Force Microscope (AFM)

AFM is a high-resolution scanning microscope which allows for imaging and measuring size at the nanoscale range. The working principle of AFM involves a sharp tip, typically made of silicon or silicon nitride, which is mounted on a flexible cantilever. As the tip, scans across the surface of a sample, it interacts with the surface atoms of the sample, causing the cantilever to deflect. These deflections are measured using a laser beam reflected off the top of the cantilever onto a position-sensitive photodetector. The data collected by the photodetector are used to generate a detailed three-dimensional image of surface at atomic or molecular resolution. The

sample was cleaned with solvent and then dried with the help of nitrogen gas to eliminate contaminants.[171]

1.7.3.8 Dynamic Light Scattering (DLS)

Dynamic light scattering (DLS) is an analytical method to determine the size distribution of particles in suspension by measuring the fluctuations in light scattering intensity. When a laser beam passes through a sample, the particles within the suspension scatter the light. Due to Brownian motion, the particles move randomly, causing the scattering intensity to fluctuate over time. These fluctuations are analyzed to get information about the particle size. The speed of the fluctuations is related to the diffusion coefficient of the particles, which can be used to calculate their hydrodynamic radius using the Stokes-Einstein equation,

$$D = k_B T/3\pi\eta d \quad \text{.....(1.3)}$$

Where D is the diffusion coefficient, k_B is the Boltzmann constant, T is the absolute temperature, η is the viscosity of the fluid and d is the diameter of the particle.

DLS combined with zeta potential measurement provides a comprehensive analysis of nanoparticle systems, addressing both particle size and surface charge properties. DLS ensures the sample is at an optimal concentration, free of contaminants, and properly dispersed to avoid multiple scattering or insufficient scattering intensity. The particles were dispersed in the solvent and taken in a clean, rinsed vial for sonication, which helps to eliminate air bubbles. The solvent is to be compatible with both the sample and the DLS instrument, as the refractive index and viscosity of the solvent are needed for accurate analysis. Next, the sample is allowed to equilibrate to the measurement temperature, as temperature variations can impact the viscosity of the solvent, and consequently the accuracy of the size measurements.[172]

1.7.3.9 Methodology to evaluate the drug loading percentage

The percentage of PIP and TQ loaded within a biopolymeric vehicle was determined spectrophotometrically. PIP has known absorption maxima at 342-344 nm and.[173] TQ is characterized by the presence of one prominent peak (λ_{max}) at 254-257 nm regarded as a distinguishing peak for quinones.[174] During the purification of a sample, through ultracentrifugation, the supernatant was collected and the absorbance of supernatant was measured. The concentration of therapeutics i.e. PIP and TQ were assessed from the calibration curve of $[(\text{Absorbance})\ \lambda_{max}]_{PIP}$ vs. PIP concentration and $[(\text{Absorbance})\ \lambda_{max}]_{TQ}$ vs. TQ concentration respectively (figure 1.4 and 1.5). The drug loading content (DLC) and drug

loading efficiency (DLE) were assessed by following equations.[175] Effective concentration of PIP and TQ were also measured spectroscopically and calculated from calibration curves.

$$\textbf{DLC (\%)} = \frac{W_{\text{total drug}} - W_{\text{free drug}}}{W_{\text{drug loaded vehicle}}} \times 100 \quad \text{......(1.4)}$$

$$\textbf{DLE (\%)} = \frac{W_{\text{total drug}} - W_{\text{free drug}}}{W_{\text{total drug}}} \times 100 \quad \text{......(1.5)}$$

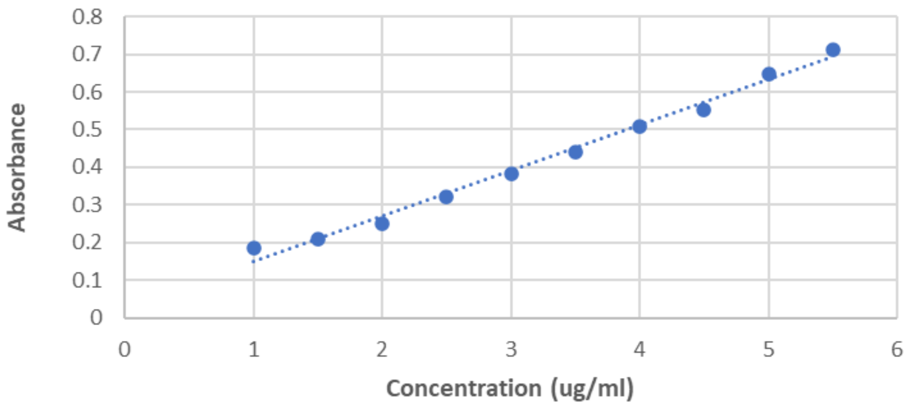

Figure 1.4: *Calibration curve of thymoquinone.*

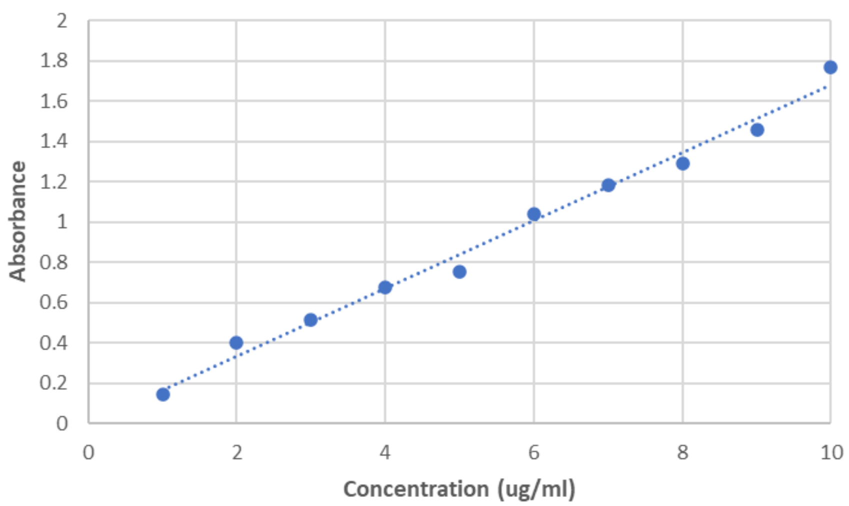

Figure 1.5: *Calibration curve of piperine.*

1.7.3.10 Methodology to determine drug release profile

The rate of release of PIP and TQ from the sample was determined by the dialysis method.[176] Purified nanocomposite suspension was taken in a dialysis bag which was dipped in a beaker containing PBS. Dialysis was allowed under gentle stirring for 100 hrs at 37ºC. At different time intervals, 1 mL solution was withdrawn followed by refilling the volume by adding fresh PBS into the beaker. The amount of released therapeutics (PIP or TQ) in the withdrawn aliquot was evaluated by measuring absorbance and then by estimating the corresponding concentration from the calibration curve of therapeutics (figure 1.4 and 1.5)

1.7.4 Methodology to assess antibacterial activity

1.7.4.1 Determination of MIC, MBC, and tolerance level

The antimicrobial activities of synthesized materials were evaluated against different Gram-negative and Gram-positive bacterial strains by colony counting method.[177] To evaluate the antimicrobial efficacy minimal inhibitory concentration (MIC) and minimum bactericidal concentration (MBC) were assessed. The concentration of an antibacterial agent that causes complete growth inhibition of a bacterial population during 18 to 20 hrs of incubation is defined as MIC, whereas MBC refers to the concentration that is responsible for 99.9% killing of the bacterial population under the same incubation condition.[178]

To evaluate the antibacterial properties, different concentrations of samples were added to this fresh bacterial culture (5×10^6 CFU ml^{-1}) containing nutrient broth (5 ml) and allowed to incubate on a rotary shaker for 18 hrs. Finally, to measure the growth inhibition, an equal amount of treated culture was withdrawn and serially diluted. Microbial growth was assessed and compared with control after plating the diluted culture on nutrient agar plates followed by overnight incubation. Each experiment was done thrice and strictly performed in a bio-safety cabinet. The mortality percentage of bacterial strains was calculated using the equation.[179]

$$M\,(\%) = [(C - T)/C] \times 100 \quad \text{.....(1.6)}$$

Where M represents the mortality percentage of bacteria, C is the mean number of bacterial colonies observed on the control plate, and T represents the mean number of colonies observed on the treated plate.

The tolerance levels of each bacterial strain against our samples were determined by the MBC and MIC values of our experiments. High tolerance demonstrates a reduced susceptibility to

antibacterial agents. Tolerance level (MBC) / (MIC) gives a clear indication of the antimicrobial potential.[180]

1.7.4.2 Agar well diffusion study

In the agar well diffusion study, the bacterial strain was allowed to grow until the turbidity of the culture reached 0.5 McFarland standards. Then 100 μL of this bacterial culture was spread on the entire agar surface of the plate filled with 30 mL of Mueller Hinton Agar. Afterward, agar wells were made in each plate having a diameter of approximately 0.563 cm. Antibacterial materials at their respective MBC concentration were transferred into the agar wells separately and were allowed to incubate overnight at a temperature of 37°C. The antibacterial agent diffuses through the agar medium and inhibits the growth of test bacteria. At the end of the incubation, the zone of inhibition was measured and recorded.[181]

1.7.4.3 Time dependent antibacterial study

For the time-dependent colony counting method antibacterial films were added to the bacterial culture (cell density 10^7 CFU mL^{-1}) containing 5mL nutrient broth and incubated on a rotary shaker at 37 °C. Finally microbial growth was assessed by plating the treated culture on nutrient agar plates after 2, 4, 12 and 24 hrs. The microbial culture without any antibacterial films was considered a control. In the case of control, after the incubation, the inoculum was plated on a nutrient agar plate and bacterial colonies were counted after 24 hrs. The antibacterial efficacy was calculated using the previously mentioned equation 1.6.

1.7.4.4 Agar diffusion study

For the agar-diffusion method, 100 μL of overnight grown bacterial culture (cell density 10^7 CFU mL^{-1}) was dispersed over the petri dish. The antibacterial films were positioned on the petri plate containing solid media with direct contact with the surface. Then the plates were incubated at 37 ºC overnight.[182]

1.7.4.5 Estimation of bacterial reactive oxygen species (ROS)

To evaluate the bacterial ROS (reactive oxygen species) generation $DCFH_2$-DA (2, 7 - dichlorodihydrofluorescein diacetate) dye was used and fluorescence intensity was measured using a spectroscope (Hitachi, Japan). The DCF-DA dye reacts with intracellular ROS after cell penetration which generates a bright green fluorescent compound, dichlorofluorescein (DCF). Finally, the intensity of this green fluorescence was measured spectroscopically by

using a fluorescence microscope (DM 2500, Leica, Germany) at wavelengths of 485 nm (excitation) and 520 nm (emission).[183]

1.7.4.6 Bacterial cell morphology study by FESEM

To evaluate the bacterial cell morphology FESEM was used. FESEM micrographs of control or untreated bacterial cells, as well as treated cells (exposed to MIC dose of the respective sample), were studied. To prepare a bacterial sample for FESEM, the bacterial broth was centrifuged and washed the pellet with phosphate buffer saline thrice. After that, the cells were fixed in 2.5% glutaraldehyde in PBS buffer for 1 hr. After that cells were rinsed in PBS and a pellet was collected by centrifugation. Then serial dehydration was achieved using a graded ethanol series (30%, 50%, 70%, 80%, 90%, and 100%) and incubated for 10 minutes in each concentration of ethanol. Finally, the samples were air-dried in a biological safety hood and FESEM analysis was performed to study cell morphology.[184]

1.7.5 Methodology to assess anticancer activity

1.7.5.1 Methodology of cell culturing

Cells were grown in Dulbecco's modified eagle's medium (DMEM) supplemented with antibiotic antimycotic solution (100 unit/mL) and 10% fetal bovine serum. The cells were maintained in a humidified CO_2 incubator at 37°C temperature in 65 mm petri plates and were allowed to grow up to 80% confluency. After that the growth media was discarded, cells were washed once with prewarmed phosphate buffer saline (PBS) and were trypsinized using 1X Trypsin-EDTA (0.25% Trypsin and 0.2% EDTA). The percentage of viable cell number was calculated by haemocytometry and the desired number of cells was seeded in well plates for subsequent experiments.

1.7.5.2 MTT assay

The anticancer activity of synthesized samples against different cancer cell lines was investigated by MTT assay.[185] Cell-permeable MTT [3-(4,5-dimethylthiazol-2-yl)-2,5-diphenyl-tetrazoliumbromide] is broken by active mitochondrial dehydrogenase enzyme of live cells, resulting in purple formazan crystals that are soluble in dimethyl sulfoxide (DMSO) or acidified isopropanol. The intensity of the resulting purple-coloured solution can be measured spectrophotometrically by measurement of [$(Absorbance)_{570nm}$] which correlates to the percentage of living cells in a cell population. For this study, cells were seeded at a concentration of 3×10^5 cells/well in a 24-well plate. After proper attachment of the cells, cells

were treated with different concentrations of samples for subsequent 24 hrs. After treatment, the media containing the anticancer agent was discarded, cells were washed with prewarmed PBS and were incubated with 200 µL MTT solution (dissolved in DMEM at a concentration of 250µg/mL) for 4 hours in the dark at 37ºC. Finally, MTT was discarded and the formazan crystals were dissolved in DMSO. The [$(Absorbance)_{570nm}$] of the solution was measured. Percent cell survivability for different treatment groups was expressed with respect to control cells.

Cell survivability (%) = 100 × [$(Absorbance_{570nm})$ control – $(Absorbance_{570nm})$ treated / $(Absorbance_{570nm})$ control] %.....(*1.7)*

1.7.5.3 Intracellular ROS estimation

The intracellular reactive oxygen species (ROS) content of cells after treatment with synthesized samples (at IC_{50} dose) was studied by fluorescence microscopy technique, using 2',7'-dichlorodihydrofluorescein diacetate ($DCFH_2$-DA) fluorescent dye. $DCFH_2$-DA is cell permeable, which upon entry into cells gets deacetylated by cellular esterases to DCFH, which then gets oxidized to highly fluorescent DCF by intracellular ROS. Thus, the extent of DCF fluorescence directly correlates to the ROS content of cells. For this study same experimental steps from seeding of the cells, their attachment, drug treatment (at IC_{50} dose), and washing with PBS were followed as described previously in 1.7.5.2. The cells were then incubated with $DCFH_2$-DA (10 µm) at 37°C in the dark for 30 mins. The stained cells were then washed several times with ice-cold PBS and images were captured using a fluorescence microscope. The fluorescence intensity of the cells was measured using 'ImageJ' software. Experiments were done in three replicates and from each treatment group, 10 different images were taken. From each snap, the actual fluorescence intensity of cells (15-20 numbers) was measured by subtraction of background intensity.[186]

1.7.5.4 Intracellular NADPH and GSH assay

Intracellular GSH (Glutathione) and NADPH (Nicotinamide Adenine Dinucleotide Phosphate) sensing assay were performed. GSH-Glo™ Glutathione Assay kit (Promega) is used to measure GSH content and Amplite™ Fluorometric NADPH Assay kit (Advancing Assay & Test technologies [AAT] Bioquest, USA) is used for NADPH measurement with the aid of microplate reader (Bio-Tek).

1.7.5.5 Determination of mitochondrial membrane potential (MMP)

The MMP of treated cells was studied by fluorescence microscopy technique, using Rhodamine 123 fluorescent dye. Rhodamine-123 is a cationic dye that distributes along the inner membrane of the mitochondria of cells and its binding is proportional to the potential of the membrane. Alternation of membrane potential of mitochondria affects the amount of binding of this dye to the membrane and thus gets reflected in its fluorescence intensity which can be used to measure the MMP of the cells.[188] In our study same steps as described in 1.7.5.3 were followed with only exception of staining the cells with Rhodamine 123 (5 µM) at 37°C in the dark for 20 mins.

1.7.5.6 Analysis of nuclear damage by Hoechst staining

The degree of nuclear damage of treated cells was studied by fluorescence microscopy technique, using Hoechst 33342 fluorescent dye. Hoechst 33342 is a nucleic acid binding stain, and its uptake gets increased in decondensed chromosomal DNA present in apoptotic cells. Thus, its level of fluorescence signifies the degree of cellular nuclear damage and apoptosis.[187] For this study same steps as described in 1.7.5.3 were followed with only the exception of staining the cells with Hoechst 33342 (5 µg/mL) at 37°C in the dark for 15 mins.

1.7.6 Methodology to assess In vivo hepatoprotective properties

1.7.6.1 Animal preparation

The experiments were performed on Swiss albino mice with 23-27 gm of body weight obtained from CPCSEA, an approved animal house (Registration No. 50/CPCSEA/1999). All animals were kept in large, clean, polypropylene cages in regular standard laboratory conditions (20±2 ºC temperature, relative humidity 50–60%, 12 hrs light and dark cycle). As diet normal food pellets were provided by Hindustan Lever, Kolkata, and water *ad libitum*. Before the experiment, initially, the animals were acclimatized for 7 days. body weights of each mouse were routinely measured. Ethical issues, scientific animal care, and all experiments used in this study were performed according to the guidelines recommended by the Committee for Control and Supervision of Experiments on Animals (CPCSEA), Chennai, India and also approved by the Institutional Animal Ethics Committee (Approval No. JU/IAEC-24/75).

1.7.6.2 Methods of animal sacrifice, serum preparation, blood and tissue collection, cell lysis

Euthanasia is performed when an animal is required to be sacrificed at the termination of an experiment. The procedure should be carried out by introducing 100% carbon di-oxide (CO_2) into a bedding-free cage causing unconsciousness and followed by death within 2.5 mins. At the end of the treatment, the mice were allowed to survive overnight with a fasting condition and were sacrificed the next day by CO_2 overdose. The liver tissue was collected after the removal of blood and tissue fluid. Liver weight was recorded and kept for further experiments. The blood samples were collected by retro-orbital and cardiac puncture techniques in an EDTA container. After that, all the anticoagulant mixed blood samples were preserved from all experimental groups and used for the haematological study. The remaining part of the blood was centrifuged at 5000 rpm for 6 mins for the separation of serum and it was utilized for the analysis of biochemical assays (SGOT, SGPT, ALP, AST, ALT, etc.). Collected liver tissue was properly washed with chilled PBS, and then ice-cold PBS was added. Then the liver tissues were cut into smaller pieces. The tissue was homogenized after adding ice-cold RIPA (1X) lysis buffer. Homogenized tissue was allowed to be kept on ice for 30 mins. Lysed tissue extract was then sonicated to break the cells up.

1.7.6.3 Biochemical Analysis

a) Haematological study

Haematological parameters deal with the study of blood in different health issues where the liver performs a crucial role. Previous research studies reported that haematological abnormalities such as anaemia, platelet aggregation, and thrombocytopenia are associated with various liver dysfunctions. All EDTA-anticoagulated blood samples were used to perform haematological studies.

- ***Haemoglobin Estimation***

To measure the haemoglobin, we used a spectrophotometric method called cyanmethemoglobin or haemoglobin cyanide method with Drabkin's reagent (introduced by Drabkin and Austin in 1935). At first, blood was mixed well with Drabkin's solution (containing potassium ferricyanide and potassium cyanide) and allowed to stand at 25°C for 5 mins. A reagent containing potassium ferricyanide oxidizes haemoglobin to form methaemoglobin. The methaemoglobin further reacts with potassium cyanide to develop a

stable red-coloured complex i.e. cyanmethemoglobin. The absorbance is measured at 540 nm which is directly proportional to the quantity of haemoglobin present in the blood sample.[189]

- ***Platelet Estimation***

We used platelet diluting fluid containing neutral formaldehyde, sodium citrate, and brilliant cresyl blue in deionized water to measure the platelet. To count platelets, a haemocytometer was used. Platelet count was performed in diluted blood samples by the number of cells / mm^3 of whole blood.[190]

- ***Total count of RBC and WBC***

Both RBC and WBC counts require Neuberger's counting chamber, microscope, RBC and WBC diluting fluid, and special pipettes for diluting blood. For quantification of RBC, blood samples were diluted to 1:200 with RBC diluting fluid (Hayem's Fluid) which fixed the red blood cells without any damage. For quantification of WBC, blood samples were diluted to 1:20 with WBC diluting fluid (2% v/v acetic acid solution) which lyses the red cells, leaving only the WBC visible. After that cells were counted under a high power (40X) objective lens by using a Neubauer's chamber (Neubauer haemocytometer). The number of cells was calculated as the number of cells / mm^3 of whole blood.[191]

b) Liver Function Test (LFT)

Liver function tests were evaluated to assess liver function and diagnose hepatic disease following the standard protocol mentioned in 1.7.6.3 (b) subsection. These blood tests measure the levels of certain liver enzymes, proteins, and other components made by the liver. The liver helps in the detoxification of several metabolites, production of proteins and digestive enzymes, regulation of red blood cells (RBCs), clearing bilirubin, and glucose storage and production. LFT includes evaluation of aspartate aminotransferase (AST), alanine aminotransferase (ALT), alkaline phosphatase (ALP), total bilirubin, total protein, albumin level in blood. Bilirubin is a major yellow-coloured toxic metabolite of various heme-containing proteins (haemoglobin) which need safe detoxification from the body.[192,193] Bilirubin test estimated the amount of bilirubin in the serum. Bilirubin is a very distinctive marker that is included in biochemical assays for hepatic disorders. Bilirubin is present in the blood circulation both as an unconjugated insoluble form (indirect bilirubin) and soluble (direct bilirubin) form. If bilirubin cannot be released properly, it accumulates in the body which indicates liver dysfunction. ALT, ALP, and AST are very crucial liver enzymes and a valuable diagnostic tool to assess liver dysfunction. Aspartate aminotransferase is an enzyme found in

the liver, heart, pancreas, and kidneys, muscles.[194] In the case of hepatic disorder, AST is released into the bloodstream resulting in elevated levels of the enzyme. Alanine aminotransferase is a liver-specific enzyme. Elevated levels of ALT in the circulation specify liver damage which makes it an efficient indicator of hepatic health.[195] Alkaline phosphatase is an enzyme present in the liver and bones. Elevated levels of ALP in the blood also indicate a liver disorder.[196]

- ***Estimation of serum SGOT and SGPT***

At first serum aspartate aminotransferase or glutamate oxalate transaminase **(**SGOT) buffer (0.1 M PBS+ 0.1M L aspartate + 2mM α ketoglutarate) and alanine aminotransferase or serum glutamate pyruvate transaminase (SGPT) (0.1M PBS+ DL alanine + 2mM α ketoglutarate) buffer were prepared. 20µL serum was added to 100 µL individual buffer solution, then mixed well and incubated at 37ºC for 30 mins. Then 100 µL of 2,4-dinitrophenylhydrazine was added with the mixture and incubate for 25ºC for 20 mins. Then 0.5 mL of 0.4 N NaOH was added to the mixture solution again to stop the reaction and then measured the OD value after 5 mins. [197] SGOT and SGPT enzyme activity was expressed as µmol /mg protein.

- ***Methods of Alkaline Phosphatase (ALP) measurement****:*

In this study, 50µL tissue homogenate was added with 0.5mL of alkali buffer substrate (0.05M glycine buffer containing 5.5 mM PNPP, pH 10.5) and incubated for 30 mins at 37ºC. Then 5 mL of NaOH (0.02N NaOH) was added to the mixture and the OD was recorded at 400nm, after 5 mins. ALP activity was determined as µmol/mg protein.[198]

- ***Measurement of total protein:***

Protein was estimated by the Lowry method.[199]

- ***Estimation of Bilirubin:***

A Bilirubin assay kit from Sigma-Aldrich was used to measure the bilirubin level. Bilirubin present in blood serum reacts with diazotized sulfanilic acid to develop a colorimetric compound that can be measured in 530 nm. This bilirubin assay kit is based on the Jendrassik-Grof method and can measure total and conjugated bilirubin.[200]

- ***Measurement of Albumin:***

At pH 4.0~4.2, bromocresol green (BCG) and albumin can interact to generate the yellowish-green albumin-BCG complex. The amount of albumin present is directly correlated with the

depth of yellowish-green. The OD value at 628 nm can be used to calculate the serum albumin concentration.[201]

1.7.6.4 Methods of oxidative stress measurement

Oxidative stress biomarkers are valuable diagnostic tools to assess liver dysfunction. Oxidative stress adversely affects some crucial cellular components like proteins, lipids, and DNA and modulates their functional potentials. Protective activities against oxidative stress are performed by several enzymes and nonenzymatic compounds which involved in maintaining redox balance in cells. ROS accumulation is elevated when the capacity of this antioxidant system declines. These are superoxide dismutase, catalase and glutathione peroxidase, tocopherol, ascorbic acid, vitamin E and glutathione etc.[202]

a) Estimation of lipid peroxidation

To estimate the lipid peroxidation level in cell TBA assay (thiobarbituric acid assay) was employed. An important by-product of lipid peroxidation, malonaldehyde (MDA) is generated which can be considered as a biological marker of oxidative stress-mediated lipid peroxidation. Aldehyde-like MDA can be identified by reacting with TBA which produces a pink-coloured substance with absorbance at 532 nm. First of all, TCA-TBA-HCL reagent was prepared where TBA was dissolved in 0.25N HCL. After that, cell lysate was centrifuged (14000 rpm for 15 mins at 4ºC) to obtain supernatant. 200 µL TCA-TBA-HCL mixture was added to 100 µL of tissue supernatant and the mixture was allowed to boil in a water bath for 15 mins. After cooling, the absorbance of the solution was observed at 532 nm. The MDA concentration of the sample was estimated using the extinction coefficient of 1.56×10^5 M^{-1} cm^{-1}.[203]

b) Estimation of superoxide dismutase (SOD)

1mM diethylene triamine penta-acetic acid was added with 3 mL Tris buffer (50 mM, pH 8.2) and 45 µL pyrogallol mixture (10 mM Pyrogallol added in 10 mM HCL). Then 10 µL of tissue supernatant (after suitable dilution) was mixed with an aliquot of assay solution prepared earlier. An increase in absorbance was noted at 420 nm due to auto-oxidation of pyrogallol using a spectrophotometer. SOD activity was expressed as units/milligrams of protein.[204]

c) Estimation of catalase (CAT)

Catalase assessment is based on the degradation of H_2O_2 by catalase present in tissue homogenate. The tissue CAT activity was measured using the standard protocol described by Mahapatra, et al. First 0.1 mL supernatant of tissue homogenate was added with 2.9 mL phosphate buffer and the mixture was transferred in a cuvette used as a control. In another

cuvette 0.1 mL supernatant of tissue homogenate was also added with 1.9 mL phosphate buffer. Then it was mixed immediately with 1 mL H_2O_2 solution. Then the absorbances at 240 nm were measured thrice at 30 s intervals to determine the activity.[205]

d) Estimation of intracellular reactive oxygen species

A fluorometric assay was used to estimate ROS level (Reactive Oxygen Species) in hepatocytes by using the chemical 2′,7′ -dichlorodihydrofluorescein diacetate (DCFH-DA). Nonfluorescent DCFH-DA dye subsequently oxidized into a strong fluorescent compound DCF in the presence of intracellular ROS. The fluorescence intensity of DCF is the quantitative indicator of accumulated intracellular ROS. For the assay, cell lysate from liver tissue was centrifuged at 10,000 rpm for 10 min at 4ºC. The supernatant was collected and 1 µL of 10 Mm DCFH-DA was added into 200 µL supernatant containing 800 µL water. The mixture was allowed to incubate at 37ºC for 2 hrs under dark conditions. Finally, fluorescence intensity was measured with excitation and emission wavelengths set at 485 and 530 nm respectively.[206]

1.7.6.5 Histopathological study

Tissue histology refers to the examination of tissue morphology of the organ. For histological examination liver was excised, rinsed, and dried using tissue paper. Then the organ was weighed and fixed in neutral formalin buffer solution (10%), dehydrated through a graded alcohol series (50-100%), cleared in xylol, and passed through paraffin series before finally embedded in paraffin for block preparation. From the paraffin block tissue slide was prepared by microtome. Finally, the section was stained with hematoxylin and eosin (H & E) dye and examined to observe histopathological changes under a light microscope.[207]

Chapter 2

Oxidative Stress Generated Synergistic Activity of Thymoquinone and Piperine Incorporated Guar Gum Bio composite: An *in vitro* Study on Bacteria and Hepatocellular Carcinoma Cells

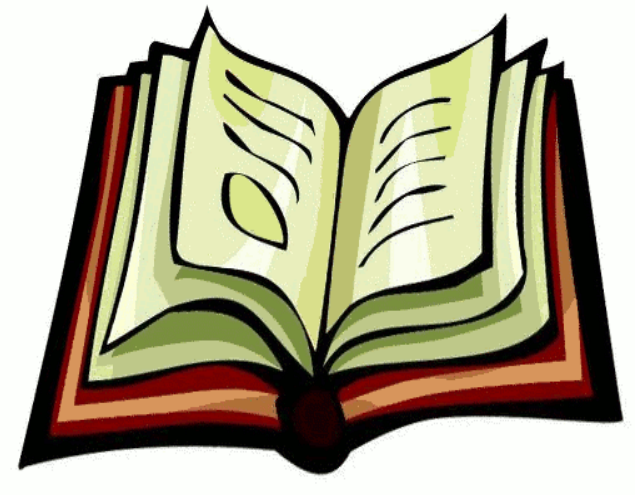

Summary

Biopolymers have become highly considerable for their inherent pharmaceutical and biomedical applications. Our study reported the synergistic antimicrobial and anticancer potentials of thymoquinone and piperine incorporated guar gum bio composite. Natural therapeutics like piperine and thymoquinone exhibited less effectivity in human medical trials due to their hydrophobicity leading to poor clinical efficacy. To overcome this problem, we have developed a delivery strategy by introducing guar gum, a natural biodegradable biopolymer. The successful tagging of phytochemicals with the biopolymer were confirmed by characterizations using different biophysical methods such as XRD, FTIR, FESEM, and UV-Vis spectra analysis etc. We reported a significant decrease in minimum inhibitory concentration (MIC) value as well as synergistic bactericidal activity against four different bacterial strains and also observed remarkably low IC_{50} value against human hepatocellular carcinoma cell lines along with pH-responsive delivery of therapeutic in the case of combinatorial dose. In our overall study, we determined, analysed and discussed the structure, efficacy, and delivery strategy of our designed natural therapeutic amalgamation to pave the way for augmenting the use of phytochemicals in successful medical applications.

2.1 Introduction

Natural therapeutics have been very much popular in revolutionizing different biomedical applications and exert antimicrobial, anti-inflammatory, and anti-cancer potentials because of their effective outcomes and almost no side effects.[208-212] Pathogens have acquired varied mechanisms to combat the currently available conventional antibiotics and expand as multi-drug therapeutics resistant forms.[213] Therefore, combinational therapy of these phytochemicals can be an intelligent therapeutic strategy in the field of applied and therapeutic sciences.[214-215] Thymoquinone (IUPAC name: 2-isopropyl-5-methyl 1,4-benzoquinone), a major bioactive component of *Nigella sativa, a* plant of Ranunculaceae family is also known as black cumin (kala jeera).[216] Piperine is extracted as a bioactive amide alkaloid constituent from *the Piper nigram* plant of the Piperaceae family.[155] Thymoquinone and piperine exhibit potent activity against a wide range of microorganisms and play an important subject in the fields of antimicrobial treatment like other therapeutic modalities.[155,217] The present experiment was aimed to study the synergistic combinational therapeutic potency of thymoquinone and piperine and their biomedical application. Studies revealed that the mode of action of a single antimicrobial drug differs from that of the same drugs when applied in combination with others.[218]

It has been reported that thymoquinone possesses hepatoprotective, antidiabetic, antifungal, anticancer, and neuroprotective properties.[219,220] It is well established that the functional mechanism of thymoquinone is to alter the biochemical reactions associated with the reactive oxygen species (ROS) generation.[216] Cellular *In vivo* studies revealed that thymoquinone induces activities of certain antioxidant enzymes glutathione transferase, superoxide dismutase (SOD), quinone reductase, glutathione (GSH). Thus, thymoquinone has a potent antioxidant property by inhibiting lipid peroxidation and preventing the generation of ROS.[216,221] Therefore, thymoquinone exerts a dual function, both antioxidant and pro-oxidant. Piperine is used as a remedy to cure inflammation, diarrhea, fungal infections, etc. The IUPAC name of piperine ($C_{17}H_{19}NO_3$) is 1-(5-[1,3-benzodioxol-5-yl]-1-oxo-2,4-pentadienyl) piperidine which is bestowed with extensive pharmacological outputs including analgesic activity, antithyroid activity, antimutagenic activity, antimetastatic activity, hepatoprotective, diuretic and anti-asthmatic activity, etc.[222,223] The important phytochemicals present in piperine are some flavonoids and phenolic contents that inhibit reactive oxygen species, lipid peroxidation, and free radicals.[224]

Despite all these promising biomedical properties, the application of thymoquinone and piperine is arrested due to several difficulties.[225-227] These two natural therapeutics have been proven to be lipophilic, thus very poorly soluble in aqueous media, restricting its therapeutic and biomedical applications.[147,226] This hydrophobic nature causes hindrance in the effective formulation may lead to unstable end products. Generally, hydrophobic components with poor bioavailability result in lowering the amounts of therapeutics in the target site when used in clinical trials.[219,228] To increase the stability of the drug, biopolymeric carrier systems can be employed which is capable of delivering the therapeutics to the target cells effectively.[229,230] One of the most stable carrier protocols, used to transport both hydrophilic and hydrophobic agents, is micro or nano-particle.[231,232] In our study, we used guar gum as vehicle loaded with piperine and thymoquinone individually and in combination. Guar gum, a natural hydrophilic nonionic polysaccharide is derived from the seeds of *Cymompsis tetraganolobus* of the Leguminaceae family.[233] Bio composite formed of biopolymers have long been employed as vehicles in natural therapeutic delivery due to their unique non-toxic, non-immunogenic, biocompatible, biodegradable, and rapid hydration properties.[85] Due to very high molecular weight, which ranges from 200,000-300,000 Da, guar gum can form highly viscous aqueous colloidal dispersion even in cold water.[85,234] The guar galactomannan has a distinctive character of imbibing a large quantity of water which makes a highly viscous solution of guar polysaccharide.[234,235] Being a natural polymer guar gum is appealing for use in natural therapeutic delivery because of its biocompatibility, nontoxicity, and biodegradability.[236]

Our present experiments with the combinations of natural therapeutics lead to damage to bacterial cell wall integration which might have caused due to excessive ROS generation or altered signalling pathway results in improper cell wall synthesis in both Gram-positive and Gram-negative bacterial strains. Thymoquinone and piperine have an impact on altered cellular metabolism inhibiting proliferation and metastasis of cancer cells. Reactive oxygen species (ROS) generation plays a crucial role in the maintenance of the redox balance in most cancer cells and an elevated ROS level may promote oxidative damage leading to cellular abnormalities or death.[237] Thymoquinone had been proven to induce cell apoptosis by increasing caspase-3 activity.[238] Caspases are one type of protease enzymes that amplify the apoptotic signalling pathway which results in cell death due to their proteolytic activity.[239,240] Induced by some initiator caspases (caspase-8, caspase-9, or caspase-10), caspase-3 mediates fragmentation of DNA within the nuclei and cytoskeletal protein degradation.[241] It has been postulated that in anticancer treatment, the activity of some drugs and bioactive compounds is

enhanced by the use of piperine.[242] Plant-derived bio-enhancers are responsible for enhancing the efficiency of some drugs having less bio-availability or in the case of long-term drug administration.[243] In the current study, we investigated the combinatorial effect of thymoquinone and piperine on bacterial cells as well as HepG2 cells.

Our study is aimed at using phytochemicals having potent antibacterial and anti-cancer properties individually or in combination. Here we have studied the effect of thymoquinone (TQ) and piperine (PIP) loaded guar gum composite (GG) on the prokaryotic and eukaryotic systems. The guar gum capped TQ and PIP (GG-PIP-TQ) has a promising synergistic effect against Gram-positive (*E. faecalis, S. aureus*) and Gram-negative (*P. aeruginosa, E. coli*) pathogenic bacterial species. In this study, we investigated the antimicrobial as well as anticancer activities of these two therapeutics against human hepatocellular carcinoma cell lines. Thus, the development of these natural therapeutics has the potential to emerge as an effective dual therapeutic agent.

2.2 Experimental section

2.2.1 Synthesis procedure

Synthesis of GG was carried out by a simple procedure in aqueous media. Initially, 0.1% (w/v) GG solution was prepared by dissolving powdered GG in lukewarm Milli-Q water and was vigorously stirred for 24 hrs. The solution became thick after the complete dissolution of the gum which was then dried in a desiccator at 60ºC temperature. The dried sample was then collected and after cooling mortared for finer grains. The sample was then named as GG and sent for characterizations.

To synthesis therapeutic loaded bio composite, first, 0.1% (w/v) GG solution was prepared in lukewarm Milli-Q water and dispersions were allowed to homogenize under vigorous stirring conditions for about 24 hrs. TQ solution (prepared in DMSO at a concentration of 1 mg mL^{-1} and sonicated) was prepared and added to gum solutions and was allowed to stir for 24 hrs. The obtained sample was centrifuged at 10,000 rpm for about 10 mins and washed three times. These solutions were then dried at 60ºC in a vacuum desiccator. Finally, the dried sample was mortared in an agate mortar to obtain finer grains. The same procedure was followed to prepare GG-PIP. We combined GG with TQ/PIP in different ratios, but the best solubility as well as the best results were observed in the ratio of 6:4 which was carried by our overall study ignoring other ratios. To prepare GG-PIP-TQ, same procedure was followed except that TQ and PIP both were added dropwise to the GG solution randomly in different ratios. As solubility in

water is regarded as an important criterion of biological samples, the solubility of all the samples was measured in water. The results suggested that the ratio of 6:2:2 showed the best solubility in water. Hence this ratio was chosen.

2.2.2 Statistical analysis

All experiments were performed in triplicate and data were presented as mean ± standard deviation (SD) for each set of experiments. Single factor one-way statistical analysis was performed using ANOVA. To determine statistical significance, value of $p < 0.05$ was considered to indicate significance or otherwise mentioned.

2.3 Results and Discussion

2.3.1 Physical Characterizations

2.3.1.1 Fourier transform infrared spectroscopy (FTIR) analysis

As figure 2.1 (a) the FTIR spectrum revealed GG absorption peak, spectra around 3328cm^{-1} is due to O–H stretching vibration of water and gum (polymer) and 772 cm^{-1} is attributed to (1–4),(1–6) linkage of galactose and mannose respectively**,** the absorption bands at 2922 cm^{-1} (C–H stretching of CH_2 group), 1644 cm^{-1} (ring stretching of mannose) and 1020 cm^{-1}(–CH_2 twisting vibration).[85,244,245] The presence of the characteristic peaks of TQ at about 1654 cm^{-1} (C=O stretch) and 1376 cm^{-1} (C–H methyl rock) established that TQ is successfully attached to the GG.[246] The presence of absorption peak due to aliphatic C–H stretching around 2942 cm^{-1} (GG-PIP) and 2942 cm^{-1} (GG-PIP-TQ) are attributed to the presence of PIP.[225] When we analyzed and compared the FTIR spectrum of GG-PIP, GG-TQ, and GG-PIP-TQ we found that they show similarities to their corresponding therapeutics indicating that they successfully attached to the polymer without any change of their chemical properties.

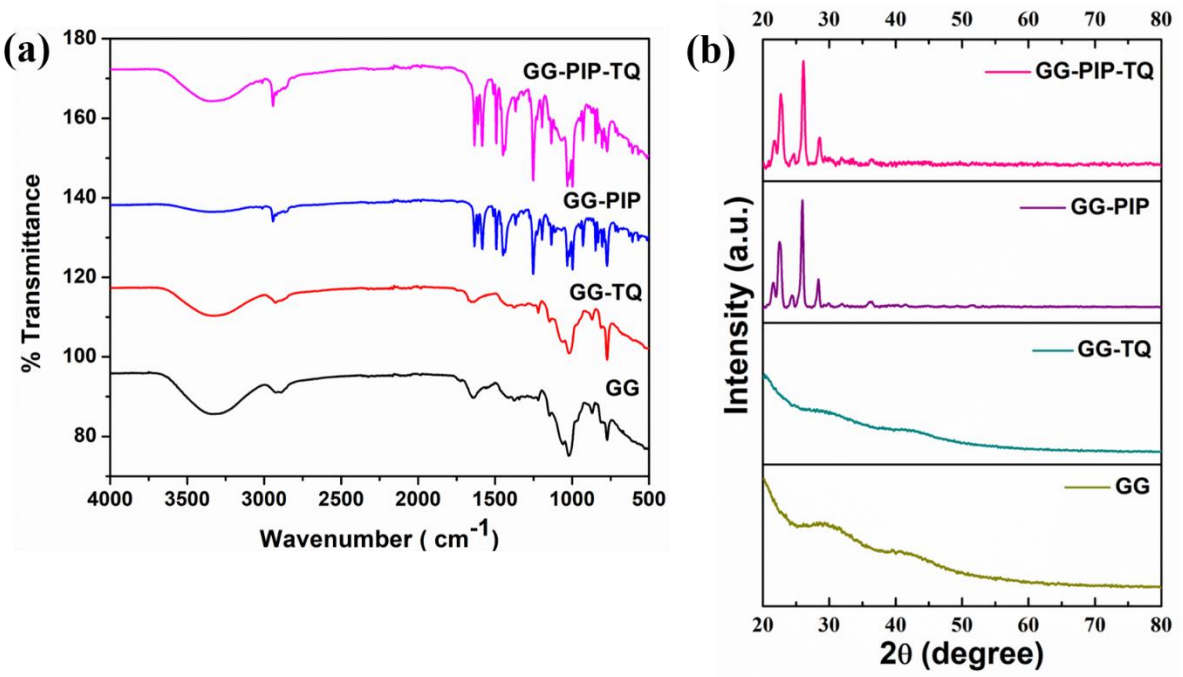

Figure 2.1: *(a) FTIR analysis of GG, GG-TQ, GG-PIP, GG-PIP-TQ (b) XRD patterns of GG, GG-TQ, GG-PIP, GG-PIP-TQ.*

2.3.1.2 X-ray diffraction (XRD) study

The incorporation of natural therapeutics in the gum vehicle was confirmed by XRD spectra are shown in figure 2.1 (b). The diffraction patterns of four samples (GG, GG-TQ, GG-PIP, GG-PIP-TQ) confirmed the incorporation of natural therapeutics in GG. GG exhibited a broad hallow which indicates very small crystallinity while on GG-TQ also depicted low intensity broader peak revealing its incorporation into the polymer matrix in the amorphous state.[244,247] The XRD pattern of GG-PIP, as well as GG-PIP-TQ, indicated the similarity with the typical pattern of PIP (JCPDS Card no: 00-043-1627).[248]

2.3.1.3 Thermal gravimetric analysis (TGA)

TGA thermograms of GG, GG-TQ, GG-PIP, GG-PIP-TQ are shown in figure 2.2(a). The curves elucidate thermal stability and the decomposition rate. The degradation has completed in two stages with increasing temperature. The initial decomposition involved a minimum weight loss which is due to the evaporation of adsorbed surface water. According to the thermogram, the initial degradation of mass at around 40–100ºC is almost 6.4%, 6.4%, 8.26% and 3.05% in case of GG, GG-TQ, GG-PIP and GG-PIP-TQ respectively. The second step of sharp degradation is associated with the combustion of organic molecules present in the sample. The second decomposition showed more significant weight loss which is about 51.92% (temperature range 180–313ºC) in GG, 65.69% in GG-TQ (temperature range 221–337ºC),

49.66% in GG-PIP (temperature range 215–322ºC) and about 68% in GG-PIP-TQ (temperature range 213-330ºC). According to the thermogram GG-PIP-TQ showed least initial weight loss up to 200ºC temperature. On the other hand, GG-TQ and GG-PIP-TQ showed almost similar total weight loss at 400ºC.

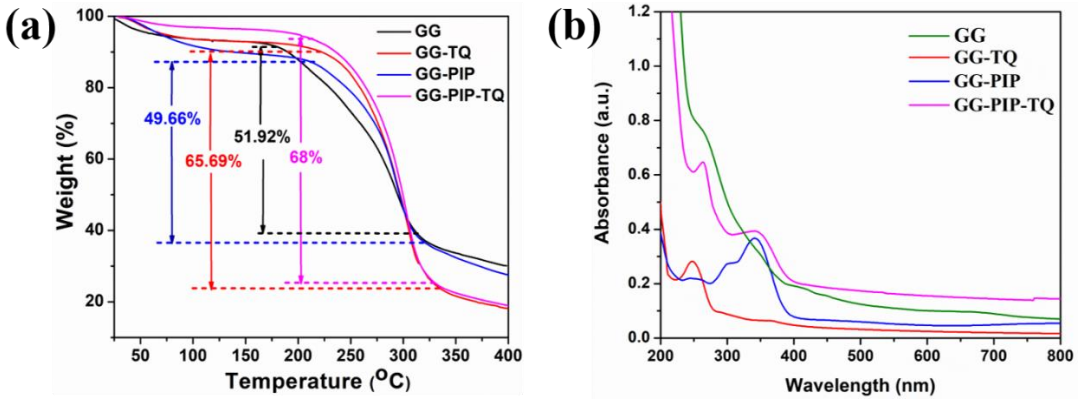

Figure 2.2: *(a) TGA analysis (b) UV-Vis spectra of GG, GG-TQ, GG-PIP, GG-PIP-TQ.*

2.3.1.4 UV Visible Spectroscopy

The optical behaviour of our formulated therapeutics was characterized by UV-vis spectroscopy stated in figure 2.2 (b). UV-vis absorbance spectrum of GG did not show any characteristic peak in its spectrum due to its UV inactiveness whereas GG-PIP and GG-TQ exhibited prominent peaks at 342 nm and 248 nm respectively which confirm the successful attachment of PIP in GG-PIP as well as TQ in GG-TQ. GG-PIP-TQ displayed two sharp peaks at 262 nm and 343 nm which ascertained the successful incorporation of TQ and PIP.[249]

2.3.1.5 Field Emission Scanning Electron Microscope (FESEM) analysis

The surface morphology of GG and GG-PIP-TQ are determined by the FESEM study. Figure 2.3 (a) showed FESEM image of GG which indicated a discontinuous and irregular structure of GG whereas a noticeable change is observed in the case of GG-PIP-TQ (figure 2.3b) indicating a clear attachment of natural therapeutics (PIP and TQ) with GG which confirmed by the reduction of porosity of bio composite.

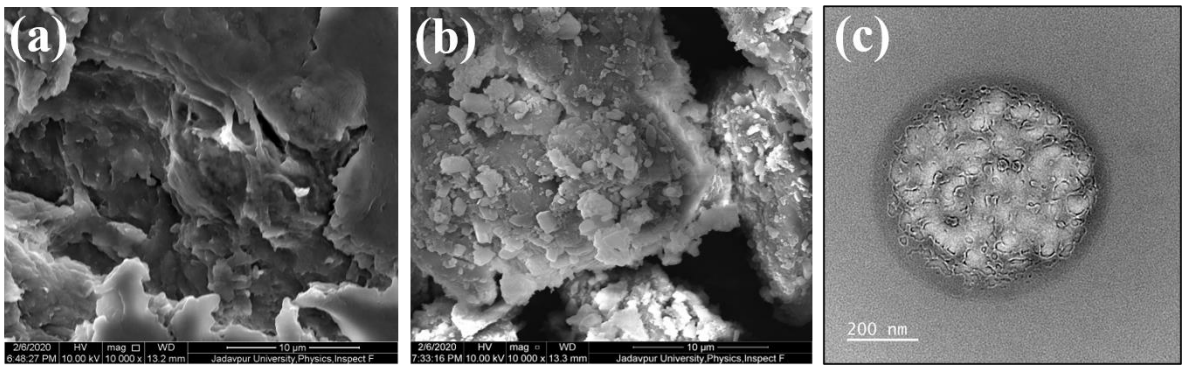

Figure 2.3: *FESEM analysis of (a) GG and (b) GG-PIP-TQ (c) TEM image of GG-PIP-TQ.*

2.3.1.6 Transmission electron microscope (TEM) analysis

In TEM image, GG-PIP-TQ particles are appeared to be round shaped with about (600 ± 6) nm in diameter shown in figure 2.3 (c). TEM image demonstrates spherical shaped mono-dispersed particles.

2.3.1.7 Dynamic light scattering (DLS) study

Table 2.1: *Represents the Hydrodynamic Diameter, Polydispersity Index and Zeta potential of GG, GG-PIP, GG-TQ, GG-PIP-TQ.*

Sample	*Hydrodynamic Diameter (nm)*	*Polydispersity Index*	*Zeta potential*
GG	176±3.4	0.16	12.34±2.8
GG-PIP	197±3.8	0.24	14.54±1.4
GG-TQ	204±2.2	0.27	11.34±2.4
GG-PIP-TQ	215±2.5	0.29	13.27±4.4

GG-PIP-TQ showed a zeta potential of 13.27±4.4 mV and hydrodynamic diameter of 215±2.5 (table 2.1). TQ or PIP loading do not alter the zeta potential drastically, but increases the hydrodynamic diameter. The presence of therapeutics inside the matrix also increases the size of the composite than the bare ones. The corresponding polydispersity index (PDI) values of the samples are a quite low, suggesting that they form a homogenous solution that is desirable for any biological application.

2.3.1.8 Loading percentage of natural therapeutic in GG

The loading efficiencies of any therapeutic in the vehicle depend on the molecular structure and the interactions between the polymer vehicle and therapeutics used. The percentage of PIP and

TQ loaded within GG was determined spectrophotometrically (as mentioned in subsection 1.7.3.9). The natural therapeutic loading profile stated that in GG, drug loading efficiencies of TQ and PIP were 75% and 79%, respectively. The high natural therapeutics loading efficiency is due to the extensive large surface area of the composite material.

2.3.1.9 Release profile of natural therapeutic from GG

The rate of release of PIP and TQ from GG was determined by dialysis method mentioned in subsection 1.7.3.10. Approximately 28% and 34% TQ release was observed from GG-PIP-TQ after 12 hrs and 24 hrs, respectively at pH 7.4 whereas at pH 5.5, the corresponding release was 44% and 58% respectively. The release profile of PIP from GG-PIP-TQ after 12 hrs and 24 hrs were 23% and 29% respectively at pH 7.4 whereas at pH 5.5, the corresponding release was 41% and 56% respectively. This controlled release of natural therapeutics is very much effective to combat the problem of rapid elimination from the system as well as an increase in therapeutic efficiency.[250]

2.3.2 Evaluation of antibacterial activity

2.3.2.1 Determination of MIC and MBC

To assess minimum inhibitory concentration (MIC) and minimum bactericidal concentration (MBC), different concentrations (50 µg/mL, 100 µg/mL, 200 µg/mL, 400 µg/mL, 600 µg/mL) of synthesized composite were used against four bacterial strains i.e. Gram-positive *S. aureus, E. faecalis* and Gram-negative *E. coli, P. aeruginosa.* The experimental procedure was mentioned in subsection 1.7.4.1. To develop an alternative way to combat bacterial pathogens and to minimize the adversity associated with the conventional antibiotics, PIP and TQ incorporated GG were screened singly and in combination with each other to determine their synergistic, additive, or antagonist interactions against *S. aureus, P. aeruginosa, E. faecalis* and *E. coli.* Figure 2.4 showed that with increasing concentration of therapeutics the bacterial growth was gradually decreasing which confirmed the antibacterial efficacy of therapeutic loaded GG. This decrease is more significant in the case of Gram-positive bacteria. Experimental results showed that MIC values were decreased in treatment with both TQ and PIP i.e. GG-PIP-TQ against all four pathogenic bacterial strains which depicted in table 2.2. Bare GG does not possess any antimicrobial property. Well diffusion study (figure 2.4e) demonstrated that GG-PIP-TQ have prominent synergistic antibacterial activity against all four pathogenic strains, especially against Gram-positive bacteria (*S. aureus, E. faecalis*).

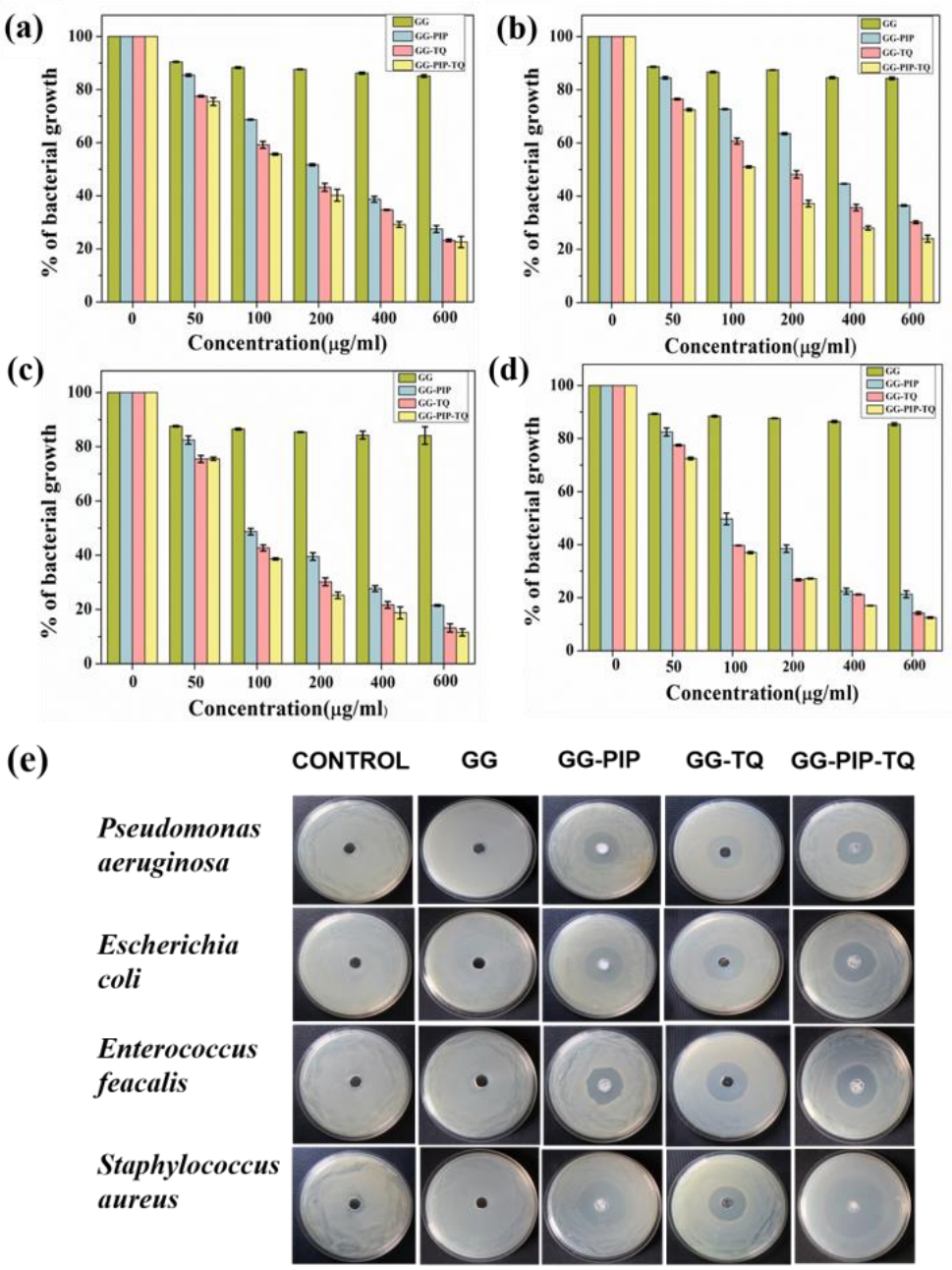

Figure 2.4: *Analysis of antibacterial activity of GG, GG-PIP, GG-TQ, GG-PIP-TQ by MIC method in (a)Pseudomonas aeruginosa (b) Escherichia coli (c) Enterococcus faecalis (d) Staphylococcus aureus; (e) Well diffusion method indicating synergistic activity of GG-PIP-TQ.*

Table 2.2: *Represents MIC, MBC and Tolerance level of bacterial strains against GG, GG-PIP, GG-TQ, GG-PIP-TQ.*

Bacteria	*Sample*	*MIC*	*MBC*	*Tolerance Level*
Pseudomonas aeruginosa	*GG*	-	-	-
	GG-PIP	331.55	1160.43	3.5
	GG-TQ	281.82	1018.55	3.61
	GG-PIP-TQ	259.37	907.8	3.5
Escherichia coli	*GG*	-	-	-
	GG-PIP	397.65	1391.76	3.5
	GG-TQ	309.66	1052.85	3.4
	GG-PIP-TQ	244.88	883.57	3.6
Enterococcus faecalis	*GG*	-	-	-
	GG-PIP	253.73	867.76	3.42
	GG-TQ	202.38	684.04	3.38
	GG-PIP-TQ	184.71	600.30	3.25
Staphylococcus aureus	*GG*	-	-	-
	GG-PIP	245.1	808.83	3.3
	GG-TQ	196.72	674.75	3.43
	GG-PIP-TQ	178.89	572.45	3.2

2.3.2.2 Determination of tolerance level

Tolerance level is an important parameter which reflects the bactericidal capacity of natural therapeutics. For a particular bacterium, if the MBC/MIC ratio is less than or equal to 4, then are considered as a bactericidal agent. Table 2.2 stated that GG-PIP, GG-TQ, GG-PIP-TQ shows bactericidal activity.

2.3.2.3 Determination of ROS Generation

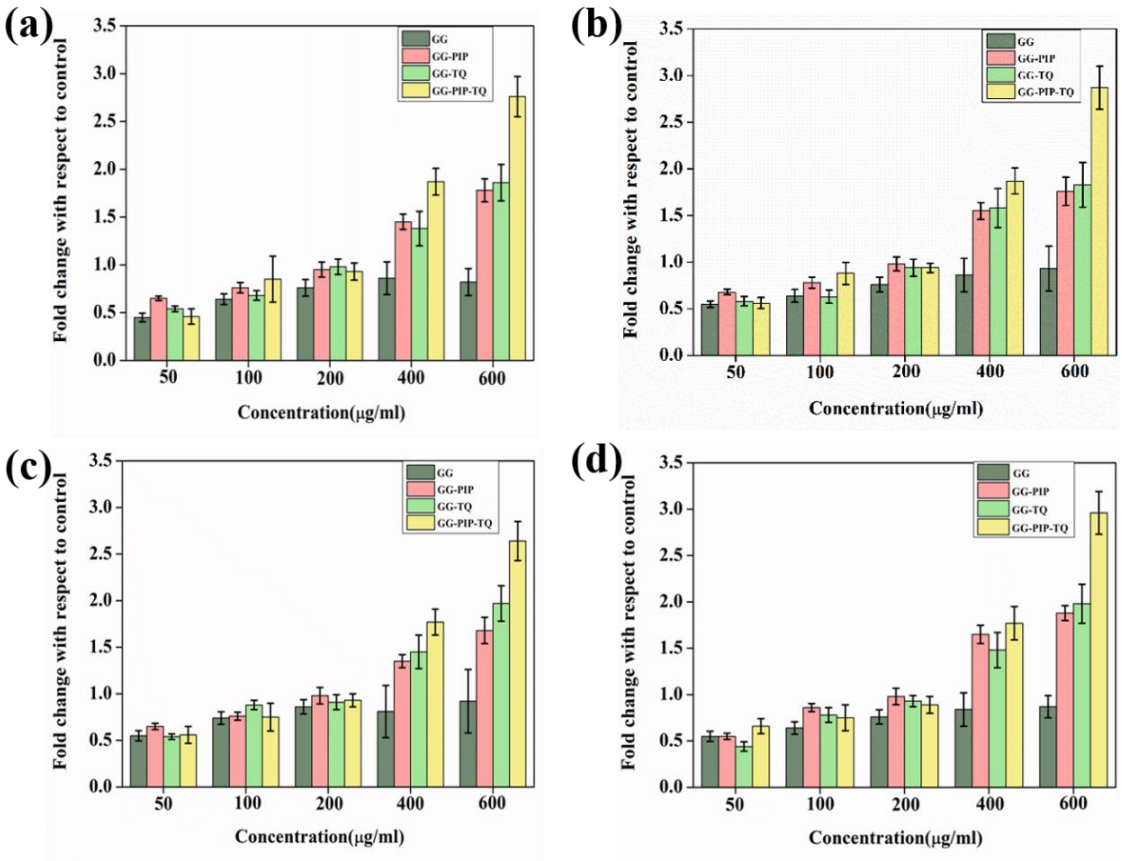

Figure 2.5: *Determination of bacterial ROS by DCFDA assay in (a) Pseudomonas aeruginosa (b) Escherichia coli (c) Enterococcus faecalis (d) Staphylococcus aureus.*

To estimate intracellular ROS generation 2, 7-dichlorofluorescein diacetate ($DCFH_2$-DA) assay was used where bacterial cells were treated with different concentrations (50µg/mL, 100µg/mL, 200 µg/mL, 400µg/mL, 600µg/mL) of GG, GG-TQ, GG-PIP, GG-PIP-TQ (as mentioned in subsection 1.7.4.5). Reactive oxygen species (ROS) like peroxides, superoxide, hydroxyl radical, singlet oxygen is generated by the inappropriate transferring of electrons to O_2.[240] Bacterial cells are susceptible to raised intracellular ROS level which cause loss of cellular integrity.[241] We found a remarkable difference in the intracellular ROS generation between GG treated and GG-PIP-TQ treated cells as shown in figure 2.5. Experimental data also showed that when treated with GG-PIP-TQ, ROS accumulations were almost 2.5-3 fold higher than control in case of all four bacterial strains. Our study indicated the efficacy of GG-PIP-TQ which significantly increase intracellular ROS generation compared to GG-PIP and GG-TQ treated cells in the case of all the four pathogenic strains confirming the synergistic activity of combinational treatment.

2.3.2.4 Bacterial morphology study by FESEM

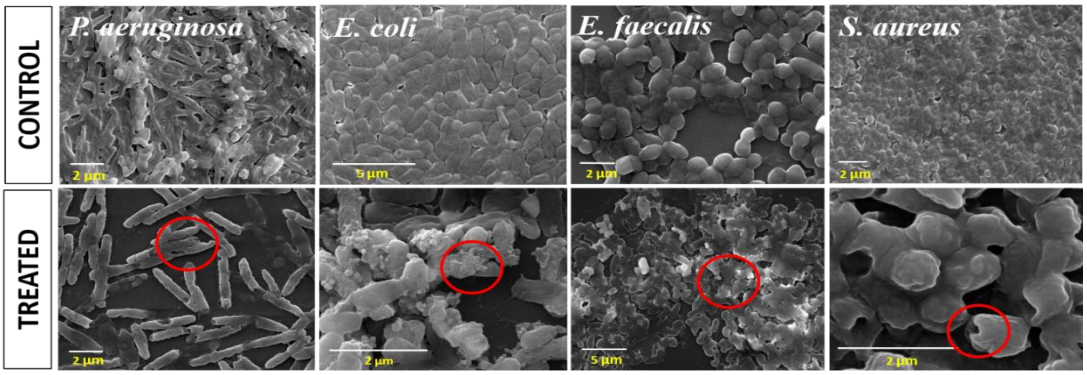

Figure 2.6: *FESEM micrographs showing morphological characteristics of control and treated (after treatment with GG-PIP-TQ) Pseudomonas aeruginosa, Escherichia coli, Enterococcus faecalis and Staphylococcus aureus cells.*

FESEM detected ultrastructural and morphological changes in bacteria after exposed to the MIC values of synthesized composites as shown in figure 2.6. All untreated bacterial cells looked undamaged with a smooth and intact surface morphology. GG-PIP-TQ treated bacterial cells become uneven and distorted in shape. Red circled parts in FESEM images of treated *P. aeruginosa* revealed shrivelled cellular surface and cell perforations whereas treated *E. coli* cells appeared to be shrunk and deformed. Image of treated *E. faecalis* cells revealed cell deformation with disintegrated cell surface whereas treated *S. aureus* cells appeared to be deformed with perforated cell surface. Cell deformations and membrane damage confirmed GG-PIP-TQ induced loss of cellular integrity in Gram-positive as well as Gram-negative strains.

2.3.3 Assessment of anticancer activity

2.3.3.1 Cytotoxicity Study

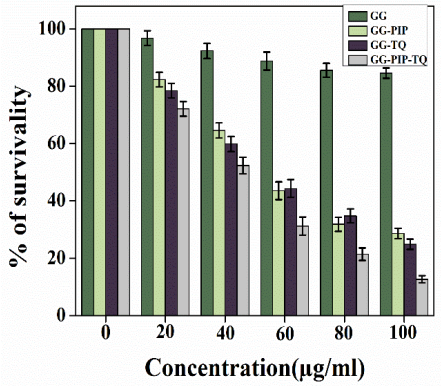

Figure 2.7*: MTT assay on HepG2 cell line after treatment with GG, GG-PIP, GG-TQ, GG-PIP-TQ.*

Table 2.3: *IC_{50} values of GG, GG-PIP, GG-TQ, GG-PIP-TQ.*

Sample	*IC_{50} Values (µg/mL)*
GG	-
GG-PIP	61.24
GG-TQ	59.46
GG-PIP-TQ	48.03

The HepG2 cell viability was assayed by employing 3-(4, 5-dimethylthiazol-2-yl) -2, 5-diphenyltetrazolium bromide (MTT) assay. The experimental procedure was mentioned in subsection 1.7.5.2. The anticancer activity was examined after exposure to GG, GG-TQ, GG-PIP, GG-PIP-TQ at the concentrations of 20µg/mL, 40µg/mL, 60µg/mL, 80µg/mL, 100µg/mL. Untreated cells were considered as control. Figure 2.7 exhibited that GG-PIP, GG-TQ, GG-PIP-TQ exerted a decrease in the cell survivability in a dose-dependent manner. On the other hand, bare GG showed no such cytotoxic activity. Table 2.3 stated the significantly low IC_{50} value of GG-PIP-TQ against HepG2 cells compared to GG-TQ and GG-PIP.

2.3.3.2 Study of Intracellular ROS generation

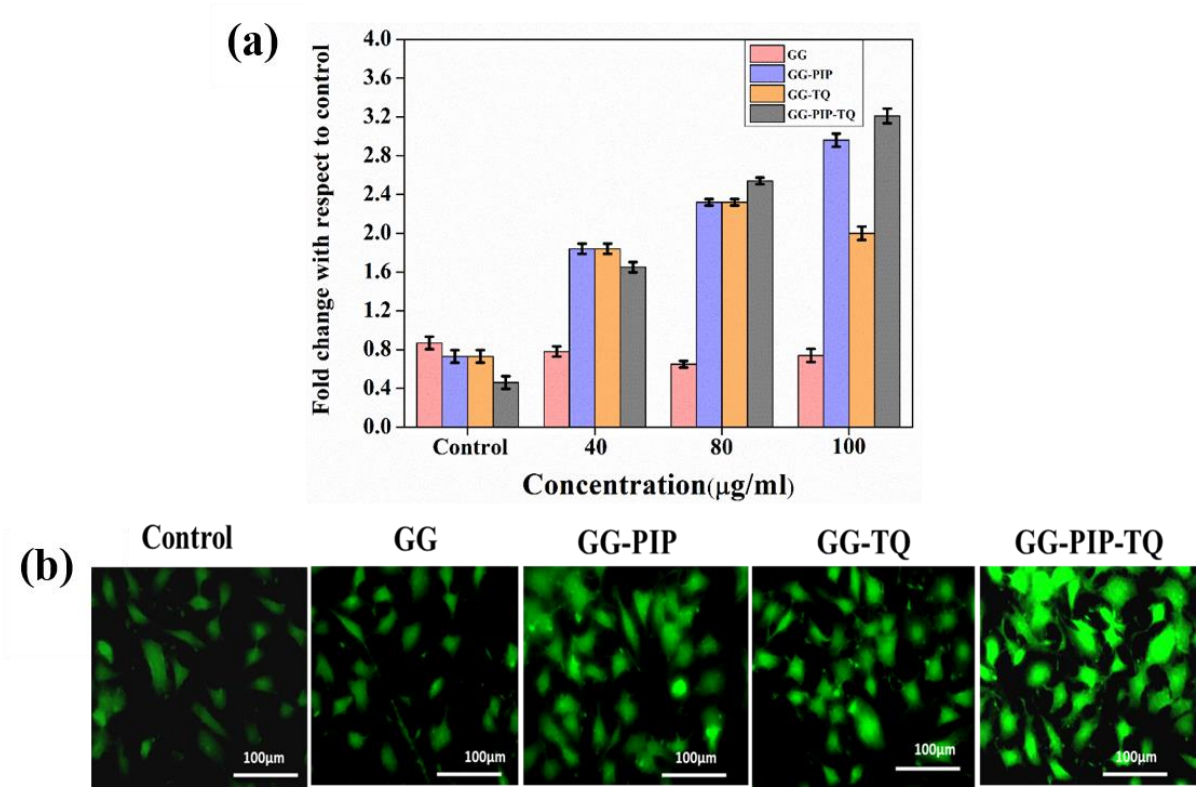

Figure 2.8: *(a) Graphical representation of mean fluorescent intensity for ROS generation in HepG2 cells (b) Fluorescence microscopic image of intracellular ROS generation in HepG2 cells.*

The generation of reactive oxygen species was estimated after treatment of HepG2 with GG, GG-PIP, GG-TQ, GG-PIP-TQ at concentrations of 40µg/mL, 80µg/mL, 100µg/mL. The experimental procedure was mentioned in subsection 1.7.5.3. Figure 2.8 (a) exhibited that treatment with GG-PIP, GG-TQ, GG-PIP-TQ cause increase in ROS accumulation in a dose-dependent manner. The fluorescence microscopic images clearly depicted the gradual enhancement of green fluorescence intensity (figure 2.8 b). On treated with GG, GG-PIP, GG-TQ, GG-PIP-TQ at their respective IC_{50} dose, enhancement of ROS accumulation was measured spectroscopically. Untreated control cells and GG treated cells displayed almost similar fluorescence intensity. GG-PIP-TQ treatment resulted in generation of higher levels of intracellular ROS which contributed to higher cell cytotoxicity and its anticancer properties corroborating with the results of MTT assay.

2.3.3.3 Determination of NADPH and GSH level

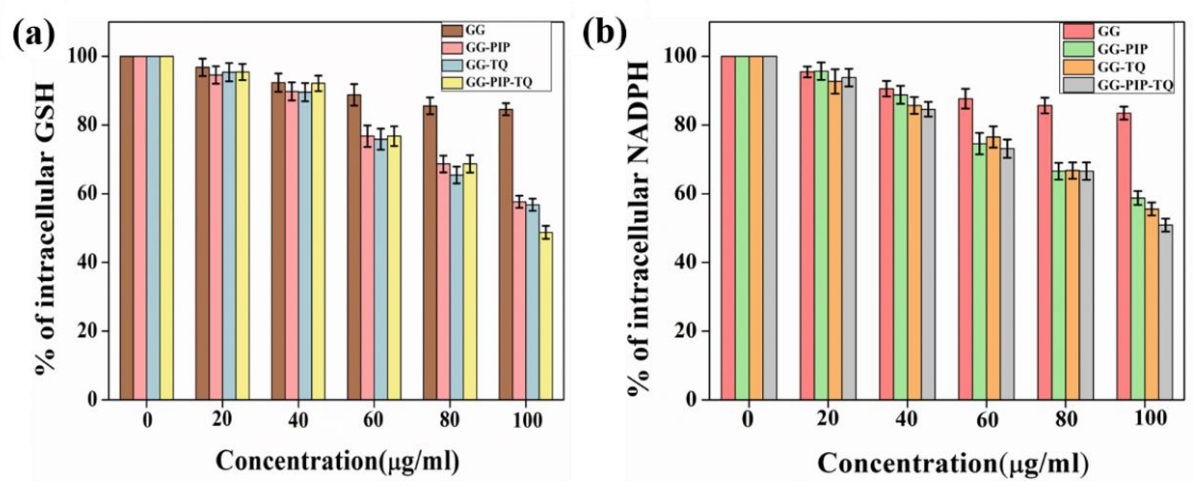

Figure 2.9: *(a) Graphical representation of Intracellular depletion of GSH after treatment with GG, GG-PIP, GG-TQ, GG-PIP-TQ. (b) Graphical representation of Intracellular NADPH level after treatment with GG, GG-PIP, GG-TQ, GG-PIP-TQ.*

In order to examine the intracellular antioxidant level in HepG2 cells on treatment with different concentrations (i.e. 20µg/mL, 40µg/mL, 60µg/mL, 80µg/mL, 100 µg/mL) of GG, GG-PIP, GG-TQ, GG-PIP-TQ, the intracellular GSH and NADPH levels were estimated following standard protocol as described in subsection 1.7.5.4. The homeostasis of the ROS level is critically maintained inside the cell and solely regulated by intracellular antioxidant levels (NADPH and GSH) in mitochondria and cytosol.[251] NADPH and GSH play critical role to protect cells from oxidative stress related damages. Glutathione reductase enzyme helps to generate GSH from its oxidized form glutathione disulfide (GSSG). GSH to GSSG ratios are

crucial for maintaining overall cellular health and function. NADP is a coenzyme which exists in two forms, NADP+ (oxidized form) and NADPH (reduced form). NADPH/NADP+ ratio counteract ROS mediated oxidative stress.[252] In this experiment, the results (figure 2.9) exhibit a drastic dose-dependent diminish in the percentage of GSH and NADPH levels on the exposure of HepG2 cells to GG-PIP, GG-TQ and GG-PIP-TQ. Treatment with bare GG showed no such decrease in GSH and NADH level while GG-PIP-TQ treatment exhibited a maximum decrease. The intracellular depletion of NADPH and GSH levels suggest cellular redox imbalance mediated cell death.

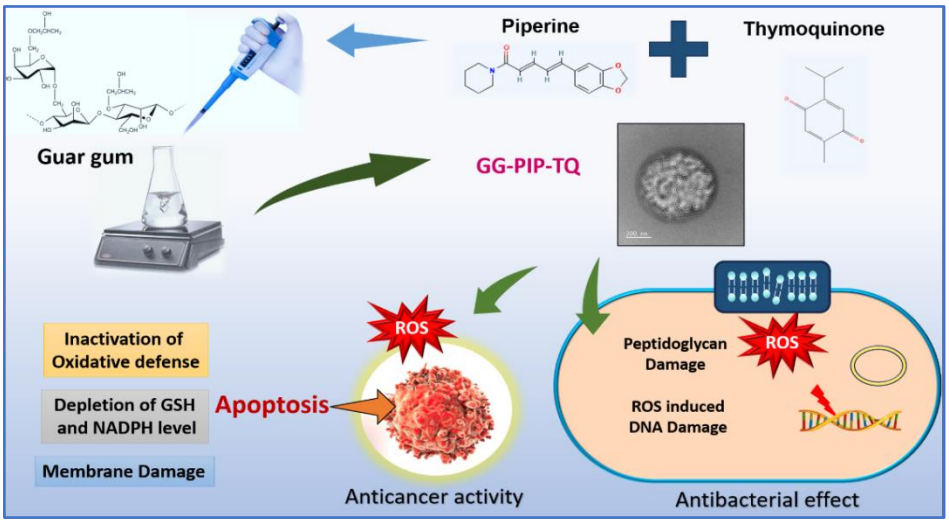

Figure 2.10: *Graphical representation of synthesis and general mechanisms for antibacterial and anticancer mode of action of GG-PIP-TQ.*

2.4 Conclusion

Several studies have been carried out to combat cancer progression and various infectious diseases without any detrimental side effects. We used an inexpensive, abundantly available natural biopolymer and assembled TQ and PIP with this polymer for synergism assay, which overcomes the poor aqueous solubility of these natural bioactive compounds. In this regard, GG-PIP, GG-TQ, GG-PIP-TQ have been assessed on four bacterial strains which are capable of causing systemic infections in human. We have also evaluated the cytotoxic activity of our samples against HepG2 cell line (figure 2.10). FTIR, XRD and UV-Vis spectroscopy data clearly demonstrated efficient interaction as well as successful incorporation of therapeutics. The solubility of hydrophobic TQ and PIP can be increased and optimum delivery can be achieved by an appropriate combination of GG. Bare GG exhibited no such activity against bacterial and cancer cells which was established by ROS estimation studies. We observed a remarkable synergistic antibacterial activity by MIC, MBC, ager well diffusion and tolerance

level study on four bacterial strains specially against Gram-positive bacteria. An effective permeability barrier of Gram-negative bacteria results in the restriction of proper penetration of bioactive phytochemicals through it. The tolerance level reflects the bactericidal capacity of natural therapeutics as obtained from MBC/MIC ratio which is less than 4. Increased level of bacterial ROS is observed possibly due to the effective penetration of natural therapeutics into the bacterial cells that causes oxidative stress and acts as an ideal bactericidal agent following bacteriostatic activity. Additionally, the pH-responsive release of natural therapeutic from porous GG suggested that the TQ and PIP release in intracellular acidic pH of cancer cell (~ 5.5) is faster than that of the normal physiological pH (~7.4). Previous study suggested that also at acidic pH guar gum could retain stability.[253] During incorporation of natural therapeutics within gum, they form a covalent linkage between them. The possible reason behind the faster release of therapeutic may be the breakage of the interlinking bonds at acidic pH, followed by the release of therapeutics gradually. In case of HepG2 cells, increased ROS generation and cytotoxic activity observed in MTT assay suggested that the natural therapeutics loaded composite could exert encouraging anticancer activity. The elimination of NADPH and GSH levels leads to oxidative stress-mediated cell death.[254] Estimated ROS, GSH and NADPH content within the cells after treatment with GG-PIP, GG-TQ, GG-PIP-TQ indicated towards the synergistic activity of TQ and PIP. GSH and NADPH levels were significantly decreased when treated with GG-PIP-TQ indicating ROS liberation. Both antibacterial and anticancer activities of GG-PIP-TQ implied that these two phytochemicals may activate each other's mode of action. Otherwise, one of them followed a mechanism that enhanced the activity of the other natural therapeutics. The bio enhancing activity of PIP was proven to be effective in synergism assay. The synergistic interaction between two drugs may lead to modified and more effective binding mechanism for the active site or it may result in delayed efflux of accumulated therapeutic complex out of the cell. Thus, combination of drugs often exerts their synergistic effect in a particular species of microorganisms either by inhibiting the cell wall synthesis or by triggering its lysis. By calculating the tolerance level of bacteria and the IC_{50} value in case of HepG2 cells, this new amalgamation of TQ and PIP with biopolymer GG suggested a remarkable synergistic effect. The pH-responsive release of therapeutics is advantageous for cancer therapy and also required for the survivability of normal healthy cells. The result of the study demonstrated that GG-PIP-TQ exerts more effect on Gram-positive than Gram-negative bacteria. Thus, the therapeutic application of our combined amalgamation can be a suitable alternative of conventional drugs to overcome the problem of side effects and antibiotic resistivity. In conclusion, we have established that the hydrophilic biocompatible GG-PIP-TQ can emerge as an ideal platform for multiple therapeutic applications.

Chapter 3

A Comparative Study on Antibacterial and Anticancer Activity of Thymoquinone Incorporated Chitosan-Sodium Alginate / Psyllium Husk Derived Biopolymeric Composite Films

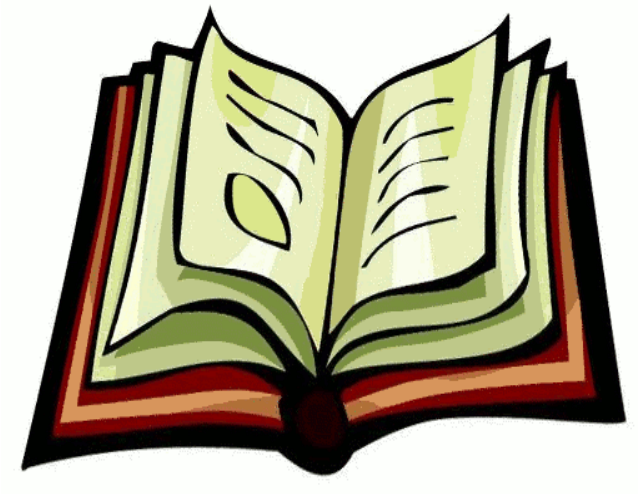

Summary

The fabrication of biopolymeric film containing natural therapeutics envisioned to develop edible, nontoxic and biodegradable composite using polymers. Our study focused on extraction of psyllium husk mucilage, a medicinally acknowledged natural polysaccharide and develop a proper composite with chitosan. We combined chitosan with both alginate and husk mucilage separately to prepare two composite films. Drug release dynamics from the complex polymeric networks was evaluated where polymeric films showed sustained release of thymoquinone, a water-insoluble phytocomponent. Structural and physico-chemical properties of the films were confirmed by FTIR, XRD, FESEM, TGA analysis. Significant antimicrobial activities against *Enterococcus faecalis* and *Pseudomonas aeruginosa* strains and strong anticancer activities against human prostate cancer cell line (PC3) and adenocarcinomic human alveolar basal epithelial cell line (A549) was observed. We also evaluated the biocompatibility of composite films on normal cell i.e. human lung fibroblasts (WI38) cell line. This biodegradable polymer combination suggests towards the possibility of potential applications for the food industry and variety of biomedical applications such as wound dressing, tissue scaffolding etc.

3.1 Introduction

Multifunctional biomaterials, polymer composite are extensively used in the field of pharmaceutical drug delivery because of their wide range of versatility, biocompatibility and stability to serve as a matrix or vehicle for drugs compared to synthetic or inorganic materials .[255,256] Polymer composites with proper ratio and modifications can be a better excipient constituent as sustained drug carrier with improved physical, mechanical, functional properties .[257,258] The stability of polymer composite could be affected by molecular weight, crystallinity, mixing ratio, presence of functional groups, pH of reaction medium, distribution of ionic groups, drying process, etc.[259]

Chitosan has been used as a positively charged polymeric drug carrier due to its biocompatibility, biodegradability and relatively low production cost.[260] Alginate is a water soluble, unbranched, biodegradable polysaccharide consisting of alternating blocks of 1–4 linked -l-guluronic (G-block) and -d-mannuronic acid (M-block) residues.[261] Carboxylic acid groups of alginate is responsible for negative charges which attribute characteristic electrostatic interaction with the positively charged molecules.[260] Alginates are extracted from brown seaweeds and marine algae such as *Laminaria hyperborea*, *Ascophyllum nodosum* and *Macrocystis pyrifera*.[262,263] Since chitosan is positively charged at low pH values (below its pKa value), it spontaneously associates with negatively charged polyions like alginate in solution to form a special type of macromolecules, the polyelectrolyte complexes.[258] Psyllium mucilage obtained from the seed coat of *Plantago ovata* and *Plantago indica* belongs to the family Plantaginaceae which can be obtained by mechanical grinding of the outer layer of the seeds.[264] Psyllium mucilage is fibrous mucilaginous hydrocolloid used in treatment of intestinal inflammation, constipation, etc.[265] Arabinoxylan, a complex heteroxylan of two pentose sugars i.e. arabinose and xylose is a highly branched hemicellulose.[266.267] Sodium alginate (AL) and chitosan (CH) are widely used as a matrix or hydrogel material to attain sustained drug release but still under widespread exploration.[268.269] Bindu et al. also reported that in combination with HPMC K4M, husk mucilage retarded the release of the drug which facilitate sustained release by reducing the instant swelling of the composite.[270] Psyllium husk mucilage (PH) was chosen to interact with chitosan (CH) to synthesis a stable complex to improve the drug loading efficiency when interacted with thymoquinone (TQ). The phyto-active component of the *Nigella sativa* essential oil (TQ) with cytotoxic, antimicrobial, antioxidant, antifungal properties is used to combine with polymer composites. According to previous studies, TQ was able to induce apoptosis via p53-dependent as well as p53-independent pathways.[271,272]

In this context, our present study is an effort toward the synthesis of high-performance biocompatible composite polymer films to obtain good antibacterial as well as cytotoxic activity with minimal side effects followed by a discussion on their probable interaction with polymer composites. Our experiments demonstrate a comparative structural characterization and therapeutic efficacy of chitosan-sodium alginate (CH-AL), chitosan-psyllium mucilage (CH-PH) films as well as thymoquinone (TQ) loaded polymeric composites (TQ@CH-AL and TQ@CH-PH).

3.2 Experimental section

3.2.1 Extraction and purification of PH

PH was extracted by mixing with deionized water in a 1:100 (w/v) ratio, for 4 h, under constant agitation at 60˚C. To prevent the water loss as a result of evaporation, water (60ºC) was added at different intervals to the system. The insoluble non-carbohydrate fractions of psyllium seeds removed by filtration. Mucilage was stirred for 10 minutes with ethanol at a ratio of 100:50 (mucilage volume: ethanol volume). After centrifuging at 2000 rpm for 3 mins the supernatant was used to quantify the non-precipitated carbohydrates. Ethanol was removed from the precipitate by using a rotary evaporator. Further, it was kept for drying in hot air oven after spreading on a glass plate at 50ºC temperature to dehydrate the carbohydrates.[273]

3.2.2 Synthesis of composite films

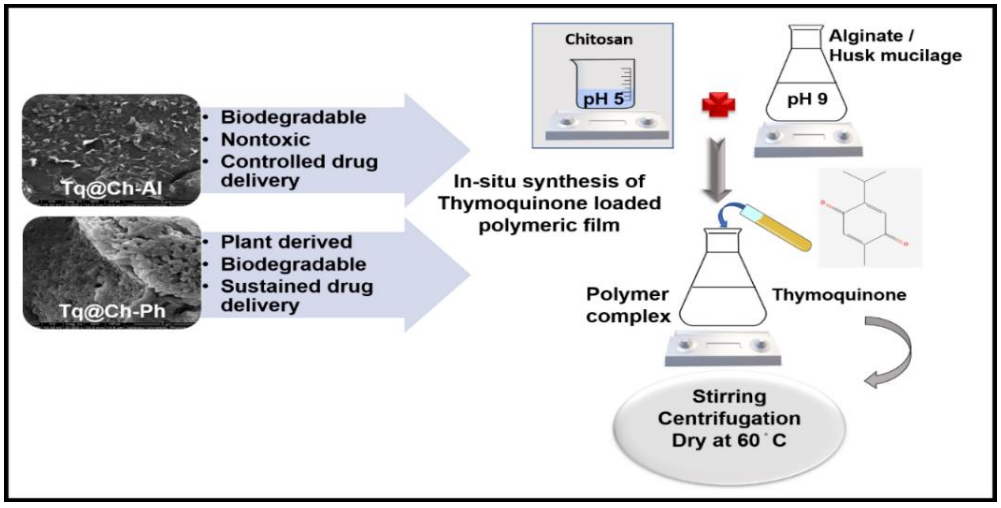

Figure 3.1: *Schematic representation of synthesis procedure of polymeric films.*

Briefly, 50 mg AL was dissolved completely in 50 mL distilled water to form a 0.1% (w/v) AL solution at room temperature. The solution was adjusted to a pH of 9. 50 mg of CH were dissolved in 50 mL of 1% (v/v) acetic acid solution to obtain a 0.1% (w/v) CH solution. pH of

the CH solution was adjusted to 5. Both dispersions were homogenized with a magnetic stirrer 4 hrs at room temperature. Then AL solution was added dropwise to CH solution under constant magnetic stirring. The resulting opalescent suspension was cast on a glass petri dish and allowed to dry at 60ºC for 24 hrs. Similar experimental procedure was followed in case of CH-PH synthesis. To incorporate TQ in to composite film, TQ was added in lukewarm millipore water (60ºC), mixed with polymer solution and was allowed to stir for 24 hrs at room temperature. The obtained sample was centrifuged at 10,000 rpm for about 10 mins and washed three times and then dried at 60ºC in a vacuum desiccator. A schematic representation of the synthesis procedure of therapeutic loaded polymeric film depicted in figure 3.1.

3.2.3 Statistical analysis

All experiments were performed in triplicate and data were presented as mean ± standard deviation (SD) for each set of experiments. Single factor one-way statistical analysis was performed using ANOVA. To determine statistical significance, value of $p < 0.05$ was considered to indicate significance or otherwise mentioned.

3.3 Results and discussion

3.3.1 Formation of polymer composite

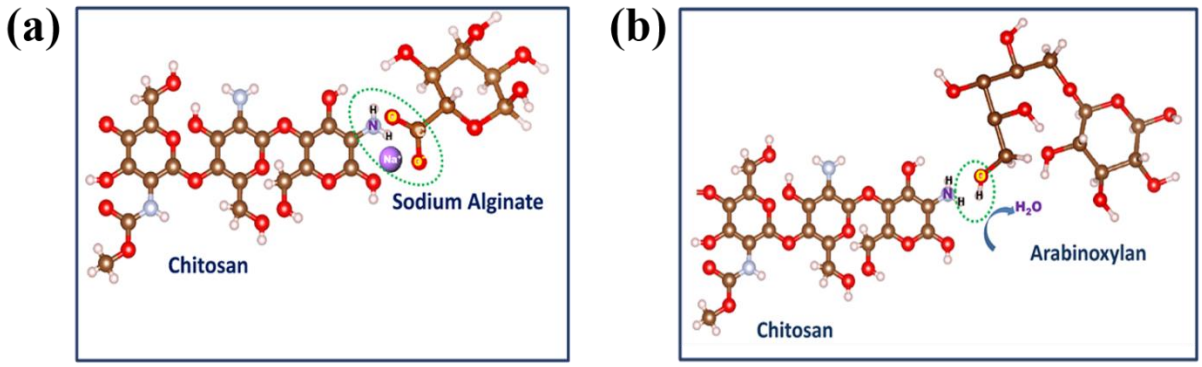

Figure 3.2: *Interaction pattern of chitosan with (b) sodium alginate and (c) arabinoxylan.*

In case of CH-AL the negatively charged carboxylic acid (–COO) groups of manuronic and guluronic acid units of AL interact electrostatically with the positively charged amino ($–NH_2$) groups of CH and form a polyelectrolyte complex.[258] In acidic environment CH becomes positively charged due the protonation of the $–NH_2$ group results in formation NH_3+ ions.[274] The CH-PH composite film is formed due to the interaction between the free amino ($–NH_2$)

group of CH with the hydroxyl (–OH) group present in arabinoxylan. Figure 3.2 demonstrate the interaction patterns of CH with AL/ PH hydrocolloid.

3.3.2 Physical Characterizations

3.3.2.1 Fourier transform infrared (FTIR) analysis

FT-IR analysis has been performed to determine the chemical structure and the presence of characteristic functional group. In figure 3.3(a) a broad absorption band at 3307.9 cm^{-1} is observed which may be due to –OH stretching of alcohols of PH. A band appearing at 2891.2 cm^{-1} in PH is due to –CH stretching of alkanes. Similar peaks are observed in CH-PH and in TQ@CH-PH.[275] The FTIR spectrum of PH (arabinoxylan) shows a peak at 894.97 cm^{-1} which represent the bending of polymer backbone of arabinoxylan.[268] Similarly, CH-PH and TQ@CH-PH shows this characteristic peak at 891.11 cm^{-1} and 889.18 cm^{-1} respectively. The absorption band at 1529.55 cm^{-1} in TQ@CH-AL and 1556.55 cm^{-1} in TQ@CH-PH corresponds to amide II groups present in CH at 1589.34 cm^{-1}.[276] Peaks at 950.96 cm^{-1} and at 883.40 cm^{-1} are observed due to the presence of uronic acid group and mannuronic acid functional group in Na-alginate. Similar peaks are appearing at FTIR spectra of CH-AL and TQ@CH-AL ascribed the presence of Na-alginate.[277] A broad peak at 3342.63 cm^{-1} correspond to the hydroxyl group .[275] The recorded peaks at 1328.95 cm^{-1} in TQ@CH-AL and 1369.46 cm^{-1} at TQ@CH-PH could be assigned the presence of TQ.[246] Further, the FTIR spectrum of TQ@CH-AL and TQ@CH-PH respectively at 3329.13 cm^{-1} and 3304.07 cm^{-1} represent O–H stretch of TQ.[246] A peak at 1398.39 cm^{-1} in CH-AL and TQ@CH-AL possibly corresponded to electrostatic interaction between –COO groups of AL with the $–NH_2$ groups of CH.[278] In case of CH-PH and TQ@CH-PH, the direct C–N bond formation via coupling of –OH group present in arabinoxylan and $–NH_2$ group of CH is which confirmed by the peak at 1251.80 cm^{-1}(C–N–C asymmetric stretch).[279]

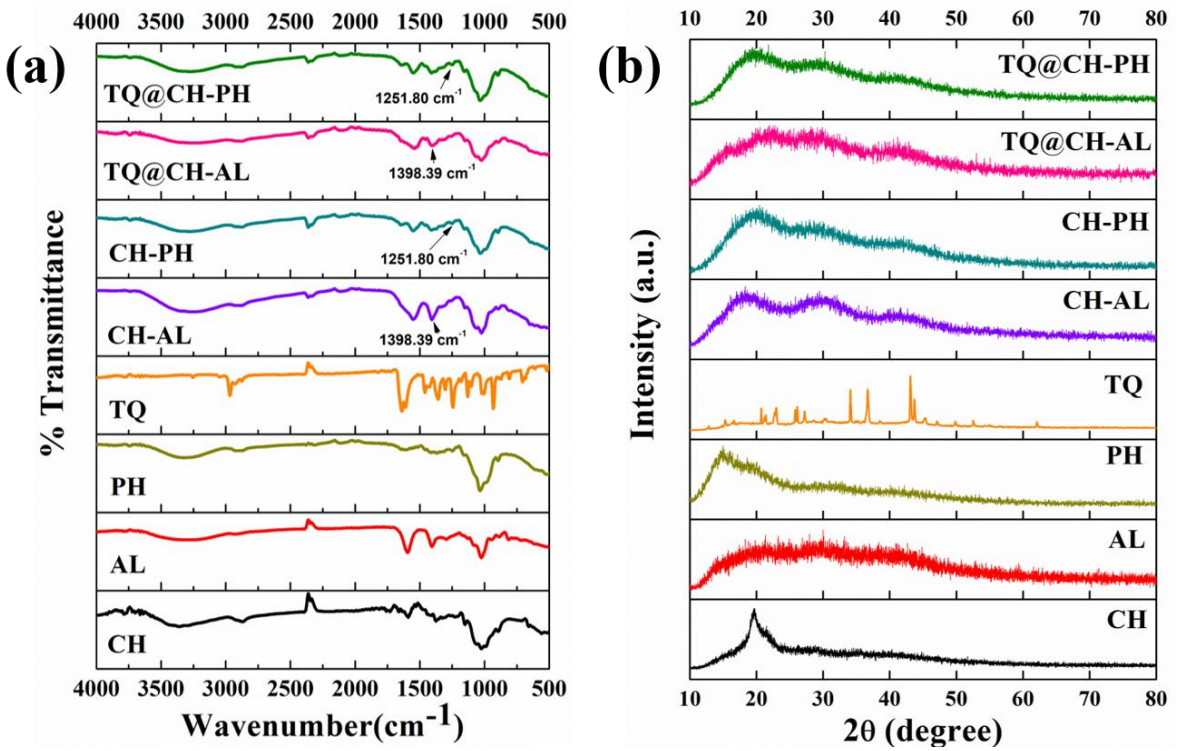

Figure 3.3: *(a) FT-IR spectra and (b) XRD pattern of synthesized polymer composites.*

3.3.2.2 X-ray diffraction (XRD) study

XRD study was performed to find out the phase and crystallinity of the composite film. Figure 3.3 (b) demonstrates the XRD spectra of PH, CH-AL, CH-PH, TQ@CH-AL and TQ@CH-PH. All four synthesized polymeric film exhibited a broad hallow which indicates very low crystallinity due to amorphous nature. Amorphous forms consist of disordered arrangements of molecule which do not have a distinguishable crystal lattice.[280] CH has very broad peaks at $2\theta = 20°$.[281] AL showed three broad humps at $2\theta = 20°$, $2\theta = 30°$, $2\theta = 40°$. The XRD pattern of PH also indicated an amorphous form with two humps at around 2θ of 15° and 20°. CH-AL, CH-PH, TQ@CH-AL and TQ@CH-PH displayed shifted hump at around 2θ of 20° and sharp peak of chitosan at $2\theta = 20°$ became weak. These results confirmed good compatibility and the interaction between CH with AL or PH to form CH-AL and CH-PH. The XRD pattern also suggested the amorphous form of composite film. The amorphous natures of polymer films were maintained after incorporation of TQ, which is beneficial for biomedical applications.

3.3.2.3 Thermal gravimetric analysis (TGA)

Thermogravimetric analysis of PH and TQ loaded composite was measured to determine the thermal stability and the decomposition temperature shown in figure 3.4 (a). It was observed that the TGA of PH, TQ@CH-AL and TQ@CH-PH showed a two-step of weight loss. Initial

weight loss may correspond to the evaporation of moisture or loss of adsorbed or bound water. The second weight loss of PH is about 49.6% in the range 230–311°C was due to the complexity of the process, which led to the degradation of the sample. At the end of 400ºC the total weight loss of sample was 56.36% in case of TQ@CH-AL and 39.68% in case of TQ@CH-PH.

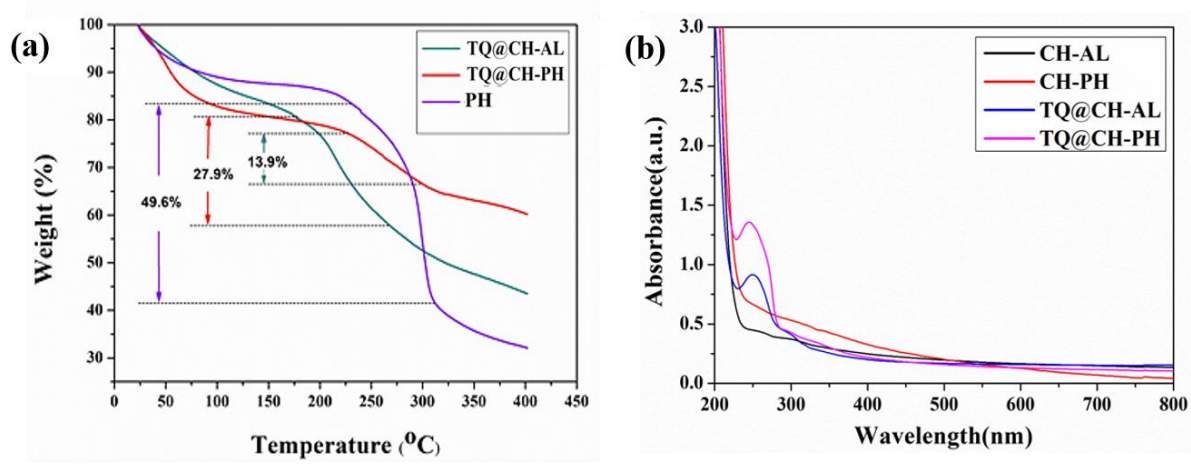

Figure 3.4: *(a) TGA curve of PH, TQ@CH-AL and TQ@CH-PH (b) UV-Vis spectra of polymer composites.*

3.3.2.4 UV–visible spectrophotometric analysis

In our study, UV-visible spectroscopy was used to study the absorption spectra of films. The UV-VIS spectra of TQ is characterized by the presence of one prominent peak (λ_{max}) at 254–257 nm regarded as a distinguishing peak for quinones.[174] As observed in figure 3.4 (b), UV–vis absorbance spectrum of TQ@CH-AL and TQ@CH-PH displayed a prominent peak at 248 nm and 252 nm respectively. The results ascertained the successful interaction with TQ.

3.3.2.5 Morphology study of composite film

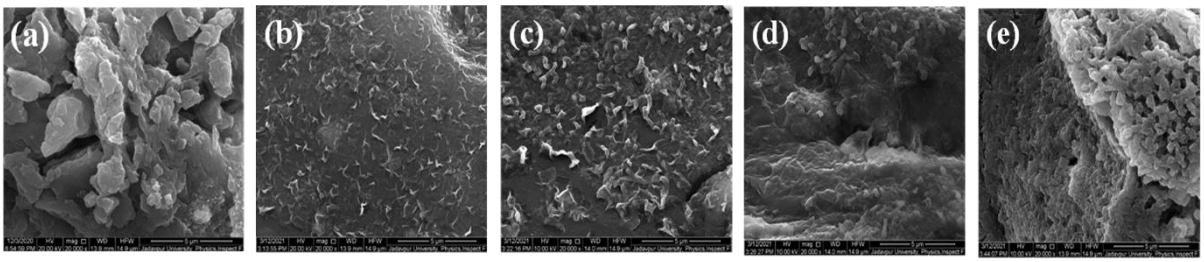

Figure 3.5: *FESEM micrograph of (a) PH (b) CH-AL, (c) TQ@CH-AL, (d) CH-PH and (e) TQ@CH-PH.*

As observed in FESEM image (figure 3.5) the surface morphologies of all these five samples are porous in nature. Figure 3.5 (a) revealed discontinuous and irregular microporous surface of PH which is also observed in image of CH-PH and TQ@CH-PH depicted in figure 3.5 (d) and (e). Figure 3.5 (b) and (c) shows flaky polymeric structure of CH-AL and TQ@CH-AL respectively. FESEM image clearly indicate the marked differences between TQ tagged polymer composites and bare polymer composites.

3.3.2.6 Estimation of therapeutic loading efficiency

The TQ loading percentage within polymeric composite film was determined by calculating the concentration of the TQ using standard procedure which was mentioned in subsection 1.7.3.9.[175] The loadings content and loading efficiencies of a wide range of natural therapeutics in polymer matrix are highly depend on the chemical nature and the interaction pattern between polymer and drug. Loading content is determined to be 36.15% in case of TQ@CH-AL and 38.10% in case of TQ@CH-PH. We report higher loading efficiency of TQ when we replace alginate with PH. Condensed porous surface of polymer composite restricted the leakage of drug from the films results in high loading efficiency of hydrophobic TQ. The loading efficiency of TQ@CH-AL and TQ@CH-PH is 78.33% and 81.30% respectively. These results indicated that the incorporation capacity of CH-PH is higher than CH-AL.

3.3.2.7 pH-responsive release of TQ

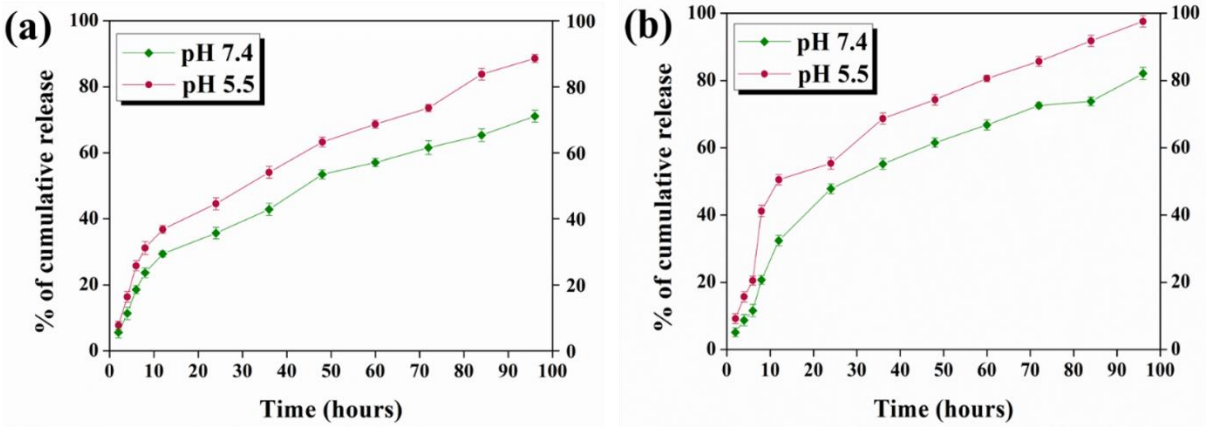

Figure 3.6: *Graphical representation of pH-responsive time-dependent release study of thymoquinone from (a)TQ@CH-AL (b)TQ@CH-PH.*

To determine the amount of TQ discharged from synthesized composite film, *in vitro* TQ release was calculated in a time dependent manner in physiological pH conditions (pH ~7.4) and intracellular pH conditions of cancer cells (pH ~ 5.5) at 37°C using standard curve of TQ (as mentioned in subsection 1.7.3.10). We verified whether these polymer complexes can

achieve stability and controlled release of TQ in physiological conditions as well as acidic environment which is essential for clinical applications. The *in vitro* release behaviour of incorporated TQ from TQ@CH-AL and TQ@CH-PH occurred in two steps, i.e., an initial rapid release within the first 12 hrs followed by a slow leaching over a period of 96 hours (figure 3.6). At pH 5.5 (acidic condition), after 24 hrs the estimated release percentage of TQ from TQ@CH-PH (approx. 55.40%) was found to be greater than TQ@CH-AL (approx. 44.60%). Release behaviour depends on the nature of interaction of therapeutics with polymer mesh. Moreover, the release profile suggested sustained but faster release in acidic condition and thus it confirms the efficacy of polymer composite to release adequate amount TQ for its anticancer applications.

3.3.3 Evaluation of antibacterial activity

3.3.3.1 Determination of antibacterial property by time dependent colony counting method

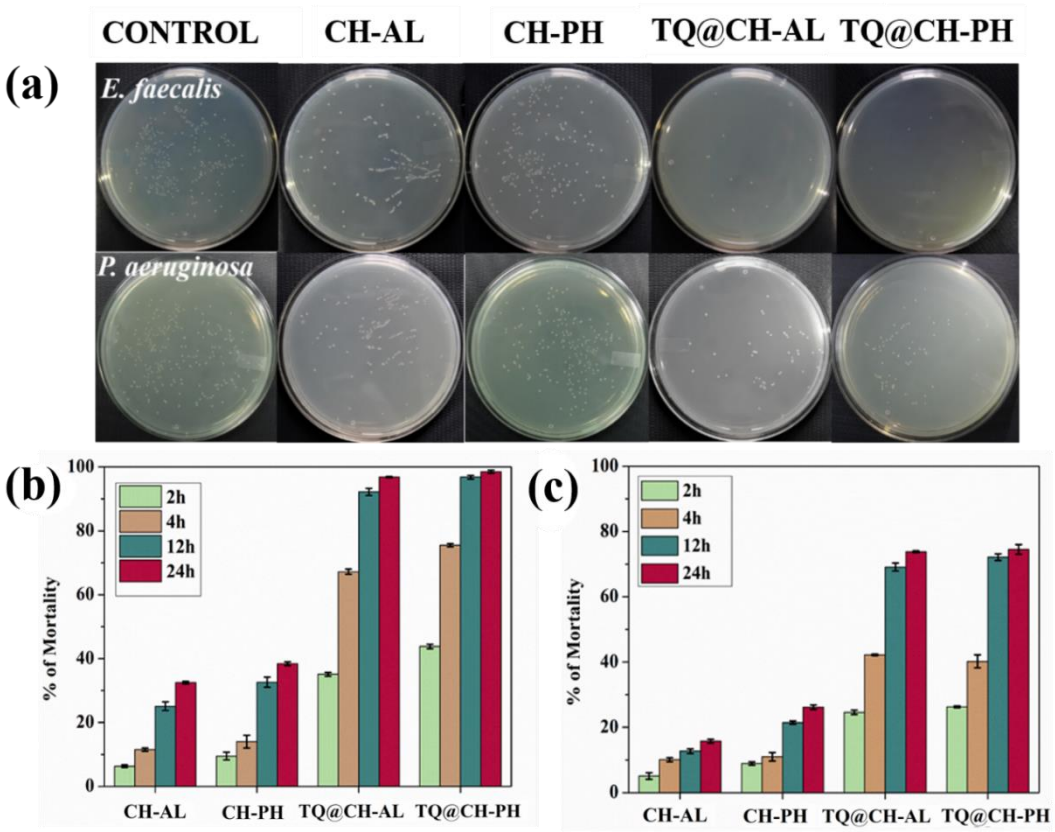

Figure 3.7: *(a) Plate count photograph showing the antibacterial efficacy of films after 24 hours of incubation. Graphical representation of the percentage of cell mortality of (b) Enterococcus faecalis and (c) Pseudomonas aeruginosa.*

Table 3.1: *Effective concentration of TQ during antibacterial assay.*

TIME (hr)	*TQ@CH-AL (µg/mL)*	*TQ@CH-PH (µg/mL)*
2	12.15	12.12
4	24.73	19.93
12	63.77	74.07
24	77.43	109.27

Antimicrobial properties of TQ loaded composite films were studied in respect of time by colony counting method on *P. aeruginosa* and *E. faecalis* (as mentioned in subsection 1.7.4.3). As because our samples are film matrix, we carried out an additional agar-diffusion method based on direct contact between the sample and the bacteria to examine their potential effectivity (as mentioned in subsection 1.7.4.4). For time dependent colony counting method a strip (weighted 3 mg) of CH-AL, CH-PH, TQ@CH-AL and TQ@CH-PH were added to bacterial culture. After incubation, microbial growth was assessed by plating treated culture on nutrient agar plates after 2, 4, 12 and 24 hrs. The microbial culture without polymer composite was considered as control. Figure. 3.7 (a) represents the antibacterial potentials of four types of composite films (namely, CH-AL, CH-PH, TQ@CH-AL and TQ@CH-PH) against *P. aeruginosa* and *E. faecalis* as determined by the plate counting method. Percent of cell mortality was plotted in time dependent manner over a period of 24 hrs to determine the effect of the composite films which were found to display significant antibacterial activity against pathogenic bacteria. Agar plates of the control and treated bacteria after 24 hrs of incubation are displayed in figure 3.7 (a). The differential antibacterial kinetics of test bacteria are checked against our four samples by time kill assay using colony count method. *E. faecalis* display 96.80% and 98.50% mortality rate when treated against TQ@CH-AL and TQ@CH-PH during the same incubation period (figure 3.7 b). Figure 3.7 (c) demonstrate that within 24 hrs of incubation period the mortality rate of *P. aeruginosa* for TQ@CH-AL and TQ@CH-PH are 73.60% and 74.50% respectively. The test result also demonstrates excessive colonies against composite without TQ i.e., CH-AL, CH-PH. Bacteriostatic activities of CH-AL and CH-PH occurred because of the antibacterial property of chitosan. PH has no such antibacterial activity when we treated our test bacteria against PH alone.

Table 3.1 demonstrate time and pH dependent effective concentration of TQ. If we compare the MIC value reported by Chaieb et al. it can be said that in case of *E. faecalis,* treatment with both TQ@CH-AL and TQ@CH-PH showed high bacterial mortality within 4 hrs even if the effective concentration of TQ is less than the MIC value.[148] However, in the 12-24 hrs range

the effective concentration of TQ is more than MIC value which correspond to the observed antibacterial activity.

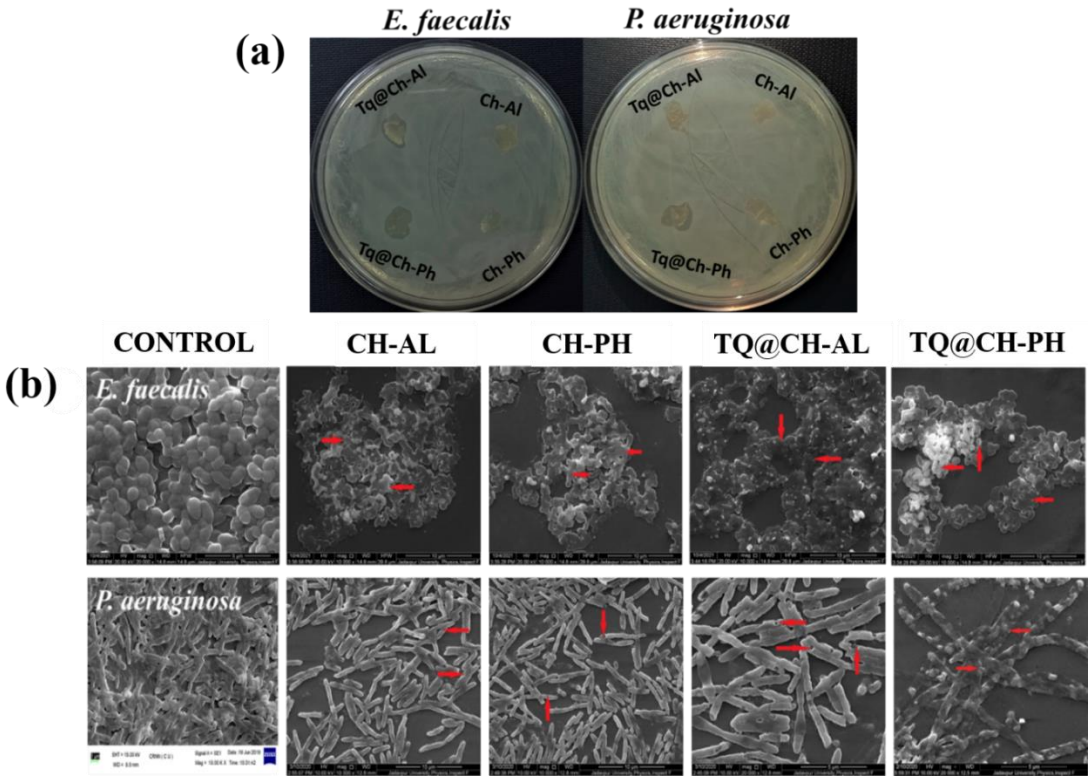

Figure 3.8: *(a) Photographic images of the antimicrobial activity of films (b) FESEM micrographs showing morphological characteristics of control and treated bacterial cells.*

3.3.3.2 Agar diffusion study

For agar-diffusion study polymer films were positioned on the petri plate for incubation following standard protocol. Figure 3.8 (a) showing agar diffusion method which revealed that CH-AL, CH-PH, did not display any significant zone of inhibition but there is no trace of bacterial biofilms formation on film surface. On the other hand, the TQ encapsulated composite films revealed a zone of inhibition. Upon contact with the TQ loaded film, the ionic interactions may occur between positively charged amino groups present in CH and negatively charged lipopolysaccharides of bacterial cell wall. The hydrophobic moieties of TQ possibly interact with the cell membrane lipopolysaccharides may results in destabilization in cellular membrane and altered permeability for TQ.[282]

3.3.3.3 Bacterial morphology study by FESEM

FESEM image of figure 3.8 (b) confirmed the damaged bacterial membrane integrity upon interaction with CH-AL, CH-PH, TQ@CH-PH and TQ@CH-AL compared to the smooth and undamaged structure of control groups.

3.3.3.4 Determination of ROS generation

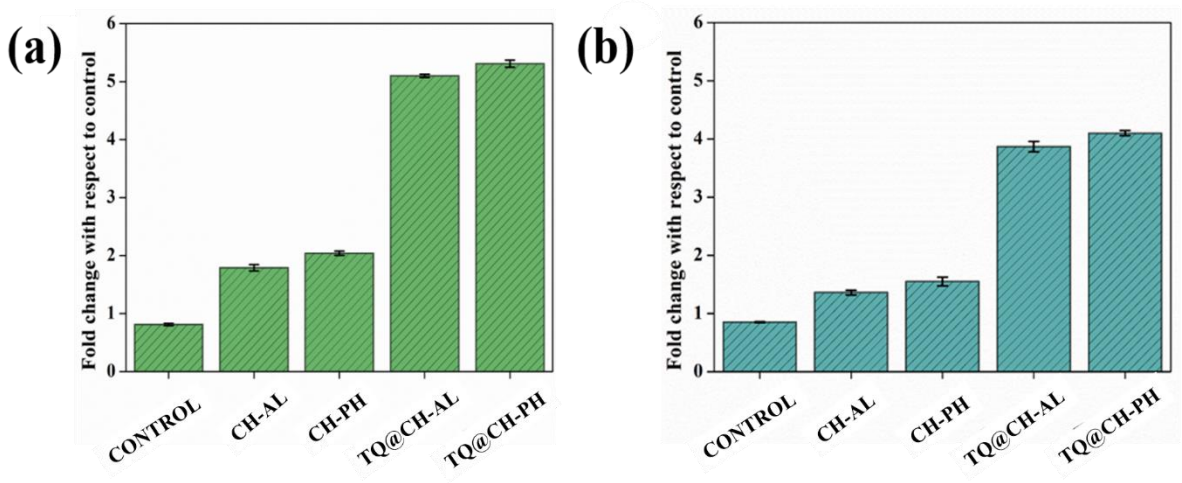

Figure 3.9: *Graphical representation of bacterial ROS generation by DCFDA assay in case of (a) Enterococcus faecalis (b) Pseudomonas aeruginosa.*

To estimate intracellular ROS generation $DCFH_2$-DA was used and fluorescence intensity was measured (as mentioned in subsection 1.7.4.5). Oxidative stress can be a major cause of disruption of cellular integrity by damaging DNA, RNA, lipids and proteins.[283] Figure 3.9 (a) and (b) also stated the higher ROS generation in bacterial cell in case of TQ@CH-PH compared to TQ@CH-AL which also correlate with the cell mortality study stated earlier. Due to ROS accumulation polyunsaturated fatty acids of bacterial membrane are attacked which initiate lipid peroxidation and alter the integrity of membrane-bound proteins.[284]

3.3.4 Assessment of anticancer properties

3.3.4.1 Cytotoxicity study

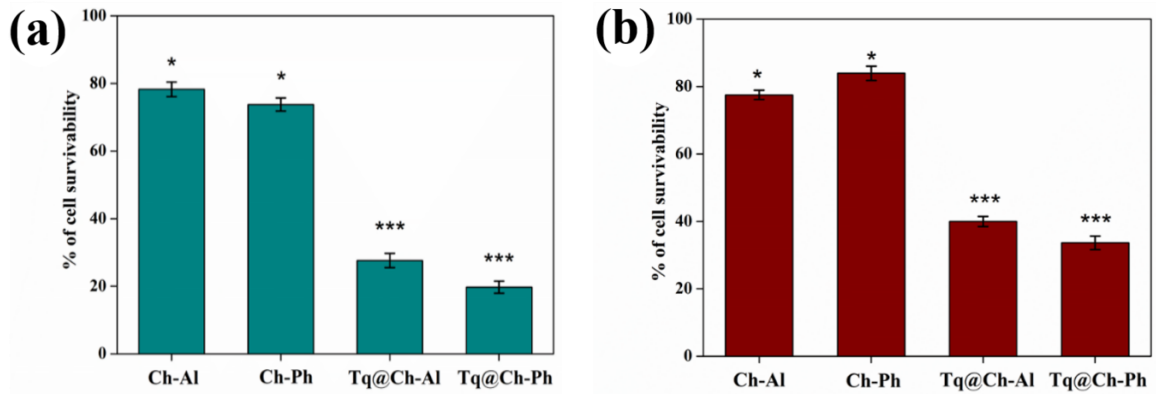

Figure 3.10: *MTT assay on (a) PC3 and (b) A549 cell line after treatment with films. The Cell*

*Survivability Percentage was expressed as a mean ± SD of three independent experiments and significance was shown as *(P<0.05), **(P<0.01) and ***(P<0.001).*

The *in vitro* cytotoxicity of synthesized films was assessed by MTT assay to human PC3 and A549 cell lines using standard protocol (as described in subsection 1.7.5.2). During incubation, cells were exposed to polymeric films (3µg/µL each) for 24 hrs. In figure 3.10 we had observed that the cell treated with TQ@CH-PH and TQ@CH-AL resulted in significant cell death in case of both cell lines compared to CH-AL and CH-PH which did not exhibit any marked cell death. In case of PC3 cell line TQ@CH-PH treated cell exhibited 19.73% cell survivability whereas 33.66% cell survivability is observed in case of A549 cells.

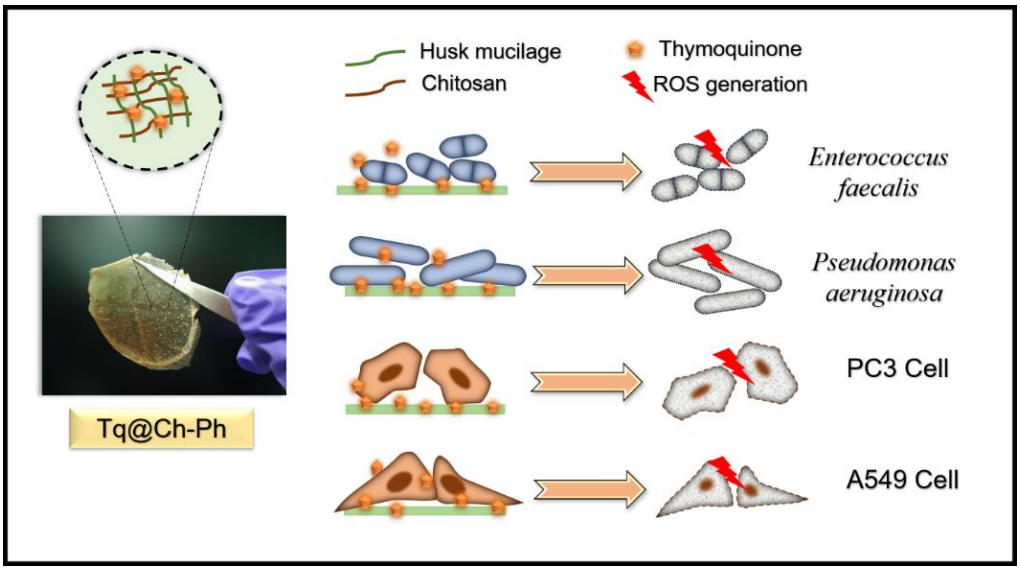

Figure 3.11: *Schematic representation showing the efficacy of polymeric film on pathogenic bacterial strains and carcinoma cells.*

3.3.4.2 Study of Intracellular ROS generation

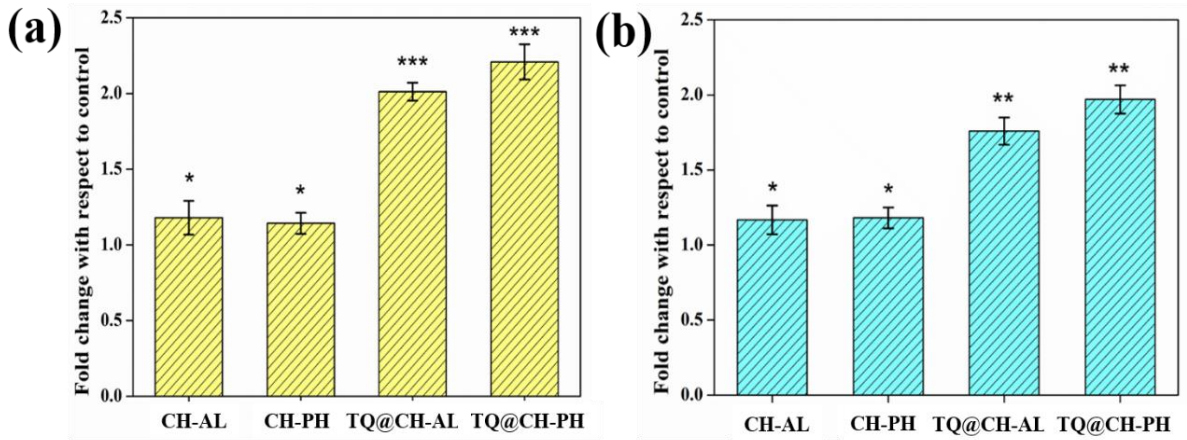

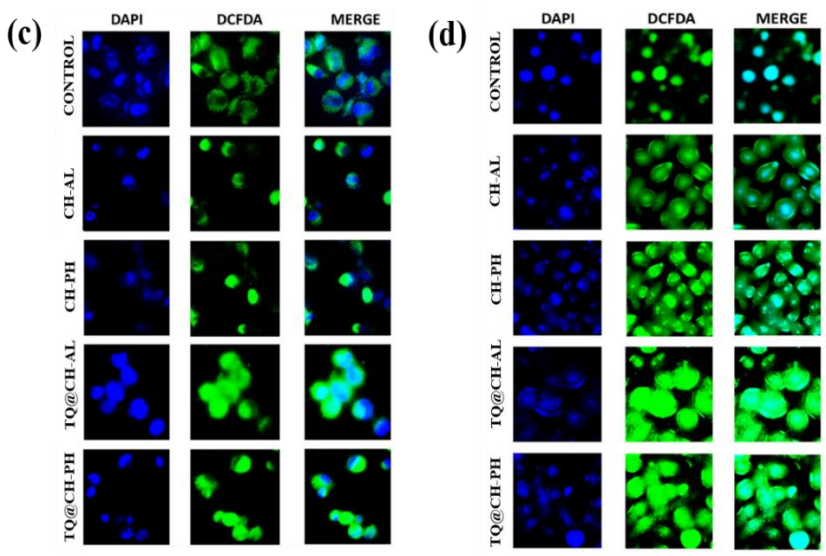

Figure 3.12: *Graphical representation of mean fluorescent intensity for ROS generation in (a)PC3 and (b)A549 cell line. The fold change with respect to control was expressed as a mean ± SD of three independent experiments and significance was shown as *(P<0.05), **(P<0.01) and ***(P<0.001). Fluorescence microscopic image of intracellular ROS generation for (c)PC3 and (d) A549 cell line.*

Monitoring intracellular ROS generated from the activity of polymer composites (dose: 3µg/µL for each film) we found out that the fold change in case of CH-AL, CH-PH both was almost similar to untreated cells whereas TQ@CH-PH and TQ@CH-AL exhibited a marked increase in the production of ROS (figure 3.12). This was confirmed by both spectrophotometry as well as fluorescence microscopy (as described in subsection 1.7.5.3).

3.3.5 Biocompatibility study

3.3.5.1 Cytotoxicity study

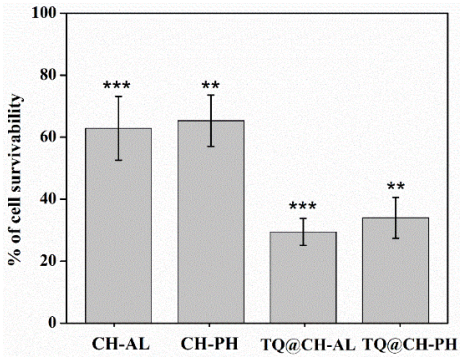

Figure 3.13: *MTT assay on WI38 cell line after treatment with films. The Cell Survivability Percentage was expressed as a mean ± SD of three independent experiments and significance was shown as *(P<0.05), **(P<0.01) and ***(P<0.001).*

In vitro cytotoxicity was evaluated with MTT assay using standard protocol (as described in subsection 1.7.5.2) where normal cell line - human lung fibroblasts (WI38) were exposed to polymeric films (3µg/µL each) for 24 hrs. In WI38 cells, TQ@CH-AL treatment exhibited 29.46% cell survivability whereas TQ@CH-PH treatment exhibited 33.98% cell survivability (figure 3.13)

3.3.5.2 Study of Intracellular ROS generation

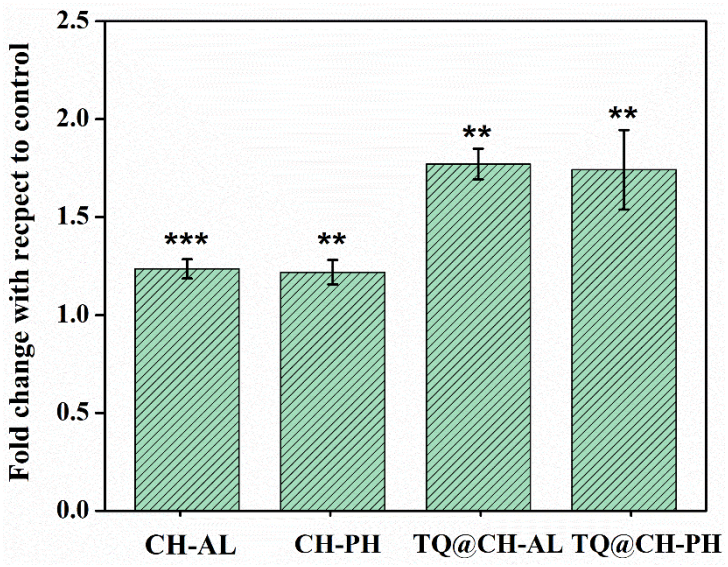

Figure 3.14: *Graphical representation of mean fluorescent intensity for ROS generation in WI38 cell line. The fold change with respect to control was expressed as a mean ± SD of three independent experiments and significance was shown as *(P<0.05), **(P<0.01) and ***(P<0.001).*

Intracellular ROS accumulation was evaluated by $DCFH_2$-DA assay using standard protocol (as described in subsection 1.7.5.3) where normal cell line- human lung fibroblasts (WI38) were exposed to polymeric films (3µg/µL each). Monitoring intracellular ROS generated from the activity of polymer composites we found out that the fold change in case of CH-AL, CH-PH both was almost similar to untreated cells whereas TQ@CH-PH and TQ@CH-AL exhibited a marked increase in the production of ROS (figure 3.14).

3.4. Conclusion

In this study, antimicrobial and anticancer composites were obtained by simply combining CH with PH or AL without the addition of any compatibilizer or chemical modification of film surfaces, thus providing a simple synthetic procedure to develop biopolymeric film with bactericidal as well as cytotoxic applications. The obtained polymer composites incorporating

TQ were characterized regarding their morphology, physico-chemical properties and thermal stability by different techniques, from which we can confirm effective interactions and good compatibility between CH and PH / AL as well as between the polymer composite and the TQ. The incorporation efficiencies and release kinetics of TQ were also evaluated and contrasted with results attained for the antimicrobial activity against bacterial strains. Notably, compared to TQ@CH-AL, TQ@CH-PH exhibited significantly improved *in vitro* TQ release as well as better antibacterial efficacy. In the FESEM study of bacterial cell, morphological changes induced by the TQ and CH in polymeric films are evident due to cell damage. An *in vitro* cytotoxicity study revealed that the TQ-loaded polymeric films showed remarkable cell death against PC3 and A549 cell lines in a highly effective manner (figure 3.11). Moreover, experimental results confirmed that the broad-spectrum antibacterial and cytotoxic activity observed due to the chitosan and TQ released from polymer film. The prepared polymeric film either adhered to the bacterial cell wall or the released TQ interact with the bacterial membrane and promote ROS generation thus destabilized the cellular integrity and membrane permeability. MTT assay against WI38 cell line also confirmed moderate biocompatibility. Hence, from overall study it has been established that PH mucilage can be used to develop effective polymeric film in combination with another polymer if properly standardised. Thus, in combination with therapeutic agents i.e., TQ, TQ@CH-PH is established as an excellent antibacterial as well as anticancer film which can be advantageous for further investigations. Thus, this type of film containing nontoxic plant derived materials has promising potential for therapeutic applications and in biomedical industry.

Chapter 4

In vitro Antibacterial and Anticancer Potentials of Piperine Incorporated Guar Gum and Psyllium Husk Derived Biopolymeric Nanocomposite

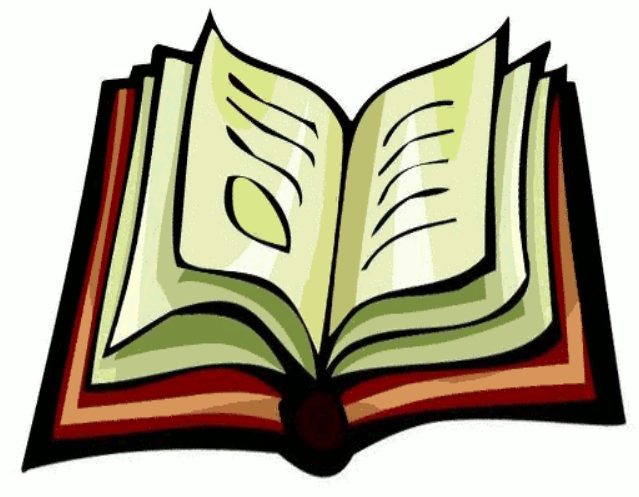

Summary

The synthesis of guar gum and psyllium husk mucilage-mediated piperine nanocomposite was reported in order to develop a modified phytochemical-based nanomaterial with potent antimicrobial and anticancer properties. Piperine was nanonized by entrapping within guar gum and psyllium husk mucilage-derived nanocomposite. We have taken guar gum and husk mucilage in three different ratios to formulate nanocomposites for comparative study. Loading percentage of piperine in nanocomposites indicated excellent incorporation efficiency. The release kinetics of piperine from nanocomposites showed sustained but faster release behaviour which confirms the availability of adequate amount of therapeutics at the site of application. The as-prepared nanocomposite showed strong oxidative stress mediated antimicrobial activities against Gram-positive *Staphylococcus aureus* and Gram-negative *Pseudomonas aeruginosa.* IC_{50} values of nanocomposites against adenocarcinomic human alveolar basal epithelial cell line were evaluated where the effective concentration of piperine was significantly low. The biocompatibility of the nanocomposite was evaluated against human lung fibroblast cell line. Moreover, the nanocomposite had the potential to induce oxidative stress, for which significant mortality of bacterial and cancer cells was detected.

4.1 Introduction

The modifications and applications of biomaterials are extensively studied for their increasing usage in the health and medical sectors. The versatile developmental procedures of nanocomposites are employed to improve the desired properties as well as introduce new interesting properties in biopolymeric composites. Natural polymers and polymer-derived structures have immense applicability due to their intrinsic pharmacological properties as well as low environmental impact.[24] Nanomaterial-based drug delivery systems (DDS) get more attention in biomedical applications resolving challenges such as poor intestinal absorption rate, ineffective delivery mechanism at target site, less solubility, and plasma inconsistency of therapeutic agents.[285,286]

A wide variety of polysaccharides have indeed been explored in synthesis of nanoparticles and nanocomposites. Guar gum and psyllium husk are suitable compounds for preparation of polymer composite, are valued for biocompatibility, biodegradability, and non-toxicity. Guar gum (GG) is isolated from the endosperm of seeds of the legume *Cyamopsis tetragonalobus,* which contains polysaccharides of galactomannans.[287] GG is used as a primary gelling agent, stabilizer, emulsifier, or thickener due to its cost-effectivity, high viscosity, and hydrophilicity.[234] GG is also known to aid obesity prevention and lowers cholesterol and glucose level.[234,287] The seed husk (psyllium husk or Ispaghula) of *Plantago ovata* plant, traditionally utilized as a dietary fibre supplement for regulation of bowel function and is also effective in both constipation and diarrhoea, two opposite gut conditions. Psyllium husk (PH) contains numerous active components i.e. 4-*O*-methylglucuronic acid, arabinoxylans, aucubin, campesterol, linoleic acid, oleic acid, palmitic acid, L-cystine, L-asparagine, rhamnose, sterol, β-sitosterol etc.[266] PH has mucilaginous properties and essential component of many commercially available laxative agents i.e. Metamucil.[116]

Several pharmacological and therapeutic procedures have been employed to repress cancerous growth often displaying partial efficacy with severe side effects.[288] It is now evident that the consumption of certain phytochemicals can play a protective role against tumorigenesis and cancer.[289] In the recent decade, this type of "chemoprevention" using some phototherapeutics with redox-mediated mechanisms has enormous capability to interfere with the proliferation of cancer cells effectively.[290] For this study, we have chosen piperine (1-[5-(1,3-Benzodioxol-5-yl)-1-oxo-2,4-pentadienyl] piperidine), a principal alkaloid extracted from *Piper longum* and *Piper nigrum* plants as a bioactive phytochemical.[291] Piperine (PIP) is recently getting attention

for its bio enhancing capacity by diminishing P-glycoprotein mediated transport as well as CYP3A4 mediated drug metabolism.[291] Studies reported the prooxidant property of PIP which induces radical mediated mitochondrial pathway of apoptosis of Hep G2 cells by repressing the peroxide-detoxifying enzyme catalase.[292] PIP is also known to induce apoptosis in rectal and colon cancer cells by ROS-mediated pathway.[293,163] Molecular docking and western blotting studies revealed the PIP- mediated inhibition of receptor tyrosine kinase and mitigation of hepatocellular carcinoma progression.[292]

Our study shows that PIP may be a promising prooxidant drug for antibacterial applications and also for the amelioration of adenocarcinomic human alveolar basal epithelial cell line (A549). Biocompatibility of nanocomposites was also measured on normal human lung fibroblasts (WI38) cell lines. In this work, we have chosen PH and GG to synthesis a stable, multifunctional nanocomposite and three different ratios of GG and PH (1:1, 2:1 and 1:2 for GG-PH-1, GG-PH-2, GG-PH-3 respectively) were taken to standardize the synthesis of nanocomposites. On the other hand, PIP was incorporated into GG-PH-1, GG-PH-2, GG-PH-3 to synthesize GG-PH@PIP-1, GG-PH@PIP-2, GG-PH@PIP-3 respectively. Our present study is an effort toward the synthesis of high-performance, biocompatible nanocomposite to attain good antibacterial and cytotoxic activity against cancer cells. This chapter describes a comparative structural characterization and clinical efficacy of three different GG and PH derived nanocomposites (GG-PH-1, GG-PH-2, GG-PH-3) as well as PIP incorporated nanocomposites (GG-PH@PIP-1, GG-PH@PIP-2, GG-PH@PIP-3).

4.2 Experimental section

4.2.1 Synthesis of bio-nanocomposite (GG-PH@PIP)

In GG-PH@PIP nanocomposite the main nano formulation was of GG-PH within which PIP was incorporated. Extraction and purification of PH was performed following the protocol which we have already mentioned in subsection 3.2.1.[294] For GG-PH@PIP-1, GG-PH@PIP-2 and GG-PH@PIP-3 the ratios of GG and PH were 1:1, 2:1 and 1:2 respectively. For GG-PH@PIP-1, 0.1% (w/v) GG solution was prepared dissolving 50 mg GG in milli-Q water. Similarly, to obtain a 0.1 % (w/v) PH solution, 50 mg of PH was dissolved in 50 mL of milli-Q water. Both dispersions were homogenized followed by dropwise addition of GG solution to PH solution under moderate magnetic stirring. After that the resulting polymer suspension was dried at 50ºC. For the synthesis of PIP-loaded nanocomposite, 3 mL PIP solution (prepared in DMSO at a concentration of 1 mg mL^{-1} and sonicated) was added dropwise to GG-PH

biopolymeric mixture and allowed to stir for further 10 hrs. The obtained reaction mixture was centrifuged at 10,000 rpm for about 10 mins, washed twice, followed by drying at 50ºC in a desiccator. A schematic diagram illustrating the synthesis procedure of piperine loaded bio nanocomposite is showed in figure 4.1.

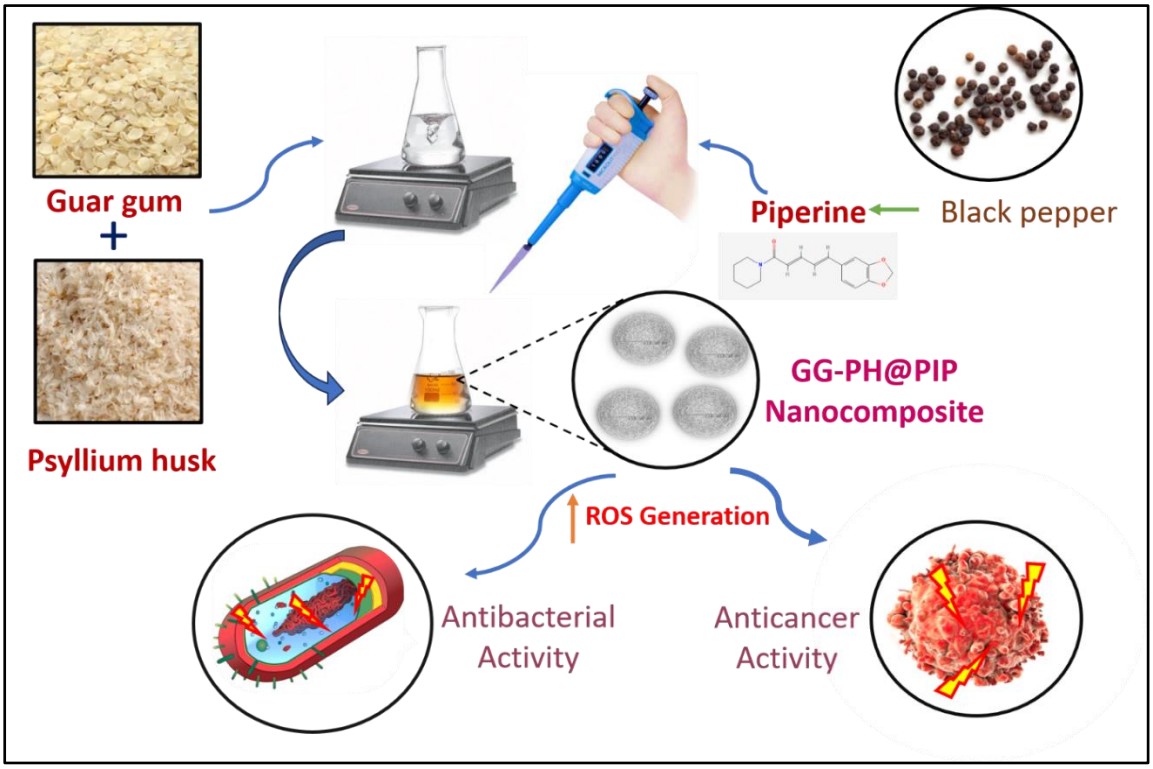

Figure 4.1: *Schematic representation describing synthesis and biological potentials of GG-PH@PIP nanocomposites.*

4.2.2 Statistical analysis

All experiments were performed in triplicate and data were presented as mean ± standard deviation (SD) for each set of experiments. Single factor one-way statistical analysis was performed using ANOVA. To determine statistical significance, value of $p < 0.05$ was considered to indicate significance or otherwise mentioned.

4.3 Results and Discussion

4.3.1 Physical Characterizations

4.3.1.1 Fourier transform infrared spectroscopy (FTIR) analysis

FT-IR spectra has been studied to determine the chemical interaction at the molecular level. As figure 4.2 (a) FTIR spectrum of GG has absorption peaks around at 792 cm^{-1} is attributed to

(1–4), (1–6) linkage of galactose and mannose, 3328 cm^{-1} (O–H stretching vibration of water and polymer), 1644 cm^{-1} (ring stretching of mannose), 1020 cm^{-1} (–CH_2 twisting vibration) and 2922 cm^{-1} (C–H stretching of CH_2 group).[244,245,295] A broad absorption band appearing at 3311 cm^{-1} represents –OH stretching of PH. A band is observed at 2904 cm^{-1} due to the –CH stretching of alkanes at the FTIR spectrum of PH. Similar peaks are observed in GG-PH and GG-PH@PIP.[275] A peak at 891 cm^{-1} is observed in the case of PH is due to the bending of the polymer backbone of PH (arabinoxylan).[268] As for PIP, the most characteristic C–O bond and the stretching of the amide group are clearly shown by peaks at 924 cm^{-1} and 1634 cm^{-1}, respectively. It also displayed peaks at 2935 cm^{-1} corresponding to aromatic C–H stretching, at 1444 cm^{-1} which corresponds to C=H stretching, and at 1248 cm^{-1} corresponding to asymmetrical stretching of =C–O–C.[225] All these characteristic peaks were retained at almost the same positions in GG-PH@PIP nanocomposite demonstrating the entrapment of PIP into the nanocomposites.

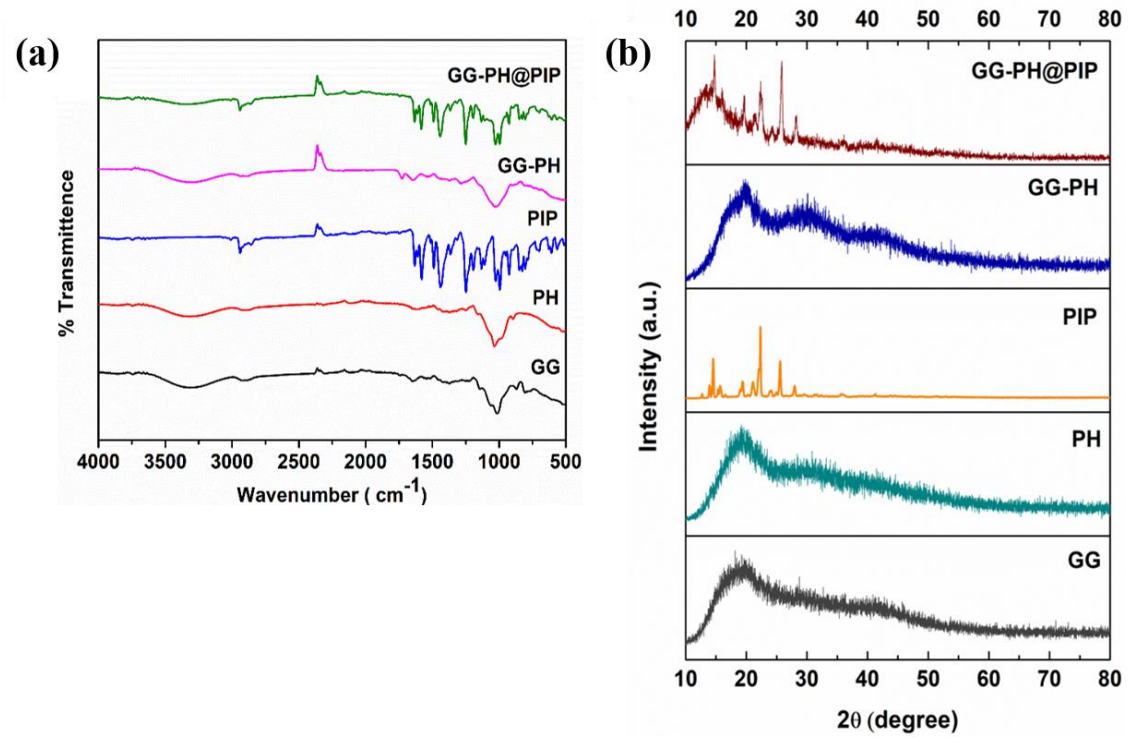

Figure 4.2: *(a) FT-IR spectra and (b) XRD spectra of nanocomposites.*

4.3.1.2 X-ray diffraction (XRD) study

XRD study shown in figure 4.2 (b) demonstrates the diffraction patterns of nanocomposite confirming the incorporation of natural therapeutic. XRD patterns of GG-PH and GG-PH@PIP nanocomposites displayed a broad hallow which implies low overall crystallinity because of

disordered molecular arrangements.[280] GG showed a very broad peaks at 2θ = 20º.[247] In XRD spectra of PH prominent humps at around 2θ of 15º and 20º were observed confirmed an amorphous nature. PIP displayed evidence of diffraction peaks at 2θ of 14º, 22º, and 25º which shows similarity with the characteristic spectra of PIP (JCPDS Card no: 00-043-1627).[248] GG-PH exhibited shifted hump at around 2θ = 20º where GG-PH@PIP showed a characteristic sharp peak of PIP which established the incorporation of PIP to form GG-PH@PIP.

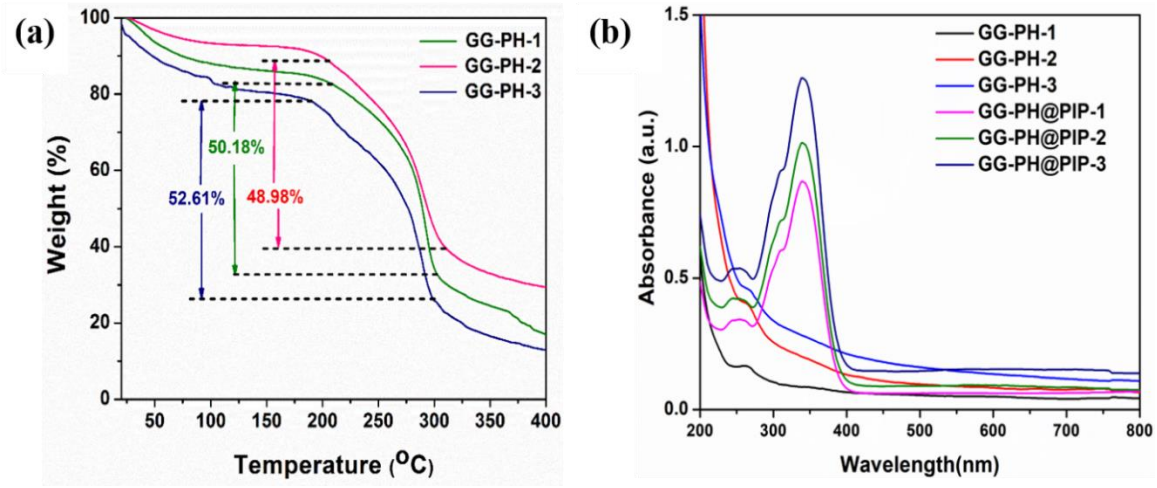

Figure 4.3: *(a) TGA curve of GG-PHs and (b) UV-Vis spectra of nanocomposites.*

4.3.1.3 Thermal gravimetric analysis (TGA)

Thermal gravimetric analysis of our bio nanocomposites was studied to evaluate the thermal stability by the TGA thermograph shown in figure 4.3 (a). It can be noticed that the TGA of GG-PH-1, GG-PH-2, and GG-PH-3 displayed a two-step weight loss with increasing temperature. Initial weight loss attributes of evaporation of adsorbed surface water. According to the thermogram of GG-PH-1, GG-PH-2, and GG-PH-3, the initial degradation of mass at around 25–100ºC is almost 12%, 7%, and 16% respectively. The second step of steady mass loss is associated with the volatilization, pyrolysis, and combustion of organic molecules of the nanocomposites. The second weight loss of GG-PH-1 is about 50.18% (temperature range 210–301ºC). The thermogravimetric curve explains it is about 48.98% (temperature range 205-310 ºC) in GG-PH-2 and 52.61% in GG-PH-3 (temperature range 190-300ºC) which led to the degradation of the samples. At 400ºC the overall mass loss was 83%, 71%, and 87% respectively according to the thermogram of GG-PH-1, GG-PH-2, and GG-PH-3.

4.3.1.4 UV–visible spectroscopy

UV–visible absorption spectra of synthesized nanocomposites have been shown in figure 4.3 (b). A prominent characteristic peak (λmax) of PIP is observed at 342–345 nm.[173] As exhibited

in figure 4.3 (b), GG-PH@PIP-1, GG-PH@PIP-2, GG-PH@PIP-3 also displayed a strongest peak at 340 nm, followed by an additional less intense peak at around 310 nm, whereas between 246 and 258 nm a low-intensity absorption band can be observed which ascertained the successful interaction with PIP.

4.3.1.5 Dynamic light scattering (DLS) study

Table 4.1: *DLS study showing hydrodynamic diameter, polydispersity index (PDI) and zeta potential of GG-PH@PIPs; and loading percentage of PIP in GG-PH@PIP.*

Nanocomposite	*Hydrodynamic Diameter (µm)*	*Polydispersity Index*	*Zeta Potential*	*Loading % of PIP in nanocomposites*
GG-PH@PIP-1	.705 ± .1	.322 ± .05	−31.1 ± .97	83 ± 1.2
GG-PH@PIP-2	1.506 ± .23	.551 ± .11	−23.8 ± 1.5	69 ± 1.4
GG-PH@PIP-3	.984 ± .13	.386 ± .08	−30.8 ± 2.3	79 ± 1.66

The size, shape and morphology of synthesized nanocomposites were determined by DLS, FESEM, TEM, and AFM study. DLS study displays the hydrodynamic diameter of any particle i.e., the size of the core particle, with additional hydration layer around it. Therefore, the size measured by DLS instrument was always larger than the actual size of any nanoparticle. As DLS study the mean size of the GG-PH@PIP-1 nanoparticle was found to be about .705 ± .1 µm with a polydispersity index (PDI) value of .322 ± .05 (table 4.1). Lower PDI values characterize the mono-dispersed nanoparticles. Therefore, the PDI value of GG-PH@PIP signified a good synthesis procedure with almost equal sized mono-dispersed nanocomposite suspension. When the ratio of the used precursor biopolymers is altered, the diameters and PDI values of the particles have changed (Table 4.1). As enhanced PDI values (.551 ± .11 of GG-PH@PIP-2) indicated lower homogeneity of the samples.

The zeta potential (ζ) of GG-PH@PIP gradually increased from (-) 23.8 ± 1.5 mV to (-) 31.1 ± .97 mV with altered ratio of the precursor biopolymers (Table 4.1). The magnitude of zeta potential signifies the potential stability of our synthesized nanocomposites. The higher (+) or (-) value of ζ indicates repulsion of particles which prevents agglomeration of particles. The stability of nanoparticles is compromised in particles with low ζ value. ζ value > ± (30) mV is normally considered as stable.[296] (-) value of zeta potential indicated (-) surface charges on

GG-PH@PIPs. Therefore, the ζ value of GG-PH@PIP-1 can be considered as more stable compared to GG-PH@PIP-2 and GG-PH@PIP-3.

4.3.1.6 Field emission scanning electron microscopy (FESEM) analysis

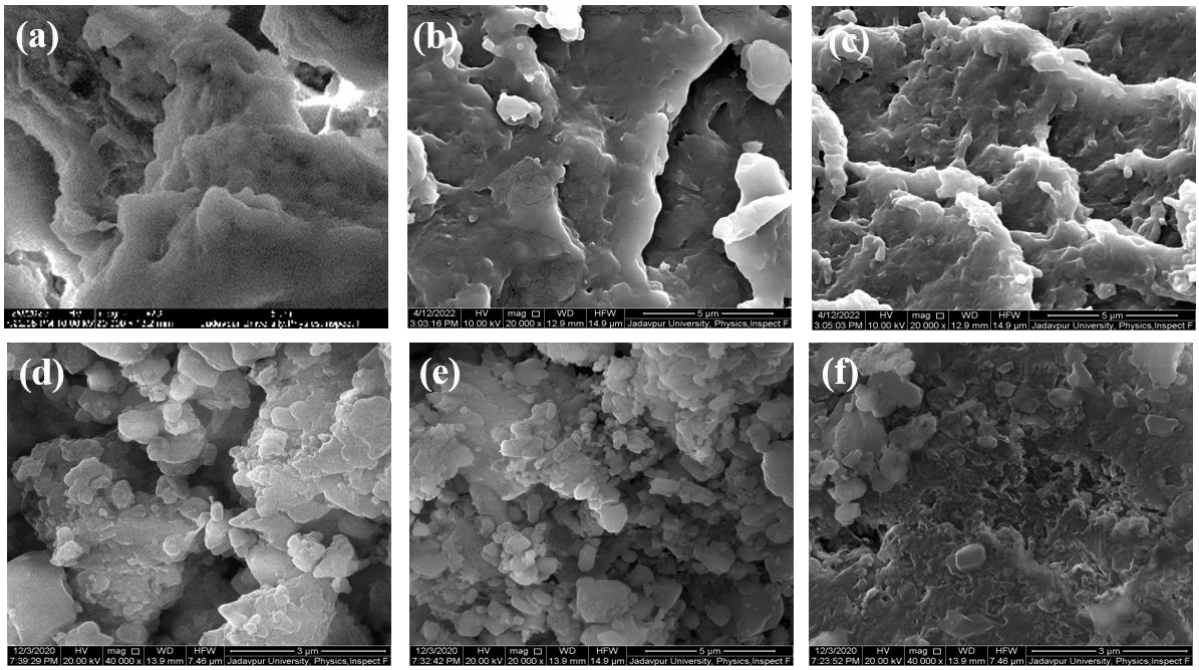

Figure 4.4: *FESEM image of (a) GG-PH-1, (b) GG-PH-2, (c) GG-PH-3, (d) GG-PH@PIP-1, (e) GG-PH@PIP-2, (f) GG-PH@PIP-3.*

FESEM image revealed the porous surface morphologies of our samples. Irregular, discontinuous, and flaky microporous surface structures appeared in the images captured from GG-PH nanocomposites (figure. 4.4 a, 4.4 b, 4.4 c) and GG-PH@PIP nanocomposites (figure. 4.4 d, 4.4 e, 4.4 f). From the FESEM image, noticeable differences can be observed between PIP-loaded composites and the bare polymer composites.

4.3.1.7 Transmission electron microscopy (TEM) analysis

TEM image demonstrates the mono-dispersed, round shaped nanoparticles. As shown in figure 4.5 (a), GG-PH@PIP-1 particles is smooth surfaced, spherical shaped and diameter was about (219 ± 6) nm.

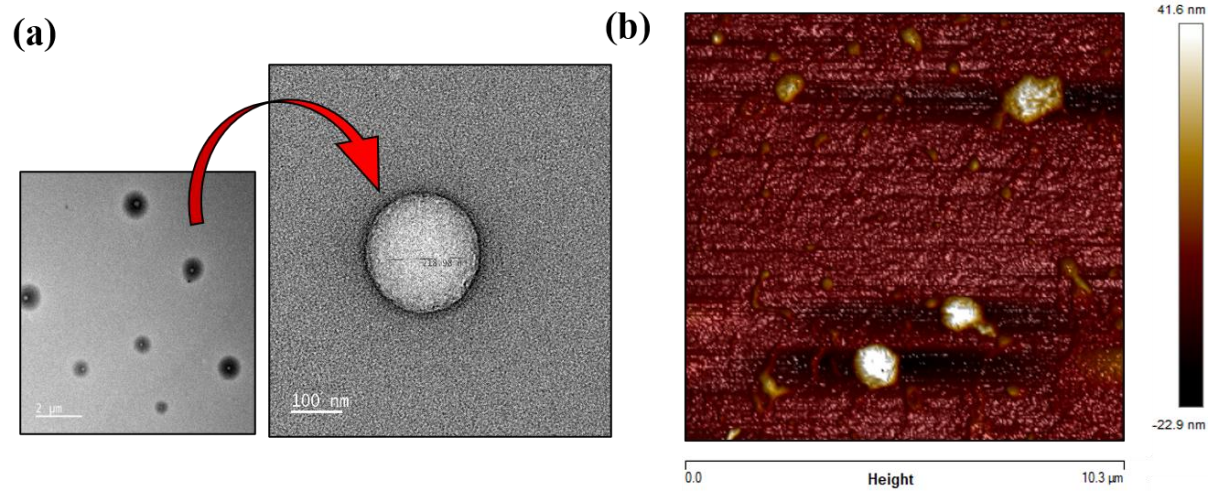

Figure 4.5: *(a) TEM image of GG-PH@PIP-1 (b) AFM image of GG-PH@PIP-1.*

4.3.1.8 Atomic force microscopy (AFM) analysis

AFM image (figure 4.5 b) illustrate that almost all particles were spherical shaped and singly dispersed. By AFM, the sizes of the GG-PH@PIP-1 were measured to be (255 ± 10) nm. In both TEM and AFM images, the nanocomposites appeared to be spherical shaped and particle size was in the overlapping zone.

4.3.1.9 Loading percentage of PIP in GG-PH@PIPs

The loading efficiencies of any therapeutic in the composite matrix highly depend on the molecular structure and the interactions between the composite and therapeutics used. The percentage of PIP loaded within GG-PH was determined spectrophotometrically (as mentioned in subsection 1.7.3.9). PIP has known absorption maxima at 344 nm.[173] The loading percentage of PIP is determined to be 79 ± 1.66 % in GG-PH@PIP-3 which is the highest among all three PIP-loaded nanocomposites. Table 4.1 shows the percentage of loaded PIP in nanocomposites which indicated very good incorporation capacity. Condensed porous mesh of biopolymeric nanocomposite constrained the release of PIP which in turn results in high loading efficiency of hydrophobic PIP.[297]

4.3.1.10 Release profile of PIP from GG-PH@PIPs

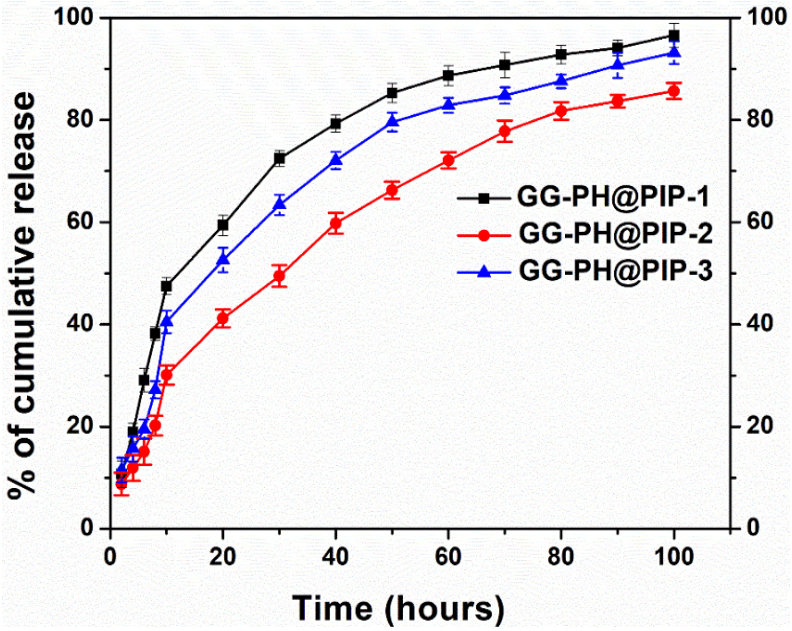

Figure 4.6: *Time-dependent release study of PIP from GG-PH@PIPs at physiological pH.*

The rate of release of PIP from GG-PH@PIP nanocomposite was determined by dialysis method mentioned in subsection 1.7.3.10. We examined whether GG-PH@PIPs can show controlled and sustained release of PIP in physiological pH (pH 7.4) throughout 100 hrs which is desirable for therapeutic applications. The *in vitro* release of PIP from GG-PH@PIPs occurred in two steps, i.e., a rapid burst release within the first 20 hrs followed by slow and controlled leaching over 100 hrs (figure. 4.6). At physiological pH, after 24 hrs the release percentage of PIP from GG-PH@PIP-1 is approximately 65% which was found to be greater than GG-PH@PIP-2 (approx. 45%) and GG-PH@PIP-3 (approx. 56%). In the case of *in vivo* experiments, drug release behaviour was supposed to be faster at the initial stage compared to the later stage of administration.[298] Initial rapid release of therapeutics could be sufficient to inhibit the primary infection and subsequent slower and sustained release might maintain the concentration of therapeutic agent required to alleviate further infection. Moreover, the release profile of PIP from GG-PH@PIPs nanocomposites ascertained sustained but faster release which confirms the effectiveness of our synthesized nanocomposites to release an adequate amount of therapeutics at the site of application.

4.3.2 Evaluation of antibacterial activity

4.3.2.1 Determination of MIC and MBC

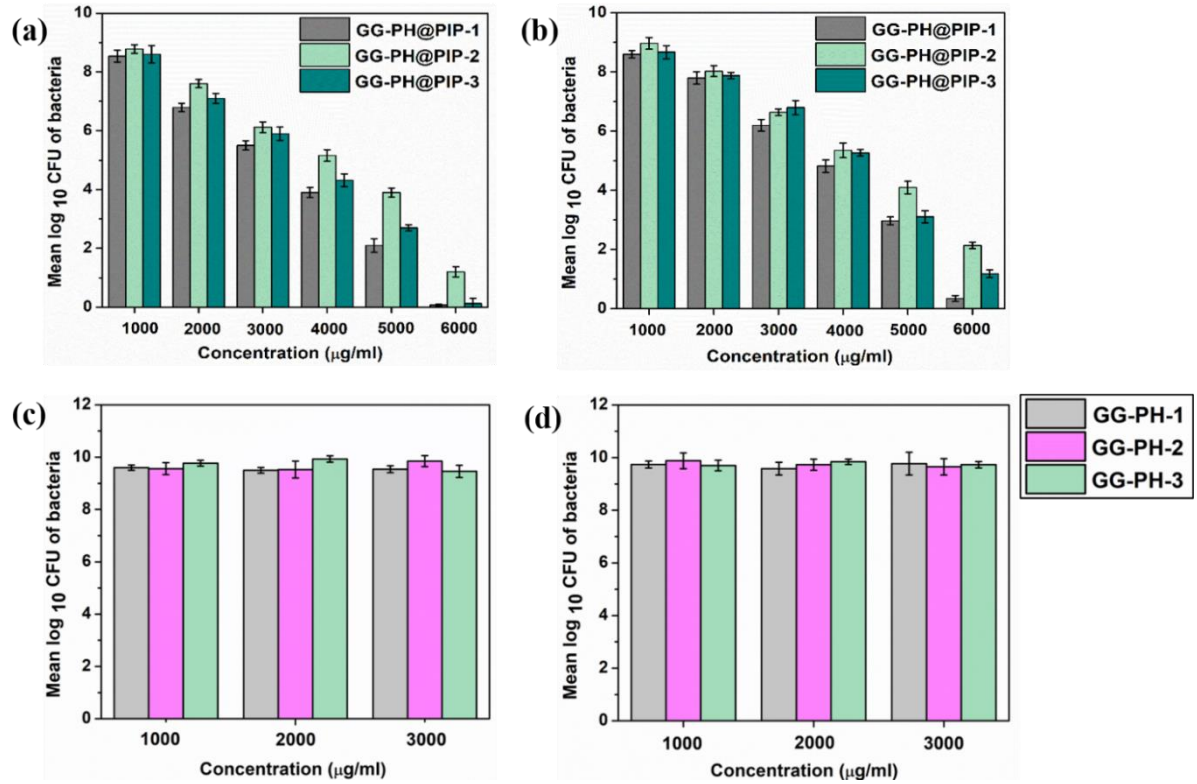

Figure 4.7: *Antibacterial activity of GG-PH@PIPs on (a) S. aureus and (b) P. aeruginosa. Graphical representation of the antibacterial activity of GG-PHs on (c) S. aureus and (d) P. aeruginosa.*

To study the antibacterial potentials of GG-PH@PIPs the bacterial cells were incubated with different concentrations (1000, 2000, 3000, 4000, 5000, 6000 µg/mL) of GG-PH@PIPs and their survivability was evaluated from colony counting method mentioned in subsection 1.7.4.1. Figure 4.7 (a) and 4.7 (b) demonstrate that GG-PH@PIP-1 have better antibacterial potential compared to GG-PH@PIP-2 and GG-PH@PIP-3. In figure 4.7 (a) the result showed that at 3 mg/mL, the bacterial cell population before and after incubation were almost equal i.e., the MIC of GG-PH@PIP-1 for *S. aureus* was around 3 mg/mL. At concentrations of 4, 5 and 6 mg/mL, around 95%, 100% and 100% mortality were observed respectively. Therefore, MBC of GG-PH@PIP-1 was between 4 and 5 mg/mL. Figure 4.7 (b) demonstrates that MIC values of GG-PH@PIP-1 for Gram-negative *P. aeruginosa* is about 4 mg/mL. At concentrations of 4, 5 and 6 mg/mL, around 89, 93 and 99.9% cells were killed respectively. Therefore, MBC of GG-PH@PIP-1 was around 6 mg/mL. The antimicrobial activities of GG-

PHs were evaluated using different concentration (1000, 2000, 3000 µg/mL) of GG-PH-1,2,3. Results portrayed that bare polymer composites (GG-PH-1,2,3) have no antibacterial activity against *S. aureus* and *P. aeruginosa* (presented in figure 4.7 c and d respectively) i.e. bacterial growth rate was not retarded by the treatment of bare GG-PH. The above antibacterial experiments confirmed that GG-PH@PIP could be a very effective antibacterial agent against different Gram-negative and Gram-positive bacterial strains. According to our experimental investigation, GG-PH@PIP has potential bactericidal properties against both Gram-positive and Gram-negative strains.

4.3.2.2 Determination of ROS generation

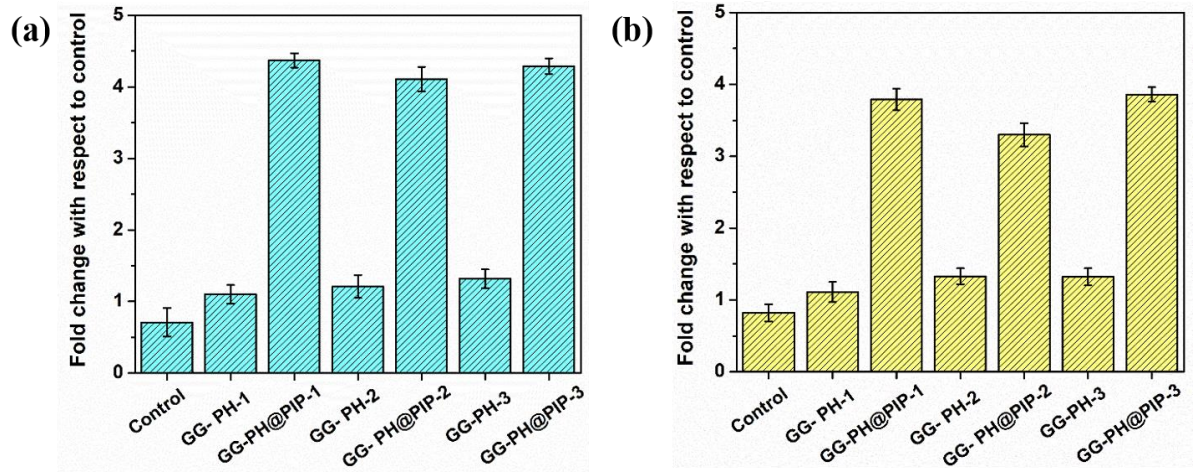

Figure 4.8*: Graphical representation of bacterial ROS generation by DCFDA assay in case of (a) S. aureus (b) P. aeruginosa.*

To evaluate the bacterial ROS generation $DCFH_2$-DA dye was used and fluorescence intensity was measured (as mentioned in subsection 1.7.4.5). ROS mediated oxidative stress is a major cause of disruption of cellular integrity mediated cell mortality.[299] Figure. 4.8 (a) and 4.8 (b) displayed the higher ROS generation in GG-PH@PIPs treated *S. aureus* and *P. aeruginosa* cells respectively compared to GG-PHs treated cells. Due to ROS accumulation in cells, bacterial membrane lipids are oxidized which initiates lipid peroxidation and free radical chain reactions which will disrupt the integrity of membrane-bound proteins.[300]

4.3.2.3 Bacterial morphology study by FESEM

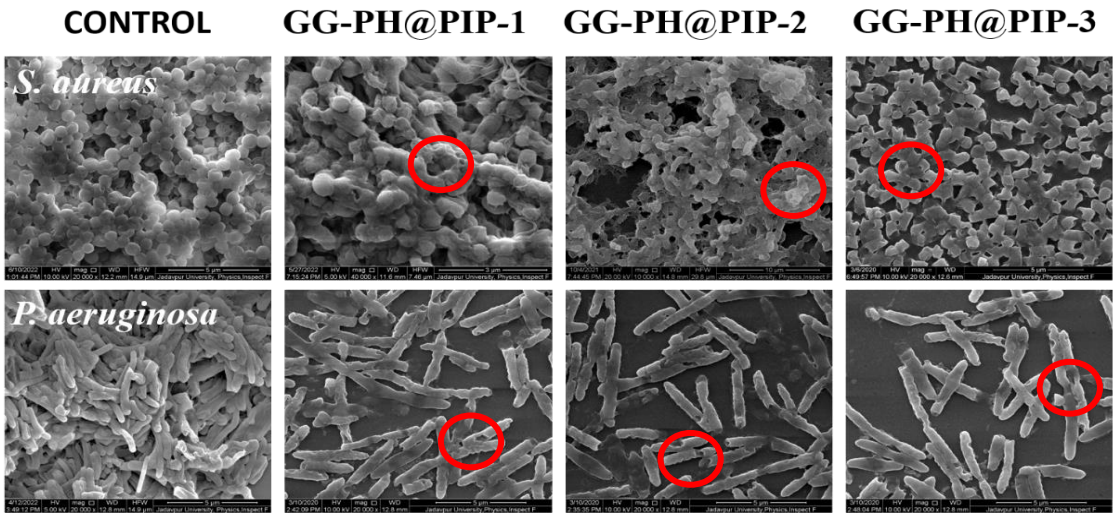

Figure 4.9: *FESEM image displaying morphological changes of bacterial cells where red circled parts indicate ruptured and damaged cell membrane.*

FESEM images of bacterial cells, exposed to MIC dose of GG-PH@PIPs, displayed ruptured surface with the damaged cell membrane (figure. 4.9) compared to the undamaged membrane of the control bacterial cells in the case of both strains. *S. aureus* cells appeared to be shrunk and surface disintegration of the cells was detected. Similar surface disintegrations and cell perforations were observed in treated *P. aeruginosa.* Thus, red circled parts marked in FESEM images confirmed membrane leakage which trigger the release of cellular materials through perforated and disintegrated cell membranes.[301] These must be the definitive causes of bacterial cell death after being treated with GG-PH@PIPs.

4.3.3 Assessment of anticancer property

4.3.3.1 Cytotoxicity Study

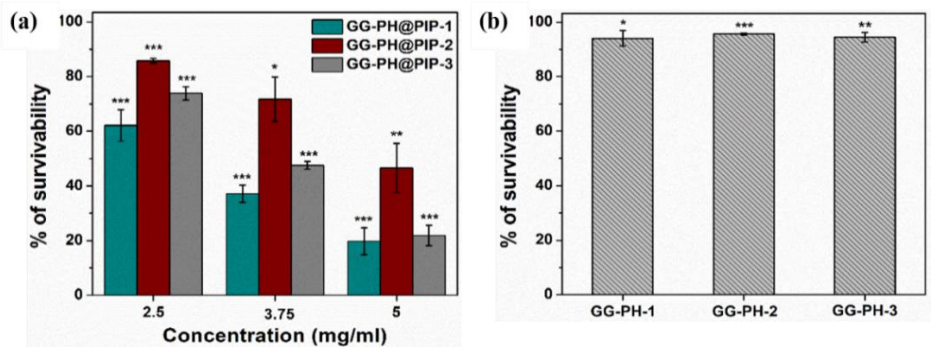

Figure 4.10: *Survivability of A549 cells after treatment by MTT assay with (a) GG-PH@PIPs and (b) GG-PHs.*

The *in vitro* anticancer properties of the nanocomposites were evaluated by MTT assay to the human A549 cell line. The A549 cells were treated with various concentrations of GG-PH@PIPs (2.5, 3.75, 5 mg/ mL) and were afterward followed by MTT assay (as described in subsection 1.7.5.2). Figure 4.10 (a) demonstrates that the cells treated with GG-PH@PIPs resulted in significant cell death. Bare nanocomposites i.e. GG-PHs did not exhibit any marked cell death after being treated with a 5 mg/ mL concentration of GG-PHs (the results are presented in Figure 4.10 b). At the highest concentration, GG-PH@PIP-1 treated cells exhibited 19.7% cell survivability whereas 46.5% and 21.9% cell survivability are observed in the case of GG-PH@PIP-2 and GG-PH@PIP-3 respectively. The IC_{50} value of GG-PH@PIP-1 was assessed to be 3.14 mg/mL which is lower than the IC_{50} values of the other two PIP incorporated samples (table. 4.2).

Table 4.2: *IC_{50} Value of GG-PH@PIPs and corresponding effective concentration of PIP.*

Nanocomposite	*IC_{50} Value (mg/mL)*	*Effective concentration of PIP (µg/mL)*
GG-PH@PIP-1	3.14	76.3
GG-PH@PIP-2	4.87	98.8
GG-PH@PIP-3	3.64	84.3

4.3.3.2 Study of Intracellular ROS generation

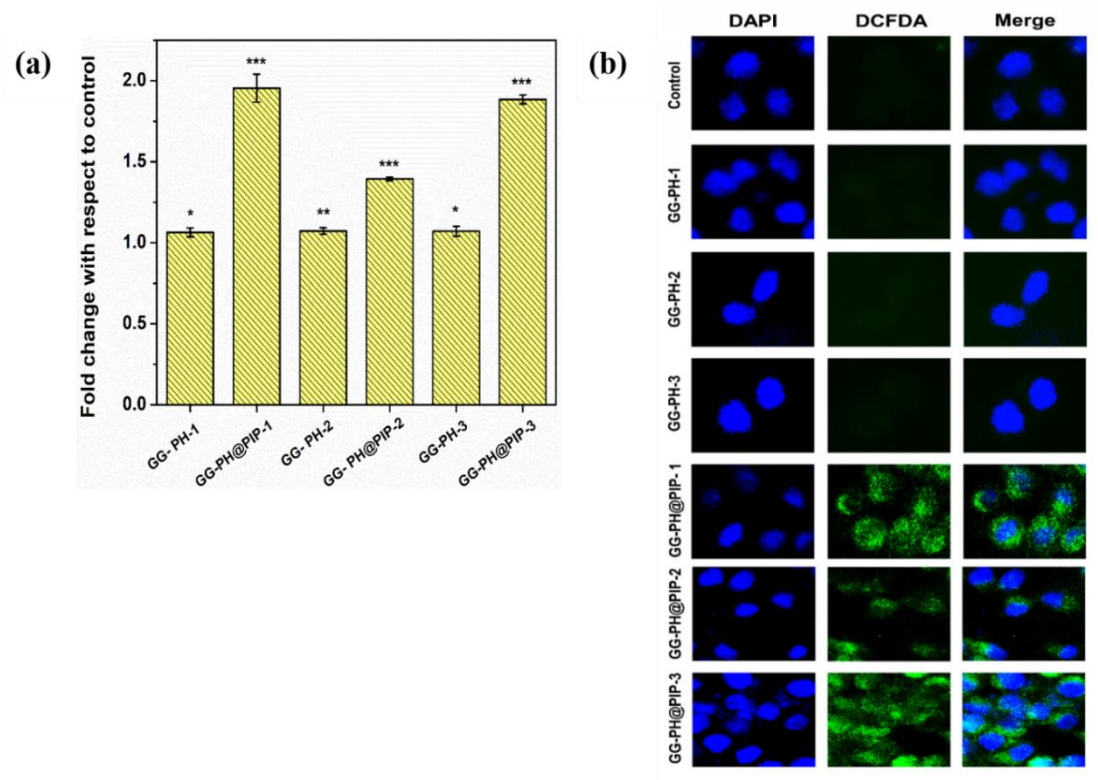

Figure 4.11: *(a) Graphical representation of ROS mediated fluorescence intensity in A549 cell line. (b) Fluorescence microscopic image of intracellular ROS generation for A549 cell line.*

To measure intracellular ROS generation in A549 cells after treatment with GG-PHs and GG-PH@PIPs (5 µg/µL each), $DCFH_2$-DA dye was used (as mentioned in subsection 1.7.5.3). GG-PHs treated cells showed very low amount of ROS generation almost similar to control cells whereas GG-PH@PIPs treated cells displayed a significant increase in ROS generation (figure 4.11 a and b). Estimated ROS content within the cells after treatment with nanocomposites indicated the highest oxidative stress in case of GG-PH@PIP-1 treated cells which was established by spectroscopically as well as by fluorescence microscopy.

4.3.4 Biocompatibility study

4.3.4.1 Cytotoxicity Study

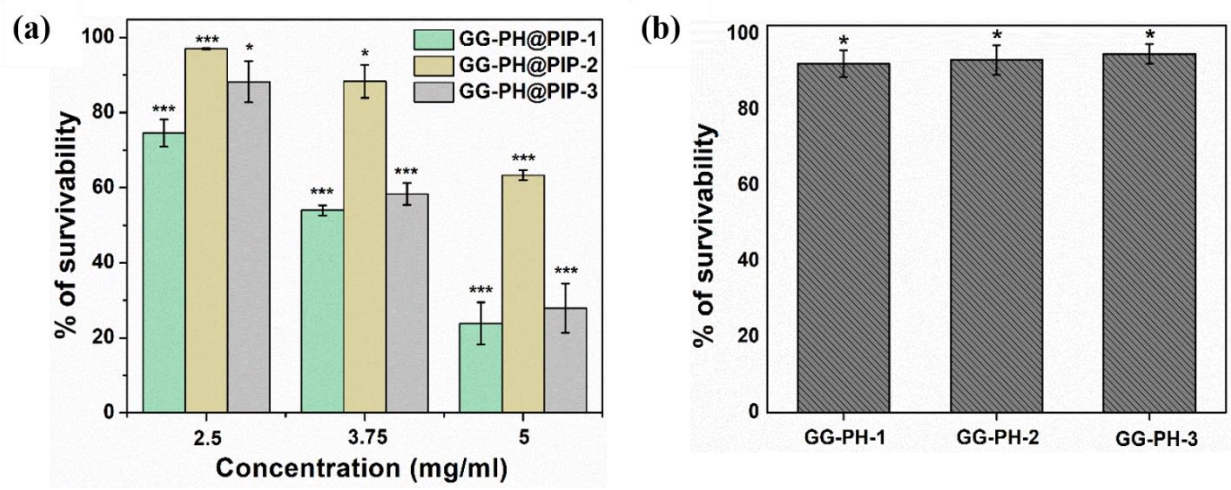

Figure. 4.12: *Graphical representation of MTT assay on WI38 cell line after treatment with (a) GG-PH@PIPs and (b) GG-PHs.*

To evaluate the biocompatibility of synthesized nanocomposites, *in vitro* cytotoxicity was estimated by MTT assay (as mentioned in subsection 1.7.5.2). Human lung fibroblasts (WI38) cells were exposed to GG-PH@PIPs with three different concentrations (2.5, 3.75, 5 mg/mL) and GG-PHs at a concentration of 5 mg/mL each. In WI38 cells, treatment with GG-PH@PIP-2 showed the highest biocompatibility. At 2.5 mg/mL dose, GG-PH@PIP-1 exhibited 54%, GG-PH@PIP-3 showed 58.3% cell survivability whereas GG-PH@PIP-2 treatment exhibited 88.3% cell survivability (figure. 4.12 a). In WI38 cells, treatment with GG-PH-1 showed 92% cell survivability whereas treatment with GG-PH-2 and GG-PH-3 exhibited respectively 93% and 94.7% cell survivability (figure. 4.12 b). From experimental results we can conclude that GG-PHs are completely biocompatible and used biopolymers do not exert any cytotoxic effect

on cells whereas in case of GG-PH@PIPs cytotoxicity can be avoided by standardize the dose of nanocomposite used.

4.3.4.2 Study of Intracellular ROS generation

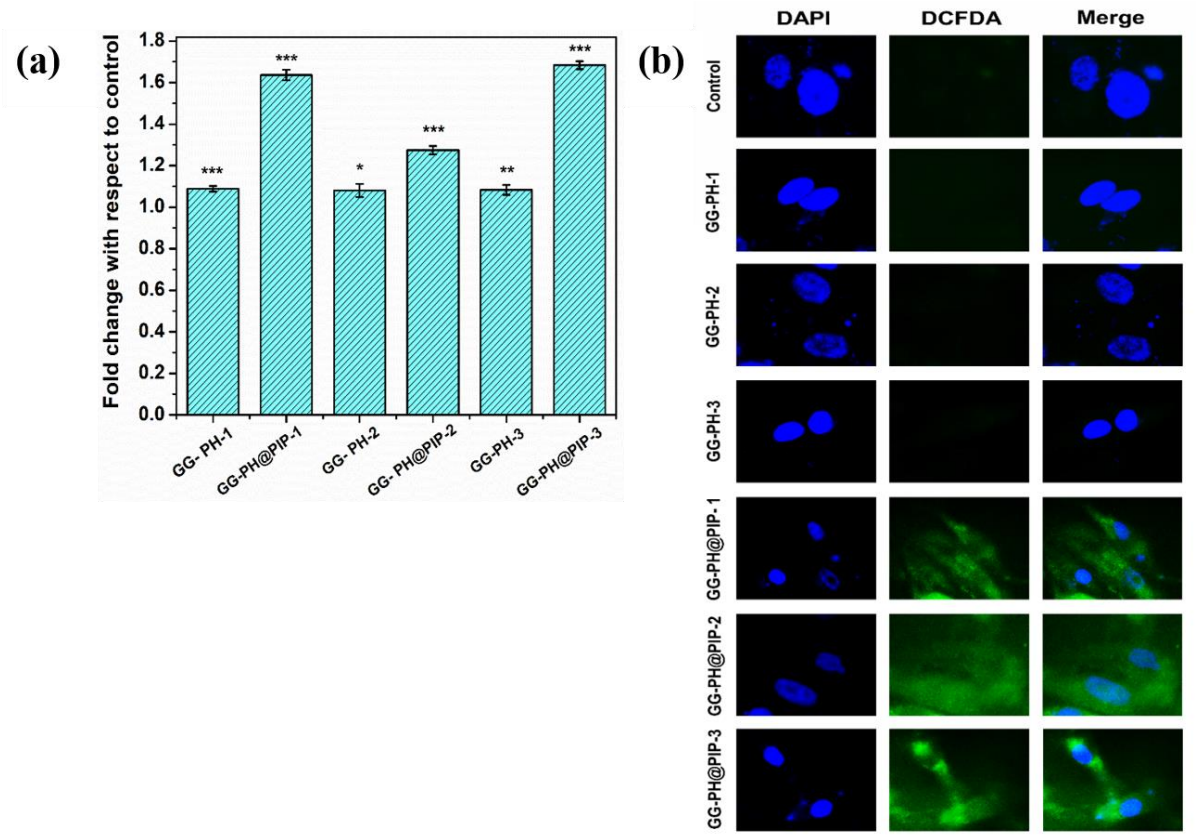

Figure. 4.13: *(a) ROS generation study in WI38 cell line. (b) Fluorescence microscopic image displayed ROS generation in WI38 cell line*

Intracellular ROS generation was evaluated when WI38 cells were exposed to GG-PH@PIPs and GG-PHs (at a concentration of 5 mg/mL each) and fluorescence intensity was measured spectroscopically (as mentioned in subsection 1.7.5.3). The graphical representation of intracellular ROS generation study (figure. 4.13 a) showed higher amount of ROS generation in GG-PH@PIPs treated cells compared to GG-PHs treated cells. Figure. 4.13 (b) exhibited a marked increase in green fluorescence in GG-PH@PIPs treated cells compared to the control and GG-PHs (bare nanocomposites) treated cells which established the ROS-mediated stress in GG-PH@PIPs treated cells. Experimental results confirmed the non-cytotoxic properties of GG-PHs in normal human lung fibroblasts (WI38) but after encapsulation of PIP the doses of GG-PH@PIPs nanocomposite should be standardized and maintained carefully to avoid the PIP-mediated side effects.

4.4 Conclusion

This chapter discussed about nanonization of a multifunctional bioactive compound PIP by loading it in the biopolymeric nanocomposite. The synthesis procedure was economical, simple and robust using only plant-derived polymers. Natural polysaccharides such as GG and PH mucilage derived nanocomposite are emerging drug delivery systems that offer promising advantages such as non-toxicity, non-immunogenicity, excellent swelling ability, biocompatibility, and most importantly having an innate pharmacological property of polysaccharides. The synthesized nanocomposites exhibited very high loading capacity i.e. up to 83% of PIP (added as precursors) was loaded in the nanocomposites. The zeta potential which signifies the stability of nanoparticles was about (-) 31 mv. The Zeta potential and loading percentage of PIP in nanocomposites decreased gradually with the change in the ratio of the precursor polymers and mucilage. The sustained release profile of PIP from GG-PH@PIPs nanocomposites confirms the efficiency of our synthesized nanocomposites. As we incorporate a very low amount of PIP in a polymer composite, a lesser concentration of PIP was found to exhibit potential antibacterial and anticancer activity. GG-PH@PIP nanocomposites have shown promising bactericidal capacities against Gram-negative *Pseudomonas aeruginosa*, and Gram-positive *Staphylococcus aureus* as well as these nanocomposites were found to have significant anticancer properties against human A549 cell lines. Experimental results also confirmed the moderate biocompatibility of these phyto-nanocomposites against normal human lung fibroblasts (WI38) cell lines. From experimental outcomes, it can be said that PH mucilage can be utilized to formulate effective bio-polymeric drug carrier in combination with other biomaterials if properly standardised. PIP, being a predominant dietary alkaloid with pro-oxidant properties might be convenient in development of a potential nanomedicine. As disease treatment frequently requires multi-dimensional drugs to combat with wide range of complications, the development of a multiple-response biopolymer-based nanocomposite like GG-PH@PIP is an urgent need to explore diverse biomedical applications.

Chapter 5

Piperine Incorporated Multi-Functional Guar Gum and Carboxymethyl Cellulose Nanocomposite: An *in vitro* Study on Bacteria and C6 glioma Cells

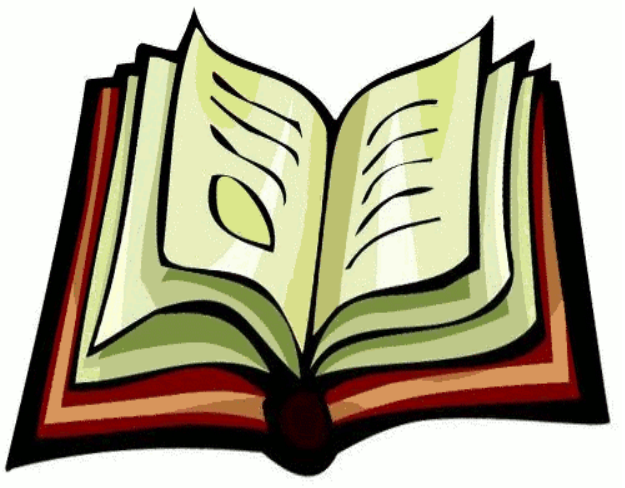

Summary

Guar gum-carboxymethyl cellulose derived piperine nanocomposite (GG-CMC@PIP) i.e., piperine loaded in guar gum-carboxymethyl cellulose composite was synthesized to develop a phytochemical-based nanomaterial by following a simple synthetic procedure. In this study, piperine was nanonized by entrapping within guar gum-carboxymethyl cellulose derived nanocomposite (GG-CMC). GG-CMC@PIPs were of (i) size (25 ± 3) nm by TEM, (ii) zeta potential (−) 33.1 ± .73 mV and (iii) entrapment efficiency 86 ± .46 %. High loading percentage of piperine in polymeric nanocomposites revealed excellent incorporation efficiency. In addition, the release behaviour of piperine from nanocomposites exhibited sustained but faster release pattern. Minimal inhibitory concentration (MIC) and minimum bactericidal concentration (MBC) of piperine- loaded nanocomposite on Gram-positive *Enterococcus faecalis* and Gram-negative *Escherichia coli, Pseudomonas aeruginosa* were in the range of 200–400 μg/mL. The nanocomposite also showed potential anticancer property against C6 glioma cell line. Excessive accumulation of reactive oxygen species (ROS), mitochondrial depolarization and higher degree of nuclear damage followed by increased mortality of C6 glioma cell were observed after the treatment with piperine loaded nanocomposite.

5.1 Introduction

There is a rising interest in the modifications and applications of biomaterials that can efficiently replace synthetic counterparts, particularly in the biomedical and pharmaceutical sectors. An important driving force to explore bio-based nanocomposites is to enhance the diversified possibilities of clinical applications of these natural compounds as well as introduce new interesting properties in biopolymeric composites. Plant derived polymers have immense applicability due to their outstanding inborn merits, such as biocompatibility, biodegradability and multifunctional applicability over synthetic polymers as well as they synergistically improve the functionality of constituent bio-materials.[302] Advanced plant-derived drug delivery systems (DDS) attract more attention in biomedical applications resolving drawbacks such as less effective rate of intestinal absorption, inefficient delivery mechanism at target site, poor solubility, and plasma inconsistency of phytocomponents.[285,286] Among the reported plant derived polysaccharides, chitosan, cellulose, guar gum, xanthan gum, alginate, and β-cyclodextrin have been efficaciously applied as a vehicle for drug encapsulation, targeted delivery and controlled release.[303] We have chosen guar gum and carboxymethyl cellulose for our study to develop bio-polymer derived nanocomposite.

Guar gum (GG) is processed from endosperm of a drought tolerant legume *Cyamopsis tetragonalobus,* which predominantly contains galactomannans.[85] GG swells to dissolves in polar solvent on dispersion by forming strong hydrogen bonds and used as a novel food additive, stabilizer, emulsifier, or thickener.[85,86] GG is degraded by *Clostridium butyricum*, a human commensal bacterium in the large intestine and prevent constipation, obesity, maintain bowel regularity, control diabetes and facilitate mineral absorption.[85,86] Carboxymethyl cellulose (CMC) is a cellulose derived hydrophilic polysaccharide possessing both carboxylate and hydroxyl groups with high chemical stability, pH-sensitivity, non-toxicity, and gel-forming properties.[121] CMC is a biocompatible macromolecule that has been used for DDS with the aim of sustained drug release.[122] It is reported that CMC has several biomedical applications such as wound healing, bioimaging, tissue engineering and drug delivery.[121]

According to World Health Organization (WHO), infectious diseases are the second important cause of universal death.[304] It is necessary to develop effective advanced multi-functional antibacterial material to alleviate the improper usage of conventional antibiotics. *Enterococcus faecalis* is a common enterococcal species associated with infections in humans and is one of the prevalent nosocomial pathogens.[305] Gram-positive *E. faecalis* resides in the gastrointestinal

as well as genitourinary tracts and is associated with bacteraemia, intra-abdominal infections, infective endocarditis, wound infections, endodontic diseases and urinary tract infections.[306] Generally, Gram-negative *Escherichia coli* is harmless and coexist in its human host with mutual benefit. However, specific pathogenic strains of *E. coli* are known to cause enteric/diarrhoeal disease, urinary tract infections and sepsis/meningitis.[307] Gram-negative *Pseudomonas aeruginosa* is an opportunistic pathogen capable of causing a range of infections including intra-abdominal infections, wound infections, urogenital sepsis and pneumonia in immunocompromised persons.[306]

Plant derived phytochemicals have been known to exert medicinal properties against numerous infectious disease due to presence of secondary metabolites.[141] Over past few decades, much attention has been given to explore "chemoprevention" by using bioactive phytocompounds for their protective role against bacterial infection, tumorigenesis, and proliferation of cancer .[290] For this study, piperine (1-[5-(1,3-Benzodioxol-5-yl)-1-oxo-2,4-pentadienyl] piperidine), a principal alkaloid extracted from the fruits of *Piper nigrum* and *Piper longum* plants have chosen as a bioactive phytochemical.[291] Diverse physiological effects of piperine (PIP) have been reported including enhanced digestion due to stimulation of gastric acid secretion, increased bioavailability of drugs by increasing their absorption, and decreasing drug metabolism by inhibition of cytochrome P450/CYP3A4.[308] Recent studies reported the cytotoxic nature of PIP for 4T1 mouse mammary carcinoma cell line and PC3 human prostate cancer cell line.[308] It is reported that PIP alone induced more potent cytotoxicity to Dalton's lymphoma ascites cells than the alcoholic extract *Piper longum*.[309] Studies showed the prooxidant property of PIP which is known to induces radical mediated mitochondrial pathway of apoptosis in Hep G2 cells.[292] In addition, PIP also functions as an inducer of apoptosis in rectal and colon cancer cells by ROS-mediated pathway.[163,293] Taken together, all these experimental reports suggest that PIP may possess therapeutic property in prevention or treatment of cancers.

Therefore, the present research was designed to study the effectivity of PIP as a promising pro-oxidant drug and offers a novel approach for the treatment of C6 glioma cells and a broad range of bacterial infections. The synthesised nanocomposites are well-characterized using XRD, FTIR, FESEM, AFM, TEM, TGA, DLS study, UV– Vis spectra and drug release dynamics etc to analyse the morphological, physical and chemical properties. We have chosen two plant derived polymers i.e. CMC and GG to synthesis a stable, multifunctional PIP incorporated nanocomposite to attain improved drug loading efficiency and sustained drug release

properties. Our experimental results report structural characterization and clinical efficacy of GG and CMC derived nanocomposites (GG-CMC) as well as PIP incorporated nanocomposites (GG-CMC@PIP). This study has focused on evaluating the anti-cancer potentials of GG-CMC@PIP against C6 glioma cells as well as bactericidal properties against Gram-positive *E. faecalis*, and Gram-negative *E. coli*, *P. aeruginosa* strains. A schematic representation of general mechanisms for antibacterial and anticancer mode of action of PIP loaded bio nanocomposite is illustrated in figure 5.1.

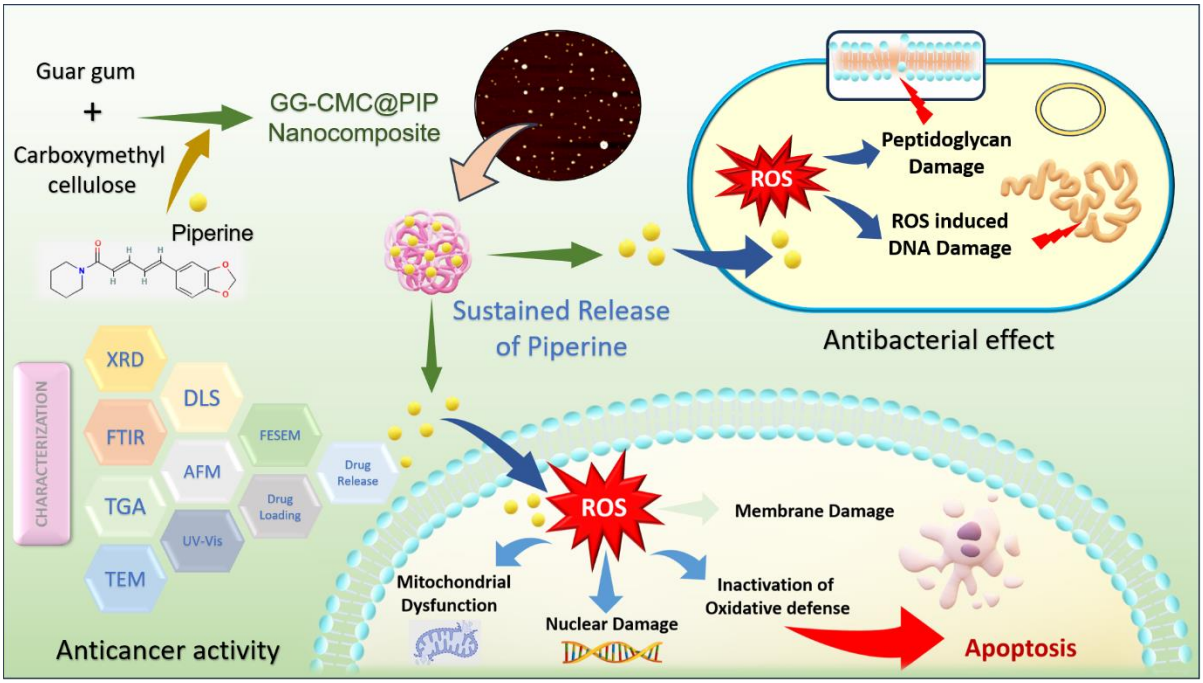

Figure 5.1: *Schematic representation of general mechanisms for antibacterial and anticancer mode of action of GG-CMC@PIP nanocomposites.*

5.2 Experimental section

5.2.1 Synthesis of bio-nanocomposite (GG-CMC@PIP)

GG-CMC@PIP nanocomposite contains the nano formulation of GG and CMC within which PIP was nanonized. Briefly, at room temperature 50 mg GG was dissolved completely in 50 mL distilled water to obtain a 0.1% (w/v) solution. 50 mg of CMC was dissolved in 50 mL of distilled water to form a 0.1 % (w/v) solution. Homogenized GG and CMC solutions were prepared using a magnetic stirrer for 2 hrs at room temperature. Under stirring condition, CMC solution was added slowly to GG solution. The resulting suspension was allowed to dry at 60ºC for 24 hrs. For the synthesis of PIP incorporated nanocomposite, 10 mL PIP solution was prepared in DMSO at a concentration of 5 mg mL^{-1} was added dropwise to the above-

mentioned polymer mixture and suspension was vigorously stirred for 8 hrs. The prepared sample were purified by centrifugation at 10,000 rpm for about 10 mins and obtained pellet was washed twice with Milli-Q water followed by drying at 60ºC in a vacuum desiccator. Ultrasonic bath sonicator is used for preparing suspensions of nanocomposite used in further studies.

5.2.2 Statistical analysis

All experiments were performed in triplicate and data were presented as mean ± standard deviation (SD) for each set of experiments. Single factor one-way statistical analysis was performed using ANOVA. To determine statistical significance, value of $p < 0.05$ was considered to indicate significance or otherwise mentioned.

5.3 Results and Discussion

5.3.1 Physical Characterizations

5.3.1.1 Fourier transform infrared spectroscopy (FTIR) analysis

Figure 5.2 (a) shows the FTIR spectra of GG, CMC, PIP, GG-CMC, GG-CMC@PIP. FTIR spectrum of GG showed peaks around at 798 cm^{-1} is assigned to (1–4), (1–6) linkage of galactose and mannose, at 1008 cm^{-1} is attributed to $–CH_2$ twisting vibration, 1647 cm^{-1} (ring stretching of mannose), 3304 cm^{-1} (O–H stretching vibration) and 2904 cm^{-1} (C–H stretching of CH_2 group).[244,245] According to the FTIR spectra of CMC a wide peak is observed at 3323 cm^{-1} (–OH stretching), at 2906 cm^{-1} (asymmetric $–CH_2$ stretching), at 1578 cm^{-1} (Asymmetrical COO–) and at 1413 cm^{-1} (Scissoring $–CH_2$).[310] Similar peaks are observed in FTIR spectra of GG-CMC and GG-CMC@PIP. As is shown in figure 5.2 (a) FTIR spectra of PIP have characteristic peaks at 928 cm^{-1} (C–O bond) and 1633 cm^{-1} (stretching of the amide group). The FTIR spectrum of PIP displays clear peaks at 1248 cm^{-1} corresponding to asymmetrical stretching of =C–O–C bond, at 1444 cm^{-1} which attributes to C=H stretching and at 2935 cm^{-1} which assigned to aromatic C–H stretching.[225] All these characteristic peaks were present in GG-CMC@PIP nanocomposite which representing the entrapment of PIP. The intensity of peaks was suppressed in FTIR spectra of GG-CMC@PIP, which indicates presence of minor ionic interaction and absence of significant chemical interaction between the PIP and polymer composite.

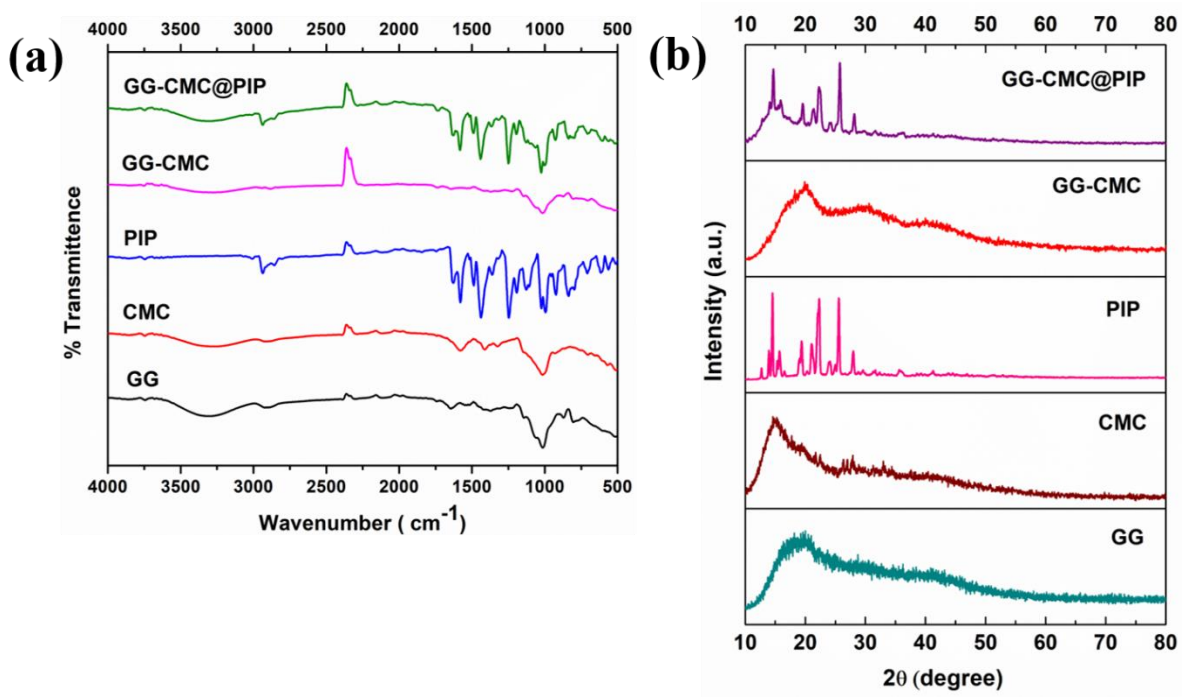

Figure 5.2: *(a) FTIR spectra, (b) XRD pattern of GG-CMC and GG-CMC@PIP nanocomposites.*

5.3.1.2. X-ray diffraction (XRD) study

XRD diffraction pattern of GG-CMC@PIP nanocomposite is shown in figure 5.2(b). GG, CMC and GG-CMC composites displayed a broad hallow which suggests the amorphous nature and low crystallinity of polymers. Disordered molecular arrangements with lack of distinguishable crystal lattices were observed in Amorphous forms.[280] GG showed a broad peak at 2θ = 20 º.[247] XRD diffraction peaks of CMC appeared at 2θ=15 º, 20 º, 34 º and 44 º.[311] XRD pattern of PIP showed diffraction peaks at 2θ = 14º, 22º, and 25º which displays resemblance with the typical pattern of PIP (JCPDS Card no: 00-043-1627).[248] XRD pattern of CMC and GG revealed that it has no crystalline structure while the XRD pattern of GG-CMC@PIP nanocomposites displayed sharp peaks represents gaining of crystalline nature due to the introduction of PIP.

5.3.1.3 Thermal gravimetric analysis (TGA)

TGA thermograms of GG-CMC, GG-CMC@PIP nanocomposites are shown in figure 5.3(a). The curves elucidate thermal stability and the decomposition rate. TGA curve of GG-CMC and GG-CMC@PIP displayed almost similar pattern and GG-CMC had a slower slope. The degradation has completed in two stages with increasing temperature. The initial decomposition involved a small weight loss which is due to the evaporation of moisture and

adsorbed surface water. According to the thermogram of GG-CMC and GG-CMC@PIP, the initial degradation of mass at around 40–150ºC is almost 10.5%, and 4% respectively. The second step of sharp degradation is associated with the pyrolysis, volatilization, and combustion of organic molecules present in the nanocomposites. The second decomposition showed more significant weight loss which is about 40.01% (temperature range 175–320ºC) in GG-CMC and about 61.41% (temperature range 183-330ºC) in GG-CMC@PIP. According to the thermograms of GG-CMC and GG-CMC@PIP, at 400 ºC the total weight loss of samples was 59% and 72% respectively.

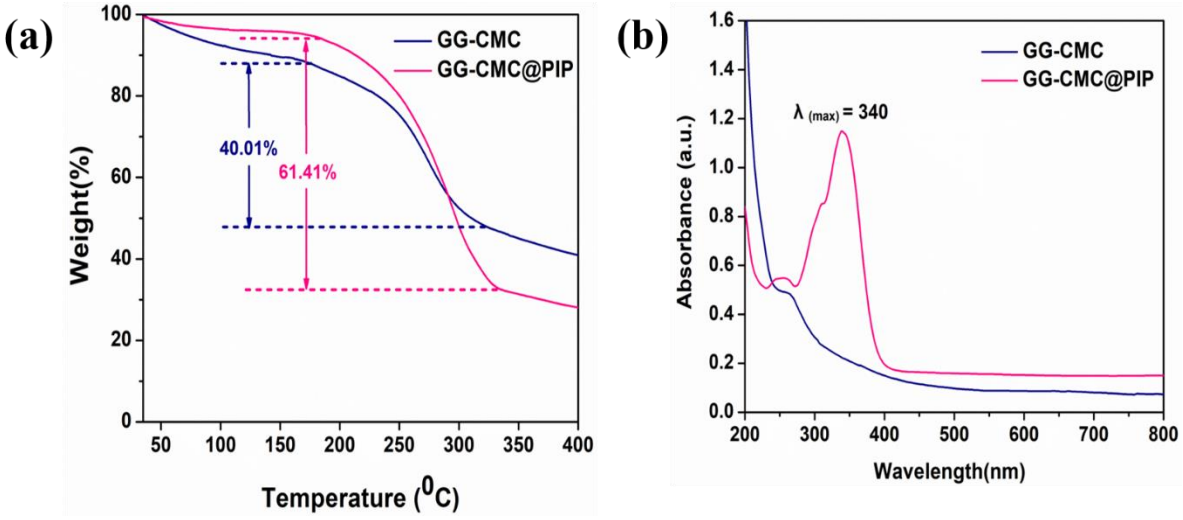

Figure 5.3: *(a) TGA curve and (b) UV-Vis spectra of GG-CMC and GG-CMC@PIP nanocomposites.*

5.3.1.4 UV–visible spectroscopy

The UV–vis spectra of GG-CMC and GG-CMC@PIP nanocomposites is shown in figure 5.3(b). PIP has a prominent characteristic peak (λmax) at 342–345 nm.[173] As observed in the spectra, GG-CMC@PIP exhibited a prominent and strongest peak at 340 nm, followed by a less intense peak at around 310 nm, whereas between 248 and 256 nm a low-intensity absorption band has been observed which established the successful incorporation of PIP into the nanocomposite.

5.3.1.5 Determination of size and shape of nanocomposites

DLS study determine the hydrodynamic diameter which includes the size of core particle together with the thick hydration layer around it. So, the hydrodynamic diameter measured in DLS study was always larger than the definite size of any particle. Therefore, actual size and shape of our synthesized nanocomposites were determined by FESEM, TEM and AFM. Poly

dispersity index (PDI) value represented the dispersibility and efficacious synthesis of nanoparticles. The mean size of the GG-CMC@PIP particle, measured by DLS instrument, was found to be about 300 nm with a poly dispersity index (PDI) value of .291. Lower PDI values of GG-CMC@PIP demonstrates the mono-dispersed and almost equal-sized nanocomposite suspension.

The zeta potential (ζ) of GG-CMC@PIP was found to be (−) 33.1 ± .73 mV. The magnitude of zeta potential implies the potential stability of nanocomposites. Negative zeta potential demonstrates the negative surface charges on GG-CMC@PIP. Higher positive or negative ζ value of nanoparticles prevent agglomeration whereas stability is compromised in decreased value of ζ by inducing aggregation of particles. As ζ value > ± 30 mV of any nanoparticle is considered as stable, therefore, GG-CMC@PIP nanocomposite can be considered stable enough for biomedical applications.[296]

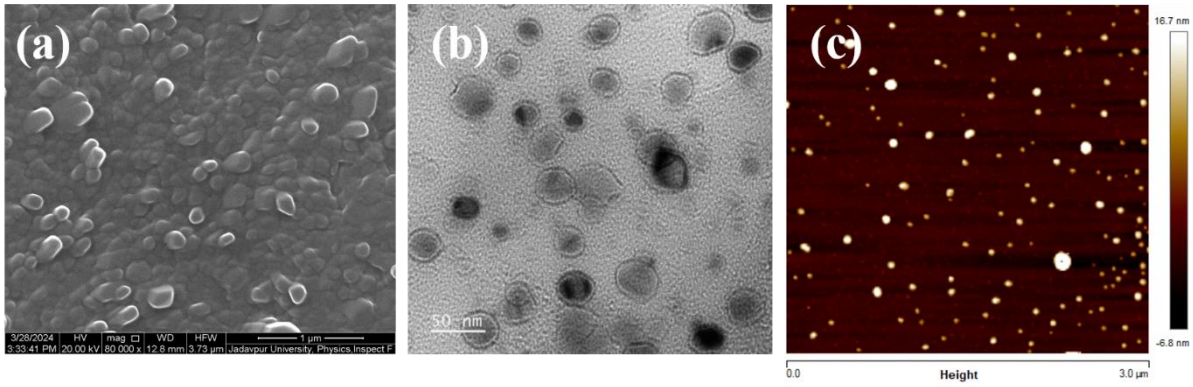

Figure 5.4: *(a) FESEM image (b) TEM image (c) AFM image of GG-CMC@PIP.*

FESEM image of GG-CMC@PIP illustrated almost spherical morphologies of nanocomposites with smooth, microporous surface structures (figure 5.4 a).

In TEM image, GG-CMC@PIP particles are appeared to be spherical shaped with about (25 ± 3) nm in diameter shown in figure 5.4 (b). TEM image demonstrates round shaped mono-dispersed particles.

AFM image (figure 5.4 c) revealed that almost all spherical shaped particles are singly dispersed. According to AFM image, the sizes of the GG-CMC@PIP were measured to be (55 ± 4) nm. All three images of FESEM, TEM and AFM exhibited the synthesized nanocomposites were spherical in shape.

5.3.1.6 Loading percentage of PIP in GG-CMC@PIP

The percentage of PIP loaded within GG-CMC was determined spectrophotometrically (as mentioned in subsection 1.7.3.9). PIP has known absorption maxima at 344 nm.[173] Loading percentage is determined to be 86 ± .46 % i.e. about 86 ± .46 % precursor PIP got loaded within the GG-CMC@PIP. The loading efficiency of any drug in composite polymer matrix are depend on the molecular interaction pattern between the polymer-composite and therapeutics used. High drug loading efficiency of PIP in nanocomposites indicated very good incorporation capacity. Condensed porous structure of nanocomposite may restrict the dissociation of PIP which can cause high drug loading efficiency of PIP loaded nanocomposites.[297]

5.3.1.7. Release profile of PIP from GG-CMC@PIP

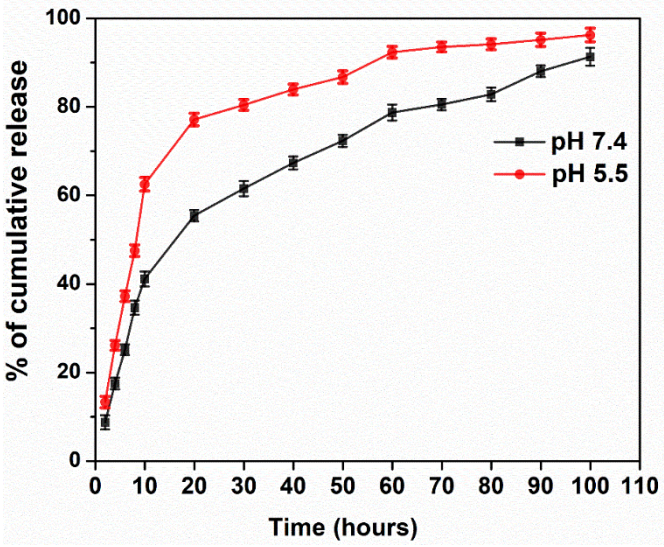

Figure 5.5: *Graphical representation of time-dependent release study of PIP from GG-CMC@PIP.*

The *in vitro* release behaviour of PIP from GG-CMC@PIP nanocomposite was assessed by dialysis method mentioned in subsection 1.7.3.10. Drug release profiles were performed in physiological pH at 7.4 and in acidic at pH 5.5. As shown in figure 5.5 we measured the release pattern of PIP from GG-CMC@PIP over a period of 100 hrs which is crucial for clinical applications. The *in vitro* release behaviour of incorporated therapeutic from GG-CMC@PIP occurred in two steps. The release pattern showed an initial burst release in the first 10 hrs followed by a slow and sustained leaching over a period of 100 hours (figure 5.5). After 24 hrs at pH 5.5 (acidic condition), the estimated release percentage of PIP (approx. 78.4%) was found to be greater than at physiological pH (approx. 58.2%). At pH 5.5 about 96% of PIP was released over a period of 100 hrs. The interaction pattern between therapeutics and polymer

composite modulates drug release behaviour. PIP that is adsorbed on to the surface of the nanocomposite might be the reason for initial bulk release. This initial release is adequate to inhibit the infectious agents and subsequent controlled release might maintain the concentration of therapeutic which is essential to alleviate spreading of infection. The release of PIP from GG-CMC@PIP was observed to be faster in acidic pH than physiological pH. As some tumours and cancer cells have poor blood vessel architecture, cellular metabolic end products tend to be accumulated in those cells resulting in lowering of pH. Hence, the accumulated nanocomposite can release its therapeutic content more efficiently in acidic pH.[312]

5.3.2 Evaluation of antibacterial activity

5.3.2.1 Determination of MIC and MBC

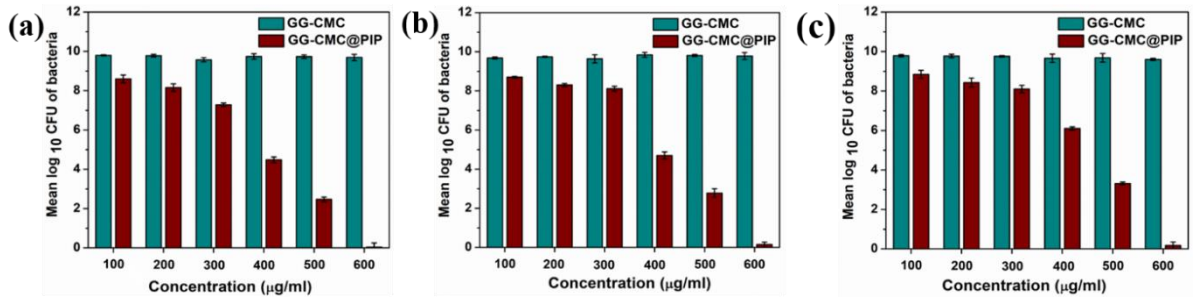

Figure 5.6: *Graphical representation of the antibacterial activity of GG-CMC@PIP on (a) Enterococcus faecalis (b) Escherichia coli and (c) Pseudomonas aeruginosa.*

To study the antibacterial potentials of GG-CMC and GG-CMC@PIP the bacterial cells were incubated with different concentrations (100, 200, 300, 400, 500, 600 µg/mL) of GG-CMC@PIP in nutrient medium and their survivability was evaluated from colony counting method on agar plates (as mentioned in subsection 1.7.4.1). The results depicted that GG-CMC does not have any potential antibacterial properties against all three bacterial strains i.e. Gram-positive *E. faecalis* and Gram-negative *E. coli* and *P. aeruginosa* as the growth rate of bacterial cells was not at all affected after treatment with GG-CMC. In figure 5.6 (a) the result portrayed that bacterial cell viability of Gram-positive *E. faecalis* is increased slowly below the concentration of 200 µg/mL of GG-CMC@PIP. The MIC of GG-CMC@PIP for *E. faecalis* was found between 200 µg/mL and 300 µg/mL. At concentrations of 400 µg/mL and 500 µg/mL, around 99.9% and 100% *E. faecalis* cells were killed respectively. Therefore, MBC of GG-CMC@PIP for *E. faecalis* was around 400 µg/mL. Figure 5.6 (b) demonstrates that MIC values of GG-CMC@PIP for Gram-negative *E. coli* was between 300 µg/mL and 400 µg/mL. At concentrations between 400 µg/mL, 500 µg/mL and 600 µg/mL, 97 %, 99.9% and 100%

cells were killed respectively. Therefore, MBC of GG-CMC@PIP for *E. coli* was around 500 µg/mL and. Figure 5.6 (c) demonstrates that MIC values of GG-CMC@PIP for Gram-negative *P. aeruginosa* was between 300 µg/mL and 400 µg/mL. At concentrations of 400, 500 and 600 µg/mL, around 98, 99.9 and 100% cells were killed respectively. Therefore, MBC of GG-CMC@PIP for *P. aeruginosa* was around 500 µg/mL. Thus, the above experimental results clearly demonstrate that the GG-CMC@PIP may come out as a potential antibacterial compound against a broad range of bacterial strains. Thus, nanonization of PIP through its loading within GG-CMC helped to gain the effective bactericidal property over the bulk PIP. However, our experimental investigations proved GG-CMC@PIP as a potential bactericidal nanocomposite against both Gram-positive and Gram-negative strains.

5.3.2.2 Estimation of bacterial ROS generation

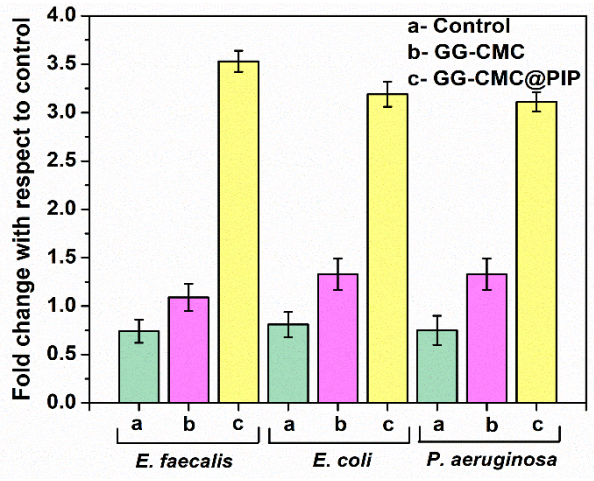

Figure 5.7: *Graphical representation of bacterial ROS generation by DCFDA assay.*

The extent of intracellular reactive oxygen species (ROS) production in bacterial cells was assessed using $DCFH_2$-DA as a visual indicator inside the cell, according to the spectrofluorimetric method (as mentioned in subsection 1.7.4.5). Reactive oxygen species (ROS) include highly reactive molecules (Peroxides, superoxide, hydroxyl radical, singlet oxygen) formed by the inappropriate transferring of electrons to O_2.[313] Bacterial cells are vulnerable to elevated intracellular ROS level as it causes disruption of cellular integrity releasing the cellular components like DNA, RNA, lipids, and proteins.[299] From figure 5.7 we found a remarkable difference in the intracellular accumulation of ROS between the GG-CMC@PIP treated and GG-CMC treated cells. In this regard, the control set (not exposed to nanocomposites) showed the lowest intracellular ROS generation. The results further revealed

that the maximum ROS accumulation was observed when treated with GG-CMC@PIP (~4.8, 3.9 and 4.1-fold higher than control in case of *E. faecalis*, *E. coli* and *P. aeruginosa* respectively). Thus, the result indicated that our synthesised PIP incorporated nanocomposite increases the accumulation of ROS in the test organism considerably that cause bacterial cell death.

5.3.2.3 Bacterial morphology study by FESEM

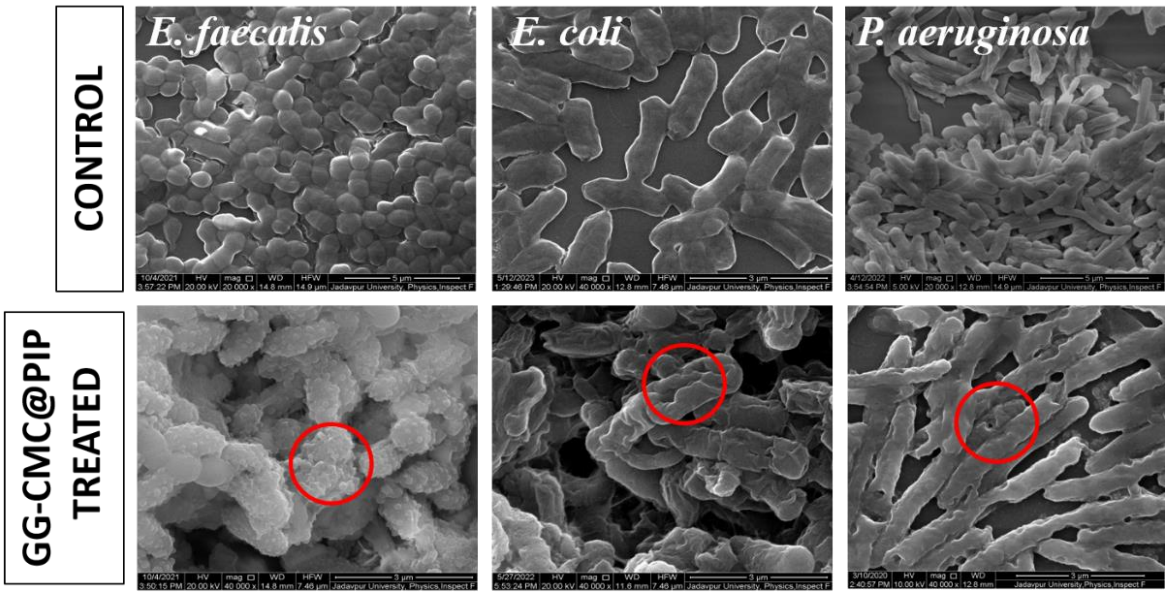

Figure 5.8: *FESEM micrographs showing morphological characteristics of bacterial cells.*

FESEM images of bacterial cells, exposed to MIC dose of GG-CMC@PIP, revealed that discontinuity of cell wall (figure 5.8) compared to the uniform and uninterrupted cell surface of the untreated control cells. Red circled parts in FESEM images of treated *E. faecalis* revealed cell deformation with uneven cell surface whereas treated *E. coli* cells appeared to be shrunk and surface disintegration was observed. Similar shrivelled surface morphologies with cell perforations were detected in treated *P. aeruginosa*. From the above findings it can be assumed that the accumulated intracellular ROS attacked polyunsaturated fatty acids of bacterial membranes and resulted in lipid peroxidation which eventually altered the integrity of membrane-bound proteins.[300] This loss of membrane uniformity caused cell leakage through ruptured, perforated and disintegrated cell membranes.[301]

5.3.3 Assessment of anticancer property

5.3.3.1 Cytotoxicity Study

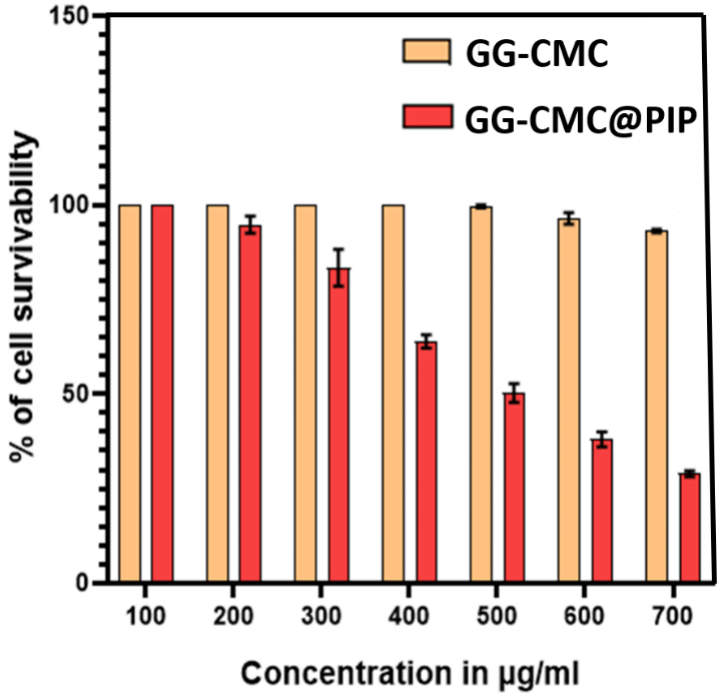

Figure 5.9: *Survivability of cells treated with different concentrations (100-700 µg/mL) of GG-CMC and GG-CMC@PIP for 24 hours as obtained by MTT assay.*

In vitro anticancer activity of both GG-CMC and GG-CMC@PIP was studied against C6 glioma cell line following standard protocol (as mentioned in subsection 1.7.5.2). Treatment of cells with different concentrations (100-700 µg/mL) of GG-CMC and GG-CMC@PIP for 24 hours showed that cytotoxicity of GG-CMC@PIP got increased in a dose-dependent manner (figure 5.9). At around 500 µg/mL dose GG-CMC@PIP resulted in ~50% cell death (IC_{50}), which showed its potential to be used as an anticancer therapeutic. On the other hand, GG-CMC had no significant cytotoxic effect on C6 glioma cells up to concentration of 500 µg/mL, beyond which slight cytotoxicity was observed (around 10% cell death at 700 µg/mL concentration).

5.3.3.2 Study of Intracellular ROS generation

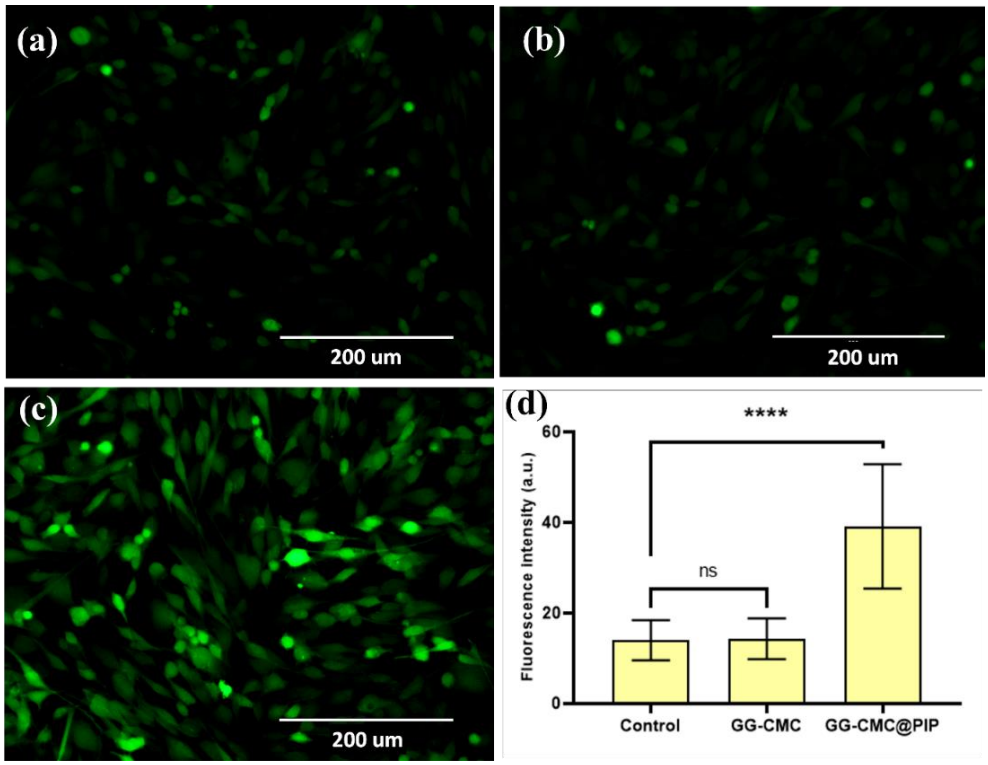

Figure 5.10: *Fluorescence microscopic images of $DCFH_2$-DA-stained (a) untreated control, (b) GG-CMC treated and (c) GG-CMC@PIP treated C6 glioma cells; (d) represents the fluorescence intensity of the images. Statistical significance was analysed with respect to control using one-way ANOVA with Dunnett's multiple comparisons test.*

The level of intracellular ROS contents of untreated control, GG-CMC and GG-CMC@PIP treated cells were investigated by fluorescence microscopy using $DCFH_2$-DA staining (as mentioned in subsection 1.7.5.3). The fluorescence intensity of untreated control cells and GG-CMC treated cells were somewhat similar with a value of (14.02±0.98) a.u. and (14.34±1.02) a.u. respectively. The fluorescence intensity of GG-CMC@PIP treated cells was comparatively higher with a value of (39.12±3.06) a.u (figure 5.10). These results showed that GG-CMC treatment had no significant effect on ROS generation in treated cells. On the other hand, GG-CMC@PIP treatment resulted in generation of higher levels of intracellular ROS which contributed to higher cell cytotoxicity and its anticancer activity, corroborating with the results of MTT assay. To maintain redox homeostasis, cancer cells display a moderate increase in ROS level together with a powerful antioxidant defense system compared to normal cells. Increased ROS level may induce emergence of malignancy, whereas an excess ROS level over the threshold will trigger apoptosis of cancer cell due to ROS mediated oxidative damage.[314]

5.3.3.3 Determination of mitochondrial membrane potential (MMP)

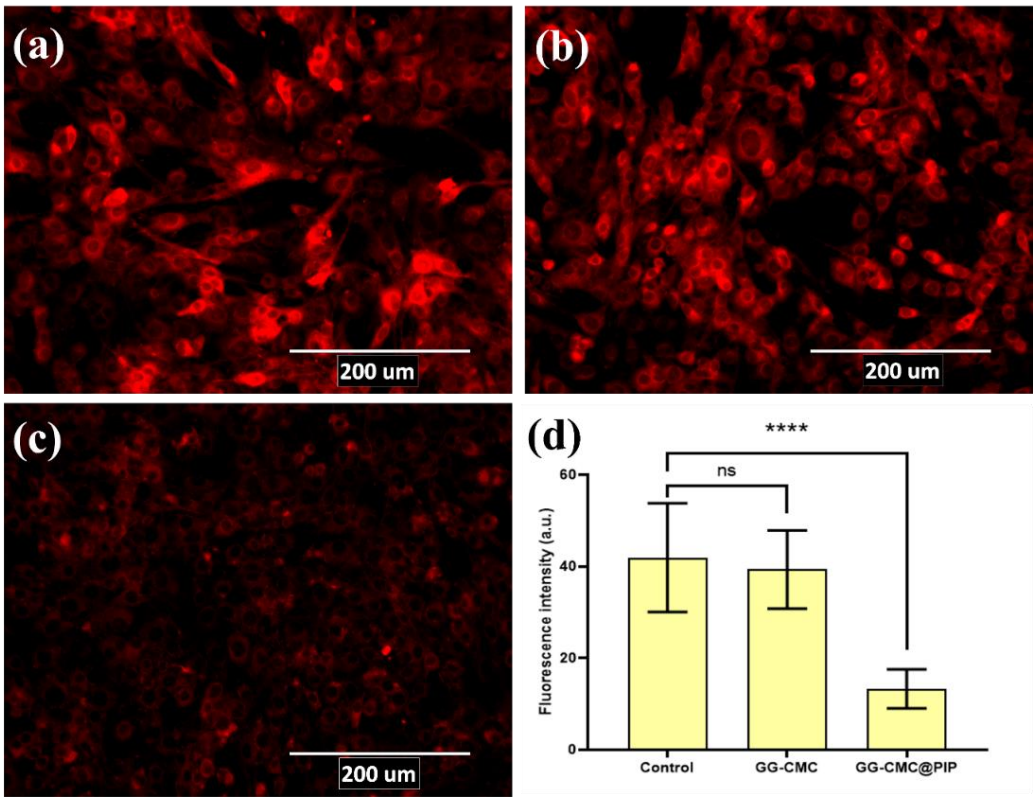

Figure 5.11: *Fluorescence microscopic images of Rhodamine 123-stained (a) untreated control, (b) GG-CMC treated and (c) GG-CMC@PIP treated C6 glioma cells; (d) represents the fluorescence intensity of the images. Statistical significance was analysed with respect to control using one-way ANOVA with Dunnett's multiple comparisons test.*

The depolarization level of mitochondrial membrane potential of GG-CMC and GG-CMC@PIP treated cells with respect to untreated control cells was studied by fluorescence microscopy using Rhodamine 123 staining (as described in subsection 1.7.5.5). The fluorescence intensity of untreated control and GG-CMC treated cells were (41.91±2.65) a.u. and (39.32±1.90) a.u. respectively. On the other hand, the fluorescence intensity of GG-CMC@PIP treated cells was (13.29±0.95) a.u., which was comparatively lower than both untreated and GG-CMC treated cells, signifying higher rate of depolarization levels of MMP (figure 5.11). Mitochondria are major target of oxidative stress in cells and disruption of MMP results in decrease of ATP production which is the main energy source for different vital biochemical reactions of cells. GG-CMC@PIP treatment caused oxidative stress mediated depolarization of MMP which contributed to its cytotoxicity and anticancer activity.

5.3.3.4 Determination of degree of nuclear damage

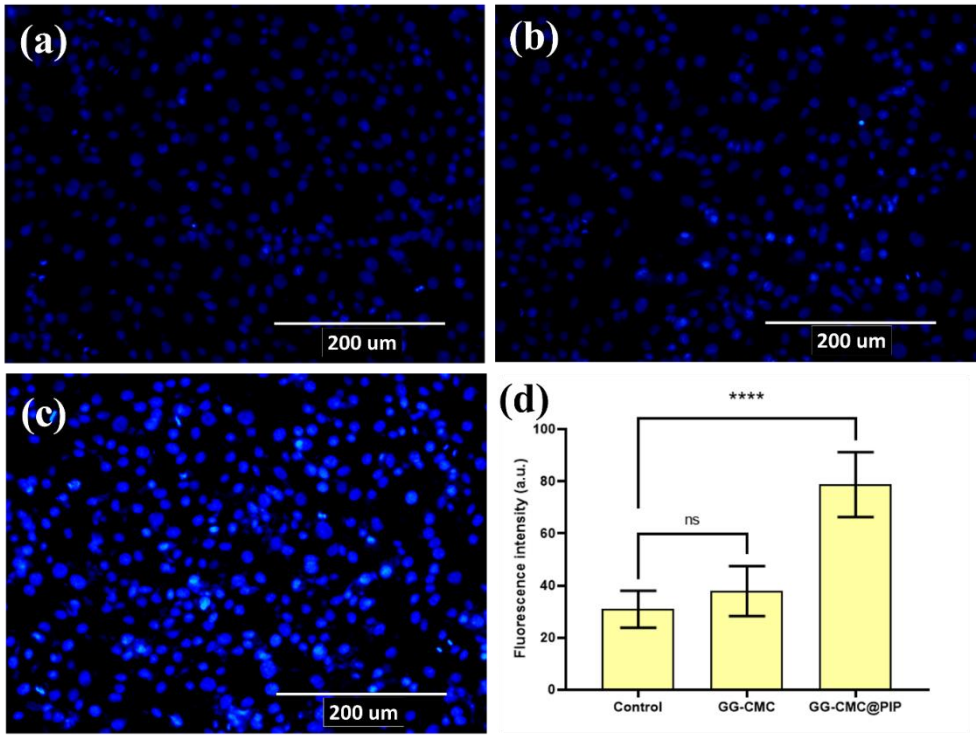

Figure 5.12: *Fluorescence microscopic images of Hoechst 33342-stained (a) untreated control, (b) GG-CMC treated and (c) GG-CMC@PIP treated C6 glioma cells; (d) represents the fluorescence intensity of the images. Statistical significance was analysed with respect to control using one-way ANOVA with Dunnett's multiple comparisons test.*

The degree of nuclear damage of untreated control, GG-CMC and GG-CMC@PIP treated cells were investigated by fluorescence microscopy using Hoechst 33342 staining (as described in subsection 1.7.5.6). The study showed that the fluorescence intensity of both untreated control and GG-CMC treated cells were lower [(30.93±1.58) a.u. and (37.86±2.14) a.u. respectively] than that of GG-CMC@PIP treated cells (78.72±2.78) a.u., (figure 5.12) implying higher degree of nuclear damage and consequent apoptosis by GG-CMC@PIP treatment and its anticancer activity.

5.4 Conclusion

In our study, we investigated antibacterial and anticancer activity of newly synthesized GG-CMC@PIP. In summary, this chapter discussed on nanonization of phyto-active compound PIP by incorporating it in the biopolymeric nanocomposite. We have successfully developed biopolymer-based GG-CMC@PIP nanocomposite using PIP for therapeutic applications. Synthesis procedure of this nanocomposite was simple, cost-effective, and robust comprising

only natural polysaccharides such as GG and CMC. GG-CMC@PIP can be an efficient drug delivery system with several promising advantages such as non-toxicity, excellent swelling ability, high drug loading capacity, sustained drug release property etc. Our study revealed a very high loading capacity (86 ± .46 %) of PIP (added as therapeutic) in GG-CMC@PIP. High zeta potential of about (−) 33.1 ± .73 mV demonstrates the good stability of nanocomposite. The sustained and controlled release profile of PIP from nanocomposites suggests the efficacy of GG-CMC@PIP as an appropriate drug delivery system. Our study has shown promising bactericidal capacity of GG-CMC@PIP nanocomposites against Gram-positive *E. faecalis* and Gram-negative *E. coli* and *P. aeruginosa.* PIP being a pro-oxidant compound, trigger ROS accumulation by disrupting intracellular defence mechanism which maintain redox homeostasis in cells. Experimental results also confirmed depolarized mitochondrion and higher degree of nuclear damage which in turn revealed prominent anticancer activity against C6 glioma cell. Thus, PIP can be considered as an interesting candidate in the ROS-mediated apoptosis in C6 glioma cell. From experimental outcomes, it can be said that natural plant derived polymers with innate pharmacological activity can be used to synthesize suitable polymeric vehicle for a broad range of drugs if properly standardised. Considering all these new observations, we believe that PIP, being an alkaloid phytochemical might be convenient as a potential nanomedicine for versatile applications. As new-generation medicinal treatment frequently requires multi-dimensional drugs to combat with wide variety of complications, the development of a multiple-response biopolymer-based nanocomposite like GG-CMC@PIP is a crucial need to explore diverse biomedical applications.

Chapter 6

An *In-vivo* Study on the Ameliorative Efficacy of Piperine Incorporated Guar Gum and Carboxymethyl Cellulose Nanocomposite Against Paracetamol-induced Liver Damage in Mice

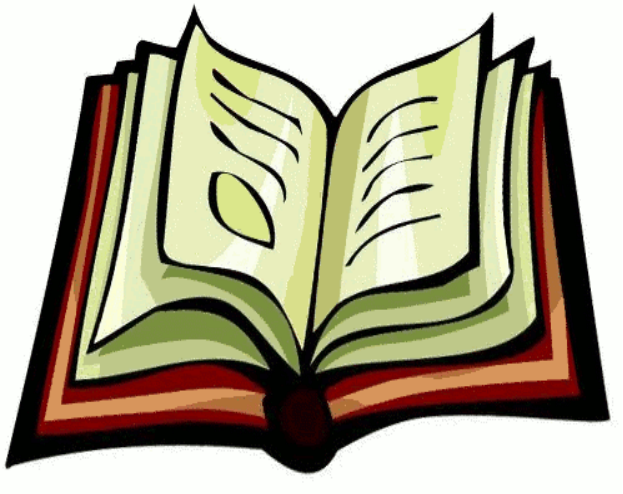

Summery

In this chapter, we investigated the effectivity of GG-CMC@PIP nanocomposite on biochemical, haematological, and histological parameters to assure the ameliorative potential of piperine in hepatotoxicity induced by the paracetamol in Swiss albino mice model. Piperine was nanonized by entrapping within a guar gum-carboxymethyl cellulose-derived polymer composite (GG-CMC). GG-CMC@PIPs were of (i) size (25 ± 3) nm measured by TEM, (ii) zeta potential (−) 33.1 ± .73 mV, and (iii) entrapment efficiency of piperine 86 ± .46 %. Nanocomposite administration (1mg/kg body weight) to paracetamol-intoxicated mice significantly reversed ($p<0.05$) the hepatic damage almost similar to silymarin. Antioxidant screening (MDA, CAT, SOD levels) was performed to study the therapeutic efficacy of synthesized nanocomposite. Oral administration of piperine-incorporated nanocomposite for 15 days significantly reduced increased serum bilirubin, aspartate transaminase, alanine transaminase, and alkaline phosphatase levels in damaged liver and showed a marked amelioration in the histopathological hepatic necrosis and boosted antioxidant enzyme levels in hepatocytes. Whereas the biochemical and antioxidant status was found to be recovered in nanocomposite-treated animals compared to that of the bulk PIP-treated animals. No significant changes in haematological parameters and antioxidant response were observed in animals after GG-CMC treatment compared to the animals which received only paracetamol treatment confirming the inert nature of bare polymer composite (GG-CMC). The results suggested that piperine as a phytochemical has promising hepatoprotective efficacy against paracetamol-induced hepatotoxicity in mice.

6.1 Introduction

The liver is a critical organ responsible for various functions, including micro- and macromolecular metabolism, bile production, and removal of bilirubin, cholesterol, hormones, toxins, drugs, and other harmful substances.[315] There is a rising concern in the search of alternative plant-derived medicines for treating acute and chronic liver diseases. Phytochemicals and their derivatives might be suitable candidates to treat different liver disorders. One of them is silymarin, a flavonolignan extracted from the milk thistle, or *Silybum marianum* which is widely used as a hepatoprotective component.[316] Silymarin contains several flavoligands and the flavonoid taxifolin.[317] The hepatoprotective property of silymarin is caused by its high antioxidant assets which cut off excess free radicals produced from the metabolism of toxic materials such as paracetamol, ethanol, etc. It has also been found that silymarin stimulates protein synthesis in hepatocytes by activating the RNA polymerase I enzyme and positively regulates new hepatocyte growth.[317,318]

In this chapter, we have investigated the hepatoprotective effect of piperine, an alkaloid phytochemical with immense therapeutic properties isolated from *Piper nigrum* or *Piper longum* plants in paracetamol-intoxicated liver disease of Swiss albino mice.[291] A wide range of medicinal potentials have been attributed to PIP in animal models, such as suppression of tumour growth, hepatotoxicity, metastasis, and inflammation, etc.[308,309] Molecular docking studies showed PIP decreases drug metabolism by inhibiting cytochrome P450/CYP3A4.[308] Several experimental outcomes reported about the prooxidant property of PIP which can induce radical mediated mitochondrial pathway of apoptosis in Hep G2 cells.[292] Recently advanced bio-based drug delivery systems (DDS) are gaining attention in biomedical applications resolving disadvantages of phytochemicals like PIP such as less effective rate of intestinal absorption, inefficient delivery mechanism at target site, poor solubility, and plasma inconsistency.[285,286] As PIP is hydrophobic we introduced two naturally abundant polysaccharides, guar gum and carboxymethyl cellulose to develop bio-polymer derived nanocomposite and nanonize PIP to incorporate into the polymeric nanocomposite (GG-CMC@PIP). The simple and robust synthesis procedure and characterization techniques were explained in subsection 5.2.

Acetaminophen or paracetamol (N-acetyl-para-aminophenol) is a non-opioid drug possessing analgesic, anti-inflammatory, and antipyretic properties.[319] Even though paracetamol is considered a safe medication at its normal therapeutic doses, chronic usage often leads to

hepatotoxicity in a dose-dependent manner.[320] According to several investigations paracetamol is metabolically activated in the liver by cytochrome P450 to form N-acetyl-p-benzoquinone imine (NAPQI), one type of reactive metabolite that is capable of covalently binding to various essential proteins lead to the formation of inactive conjugates. NAPQI is detoxified in the liver by glutathione (GSH) by developing a paracetamol-glutathione conjugate. These conjugates result in serious damage to hepatocytes causing liver necrosis.[321] The centrilobular zone of the liver is the prime site of hepatic necrosis caused by paracetamol as cytochrome P450 is abundant in this portion of the liver.[322] Experimental results showed that several animals as well as humans may develop fulminate acute centrilobular hepatic necrosis due to an overdose of paracetamol.[323,324] Excessive accumulation of reactive oxygen species within hepatocytes and depletion of antioxidant enzymes are the critical factors that lead to acetaminophen-induced hepatotoxicity.[325]

In this study, the hepatoprotective potential of GG-CMC@PIP nanocomposite was measured against the hepatotoxicity induced by paracetamol overdose in Swiss albino mice. Estimation of liver markers (total bilirubin, ALT, ALP, and AST) were carried out in serum, while the antioxidant status (SOD, CAT, MDA, ROS level) was determined in liver homogenate. Hepatoprotection has been documented by liver histopathological changes for evaluation of hepatic toxicity as well as recovery aided by synthesized nanocomposite.

6.2 Experimental section

6.2.1 Synthesis procedure

The synthesis procedure of GG-CMC and GG-CMC@PIP was mentioned in subsection 5.2.1. Characterizations of synthesized nanocomposites were discussed in subsection 5.3.1.

6.2.2 Experimental design

Animal preparation and other methodology explaining animal sacrifice, serum preparation, blood and tissue collection, and cell lysis are described in subsection 1.7.6. After acclimatization for 7 days, all mice were randomly assigned to 6 groups (n = 4). Group I without any treatment was assigned as a control group. Group II was designated as a toxic group and treated with paracetamol (75 mg /kg, 1:1 combination with olive oil) for 15 days (almost 5 times less than the LD_{50} value).[326] Group III was graded as the therapy with GG-CMC which first treated with paracetamol (75 mg/kg BW) for 15 days followed by GG-CMC (1mg/kg BW) for another 15 days. Group IV was graded as the therapy with PIP which first

treated with paracetamol (75 mg/kg BW) for 15 days followed by PIP (1mg/kg BW) for 15 days. Group V was graded as the therapy with GG-CMC@PIP which was first administered with paracetamol (75 mg/kg BW) for 15 days followed by GG-CMC@PIP (1mg/kg BW) for 15 days. Group VI was designated as the therapy with silymarin which was first administered with paracetamol (75 mg/kg BW) for 15 days followed by silymarin (1mg/kg BW) for 15 days. Mice belonging to Group-II to Group VI were administrated with paracetamol (75 mg/kg BW) for 15 days, and group-III to VI received therapeutic treatment with 1 mg/kg BW. Groups III, IV, V and VI mice were treated with respective sample therapeutics for 15 consecutive days.

Table 6.1 *Represents the animal experimental design and treatment protocol.*

Animal Group n=4	***Drug Administration***		***Remarks***
Group I	N.A.	N.A.	Control
Group II	Paracetamol (75 mg/ kg BW)	N.A.	Paracetamol
Group III	Paracetamol (75 mg / kg BW)	Biopolymer composite (GG-CMC) (1mg/kg BW)	Paracetamol + GG-CMC
Group IV	Paracetamol (75 mg / kg BW)	PIP (1mg/kg BW)	Paracetamol + PIP
Group V	Paracetamol (75 mg / kg BW)	Nanocomposite (GG-CMC@PIP) (1mg/kg BW)	Paracetamol+ GG-CMC@PIP
Group VI	Paracetamol (75 mg / kg BW)	Silymarin (1mg/kg BW)	Paracetamol+ Silymarin

6.2.3 Statistical analysis

All experimental data were represented as Mean ± Standard Error (SE) of the mean. The statistical significance was determined by using a one-way analysis of variance (ANOVA). $p < 0.05$ was considered to be an indication of statistical significance.

6.3 Results and Discussion

6.3.1. Cell Cytotoxicity study and dose determination of PIP

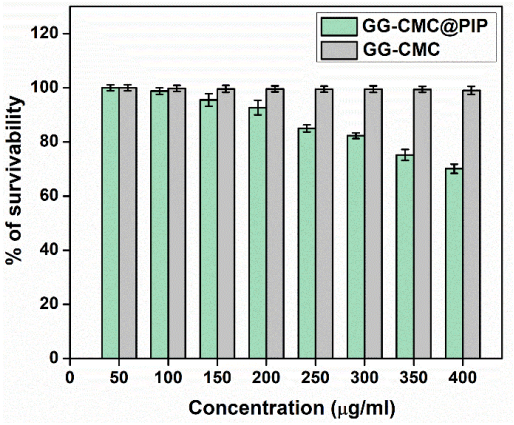

Figure 6.1: *Graphical representation of MTT assay on WI38 cell line after treatment with GG-CMC@PIP and GG-CMC.*

Table 6.2: *Concentration of GG-CMC@PIP in cytotoxicity study and corresponding effective concentration of PIP. All data are represented as Mean ± SEM, P values calculated by ANOVA test, a test of significance $p<0.05$ implies.*

Dose of GG-CMC@PIP (µg/mL)	*Effective concentration of PIP (µg/mL)*
50	15.06
100	30.13
150	45.19
200	60.25
250	75.31
300	90.38
350	105.44
400	120.50

To evaluate the biocompatibility of synthesized nanocomposites, *in vitro* cytotoxicity was estimated by MTT assay following standard protocol (as mentioned in subsection 1.7.5.2). Human lung fibroblast (WI38) cells were exposed to GG-CMC and GG-CMC@PIPs of different concentrations (50-400 µg/mL). Experimental outcomes displayed 99-100% cell viability which confirmed the nontoxic nature of GG-CMC composite. Treatment with GG-CMC@PIP also showed excellent biocompatibility. At 400 µg/mL dose, GG-CMC@PIP

exhibited 70.1% cell survivability (figure 6.1). From experimental results we can conclude that GG-CMC@PIP is biocompatible and cytotoxicity can be avoided by proper standardization of doses. Biopolymeric composite without PIP (GG-CMC) does not exert any cytotoxic effect on WI38 cells.

Table 6.2 displayed the effective concentration of PIP corresponding to the concentration of GG-CMC@PIP used in the cytotoxicity study (experimental procedure was mentioned in subsection 1.7.3.9). At a concentration of 400 µg/mL of GG-CMC@PIP, the effective concentration of PIP was found to be 120.5 µg/mL which is responsible for only 29.9% cell mortality.

A previous study suggested that 1.12 mg of PIP /kg BW showed no immuno-toxicological effects in Swiss albino male mice. As this concentration of PIP is immunologically safe for mice, it can be considered as no observed adverse effect level (NOAEL) dose.[327] Therefore, we chose a dose of 1mg/kg BW for all experimental samples i.e. PIP, GG-CMC, GG-CMC@PIP, and silymarin. In 1mg/mL solution of GG-CMC@PIP, the effective concentration of PIP is approximately 301.25µg/mL (suggested by Table 6.2) which is significantly less than the NOAEL dose of PIP.

6.3.2 Study of haematological parameters

Table 6.3: *Effect of GG-CMC@PIP on haematological parameters in paracetamol-intoxicated mice. All data are represented as Mean ± SEM, P values calculated by ANOVA test, a test of significance $p<0.05$ implies.*

Parameters	*Group I Control*	*Group II Paracetamol*	*Group III Paracetamol +GG-CMC*	*Group IV Paracetamol +PIP*	*Group V Paracetamol + GG-CMC@PIP*	*Group VI Paracetamol + Silymarin*
Hb% (g/dL)	13.1± 1.1	10.2±.5	10.9±.4	11.1±1.2	12.7±.7	11.9±.2
Platelet (10^3/cu.mm)	711.32±2.1	688±3.5	690±2.2	720±2.4	737±3.2	733±3.1
WBC (x 10^3)	5.2±.50	6.3±.71	6.4±.53	6.1±.30	5.4±.62	5.7±.41

The experiment was conducted to examine the adverse effects of orally administered paracetamol and to investigate the ameliorative effect of GG-CMC@PIP on haematological changes in mice following the standard protocol mentioned in 1.7.6.3 (a) subsection. The study

showed that the paracetamol-treated (auto-recovery) group (Gr-II) and GG-CMC-treated group (Gr-III) have a lower platelet count when compared to the control group (Gr-I). On the other hand, the paracetamol-intoxicated GG-CMC-treated group (Gr-III) showed a reduced platelet count than PIP-treated (Gr-IV), GG-CMC@PIP treated (Gr-V) and silymarin-treated (Gr-IV) group. Abnormalities in haematological parameters are often found in liver diseases. The liver plays a crucial role in regulating iron homeostasis by producing the hepcidin hormone. The hepatic disorder causes an overactive spleen called hypersplenism which leads to thrombocytopenia i.e. low platelet count and anaemia.[328] Elevated liver enzyme levels can also result in low platelet counts. In group II Hb% level is found to be dropped (10.2±.5 g/dL). Subsequently, the paracetamol-treated group (Gr-II) and the groups treated with GG-CMC (Gr-III) had significantly ($P<0.05$) lower levels of haemoglobin compared to the groups treated with bulk PIP (11.1±1.2 g/dL), GG-CMC@PIP (12.7±.7 g/dL) and silymarin (11.9±.2 g/dL). The WBC level of the GG-CMC@PIP treated group (Gr-V) was much lower than the auto recovery group (Gr-II) while the PIP treated Group (Gr IV) showed a lower level of WBC level than Gr-III. Haematological parameters of Table 6.3 showed that the Hb%, platelet, and WBC levels of the paracetamol-treated group (Gr-II) are closer to the GG-CMC treated group (Gr-III). The positive control mice group, which received silymarin treatment showed a decrease in WBC levels which is closer to the control group. This result implies that all treated mice have higher levels of inflammation than GG-CMC@PIP treated mice which showed closer WBC level to control group.

6.3.3 Measurement of body weight

The changes in body weight during treatment are summarized in Table 6.4. In this experiment, we monitored body weight at regular intervals as a vital indicator of health issues associated with paracetamol doses. Slow weight gain or weight loss is generally the first sign of negative effects. The body weights of mice under six different circumstances are depicted in Table 6.4. The findings revealed that all paracetamol-intoxicated mice groups showed decreased weight gain till the 15th day. The delivery of bulk PIP, silymarin, and GG-CMC@PIP nanocomposite almost restores the normal physiological condition of mice which is confirmed by a steady increase in body weight. After treatment with GG-CMC@PIP nanocomposite in (Gr-V) body weight was significantly ($p<0.05$) increased which was almost similar to the control group. The obtained data implied a significant decrease in weight gain in group II and group III mice when compared to the control and other treated groups.

Table 6.4: *Measurement of body weight (gm) in control and treated mice. All data are represented as Mean ± SEM, P values calculated by ANOVA test, the test of significance p<0.05 implies.*

Days	*Group I Control*	*Group II Paracetamol*	*Group III Paracetamol + GG-CMC*	*Group IV Paracetamol + PIP*	*Group V Paracetamol + GG-CMC@PIP*	*Group VI Paracetamol + Silymarin*
1th	23±0.14	23±0.84	23±0.33	23±0.80	23±0.22	23±0.71
3th	24±0.54	23±0.53	23±0.64	23±0.17	23±0.94	23±0.77
5th	25±0.11	24±0.46	24±0.74	24±0.74	24±0.74	24±0.74
7th	25±0.74	24±0.45	24±1.12	24±0.98	24±0.76	24±0.88
9th	26±0.90	24±0.56	24±0.87	25±0.74	25±0.68	25±0.91
11th	26±0.88	25±0.83	25±0.48	25±0.63	26±0.71	25±0.80
13th	27±1.12	25±0.34	25±0.65	25±0.57	26±0.47	25±0.81
15th	27±1.14	26±0.54	26±0.11	26±0.42	26±0.86	26±0.45
17th	28±0.68	27±0.21	26±0.20	27±0.34	27±0.50	26±0.72
19th	28±0.75	27±0.35	26±0.51	27±0.56	28±0.67	26±0.53
21th	29±0.80	27±0.44	26±0.68	27±0.34	28±0.48	27±0.49
23th	30±1.22	27±0.71	27±0.41	28±0.24	29±0.62	28±0.51
25th	30±1.30	27±0.85	27±0.63	28±0.67	29±0.48	28±0.96
27th	31±1.11	28±0.41	27±0.88	29±0.52	30±0.69	29±0.30
29th	32±0.40	28±0.55	28±0.73	29±0.21	30±0.80	29±0.67
31th	32±1.10	28±0.90	28±1.04	30±0.49	31±1.38	30±0.35

6.3.4 Measurement of organ weight (Liver)

Measurement of organ weight was performed immediately after the isolation of the liver (figure 6.2) from sacrificed animals. This study demonstrated that the liver weight (table 6.5) of paracetamol treated group (1.39±0.4 gm) was increased compared to the control group (0.98 ±0.06 gm), whereas the paracetamol treated group (Gr-II) and GG-CMC treated group (Gr-III) revealed an almost similar increase in organ weight which are 1.39±0.4 gm and 1.36±0.08 gm respectively. Here, in these experiments, the liver weight of PIP treated group (1.27±0.08 gm) was found to be increased than the GG-CMC@PIP treated group. In GG-CMC@PIP treated group (Gr-V) the organ weight (1.1±0.04 gm) was significantly ($p<0.05$) restored and the weight was found to be near to the silymarin treated group (.99±0.07).

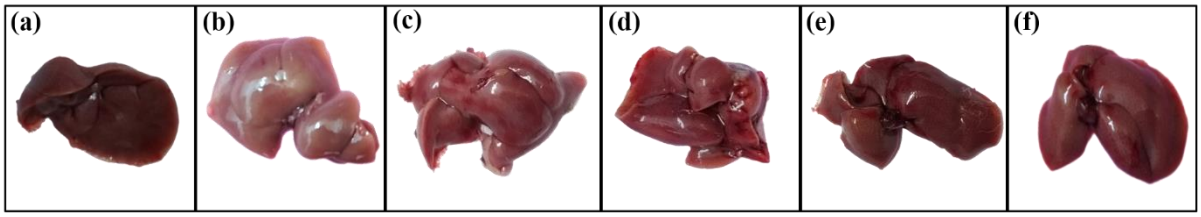

Figure 6.2: *Morphology of isolated liver from (a) Control (b) Paracetamol treated (c)Paracetamol +GG-CMC treated (d) Paracetamol +PIP treated (e) Paracetamol + GG-CMC@PIP treated (f) Paracetamol +Silymarin treated mice.*

Table 6.5*: Organ weight of control and paracetamol intoxicated mice. All data represent as Mean ± SEM, P values calculated by ANOVA test, test of significance p<0.05 implies.*

	Group I Control	*Group II Paracetamol*	*Group III Paracetamol + GG-CMC*	*Group IV Paracetamol + PIP*	*Group V Paracetamol + GG-CMC@PIP*	*Group VI Paracetamol + Silymarin*
Liver weight (gm)	0.98±0.06	1.39±0.4	1.36±0.08	1.27±0.08	1.1±0.04	.99±0.07

6.3.5 Study of liver biomarkers

We assessed the serum level of liver biomarkers following the standard protocol mentioned in 1.7.6.3 (b) subsection. The results obtained from the mice that received oral administration of GG-CMC@PIP nanocomposite showed a significant ($P < 0.05$) decrease in all the serum enzymes in comparison with the PIP-treated group. Our study demonstrated that excessive paracetamol treatment raised the bilirubin and other liver enzyme levels while lowering total protein i.e. albumin and globulin levels. According to figure 6.3, compared to group I all paracetamol-treated mice were determined to have significantly increased serum ALT, AST, ALP and total bilirubin levels after treatment. Figure 6.3(a) demonstrated that the PIP and GG-CMC@PIP treated group had lower bilirubin levels than the paracetamol-treated group (Gr-II). Figure 6.3 (b) and (c) showed serum AST and ALT activity of the GG-CMC@PIP and the silymarin-treated group was significantly decreased when compared to GG-CMC treated group (Gr-III) which confirms the hepatoprotective activity of PIP and silymarin respectively. Figure 6.3 (d) showed almost similar decrease in serum ALP levels in group V and VI mice compared to group II, III, and IV mice. Table 6.6 displayed paracetamol overdoses reduced the total protein level in group II mice which received only paracetamol treatment. While in GG-CMC@PIP treated animals the total protein level was increased significantly ($p<0.05$) compared to other treatment groups. Elevated total cholesterol level was observed in group II

and group III mice whereas increased total cholesterol level was markedly depleted after treatment with PIP, GG-CMC@PIP, and silymarin. Furthermore, elevated levels of serum ALT, AST, and ALP levels in group II implied the dysfunctional condition of the liver. The result showed that the bilirubin level in the GG-CMC-treated group was not significantly reduced to the control group. On the other hand, nanocomposite treated group (Gr-V) the bilirubin level was reduced which was almost near to the control group. Total protein as well as albumin and globulin ratio (A/G ratio) can be a crucial indicator of liver disease. It was observed that in the case of paracetamol, treated group (Gr-II) the albumin level (2.3±.2 gm/dL) was significantly reduced compared to the control group (3.4±.33 gm/dL). Whereas in GG-CMC@PIP treated animals the albumin and total protein levels showed significant ($p<0.05$) elevation compared to the paracetamol-treated group (Gr-II). In this study, it was observed that in a positive control group i.e. silymarin treated group and GG-CMC@PIP treated group the level of bilirubin was reduced to .32±0.05 mg/dL and .29±0.03 mg/dL respectively. Results suggested the ameliorative effect of GG-CMC@PIP was more efficient than silymarin in respect to the control group. Simultaneously it was also observed that the serum activities of aminotransferases (ALT and AST) and ALP levels in the nanocomposite treated group was significantly reduced than the group treated with PIP.

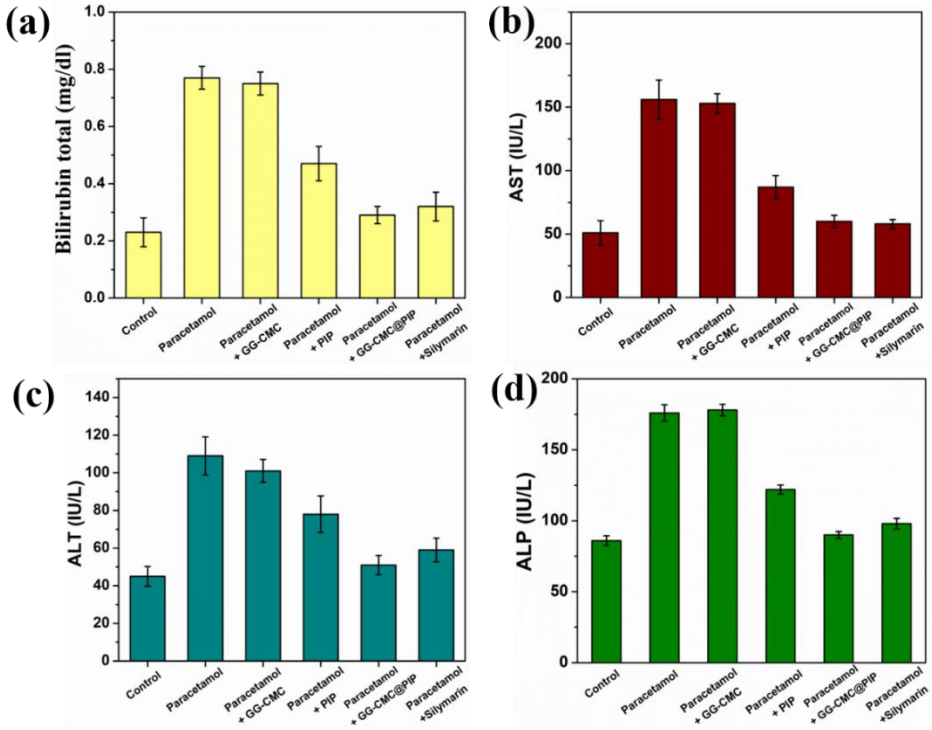

Figure 6.3: *(a) Serum bilirubin level (b)serum AST level (c) serum ALT level (d) serum ALP level of control and treated mice groups. All data represent as Mean ± SEM, P values calculated by ANOVA test, test of significance $p<0.05$ implies.*

Table 6.6: *Total protein, albumin and total cholesterol level of control and treated mice. All data represent as Mean ± SEM, P values calculated by ANOVA test, test of significance p<0.05 implies.*

Parameters	*Group I Control*	*Group II Paracetamol*	*Group III Paracetamol + GG-CMC*	*Group IV Paracetamol + PIP*	*Group V Paracetamol + GG-CMC@PIP*	*Group VI Paracetamol + Silymarin*
Total Protein (gm/dL)	6.6±.54	4.9±.23	4.3±.51	5.5±.71	7.1±.46	6.3±.69
Albumin (gm/dL)	3.4±.33	2.3±.2	2.2±.06	3.1±.41	3.9±.22	3.3±.24
Total Cholesterol (mg/dL)	90±5.4	168±3.13	165±4.6	152±3.1	110±3.1	118±4.1

6.3.6 Study on oxidative stress and antioxidant responses

6.3.6.1 Hepatic MDA Activity

Lipid peroxidation is considered to be one of the main factors affected by paracetamol induced hepatotoxicity. Malondialdehyde (MDA) is produced in response of peroxidation of polyunsaturated fatty acids under antioxidant deficiency. A distinct enhance in free radicals in system caused hyperproduction of MDA.[329] Thus, MDA level is used as a biomarker to assess oxidative damage and lipid peroxidation in different tissues (as mentioned in subsection 1.7.6.4 a). Table 6.7 illustrates that the paracetamol treated mice develop a significantly ($p<0.05$) higher level of MDA in liver homogenate (2.1±.11 nmol/mg protein) than the control group (1.12±.07 nmol/mg protein) which is due to the paracetamol induced lipid peroxidation. In comparison between PIP treated group and the GG-CMC@PIP treated group, MDA level is significantly depleted in GG-CMC@PIP treated mice which suggests better effectivity of GG-CMC@PIP nanocomposite, whereas GG-CMC treated mice showed significantly increased level of MDA compared to control mice.

6.3.6.2 Hepatic SOD activity

Superoxide dismutase (SOD) is an effective antioxidant enzyme and front-line defense system against oxidative stress-mediated injury.[330] SOD level of liver homogenate was estimated following standard protocol as mentioned in subsection 1.7.6.4 b. Table 6.7 showed that

treatment with paracetamol caused a significant decrease in the SOD activity in liver tissue. The increased production of free radicals caused by administration of paracetamol is a major cause of reduced SOD activity. Experimental data showed that the SOD activity significantly increased ($P < 0.05$) in mice treated with GG-CMC@PIP nanocomposite compared with those of paracetamol treated as well as GG-CMC-treated mice. Administration of PIP also caused an increase in SOD activity in liver tissues. But the elevation in SOD level is significantly higher in GG-CMC@PIP and silymarin-treated group compared to PIP treated group. Thus, a significant recovery related to SOD was observed in response to the presence of nanocomposite.

Table 6.7: *Liver MDA levels, SOD and CAT activities of the control and treated groups. All data represent as Mean ± SEM, P values calculated by ANOVA test, test of significance p<0.05 implies.*

Parameters	*Group I Control*	*Group II Paracetamol*	*Group III Paracetamol + GG-CMC*	*Group IV Paracetamol + PIP*	*Group V Paracetamol + GG-CMC@PIP*	*Group VI Paracetamol + Silymarin*
MDA (nmol/mg protein)	1.12±.07	2.1±.11	2.17±.13	1.97±.13	1.3±.14	1.7±.07
SOD (U/mg protein)	3.5±.05	2.2±.13	2.11±.14	2.61±.08	2.98±.2	2.77±.14
CAT (U/mg protein)	2.32±0.1	1.45±.09	1.39±.07	1.88±.15	2.28±.08	2.04±.1

6.3.6.3 Hepatic CAT Activity

Catalase is a vital enzyme responsible for breaking down H_2O_2 in cells to maintain redox balance.[331] Estimation of CAT level in tissue homogenate was performed following standard protocol mentioned in subsection 1.7.6.4 c. Table 6.7 demonstrates CAT activity in the liver homogenate. The catalase activity was shown to be depleted after paracetamol treatment in all examined tissues. There was an insignificant increase of CAT activity in PIP-treated (1.88±.15 U/mg protein) mice than in the silymarin-treated group (2.04±.1 U/mg protein). It was also found that the liver homogenate of the GG-CMC@PIP-treated group had noticeably enhanced CAT activity than the PIP-treated group. There was a significant increase in liver CAT activity in PIP-treated mice than in the paracetamol-treated group II. Furthermore, significantly

($p<0.05$) enhanced CAT activity in the nanocomposite (GG-CMC@PIP) treated group than other treated groups was also observed. The increase in CAT activity mainly signifies the functional anti-oxidant mechanism in the GG-CMC@PIP treated group. Therefore, experimental results confirmed that nanonized PIP in GG-CMC@PIP nanocomposite possesses improved ameliorative potential than bulk PIP to regain hepatic CAT enzyme activity to restore liver function.

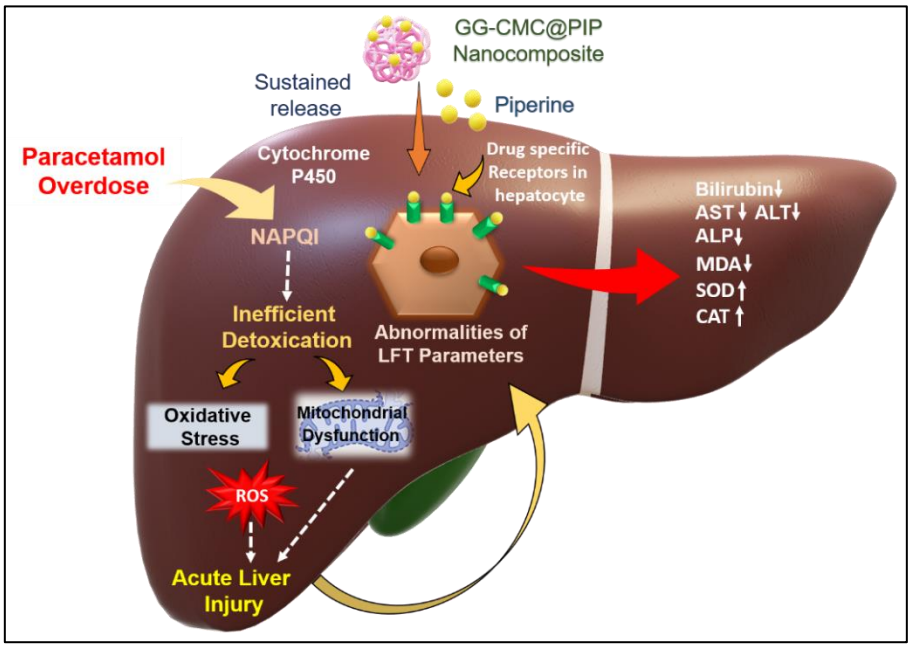

Figure 6.4: *Schematic representation showing mode of action of GG-CMC@PIP nanocomposites in paracetamol induced hepatotoxicity.*

6.3.6.4 Evaluation of ROS in liver hepatocytes

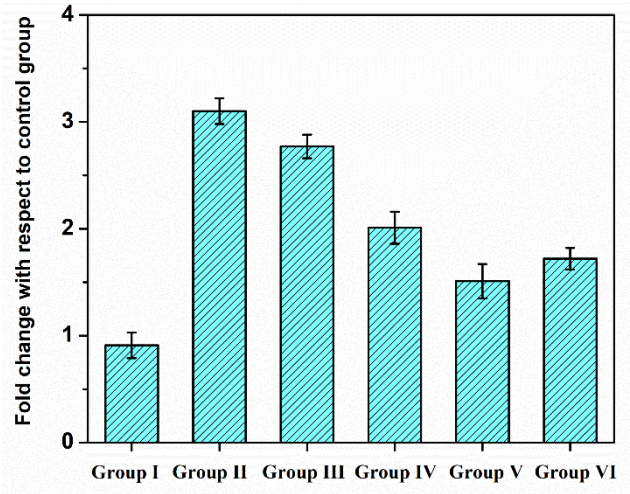

Figure 6.5: *Study of ROS generation by DCFDA method in liver hepatocytes in control and treated mice.*

To measure the overall oxidative status of liver tissue, ROS was measured with a DCFDA probe in the liver homogenates (as mentioned in subsection 1.7.6.4 d). In paracetamol-induced hyperbilirubinemia, excessive bilirubin production triggers the generation of reactive oxygen species (ROS) which induces oxidative stress.[332] Increased ROS levels with paracetamol treatment were suppressed by the administration of GG-CMC@PIP nanocomposite as shown in figure 6.5. ROS level in paracetamol and GG-CMC treated group III was significantly ($p<0.05$) closer to the paracetamol treated group. The ROS level was marginally higher in the PIP-treated group than silymarin-treated mice and it was significantly ($P<0.05$) higher than GG-CMC@PIP treated group. Reduced ROS levels in the nanocomposite-treated group indicate the hepatoprotective activity of nanonized PIP.

6.3.7 Liver histopathology study

The effect of nanocomposite on paracetamol-induced mice was assessed by observing the histopathological changes in liver sections stained with hematoxylin and eosin (H&E) under a light microscope (figure 6.6) following the standard protocol mentioned in 1.7.6.5 subsection. Livers of the control group (Gr-I) showed normal liver morphology with lobular architecture, and central veins with hepatic cords with no signs of inflammation. Within each lobule, hepatic cords comprising hepatocytes radiated from the central vein. No histological abnormalities were observed. In contrast, the liver sections from paracetamol-induced mice (Gr II) showed

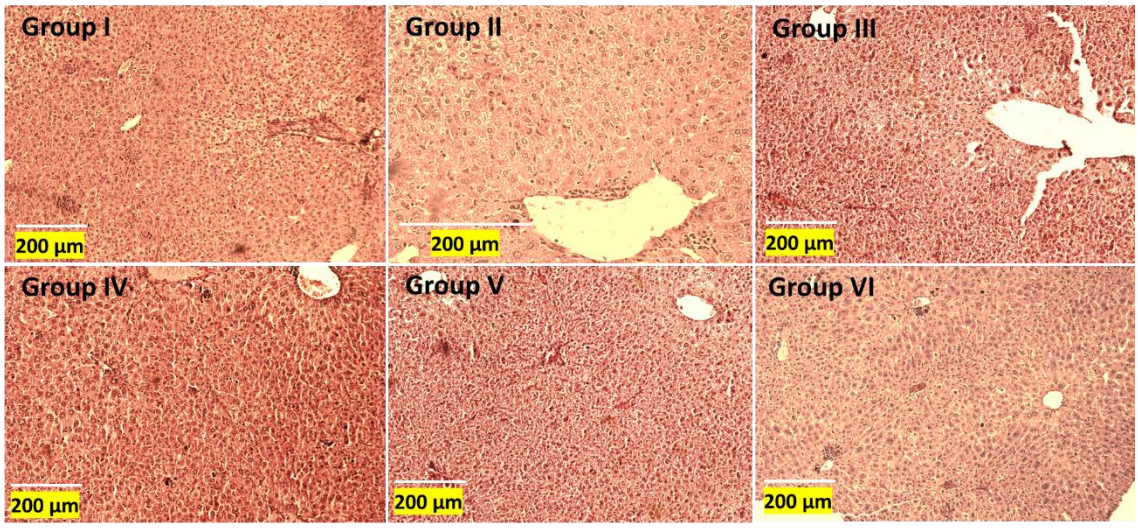

Figure 6.6: *Photomicrographs of hematoxylin-eosin-stained histological sections of the liver of control and experimental mice.*

endothelial sloughing, mild sinusoidal dilation, necrosis, vacuolization in liver parenchyma with distorted tissue architecture. Notably, these pathologic changes were markedly reduced in

the livers of PIP, GG-CMC@PIP, and silymarin-treated groups. In the case of group-IV and VI animals that received PIP and silymarin treatment respectively after paracetamol induction displayed mild endothelial sloughing in liver parenchyma compared to group-V mice. Histological study of the liver section of group-V mice displayed signs of recovery from necrosis and damaged cellular architecture induced by paracetamol. All the experimental results suggested the efficacy of GG-CMC@PIP nanocomposite which has very prominent hepatoprotective activity against paracetamol-induced oxidative damage.

6.4 Discussion

The co-morbidity, mortality, and economic burden of chronic liver disease (CLD) and its related complications i.e. cirrhosis, and liver cancer are substantial. The burden of CLD is significant and rising, according to data released by the World Health Organization and the Global Burden of Disease.[333] These days, research on appropriate herbal remedies is necessary due to the negative consequences of conventional drugs used to treat liver disorders.[334] Herbs are less toxic, easily obtained, inexpensive, and have fewer side effects than the medications now in use. Numerous research using biomarkers for hepatic function have documented the beneficial effect of piperine on liver health. Researchers have found that piperine can reduce the levels of ALT, AST, and ALP enzymes.[335]

In the present investigations, we administered paracetamol (75 mg/kg BW) to induce hepatotoxicity in the Swiss albino mice model. Experimental results indicated that paracetamol-induced hepatic damage is associated with inflammation and hyperbilirubinemia. Serum bilirubin level markedly elevated after paracetamol overdose confirming the liver damage. As seen in our studies, mice receiving paracetamol (auto recovery) had ALT and AST levels that were noticeably greater than those of the mice receiving the other treatments. This is because paracetamol damages liver cells more severely, which results in cellular leakage, a reduction in cell membrane integrity, and the release of these enzymes into the bloodstream. Paracetamol is metabolized into a toxic active metabolite NAPQI which binds to lipid, protein, and DNA macromolecules through covalent bonds which in turn reduce glutathione levels in the hepatocytes trigger mitochondrial dysfunction (figure 6.4). Depletion in antioxidant level leads to loss of functional integrity of the cell membrane of hepatocytes. Membrane leakage leads to the release of excessive serum markers i.e. AST, ALT, and ALP in the blood. Moreover, NAPQI can interact with liver tissue glutathione to remove this antioxidant causing oxidative stress and tissue necrosis.[336] The results of our study showed that group II receiving

oral doses of paracetamol (75 mg/kg BW) had higher levels of MDA level than the nanocomposite treated group. In the present study, mice treated with 1mg/kg BW GG-CMC@PIP had a significant reduction in the MDA level of the homogeneous liver tissue as compared to group II. Similarly, the changes of body weight significantly increased rapidly after the administration of GG-CMC@PIP. Possibly GG-CMC@PIP nanocomposites inhibit protein oxidation properties. Superoxide dismutase (SOD) is a very powerful free radical scavenger that converts superoxide radicals into H_2O_2 and oxygen whereas catalase (CAT) enzyme reduces oxidative stress by converting H_2O_2 into water and oxygen.[330, 331] These two antioxidant enzyme levels are restored after nanocomposite treatment.

Our biochemical results were consistent with the histological finding, and the group that received only paracetamol treatment indicated a higher degree of liver injury. Histological analysis of this auto-recovery group showed centrilobular hepatic necrosis, sinus contractions, and the presence of inflammatory cells at the site of liver haemorrhage. The normal liver function was regained and oxidative stress was found to reduce in paracetamol-induced mice by treatment with equivalent quantities (1mg/kg BW) of GG-CMC@PIP nanocomposites, PIP, and silymarin. Our findings suggested that GG-CMC@PIP nanocomposites could be effective as a traditional paracetamol antidote as PIP has promising antioxidant properties. Additionally, our results showed that the synthesized nanocomposites had no negative effects on the liver if the dose was properly standardized. Therefore, it may be suggested that the nanocomposite possesses a potentially promising therapeutic role against paracetamol-induced oxidative stress-mediated acute liver disorders.

Chapter 7

General Conclusion

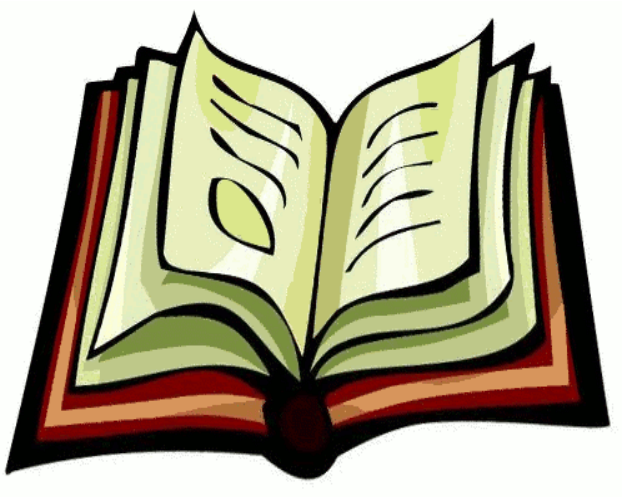

7. Conclusion

In conclusion, this thesis discussed and highlighted the significant potential of various polymer-based composite materials including TQ and PIP incorporated GG composite, TQ incorporated CH-AL and PH-AL composite film, PIP loaded GG-CMC and GG-PH nanocomposite.

In Chapter 2, a biopolymeric vehicle derived from guar gum is synthesized and two natural therapeutics PIP and TQ were incorporated to evaluate their dual therapeutic properties. The solubility of hydrophobic TQ and PIP can be increased by nanonization and optimum delivery can be achieved by an appropriate combination of GG. Synthesized biocomposites (GG-PIP, GG-TQ, GG-PIP-TQ) showed remarkable synergistic bactericidal activity against Gram-positive (*E.faecalis, S.aureus*) and Gram-negative (*P. aeruginosa, E. coli*) strains which are capable of causing systemic infections. Our study revealed that elevated level of ROS accumulation is the major cause of bacterial growth inhibition. Increased levels of bacterial ROS may be due to the effective penetration of natural therapeutics into the bacterial cells that causes oxidative stress, resulting in cell perforations, cell deformations, and membrane damage confirmed by FESEM images of treated bacteria. In hepatocellular carcinoma cell line (HepG2) GG-PIP-TQ exhibited oxidative stress-mediated synergism in cytotoxic activity confirmed by dose-dependent MTT assay. As intracellular NADPH and GSH levels are crucial in maintaining homeostasis of the ROS level, a drastic dose-dependent diminish in NADPH and GSH levels leads to oxidative stress-mediated mortality of HepG2 cells after GG-PIP-TQ treatment. Considering the tolerance level of bacteria and the IC_{50} value against HepG2 cells, this new amalgamation of TQ and PIP with biopolymer GG suggested a remarkable synergistic effect. Both antibacterial and anticancer activities of GG-PIP-TQ implied that these two phytochemicals may activate each other's mode of action leads to synergism in their bactericidal and anticancer potentials. From the overall observations, we can conclude that this novel amalgamation with porous polymeric substances can improve the efficacy of natural therapeutic delivery. The pH-responsive sustained release of therapeutics is beneficial for anticancer activity and also required for the survivability of normal healthy cells. Thus, the therapeutic application of our combined amalgamation can be a suitable alternative to conventional drugs to overcome the problem of side effects and antibiotic resistance associated with synthetic drugs.

In chapter 3, we have synthesized high-performance biocompatible composite polymer films having antimicrobial and anticancer properties by simply combining CH with PH or AL without the addition of any stabilizer or chemical modification of film surfaces. The obtained

polymer composites incorporating TQ were characterized to evaluate their morphology, physico-chemical properties and thermal stability by different techniques, from which we can confirm effective interactions and good compatibility between precursor polymers and TQ. We observed elevated intracellular ROS-mediated cell mortality in *P. aeruginosa* and *E. faecalis* strains after treatment with the composite films. Notably, compared to TQ@CH-AL, TQ@CH-PH displayed significantly enhanced *in vitro* TQ release as well as better antibacterial efficacy. An *in vitro* cytotoxicity study by MTT assay showed that the therapeutic loaded polymeric films possess ROS mediated anticancer potentials against PC3 and A549 cell lines. MTT assay against WI38 cell line also confirmed moderate biocompatibility which suggests proper dose standardisation during therapeutic applications. Hence, from an overall study, we can conclude that husk mucilage can be used to develop effective polymeric film in combination with another polymer if properly standardized. Thus, the combination of compatible nontoxic therapeutic agents with bio-composite films can emerge as an excellent dual therapeutic material.

In chapter 4, We developed natural polysaccharides such as GG and PH mucilage-derived PIP incorporated nanocomposite following an economical and robust synthesis procedure where hydrophobic phytocomponent PIP was nanonized and loaded in the biopolymeric composite. Natural polysaccharides such as GG and PH mucilage exert promising advantages such as non-toxicity, non-immunogenicity, excellent swelling ability, biocompatibility, and most importantly having an innate pharmacological property of polysaccharides. The synthesized nanocomposites exhibited a very high loading capacity (up to 83%) and sustained release behaviour of piperine. GG-PH@PIP nanocomposites have shown promising bactericidal capacities against Gram-negative *P. aeruginosa*, and Gram-positive *S. aureus.* Therapeutic loaded nanocomposites have elevated oxidative stress mediated anticancer properties against human A549 cell lines as well as moderate biocompatibility against normal human lung fibroblasts (WI38) cell lines. From experimental outcomes, it can be said that PH mucilage can be utilized to formulate effective bio-polymeric drug carriers in combination with other biomaterials if properly standardized. PIP, being a predominant dietary alkaloid with pro-oxidant properties might be convenient in formulation of a potential nanomedicine. The development of a multiple-response biopolymer-based nanocomposite like GG-PH@PIP is a crucial need to explore diverse biomedical applications.

In chapter 5, We have successfully developed natural polymer (GG and CMC) derived PIP incorporated nanocomposite following a cost-effective and simple synthesis procedure for dual therapeutic applications. GG-CMC@PIP can be an efficient drug delivery system with several promising advantages such as non-toxicity, excellent swelling ability, high drug loading

capacity (86 ± .46 %), sustained drug release property, etc. Our study has shown excellent bactericidal property of GG-CMC@PIP nanocomposites against Gram-positive *E. faecalis* and Gram-negative *E. coli* and *P. aeruginosa.* Oxidative stress, depolarized mitochondrion and higher degree of nuclear damage confirmed promising anticancer activity against C6 glioma cell. Considering all these new observations, we believe that PIP, being an alkaloid phytochemical might be convenient as a potential nanomedicine for versatile applications. As disease treatment frequently requires multi-dimensional drugs to combat with wide range of complications, the development of a multiple-response biopolymeric nanocomposite like GG-CMC@PIP is an urgent requirement to explore diverse pharmacological applications. In conclusion, our study established that the hydrophilic biocompatible GG-CMC@PIP can emerge as an ideal platform for multiple therapeutic applications.

In chapter 6, Nowadays, research on appropriate phyto-therapeutical remedies is necessary due to the adverse effects of conventional drugs used to treat liver disorders. Phytochemicals are less toxic, easily available, inexpensive, and biocompatible. We synthesized natural polymer (GG and CMC) derived PIP incorporated nanocomposite to investigate *in-vivo* hepatoprotective activity of synthesized GG-CMC@PIP in Swiss albino mice model. The induction with paracetamol leads to hyperbilirubinemia and a significant increase in liver enzymes such as AST, ALT, and ALP levels in all the paracetamol-treated groups when compared to the normal control. SOD and CAT enzyme levels are associated with the antioxidant defense system of liver cells. The stored antioxidant enzyme pool is depleted quickly resulting in oxidative stress-mediated liver injury and hyperbilirubinemia after a paracetamol overdose. GG-CMC@PIP treatment significantly increased these antioxidant enzyme activities. The ROS accumulation in the hepatocytes of paracetamol-treated animals was significantly higher than that in the control animals but significantly reduced in the livers of GG-CMC@PIP treated mice. After that, all the results of body weight demonstrated that the group receiving paracetamol treatment gained satisfactory weight after initiation of nanocomposite treatment. Whereas GG-CMC treated group displayed similar retarded weight gain when compared to paracetamol treated auto-recovery group. Moreover, our study suggested the enhanced efficacy of orally administered GG-CMC@PIP compared to bulk PIP as well as silymarin, a well-known hepatoprotective therapeutic. Therefore, it can be concluded that synthesized nanocomposite had promising hepatoprotective property against paracetamol-induced liver disorder.

References

1. Dutta, A., Lal, N., Naaz, M., Ghosh, A. and Verma, R., 2014. Ethnological and Ethno-medicinal importance of Aegle marmelos (L.) Corr (Bael) among indigenous people of India. *American journal of ethnomedicine*, *1*(5), pp.290-312.
2. Ur-Rahman, I., Sher, H. and Bussmann, R.W. eds., 2019. Reference guide on high value medicinal and aromatic plants–sustainable management and cultivation practices. *University of Swat, Pakistan*.
3. Das, B. and Patra, S., 2017. Antimicrobials: meeting the challenges of antibiotic resistance through nanotechnology. In *Nanostructures for antimicrobial therapy* (pp. 1-22). Elsevier.
4. Gajdács, M., Spengler, G. and Urbán, E., 2017. Identification and antimicrobial susceptibility testing of anaerobic bacteria: Rubik's cube of clinical microbiology?. *Antibiotics*, *6*(4), p.25.
5. Alekshun, M.N. and Levy, S.B., 2007. Molecular mechanisms of antibacterial multidrug resistance. *Cell*, *128*(6), pp.1037-1050.
6. Rahman, H.S., Othman, H.H., Hammadi, N.I., Yeap, S.K., Amin, K.M., Abdul Samad, N. and Alitheen, N.B., 2020. Novel drug delivery systems for loading of natural plant extracts and their biomedical applications. *International journal of nanomedicine*, pp.2439-2483.
7. Nath, R., Roy, R., Barai, G., Bairagi, S., Manna, S. and Chakraborty, R., 2021. Modern developments of nano based grug delivery system by combined with phytochemicals-presenting new aspects. *Int. J. Sci. Res. Sci. Technol*, *8*, pp.107-129.
8. Gupta, M., Chauhan, D.N., Sharma, V. and Chauhan, N.S. eds., 2019. *Novel drug delivery systems for phytoconstituents*. CRC Press.
9. Patwardhan, B. and Partwardhan, A., 2005. *Traditional Medicine: Modern Approach for affordable global health* (pp. 1-172). Switzerland: World Health Organization.
10. Rosangkima, G. and Prasad, S.B., 2004. Antitumour activity of some plants from Meghalaya and Mizoram against murine ascites Dalton's lymphoma.
11. Estrada Meza, C., The effect of thymoquinone on key onco-and tumor suppressor miRNAs in HCT-15 colorectal cancer cell line.
12. Zhu, M., Sun, Y., Su, Y., Guan, W., Wang, Y., Han, J., Wang, S., Yang, B., Wang, Q. and Kuang, H., 2024. Luteolin: A promising multifunctional natural flavonoid for human diseases. *Phytotherapy Research*.

13. Yousefi, M., Narmani, A. and Jafari, S.M., 2020. Dendrimers as efficient nanocarriers for the protection and delivery of bioactive phytochemicals. *Advances in colloid and interface science*, *278*, p.102125.

14. Jeetah, R., Bhaw-Luximon, A. and Jhurry, D., 2014. Nanopharmaceutics: phytochemical-based controlled or sustained drug-delivery systems for cancer treatment. *Journal of biomedical nanotechnology*, *10*(9), pp.1810-1840.

15. Upaganlawar, A., Polshettiwar, S., Raut, S., Tagalpallewar, A. and Pande, V., 2022. Effective cancer management: Inimitable role of phytochemical based nano-formulations. *Current Drug Metabolism*, *23*(11), pp.869-881.

16. Shariatinia, Z., 2020. Biopolymeric nanocomposites in drug delivery. *Advanced Biopolymeric Systems for Drug Delivery*, pp.233-290.

17. Shahcheraghi, N., Golchin, H., Sadri, Z., Tabari, Y., Borhanifar, F. and Makani, S., 2022. Nano-biotechnology, an applicable approach for sustainable future. *3 Biotech*, *12*(3), p.65.

18. Kumar, M.S., PZ: 01 Solid lipid nanoparticles-a new approach to increase bioavailability.

19. Sohail, M., Rabbi, F., Younas, A., Hussain, A., Yu, B., Li, Y., Iqbal, S., Ullah, K.H., Qadeer, A., Aquib, M. and Iqbal, H., 2022. Herbal bioactive–based nano drug delivery systems. In *Herbal Bioactive-Based Drug Delivery Systems* (pp. 169-193). Academic Press.

20. Jain, K.K., 2020. An overview of drug delivery systems. *Drug Delivery Systems*, pp.1-54.

21. Saghazadeh, S., Rinoldi, C., Schot, M., Kashaf, S.S., Sharifi, F., Jalilian, E., Nuutila, K., Giatsidis, G., Mostafalu, P., Derakhshandeh, H. and Yue, K., 2018. Drug delivery systems and materials for wound healing applications. *Advanced drug delivery reviews*, *127*, pp.138-166.

21. Adepu, S. and Ramakrishna, S., 2021. Controlled drug delivery systems: current status and future directions. *Molecules*, *26*(19), p.5905.

22. Syed, M.H., Zahari, M.A.K.M., Khan, M.M.R., Beg, M.D.H. and Abdullah, N., 2023. An overview on recent biomedical applications of biopolymers: Their role in drug delivery systems and comparison of major systems. *Journal of Drug Delivery Science and Technology*, *80*, p.104121.

23. Mondal, A., Nayak, A.K., Chakraborty, P., Banerjee, S. and Nandy, B.C., 2023. Natural polymeric nanobiocomposites for anti-cancer drug delivery therapeutics: A recent update. *Pharmaceutics*, *15*(8), p.2064.

24. Xiong, R., Grant, A.M., Ma, R., Zhang, S. and Tsukruk, V.V., 2018. Naturally-derived biopolymer nanocomposites: Interfacial design, properties and emerging applications. *Materials Science and Engineering: R: Reports*, *125*, pp.1-41.

25. Bhatia, S. and Bhatia, S., 2016. Natural polymers vs synthetic polymer. *Natural polymer drug delivery systems: nanoparticles, plants, and algae*, pp.95-118.

26. Kakkalameli, S., Daphedar, A.B., Faniband, B., Sharma, S., Nadda, A.K., Ferreira, L.F.R., Bilal, M., Américo-Pinheiro, J.H.P. and Mulla, S.I., 2022. Biopolymers and environment. In *Biopolymers: Recent Updates, Challenges and Opportunities* (pp. 19-33). Cham: Springer International Publishing.

27. Nayak, A.K., Hasnain, M.S. and Pal, D. eds., 2019. *Natural Polymers for Pharmaceutical Applications: Volume 1: Plant-Derived Polymers*. CRC Press.

28. Park, J.H., Saravanakumar, G., Kim, K. and Kwon, I.C., 2010. Targeted delivery of low molecular drugs using chitosan and its derivatives. *Advanced drug delivery reviews*, *62*(1), pp.28-41

29. Ogaji, I.J., Nep, E.I. and Audu-Peter, J.D., 2012. Advances in natural polymers as pharmaceutical excipients.

30. Adepu, S. and Ramakrishna, S., 2021. Controlled drug delivery systems: current status and future directions. *Molecules*, *26*(19), p.5905.

31. Rouf, T.B. and Kokini, J.L., 2018. Natural biopolymer-based nanocomposite films for packaging applications. *Bionanocomposites for packaging applications*, pp.149-177.

32. Zewde, B., Atoyebi, O., Zvonkina, I.J., Thomspon, T., Hargrove, A., Scott, A. and Raghavan, D., 2020. Biopolymer Nanocomposites and Their Applications. In *Soft Matter and Biomaterials on the Nanoscale: The WSPC Reference on Functional Nanomaterials—Part I Volume 2: Polymers on the Nanoscale: Nano-structured Polymers and Their Applications* (pp. 45-108).

33. Kumari, S.V.G., Manikandan, N.A., Pakshirajan, K. and Pugazhenthi, G., 2020. Sustained drug release and bactericidal activity of a novel, highly biocompatible and biodegradable polymer nanocomposite loaded with norfloxacin for potential use in antibacterial therapy. *Journal of Drug Delivery Science and Technology*, *59*, p.101900.

34. Maji, B., 2019. Introduction to natural polysaccharides. In *Functional polysaccharides for biomedical applications* (pp. 1-31). Woodhead Publishing.

35. Kabir, S.F., Rahman, A., Yeasmin, F., Sultana, S., Masud, R.A., Kanak, N.A. and Haque, P., 2022. Occurrence, distribution, and structure of natural polysaccharides. In *Radiation-processed polysaccharides* (pp. 1-27). Academic Press.

36. Lu, X., Chen, J., Guo, Z., Zheng, Y., Rea, M.C., Su, H., Zheng, X., Zheng, B. and Miao, S., 2019. Using polysaccharides for the enhancement of functionality of foods: A review. *Trends in Food Science & Technology*, *86*, pp.311-327.

37. Yu, L., Dean, K. and Li, L., 2006. Polymer blends and composites from renewable resources. *Progress in polymer science*, *31*(6), pp.576-602.

38. Paul, D.R. and Barlow, J.W., 1980. Polymer blends. *Journal of Macromolecular Science—Reviews in Macromolecular Chemistry*, *18*(1), pp.109-168.

39. Zhang, Z.P., Rong, M.Z. and Zhang, M.Q., 2018. Polymer engineering based on reversible covalent chemistry: A promising innovative pathway towards new materials and new functionalities. *Progress in Polymer Science*, *80*, pp.39-93.

40. Tillet, G., Boutevin, B. and Ameduri, B., 2011. Chemical reactions of polymer crosslinking and post-crosslinking at room and medium temperature. *Progress in polymer science*, *36*(2), pp.191-217.

41. Nielsen, L.E., 1969. Cross-linking–effect on physical properties of polymers. *Journal of Macromolecular Science, Part C*, *3*(1), pp.69-103.

42. Ghosh, M., Halperin-Sternfeld, M. and Adler-Abramovich, L., 2019. Bio mimicking of extracellular matrix. *Biological and Bio-inspired Nanomaterials: Properties and Assembly Mechanisms*, pp.371-399.

43. Khan, M.U.A., Aslam, M.A., Abdullah, M.F.B., Hasan, A., Shah, S.A. and Stojanović, G.M., 2023. Recent perspective of polymeric biomaterial in tissue engineering–a review. *Materials Today Chemistry*, *34*, p.101818.

44. Das, A., Ringu, T., Ghosh, S. and Pramanik, N., 2023. A comprehensive review on recent advances in preparation, physicochemical characterization, and bioengineering applications of biopolymers. *Polymer Bulletin*, *80*(7), pp.7247-7312.

45. Polman, E.M., Gruter, G.J.M., Parsons, J.R. and Tietema, A., 2021. Comparison of the aerobic biodegradation of biopolymers and the corresponding bioplastics: A review. *Science of the Total Environment*, *753*, p.141953.

46. Asthana, N., Pal, K., Khan, A.A. and Malik, A., 2024. Novel biopolymeric materials potential utilization for environmental practices. *Journal of Molecular Structure*, p.138390.

47. Arif, Z.U., Khalid, M.Y., Sheikh, M.F., Zolfagharian, A. and Bodaghi, M., 2022. Biopolymeric sustainable materials and their emerging applications. *Journal of Environmental Chemical Engineering*, *10*(4), p.108159.

48. Fazal, T., Murtaza, B.N., Shah, M., Iqbal, S., Rehman, M.U., Jaber, F., Dera, A.A., Awwad, N.S. and Ibrahium, H.A., 2023. Recent developments in natural biopolymer based drug delivery systems. *RSC advances*, *13*(33), pp.23087-23121.

49. Verma, M.L., Dhanya, B.S., Rani, V., Thakur, M., Jeslin, J. and Kushwaha, R., 2020. Carbohydrate and protein based biopolymeric nanoparticles: current status and biotechnological applications. *International journal of biological macromolecules*, *154*, pp.390-412.

50. Tardy, B.L., Mattos, B.D., Otoni, C.G., Beaumont, M., Majoinen, J., Kämäräinen, T. and Rojas, O.J., 2021. Deconstruction and reassembly of renewable polymers and biocolloids into next generation structured materials. *Chemical reviews*, *121*(22), pp.14088-14188.

51. Mori, R., 2023. Replacing all petroleum-based chemical products with natural biomass-based chemical products: a tutorial review. *RSC Sustainability*, *1*(2), pp.179-212.

52. Udayakumar, G.P., Muthusamy, S., Selvaganesh, B., Sivarajasekar, N., Rambabu, K., Banat, F., Sivamani, S., Sivakumar, N., Hosseini-Bandegharaei, A. and Show, P.L., 2021. Biopolymers and composites: Properties, characterization and their applications in food, medical and pharmaceutical industries. *Journal of Environmental Chemical Engineering*, *9*(4), p.105322.

53. Kouhi, M., Prabhakaran, M.P. and Ramakrishna, S., 2020. Edible polymers: An insight into its application in food, biomedicine and cosmetics. *Trends in Food Science & Technology*, *103*, pp.248-263.

54. Alias, N.H., Abdullah, N., Othman, N.H., Marpani, F., Zainol, M.M. and Shayuti, M.S.M., 2022. Sustainability challenges and future perspectives of biopolymer. In *Biopolymers: Recent Updates, Challenges and Opportunities* (pp. 373-389). Cham: Springer International Publishing.

55. Mtibe, A., Motloung, M.P., Bandyopadhyay, J. and Ray, S.S., 2021. Synthetic biopolymers and their composites: Advantages and limitations—An overview. *Macromolecular rapid communications*, *42*(15), p.2100130.

56. Patti, Antonella, and Domenico Acierno. "Towards the sustainability of the plastic industry through biopolymers: properties and potential applications to the textiles world." *Polymers* 14, no. 4 (2022): 692.

57. Kartik, A., Akhil, D., Lakshmi, D., Gopinath, K.P., Arun, J., Sivaramakrishnan, R. and Pugazhendhi, A., 2021. A critical review on production of biopolymers from algae biomass and their applications. *Bioresource Technology*, *329*, p.124868.

58. Kreyenschulte, D., Krull, R. and Margaritis, A., 2014. Recent advances in microbial biopolymer production and purification. *Critical reviews in biotechnology*, *34*(1), pp.1-15.

59. Pires, J.R.A., Souza, V.G.L., Fuciños, P., Pastrana, L. and Fernando, A.L., 2022. Methodologies to assess the biodegradability of bio-based polymers—current knowledge and existing gaps. *Polymers*, *14*(7), p.1359.

60. He, Q., Chen, J., Yan, J., Cai, S., Xiong, H., Liu, Y., Peng, D., Mo, M. and Liu, Z., 2020. Tumor microenvironment responsive drug delivery systems. *Asian Journal of Pharmaceutical Sciences*, *15*(4), pp.416-448.

61. Abuwatfa, W.H., Awad, N.S., Pitt, W.G. and Husseini, G.A., 2022. Thermosensitive polymers and thermo-responsive liposomal drug delivery systems. *Polymers*, *14*(5), p.925.

62. Mura, S., Nicolas, J. and Couvreur, P., 2013. Stimuli-responsive nanocarriers for drug delivery. *Nature materials*, *12*(11), pp.991-1003.

63. Raza, A., Rasheed, T., Nabeel, F., Hayat, U., Bilal, M. and Iqbal, H.M., 2019. Endogenous and exogenous stimuli-responsive drug delivery systems for programmed site-specific release. *Molecules*, *24*(6), p.1117.

64. Liu, D., Bimbo, L.M., Mäkilä, E., Villanova, F., Kaasalainen, M., Herranz-Blanco, B., Caramella, C.M., Lehto, V.P., Salonen, J., Herzig, K.H. and Hirvonen, J., 2013. Co-delivery of a hydrophobic small molecule and a hydrophilic peptide by porous silicon nanoparticles. *Journal of Controlled Release*, *170*(2), pp.268-278.

65. Zhang, L., Radovic-Moreno, A.F., Alexis, F., Gu, F.X., Basto, P.A., Bagalkot, V., Jon, S., Langer, R.S. and Farokhzad, O.C., 2007. Co-delivery of hydrophobic and hydrophilic drugs from nanoparticle–aptamer bioconjugates. *ChemMedChem: Chemistry Enabling Drug Discovery*, *2*(9), pp.1268-1271.

66. Medina, C., Santos-Martinez, M.J., Radomski, A., Corrigan, O.I. and Radomski, M.W., 2007. Nanoparticles: pharmacological and toxicological significance. *British journal of pharmacology*, *150*(5), pp.552-558.

67. Shim, M.S. and Kwon, Y.J., 2012. Stimuli-responsive polymers and nanomaterials for gene delivery and imaging applications. *Advanced drug delivery reviews*, *64*(11), pp.1046-1059.

68. Sun, R., Liu, Y., Li, S.Y., Shen, S., Du, X.J., Xu, C.F., Cao, Z.T., Bao, Y., Zhu, Y.H., Li, Y.P. and Yang, X.Z., 2015. Co-delivery of all-trans-retinoic acid and doxorubicin for cancer therapy with synergistic inhibition of cancer stem cells. *Biomaterials*, *37*, pp.405-414

69. Zhang, P., Liu, G. and Chen, X., 2017. Nanobiotechnology: cell membrane-based delivery systems. *Nano today*, *13*, pp.7-9.

70. Lee, S.M., Park, H., Choi, J.W., Park, Y.N., Yun, C.O. and Yoo, K.H., 2011. Multifunctional nanoparticles for targeted chemophotothermal treatment of cancer cells. *Angewandte Chemie International Edition*, *50*(33), pp.7581-7586.

71. Kumar, S., Michael, I.J., Park, J., Granick, S. and Cho, Y.K., 2018. Cloaked exosomes: biocompatible, durable, and degradable encapsulation. *Small*, *14*(34), p.1802052.

72. Xue, J., Zhao, Z., Zhang, L., Xue, L., Shen, S., Wen, Y., Wei, Z., Wang, L., Kong, L., Sun, H. and Ping, Q., 2017. Neutrophil-mediated anticancer drug delivery for suppression of postoperative malignant glioma recurrence. *Nature nanotechnology*, *12*(7), pp.692-700.

73. Fang, R.H., Hu, C.M.J. and Zhang, L., 2012. Nanoparticles disguised as red blood cells to evade the immune system. *Expert opinion on biological therapy*, *12*(4), pp.385-389.

74. Kuai, R., Ochyl, L.J., Bahjat, K.S., Schwendeman, A. and Moon, J.J., 2017. Designer vaccine nanodiscs for personalized cancer immunotherapy. *Nature materials*, *16*(4), pp.489-496.

75. Peppas, N.A., 2004. Intelligent therapeutics: biomimetic systems and nanotechnology in drug delivery. *Advanced drug delivery reviews*, *56*(11), pp.1529-1531.

76. Yoo, J.W., Irvine, D.J., Discher, D.E. and Mitragotri, S., 2011. Bio-inspired, bioengineered and biomimetic drug delivery carriers. *Nature reviews Drug discovery*, *10*(7), pp.521-535.

77. Peng, S., Wang, Y., Li, N. and Li, C., 2017. Enhanced cellular uptake and tumor penetration of nanoparticles by imprinting the “hidden” part of membrane receptors for targeted drug delivery. *Chemical communications*, *53*(81), pp.11114-11117.

78. Muro, S., 2012. Challenges in design and characterization of ligand-targeted drug delivery systems. *Journal of Controlled Release*, *164*(2), pp.125-137.

79. Ruan, S., Zhou, Y., Jiang, X. and Gao, H., 2021. Rethinking CRITID procedure of brain targeting drug delivery: circulation, blood brain barrier recognition, intracellular transport, diseased cell targeting, internalization, and drug release. *Advanced Science*, *8*(9), p.2004025.

80. Ling, D., Hackett, M.J. and Hyeon, T., 2014. Surface ligands in synthesis, modification, assembly and biomedical applications of nanoparticles. *Nano Today*, *9*(4), pp.457-477

81. Dehaini, D., Fang, R.H. and Zhang, L., 2016. Biomimetic strategies for targeted nanoparticle delivery. *Bioengineering & translational medicine*, *1*(1), pp.30-46.

82. Singh, A.K., Harrison, S.H. and Schoeniger, J.S., 2000. Gangliosides as receptors for biological toxins: development of sensitive fluoroimmunoassays using ganglioside-bearing liposomes. *Analytical chemistry*, *72*(24), pp.6019-6024.

83. Tong, H.H., McIver, M.A., Fisher, L.M. and DeMaria, T.F., 1999. Effect of lacto-N-neotetraose, asialoganglioside-GM1 and neuraminidase on adherence of otitis media-associated serotypes ofStreptococcus pneumoniaeto chinchilla tracheal epithelium. *Microbial pathogenesis*, *26*(2), pp.111-119.

84. Davidson, R.L., 1980. Handbook of water-soluble gums and resins.

85. Mudgil, D., Barak, S. and Khatkar, B.S., 2014. Guar gum: processing, properties and food applications—a review. *Journal of food science and technology*, *51*, pp.409-418.

86. Sharma, G., Sharma, S., Kumar, A., Ala'a, H., Naushad, M., Ghfar, A.A., Mola, G.T. and Stadler, F.J., 2018. Guar gum and its composites as potential materials for diverse applications: A review. *Carbohydrate polymers*, *199*, pp.534-545.

87. Dutta, K., Das, B., Mondal, D., Adhikari, A., Rana, D., Chattopadhyay, A.K., Banerjee, R., Mishra, R. and Chattopadhyay, D., 2017. An ex situ approach to fabricating nanosilica reinforced polyacrylamide grafted guar gum nanocomposites as an efficient biomaterial for transdermal drug delivery application. *New Journal of Chemistry*, *41*(17), pp.9461-9471.

88. Bahamdan, A. and Daly, W.H., 2007. Hydrophobic guar gum derivatives prepared by controlled grafting processes. *Polymers for Advanced Technologies*, *18*(8), pp.652-659.

89. Prabaharan, M., 2011. Prospective of guar gum and its derivatives as controlled drug delivery systems. *International journal of biological macromolecules*, *49*(2), pp.117-124.

90. Bharaniraja, B., Jayaram Kumar, K., Prasad, C.M. and Sen, A.K., 2011. Modified katira gum for colon targeted drug delivery. *Journal of Applied Polymer Science*, *119*(5), pp.2644-2651.

91. Thakur, S., Chauhan, G.S. and Ahn, J.H., 2009. Synthesis of acryloyl guar gum and its hydrogel materials for use in the slow release of l-DOPA and l-tyrosine. *Carbohydrate Polymers*, *76*(4), pp.513-520.

92. Altaf, S.A., Yu, K., Parasrampuria, J. and Friend, D.R., 1998. Guar gum-based sustained release diltiazem. *Pharmaceutical research*, *15*, pp.1196-1201.

93. Al-Saidan, S.M., Krishnaiah, Y.S.R., Satyanarayana, V., Bhaskar, P. and Karthikeyan, R.S., 2004. Pharmacokinetic evaluation of guar gum-based three-layer matrix tablets for oral controlled delivery of highly soluble metoprolol tartrate as a model drug. *European journal of pharmaceutics and Biopharmaceutics*, *58*(3), pp.697-703.

94. Baweja, J.M. and Misra, A.N., 1997. Studies on kinetics of drug release from modified guar gum hydrophilic matrices. *Indian journal of pharmaceutical sciences*, *59*(6), pp.316-320.

95. Kumari, S. and Kishor, R., 2020. Chitin and chitosan: origin, properties, and applications. In *Handbook of chitin and chitosan* (pp. 1-33). Elsevier.

96. Krajewska B. Membrane-based processes performed with use of chitin/chitosan materials. Sep Purif Technol 2005;41:305e12.

97. Gutiérrez, T.J., 2017. Chitosan applications for the food industry. *Chitosan: Derivatives, composites and applications*, pp.183-232.

98. Singh, P., Mishra, G. and Dinda, S.C., 2021. Natural excipients in pharmaceutical formulations. *Evidence Based Validation of Traditional Medicines: A comprehensive Approach*, pp.829-869.

99. Ariful Islam, M., Park, T.E., Reesor, E., Cherukula, K., Hasan, A., Firdous, J., Singh, B., Kang, S.K., Choi, Y.J., Park, I.K. and Cho, C.S., 2015. Mucoadhesive chitosan derivatives as novel drug carriers. *Current pharmaceutical design*, *21*(29), pp.4285-4309.

100. Ranjbar-Mohammadi, M., Arami, M., Bahrami, H., Mazaheri, F. and Mahmoodi, N.M., 2010. Grafting of chitosan as a biopolymer onto wool fabric using anhydride bridge and its antibacterial property. *Colloids and Surfaces B: Biointerfaces*, *76*(2), pp.397-403.

101. Vasudev, S.C., Chandy, T. and Sharma, C.P., 1997. Development of chitosan/polyethylene vinyl acetate co-matrix: controlled release of aspirin-heparin for preventing cardiovascular thrombosis. *Biomaterials*, *18*(5), pp.375-381.

102. Sahasathian T., Kerdcholpetch T., Chanweroch A., Praphairaksit N., Suwonjandee N., Muangsin N.: Sustained release of amoxicillin from chitosan tablets. Arch. Pharm. Res. (2007), 304, 526-531.

103. H. Bao, Y. Pan, Y. Ping, N.G. Sahoo, T. Wu, L. Li, J. Li, L.H. Gan, Chitosan-Functionalized graphene oxide as a nanocarrier for drug and gene delivery, Small 7 (2011) 1569–1578, http://dx.doi.org/10.1002/smll.201100191.

104. Xie, M., Lei, H., Zhang, Y., Xu, Y., Shen, S., Ge, Y., Li, H. and Xie, J., 2016. Non-covalent modification of graphene oxide nanocomposites with chitosan/dextran and its application in drug delivery. *RSC advances*, *6*(11), pp.9328-9337.

105. Reddy, K.M., Babu, V.R., Sairam, M., Subha, M.C.S., Mallikarjuna, N.N., Kulkarni, P.V. and Aminabhavi, T.M., 2006. Development of chitosan-guar gum semi-interpenetrating polymer network microspheres for controlled release of cefadroxil. *Designed monomers and polymers*, *9*(5), pp.491-501.

106. Yadav, M. and Ahmadi, Y., 2019. Alginates: Source, chemistry, and properties. In *Alginates* (pp. 1-24). Apple Academic Press

107. Liew CV, Chan LW, Ching AL, Heng PWS. Evaluation of sodium alginate as drug release modifier in matrix tablets. *Int J Pharm* 2006, 309, 25-37.

108. Draget, K.I., Skjåk-Bræk, G. and Smidsrød, O., 1997. Alginate based new materials. *International journal of biological macromolecules*, *21*(1-2), pp.47-55.

109. Miyazaki S., Nakayama A., Oda M., Takada M., Attwood D.: Chitosan and sodium alginate based bioadhesive tablets for intraoral drug delivery. Biol. Pharm. Bull. (1994), 17, 5, 745-747.

110. Goel H., Tiwary A. K., Rana V.: Fabrication and optimization of fast disintegrating tablets employing interpolymeric chitosan-alginate complex and chitin as novel superdisintegrants. Acta Pol. Pharm. (2011), 68, 4, 571-583.

111. Anirudhan, T.S. and Nair, S.S., 2019. Polyelectrolyte complexes of carboxymethyl chitosan/alginate based drug carrier for targeted and controlled release of dual drug. *Journal of Drug Delivery Science and Technology*, *51*, pp.569-582.

112. Van Craeyveld, V., Delcour, J.A. and Courtin, C.M., 2009. Extractability and chemical and enzymic degradation of psyllium (Plantago ovata Forsk) seed husk arabinoxylans. *Food chemistry*, *112*(4), pp.812-819.

113. Singh, B., 2007. Psyllium as therapeutic and drug delivery agent. *International journal of pharmaceutics*, *334*(1-2), pp.1-14.

114. Kumar et al., 2017. D. Kumar, J.Pandey, P.Kumar, V. Raj. Psyllium Mucilage and Its Use in Pharmaceutical Field: An Overview. Current Synthetic and Systems Biology, 5 (1), (2017). DOI: 10.4172/2332-0737.1000134

115. Jani, G.K., Shah, D.P., Prajapati, V.D. and Jain, V.C., 2009. Gums and mucilages: versatile excipients for pharmaceutical formulations. *Asian J Pharm Sci*, *4*(5), pp.309-323.].

116. Mehmood, M.H., Aziz, N., Ghayur, M.N. and Gilani, A.H., 2011. Pharmacological basis for the medicinal use of psyllium husk (Ispaghula) in constipation and diarrhea. *Digestive Diseases and Sciences*, *56*, pp.1460-1471

117. Singh, B., Bala, R. and Chauhan, N., 2008. In vitro release dynamics of model drugs from psyllium and acrylic acid based hydrogels for the use in colon specific drug delivery. *Journal of Materials Science: Materials in Medicine*, *19*, pp.2771-2780.

118. Rosu, M.C. and Bratu, I., 2014. Promising psyllium-based composite containing TiO2 nanoparticles as aspirin-carrier matrix. *Progress in Natural Science: Materials International*, *24*(3), pp.205-209.

119. Kumar, D., Gautam, A. and Kundu, P.P., 2022. Synthesis of pH-sensitive grafted psyllium: Encapsulation of quercetin for colon cancer treatment. *Journal of Applied Polymer Science*, *139*(4), p.51552.

120. Patil, B.S., Mastiholimath, V.S. and Kulkarni, A.R., 2011. Development and evaluation of psyllium seed husk polysaccharide based wound dressing films. *Oriental pharmacy and experimental medicine*, *11*, pp.123-129.

121. Javanbakht, S. and Shaabani, A., 2019. Carboxymethyl cellulose-based oral delivery systems. *International journal of biological macromolecules*, *133*, pp.21-29.

122. Butun, S., Ince, F.G., Erdugan, H. and Sahiner, N., 2011. One-step fabrication of biocompatible carboxymethyl cellulose polymeric particles for drug delivery systems. *Carbohydrate polymers*, *86*(2), pp.636-643.

123. Pourmadadi, M., Rahmani, E., Shamsabadipour, A., Samadi, A., Esmaeili, J., Arshad, R., Rahdar, A., Tavangarian, F. and Pandey, S., 2023. Novel carboxymethyl cellulose based nanocomposite: A promising biomaterial for biomedical applications. *Process Biochemistry*.

124. Song, Y., Zhou, J., Li, O., Guo, Y., & Zhang, L. (2009). Preparation and characterization of novel quaternized cellulose nanoparticles as protein carriers. Macromolecular Bioscience, 9, 857–863.

125. He, F., Liu, J., Roberts, C. B., & Zhao, D. (2009). One-step "green" synthesis of Pd nanoparticles of controlled size and their catalytic activity for trichloroethene hydrodechlorination. Industrial & Engineering Chemistry Research, 48, 6550–6557.

126. Ng, S.F. and Jumaat, N., 2014. Carboxymethyl cellulose wafers containing antimicrobials: A modern drug delivery system for wound infections. *European Journal of Pharmaceutical Sciences*, *51*, pp.173-179.

127. Sarkar, C., Chowdhuri, A.R., Kumar, A., Laha, D., Garai, S., Chakraborty, J. and Sahu, S.K., 2018. One pot synthesis of carbon dots decorated carboxymethyl cellulose-hydroxyapatite nanocomposite for drug delivery, tissue engineering and Fe3+ ion sensing. *Carbohydrate polymers*, *181*, pp.710-718.

128. Madusanka, N., de Silva, K.N. and Amaratunga, G., 2015. A curcumin activated carboxymethyl cellulose–montmorillonite clay nanocomposite having enhanced curcumin release in aqueous media. *Carbohydrate polymers*, *134*, pp.695-699.

129. Pirsa, S., Farshchi, E. and Roufegarinejad, L., 2020. Antioxidant/antimicrobial film based on carboxymethyl cellulose/gelatin/TiO 2–Ag nano-composite. *Journal of Polymers and the Environment*, *28*, pp.3154-3163.

130. George, B.P., Chandran, R. and Abrahamse, H., 2021. Role of phytochemicals in cancer chemoprevention: Insights. *Antioxidants*, *10*(9), p.1455.

131. Najmi, A., Javed, S.A., Al Bratty, M. and Alhazmi, H.A., 2022. Modern approaches in the discovery and development of plant-based natural products and their analogues as potential therapeutic agents. *Molecules*, *27*(2), p.349.

132. Sharma, G., Prakash, D., Gupta, C., Prakash, D. and Sharma, G., 2014. Phytochemicals of nutraceutical importance: do they defend against diseases. *Phytochemicals of nutraceutical importance*, *1*.

133. Kaushik, B., Sharma, J., Kumar, P. and Shourie, A., 2021. Phytochemical properties and pharmacological role of plants: secondary metabolites. *Biosciences Biotechnology Research Asia*, *18*(1), p.23.

134. Lobo, M.G., Hounsome, N. and Hounsome, B., 2018. Biochemistry of vegetables: secondary metabolites in vegetables—terpenoids, phenolics, alkaloids, and sulfur-containing compounds. *Handbook of vegetables and vegetable processing*, pp.47-82.

135. Alamgir, A.N.M., 2017. *Therapeutic use of medicinal plants and their extracts: volume 1*. Springer International Publishing AG.

136. Pillai, R.K. and Jayasree, K., 2017. Rare cancers: Challenges & issues. *Indian Journal of Medical Research*, *145*(1), pp.17-27.

137. Karunamoorthi, K., Jegajeevanram, K., Vijayalakshmi, J. and Mengistie, E., 2013. Traditional medicinal plants: a source of phytotherapeutic modality in resource-constrained health care settings. *Journal of Evidence-Based Complementary & Alternative Medicine*, *18*(1), pp.67-74.

138. Yan, Y., Li, X., Zhang, C., Lv, L., Gao, B. and Li, M., 2021. Research progress on antibacterial activities and mechanisms of natural alkaloids: A review. *Antibiotics*, *10*(3), p.318.

139. Isah, T., 2016. Anticancer alkaloids from trees: Development into drugs. *Pharmacognosy reviews*, *10*(20), p.90.

140. Cushnie, T.T. and Lamb, A.J., 2005. Antimicrobial activity of flavonoids. *International journal of antimicrobial agents*, *26*(5), pp.343-356

141. Barbieri, R., Coppo, E., Marchese, A., Daglia, M., Sobarzo-Sánchez, E., Nabavi, S.F. and Nabavi, S.M., 2017. Phytochemicals for human disease: An update on plant-derived compounds antibacterial activity. *Microbiological research*, *196*, pp.44-68.

142. Merkl, R., Hradkova, I., Filip, V. and Šmidrkal, J., 2010. Antimicrobial and antioxidant properties of phenolic acids alkyl esters

143. Cueva, C., Moreno-Arribas, M.V., Martín-Álvarez, P.J., Bills, G., Vicente, M.F., Basilio, A., Rivas, C.L., Requena, T., Rodríguez, J.M. and Bartolomé, B., 2010. Antimicrobial activity of phenolic acids against commensal, probiotic and pathogenic bacteria. *Research in microbiology*, *161*(5), pp.372-382.

144. Petropoulos, S., Di Gioia, F. and Ntatsi, G., 2017. Vegetable organosulfur compounds and their health promoting effects. *Current pharmaceutical design*, *23*(19), pp.2850-2875.

145. Gutiérrez-del-Río, I., Fernández, J. and Lombó, F., 2018. Plant nutraceuticals as antimicrobial agents in food preservation: Terpenoids, polyphenols and thiols. *International journal of antimicrobial agents*, *52*(3), pp.309-315.

146. Farkhondeh, T., Samarghandian, S., Shahri, A.M.P. and Samini, F., 2018. The neuroprotective effects of thymoquinone: a review. *Dose-response*, *16*(2), p.1559325818761455.]

147. Khan, M.A. (2018). Antimicrobial Action of Thymoquinone. In: Younus, H. (eds) Molecular and Therapeutic actions of Thymoquinone. Springer, Singapore. https://doi.org/10.1007/978-981-10-8800-1_5]

148. Chaieb, K., Kouidhi, B., Jrah, H. *et al.* Antibacterial activity of Thymoquinone, an active principle of *Nigella sativa* and its potency to prevent bacterial biofilm formation. *BMC Complement Altern Med* **11**, 29 (2011). https://doi.org/10.1186/1472-6882-11-29]

149. Haq, A., Kumar, S., Mao, Y., Berthiaume, F. and Michniak-Kohn, B., 2020. Thymoquinone-loaded polymeric films and hydrogels for bacterial disinfection and wound healing. *Biomedicines*, *8*(10), p.386.

150. Roepke, M., Diestel, A., Bajbouj, K., Walluscheck, D., Schonfeld, P., Roessner, A., Schneider-Stock, R. and Gali-Muhtasib, H., 2007. Lack of p53 augments thymoquinone-induced apoptosis and caspase activation in human osteosarcoma cells. *Cancer biology & therapy*, *6*(2), pp.160-169.

151. Imran, M., Rauf, A., Khan, I.A., Shahbaz, M., Qaisrani, T.B., Fatmawati, S., Abu-Izneid, T., Imran, A., Rahman, K.U. and Gondal, T.A., 2018. Thymoquinone: A novel strategy to combat cancer: A review. *Biomedicine & Pharmacotherapy*, *106*, pp.390-402.

152. X. Liu, J. Dong, W. Cai, Y. Pan, R. Li, B. Li, The effect of thymoquinone on apoptosis of SK-OV-3 ovarian cancer cell by regulation of Bcl-2 and Bax, Int. J. Gynecol. Cancer 27 (8) (2017) 1596–1601.

153. A.S. Haron, S.S. Syed Alwi, L. Saiful Yazan, R. Abd Razak, Y.S. Ong, F.H. Zakarial Ansar, H. Roshini Alexander, Cytotoxic effect of thymoquinone-loaded nanostructured lipid carrier (TQ-NLC) on liver cancer cell integrated with hepatitis B genome, Hep3B, Evid. Based Complement. Altern. Med., 2018.

154. Quijia, C. R. and Chorilli, M. (2020) 'Characteristics, Biological Properties and Analytical Methods of Piperine: A Review', *Critical Reviews in Analytical Chemistry,* 50(1), pp. 62–77. doi: 10.1080/10408347.2019.1573656.

155. Hikal, D.M., 2018. Antibacterial activity of piperine and black pepper oil. *Biosciences biotechnology research Asia*, *15*(4), p.877.

156. J Rao, P., D Kolla, S., Elshaari, F., Elshaari, F., El Awamy, H., Elfrady, M., Singh, R., Belkhier, A., Srikumar, S., R Said, A. and J Dhopoide, S., 2015. Effect of piperine on liver function of CF-1 albino mice. *Infectious Disorders-Drug Targets (Formerly Current Drug Targets-Infectious Disorders)*, *15*(2), pp.131-134.

157. Sethiya, N.K., Shah, P., Rajpara, A., Nagar, P.A. and Mishra, S.H., 2015. Antioxidant and hepatoprotective effects of mixed micellar lipid formulation of phyllanthin and piperine in carbon tetrachloride-induced liver injury in rodents. *Food & function*, *6*(11), pp.3593-3603.].

158. Zadorozhna, M., Tataranni, T., & Mangieri, D. (2019). Piperine: Role in prevention and progression of cancer. Molecular Biology Reports, 46(5), 5617–5629.

159. Ding, Y., Ding, Y., Wang, Y., Wang, C., Gao, M., Xu, Y., Ma, X., Wu, J. and Li, L., 2020. Soluplus®/TPGS mixed micelles for co-delivery of docetaxel and piperine for combination cancer therapy. *Pharmaceutical development and technology*, *25*(1), pp.107-115.

160. Sehgal, A., Kumar, M., Jain, M. and Dhawan, D.K., 2012. Piperine as an adjuvant increases the efficacy of curcumin in mitigating benzo (a) pyrene toxicity. *Human & experimental toxicology*, *31*(5), pp.473-482.

161. Yoo, E.S., Choo, G.S., Kim, S.H., Woo, J.S., Kim, H.J., Park, Y.S., Kim, B.S., Kim, S.K., Park, B.K., Cho, S.D. and Nam, J.S., 2019. Antitumor and apoptosis-inducing effects of piperine on human melanoma cells. *Anticancer Research*, *39*(4), pp.1883-1892.

162. Rad, J. G., & Hoskin, D. W. (2020). Delivery of apoptosis-inducing Piperine to triple-negative breast Cancer cells via co-polymeric nanoparticles. Anticancer Research, 40(2), 689–694.

163. Yaffe, P.B., Power Coombs, M.R., Doucette, C.D., Walsh, M. and Hoskin, D.W., 2015. Piperine, an alkaloid from black pepper, inhibits growth of human colon cancer cells via G1 arrest and apoptosis triggered by endoplasmic reticulum stress. *Molecular carcinogenesis*, *54*(10), pp.1070-1085.

164. Liang, X., Zhang, L., Li, F., Luan, S., He, C., Yin, L., Yin, Z., Zou, Y., Yue, G., Li, L. and Song, X., 2020. Autophagy-regulating N-heterocycles derivatives as potential anticancer agents. *Future Medicinal Chemistry*, *12*(3), pp.223-242.

165. Baker, M.J., Trevisan, J., Bassan, P., Bhargava, R., Butler, H.J., Dorling, K.M., Fielden, P.R., Fogarty, S.W., Fullwood, N.J., Heys, K.A. and Hughes, C., 2014. Using Fourier transform IR spectroscopy to analyze biological materials. *Nature protocols*, *9*(8), pp.1771-1791.

166. Instrumentation, G., Analysis, Barbara L Dutrow, Louisiana State University, Christine M. *Clark, Eastern Michigan University*.

167. Coats, A.W. and Redfern, J.P., 1963. Thermogravimetric analysis. A review. *Analyst*, *88*(1053), pp.906-924.

168. Vogt, C., Wondergem, C.S. and Weckhuysen, B.M., 2023. Ultraviolet-visible (uv-vis) spectroscopy. In *Springer handbook of advanced catalyst characterization* (pp. 237-264). Cham: Springer International Publishing.

169. Arunachalam, K. and Davoodbasha, M., 2021. Imaging bacteria and biofilm by field emission scanning electron microscopy. *Analytical Methodologies for Biofilm Research*, pp.205-222.

170. Legros, M., Cabié, M. and Gianola, D.S., 2009. In situ deformation of thin films on substrates. *Microscopy Research and Technique*, *72*(3), pp.270-283.

171. Binnig, G., Quate, C.F. and Gerber, C., 1986. Atomic force microscope. *Physical review letters*, *56*(9), p.930.

172. Stetefeld, J., McKenna, S.A. and Patel, T.R., 2016. Dynamic light scattering: a practical guide and applications in biomedical sciences. *Biophysical reviews*, *8*, pp.409-427.

173. Zsila, F., Hazai, E. and Sawyer, L., 2005. Binding of the pepper alkaloid piperine to bovine β-lactoglobulin: circular dichroism spectroscopy and molecular modeling study. *Journal of agricultural and food chemistry*, *53*(26), pp.10179-10185.

174. Salmani et al., 2014. M.J.M. Salmani, S.Asghar, L.Huixia, J. Zhou. Aqueous Solubility and Degradation Kinetics of the Phytochemical Anticancer Thymoquinone; Probing the Effects of Solvents, pH and Light. Molecules, 19 (5), (2014), pp. 5925-5939. doi:10.3390/molecules19055925.

175. Wang, Y., Luo, Q., Gao, L., Gao, C., Du, H., Zha, G., Li, X., Shen, Z. and Zhu, W., 2014. A facile strategy to prepare redox-responsive amphiphilic PEGylated prodrug with high drug loading content and low critical micelle concentration. *Biomaterials science*, *2*(10), pp.1367-1376.

176. Yu, M., Yuan, W., Li, D., Schwendeman, A. and Schwendeman, S.P., 2019. Predicting drug release kinetics from nanocarriers inside dialysis bags. *Journal of Controlled Release*, *315*, pp.23-30.

177. Kis, B., Unay, M., Ekimci, G.D., Ercan, U.K. and Akan, A., 2019, October. Counting bacteria colonies based on image processing methods. In *2019 Medical Technologies Congress (TIPTEKNO)* (pp. 1-4). IEEE.

178. Kowalska-Krochmal, B. and Dudek-Wicher, R., 2021. The minimum inhibitory concentration of antibiotics: Methods, interpretation, clinical relevance. *Pathogens*, *10*(2), p.165.

179. Bagchi, B., Dey, S., Bhandary, S., Das, S., Bhattacharya, A., Basu, R. and Nandy, P., 2012. Antimicrobial efficacy and biocompatibility study of copper nanoparticle adsorbed mullite aggregates. *Materials Science and Engineering: C*, *32*(7), pp.1897-1905.

180. May, J., Shannon, K., King, A. and French, G., 1998. Glycopeptide tolerance in Staphylococcus aureus. *The Journal of antimicrobial chemotherapy*, *42*(2), pp.189-197.

181. Boyanova, L., Gergova, G., Nikolov, R., Derejian, S., Lazarova, E., Katsarov, N., Mitov, I. and Krastev, Z., 2005. Activity of Bulgarian propolis against 94 Helicobacter pylori strains in vitro by agar-well diffusion, agar dilution and disc diffusion methods. *Journal of medical microbiology*, *54*(5), pp.481-483.

182. Banerjee, S., Bagchi, B., Bhandary, S., Kool, A., Hoque, N.A., Biswas, P., Pal, K., Thakur, P., Das, K., Karmakar, P. and Das, S., 2018. Antimicrobial and biocompatible fluorescent hydroxyapatite-chitosan nanocomposite films for biomedical applications. *Colloids and Surfaces B: Biointerfaces*, *171*, pp.300-307.

183. Jiang, Q., E, F., Tian, J., Yang, J., Zhang, J. and Cheng, Y., 2020. Light-excited antibiotics for potentiating bacterial killing via reactive oxygen species generation. *ACS applied materials & interfaces*, *12*(14), pp.16150-16158.

184. Dutta Sinha, S., Chatterjee, S., Maiti, P.K., Tarafdar, S. and Moulik, S.P., 2017. Evaluation of the role of substrate and albumin on Pseudomonas aeruginosa biofilm morphology through FESEM and FTIR studies on polymeric biomaterials. *Progress in biomaterials*, *6*, pp.27-38.

185. D. A. Scudiero, R. H. Shoemaker, K. D. Paull, A. Monks, S. Tierney, T. H. Nofziger, M. J. Currens, D. Seniff and M. R. Boyd, Evaluation of a soluble tetrazolium/formazan assay for cell growth and drug sensitivity in culture using human and other tumor cell lines, Cancer Res., 48(17) (1988) 4827–4833

186. M. Patra, M. Banik, P. Bandopadhyay, D. Dutta, R. Mukherjee, S. Das, N. A. Begum and T. Basu, Nanonization of a chemically synthesized flavone HMDF (3-hydroxy-3',4'-methylenedioxyflavone) by entrapping within calcium phosphate nanoparticles and exploring its antioxidant role on neural cells in vitro and zebrafish in vivo, Nanotechnology, 32 (2021) 23

187. L. C. Crowley, B. J. Marfell and N. J. Waterhouse, Analyzing Cell Death by Nuclear Staining with Hoechst 33342, Cold Spring Harb Protoc., 9 (2016)

188. B. Chazotte, Labeling mitochondria with rhodamine 123, Cold Spring Harbor protocols, 7 (2011) 892–894

189. Beghdad, A., 2023. *Study and realization of a system for measuring hemoglobin: hemoglobinometer* (Doctoral dissertation, University of Tlemcen).

190. Rees, H.M. and Ecker, E.E., 1923. An improved method for counting blood platelets. *Journal of the American Medical Association*, *80*(9), pp.621-622.

191. Pintus, E., Ric, D. and Ros-Santaella, J.L., Laboratory Protocols in Animal Physiology Part I: Blood Analysis in Mammals.

192. Creeden, J.F., Gordon, D.M., Stec, D.E. and Hinds Jr, T.D., 2021. Bilirubin as a metabolic hormone: the physiological relevance of low levels. *American Journal of Physiology-Endocrinology and Metabolism*, *320*(2), pp.E191-E207.

193. Guerra Ruiz, A.R., Crespo, J., López Martínez, R.M., Iruzubieta, P., Casals Mercadal, G., Lalana Garcés, M., Lavin, B. and Morales Ruiz, M., 2021. Measurement and clinical usefulness of bilirubin in liver disease. *Advances in Laboratory Medicine/Avances en Medicina de Laboratorio*, *2*(3), pp.352-361.

194. Ndrepepa, G., 2021. Aspartate aminotransferase and cardiovascular disease—a narrative review. *Journal of Laboratory and Precision Medicine*, *6*.

195. Liu, Z., Que, S., Xu, J. and Peng, T., 2014. Alanine aminotransferase-old biomarker and new concept: a review. *International journal of medical sciences*, *11*(9), p.925.

196. Lowe, D., Sanvictores, T., Zubair, M. and John, S., 2023. Alkaline phosphatase. *StatPearls*.

197. Bergmeyer, H. U. (Ed.). (2012). *Methods of enzymatic analysis*. Elsevier.

198. Bowers Jr, G.N. and McComb, R.B., 1966. A continuous spectrophotometric method for measuring the activity of serum alkaline phosphatase. *Clinical chemistry*, *12*(2), pp.70-89.

199. Peterson, G.L., 1977. A simplification of the protein assay method of Lowry et al. which is more generally applicable. *Analytical biochemistry*, *83*(2), pp.346-356.

200. Fossati, P., Ponti, M., Prencipe, L. and Tarenghi, G., 1989. One-step protocol for assays of total and direct bilirubin with stable combined reagents. *Clinical chemistry*, *35*(1), pp.173-176.

201. Trivedu, V.D., Saxena, I., Siddiqui, M.U. and Qasim, M.A., 1997. Interaction of bromocresol green with different serum albumins studied by fluorescence quenching. *IUBMB Life*, *43*(1), pp.1-8.

202. Mao, G., Kraus, G.A., Kim, I., Spurlock, M.E., Bailey, T.B. and Beitz, D.C., 2011. Effect of a mitochondria-targeted vitamin E derivative on mitochondrial alteration and systemic oxidative stress in mice. *British journal of nutrition*, *106*(1), pp.87-95.

203. Emami, A.M., Homaee, H.M. and Azarbayjani, M.A., 2016. Effects of high intensity interval training and curcumin supplement on glutathione peroxidase (GPX) activity and malondialdehyde (MDA) concentration of the liver in STZ induced diabetic rats. *Iranian Journal of Diabetes and Obesity*, *8*(3), pp.129-134.

204. Mahapatra, S.K., Das, S., Bhattacharjee, S., Gautam, N., Majumdar, S. and Roy, S., 2009. In vitro nicotine-induced oxidative stress in mice peritoneal macrophages: a dose-dependent approach. *Toxicology Mechanisms and Methods*, *19*(2), pp.100-108.

205. Mahapatra, A., Panigrahi, S., Patra, R.C., Rout, M. and Ganguly, S., 2018. A study on bovine mastitis related oxidative stress along with therapeutic regimen. *Int J Curr Microbiol App Sci*, *7*, pp.247-256.

206. Liu, Q., Wu, D., Ma, Y., Cao, Y., Pang, Y., Tang, M., Pu, Y. and Zhang, T., 2022. Intracellular reactive oxygen species trigger mitochondrial dysfunction and apoptosis in cadmium telluride quantum dots-induced liver damage. *NanoImpact*, *25*, p.100392.

207. Gazzard, B.G., Portmann, B., MUREAY-LYON, I.M. and WILLIAMS, R., 1975. Causes of death in fulminant hepatic failure and relationship to quantitative histological assessment of parenchymal damage. *QJM: An International Journal of Medicine*, *44*(4), pp.615-626.

208. Thu, H.E., Hussain, Z., Mohamed, I.N. and Shuid, A.N., 2018. Recent advances in antibacterial, antiprotozoal and antifungal trends of Eurycoma longifolia: a review of therapeutic implications and future prospects. *Current Drug Targets*, *19*(14), pp.1657-1671.

209. Chen, L.H., Xue, J.F., Zheng, Z.Y., Shuhaidi, M., Thu, H.E. and Hussain, Z., 2018. Hyaluronic acid, an efficient biomacromolecule for treatment of inflammatory skin and joint diseases: A review of recent developments and critical appraisal of preclinical and clinical investigations. *International journal of biological macromolecules*, *116*, pp.572-584.

210. Tumpang, M.A., Ramli, N.A. and Hussain, Z., 2018. Phytomedicines are efficient complementary therapies for the treatment of atopic dermatitis: a review of mechanistic insight and recent updates. *Current drug targets*, *19*(6), pp.674-700.

211. Khan, S., Imran, M., Butt, T.T., Shah, S.W.A., Sohail, M., Malik, A., Das, S., Thu, H.E., Adam, A. and Hussain, Z., 2018. Curcumin based nanomedicines as efficient nanoplatform for treatment of cancer: new developments in reversing cancer drug resistance, rapid internalization, and improved anticancer efficacy. *Trends in food science & technology*, *80*, pp.8-22.

212. Thornthwaite, J.T., Shah, H.R., Shah, P., Peeples, W.C. and Respess, H., 2013. The formulation for cancer prevention & therapy.

213. Brooks, B.D. and Brooks, A.E., 2014. Therapeutic strategies to combat antibiotic resistance. *Advanced drug delivery reviews*, *78*, pp.14-27.

214. Bukhari, S.N.A., Hussain, F., Thu, H.E. and Hussain, Z., 2019. Synergistic effects of combined therapy of curcumin and Fructus Ligustri Lucidi for treatment of osteoporosis: cellular and molecular evidence of enhanced bone formation. *Journal of integrative medicine*, *17*(1), pp.38-45.

215. Chan, M.M., Chen, R. and Fong, D., 2018. Targeting cancer stem cells with dietary phytochemical-repositioned drug combinations. *Cancer letters*, *433*, pp.53-64.

216. Mohammadabadi, M.R. and Mozafari, M.R., 2018. Enhanced efficacy and bioavailability of thymoquinone using nanoliposomal dosage form. *Journal of drug delivery science and technology*, *47*, pp.445-453.

217. Halawani, E., 2009. Antibacterial activity of thymoquinone and thymohydroquinone of Nigella sativa L. and their interaction with some antibiotics. *Adv Biol Res*, *3*(5-6), pp.148-52.

218. Chanda, S., Rakholiya, K., Dholakia, K. and Baravalia, Y., 2013. Antimicrobial, antioxidant, and synergistic properties of two nutraceutical plants: Terminalia catappa L. and Colocasia esculenta L. *Turkish Journal of Biology*, *37*(1), pp.81-91.

219. Ahmad, Z., Laughlin, T.F. and Kady, I.O., 2015. Thymoquinone inhibits Escherichia coli ATP synthase and cell growth. *PLoS One*, *10*(5), p.e0127802.

220. Farrag, A.R.H., 2007. Protective effect of Nigella sativa seeds against lead-induced hepatorenal damage in male rats' Abdel-Razik H. Farrag,"Karam A. Mahdy,'Gamal H. Abdel Rahman and "Mostafa M. Osfor" Departments of Pathology,"Department of Medical Biochemistry. *J. biol. sci*, *10*(17), pp.2809-16.

221. Nallamuthu, I., Parthasarathi, A. and Khanum, F., 2013. Thymoquinone-loaded PLGA nanoparticles: antioxidant and antimicrobial properties. *Int J Curr Pharm Res*, *2*(12), pp.202-7.

222. Gorgani, L., Mohammadi, M., Najafpour, G.D. and Nikzad, M., 2017. Piperine—the bioactive compound of black pepper: from isolation to medicinal formulations. *Comprehensive reviews in food science and food safety*, *16*(1), pp.124-140.

223. Srinivasan, K., 2009. Black pepper (Piper nigrum) and its bioactive compound, piperine. In *Molecular targets and therapeutic uses of spices: Modern uses for ancient medicine* (pp. 25-64).

224. Kalunta, C.G., 2017. Antimicrobial effect of different seed extracts of Piper nigrum against Escherichia coli, Staphylococcus aureus and Candida albican. *Biotechnological Research*, *3*(3), pp.71-76.

225. Laha, A., Yadav, S., Majumdar, S. and Sharma, C.S., 2016. In-vitro release study of hydrophobic drug using electrospun cross-linked gelatin nanofibers. *Biochemical Engineering Journal*, *105*, pp.481-488.

226. Goyal, S.N., Prajapati, C.P., Gore, P.R., Patil, C.R., Mahajan, U.B., Sharma, C., Talla, S.P. and Ojha, S.K., 2017. Therapeutic potential and pharmaceutical development of thymoquinone: a multitargeted molecule of natural origin. *Frontiers in pharmacology*, *8*, p.656.

227. Shityakov, S., Bigdelian, E., Hussein, A.A., Hussain, M.B., Tripathi, Y.C., Khan, M.U. and Shariati, M.A., 2019. Phytochemical and pharmacological attributes of piperine: A bioactive ingredient of black pepper. *European journal of medicinal chemistry*, *176*, pp.149-161.

228. Alam, S., Khan, Z.I., Mustafa, G., Kumar, M., Islam, F., Bhatnagar, A. and Ahmad, F.J., 2012. Development and evaluation of thymoquinone-encapsulated chitosan nanoparticles for nose-to-brain targeting: a pharmacoscintigraphic study. *International journal of nanomedicine*, pp.5705-5718.

229. Hussain, Z., 2021. Nanotechnology guided newer intervention for treatment of osteoporosis: efficient bone regeneration by up-regulation of proliferation, differentiation and mineralization of osteoblasts. *International Journal of Polymeric Materials and Polymeric Biomaterials*, *70*(1), pp.1-13.

230. Fang, G., Zhang, Q., Pang, Y., Thu, H.E. and Hussain, Z., 2019. Nanomedicines for improved targetability to inflamed synovium for treatment of rheumatoid arthritis: multi-functionalization as an emerging strategy to optimize therapeutic efficacy. *Journal of controlled release*, *303*, pp.181-208.

231. Hussain, Z., Pandey, M., Choudhury, H., Ying, P.C., Xian, T.M., Kaur, T., Jia, G.W. and Gorain, B., 2020. Hyaluronic acid functionalized nanoparticles for simultaneous delivery of curcumin and resveratrol for management of chronic diabetic wounds: Fabrication, characterization, stability and in vitro release kinetics. *Journal of Drug Delivery Science and Technology*, *57*, p.101747.

232. Zhuo, F., Abourehab, M.A. and Hussain, Z., 2018. Hyaluronic acid decorated tacrolimus-loaded nanoparticles: Efficient approach to maximize dermal targeting and anti-dermatitis efficacy. *Carbohydrate polymers*, *197*, pp.478-489.

233. Patel, J.J., Karve, M. and Patel, N.K., 2014. Guar gum: a versatile material for pharmaceutical industries. *Int J Pharm Pharm Sci*, *6*(8), pp.13-19.

234. Thombare, N., Jha, U., Mishra, S. and Siddiqui, M.Z., 2016. Guar gum as a promising starting material for diverse applications: A review. *International journal of biological macromolecules*, *88*, pp.361-372.

235. Singh, V., Tiwari, A., Tripathi, D.N. and Sanghi, R., 2004. Grafting of polyacrylonitrile onto guar gum under microwave irradiation. *Journal of Applied Polymer Science*, *92*(3), pp.1569-1575.

236. Chaurasia, M., Chourasia, M.K., Jain, N.K., Jain, A., Soni, V., Gupta, Y. and Jain, S.K., 2006. Cross-linked guar gum microspheres: A viable approach for improved delivery of anticancer drugs for the treatment of colorectal cancer. *Aaps Pharmscitech*, *7*, pp.E143-E151.

237. Khandrika, L., Kumar, B., Koul, S., Maroni, P. and Koul, H.K., 2009. Oxidative stress in prostate cancer. *Cancer letters*, *282*(2), pp.125-136.

238. Ismail, N., Abdel–Mottaleb, Y., Ahmed, A.A.E. and El-Maraghy, N.N., 2018. Novel combination of thymoquinone and resveratrol enhances anticancer effect on hepatocellular carcinoma cell line. *Future Journal of Pharmaceutical Sciences*, *4*(1), pp.41-46.

239. Danial, N.N. and Korsmeyer, S.J., 2004. Cell death: critical control points. *Cell*, *116*(2), pp.205-219.

240. Behzadi, E. and Behzadi, P., 2012. An in vitro study on the apoptosis inducing effects of ultraviolet B light in Staphylococcus aureus. *Maedica*, *7*(1), p.54.

241. Sakahira, H., Enari, M. and Nagata, S., 1998. Cleavage of CAD inhibitor in CAD activation and DNA degradation during apoptosis. *Nature*, *391*(6662), pp.96-99.

242. Singh, R., Devi, S., Patel, J., Patel, U., Bhavsar, S. and Thaker, A., 2009. Indian herbal bioenhancers: a review. *Pharmacognosy Reviews*, *3*(5), p.90.

243. Chinta, G., B Syed, S., Coumar, M.S. and Periyasamy, L., 2015. Piperine: A comprehensive review of pre-clinical and clinical investigations. *Current Bioactive Compounds*, *11*(3), pp.156-169.

244. Gong, H., Liu, M., Chen, J., Han, F., Gao, C. and Zhang, B., 2012. Synthesis and characterization of carboxymethyl guar gum and rheological properties of its solutions. *Carbohydrate polymers*, *88*(3), pp.1015-1022.

245. Gupta, V.K., Pathania, D., Singh, P., Kumar, A. and Rathore, B.S., 2014. Adsorptional removal of methylene blue by guar gum–cerium (IV) tungstate hybrid cationic exchanger. *Carbohydrate polymers*, *101*, pp.684-691.

246. Surekha, R. and Sumathi, T., 2016. An efficient encapsulation of thymoquinone using solid lipid nanoparticle for brain targeted drug delivery: physicochemical characterization, pharmacokinetics and bio-distribution studies. *Int. J. Pharm. Clin. Res*, *8*(12), pp.1616-1624.

247. Singh, V., Kumari, P., Pandey, S. and Narayan, T., 2009. Removal of chromium (VI) using poly (methylacrylate) functionalized guar gum. *Bioresource technology*, *100*(6), pp.1977-1982.

248. Khan, Z.R., Moni, F., Sharmin, S., Al-Mansur, M.A., Gafur, A., Rahman, O. and Afroz, F., 2017. Isolation of bulk amount of piperine as active pharmaceutical ingredient (API) from black pepper and white pepper (Piper nigrum L.). *Pharmacology & Pharmacy*, *8*(7), pp.253-262.

249. Bigio, I.J. and Mourant, J.R., 1997. Ultraviolet and visible spectroscopies for tissue diagnostics: fluorescence spectroscopy and elastic-scattering spectroscopy. *Physics in Medicine & Biology*, *42*(5), p.803.

250. Uhrich, K.E., Cannizzaro, S.M., Langer, R.S. and Shakesheff, K.M., 1999. Polymeric systems for controlled drug release. *Chemical reviews*, *99*(11), pp.3181-3198.

251. Ott, M., Gogvadze, V., Orrenius, S. and Zhivotovsky, B., 2007. Mitochondria, oxidative stress and cell death. *Apoptosis*, *12*, pp.913-922.

252. Raj Rai, S., Bhattacharyya, C., Sarkar, A., Chakraborty, S., Sircar, E., Dutta, S. and Sengupta, R., 2021. Glutathione: Role in oxidative/nitrosative stress, antioxidant defense, and treatments. *ChemistrySelect*, *6*(18), pp.4566-4590.

253. Wang, Q., Ellis, P.R. and Ross-Murphy, S.B., 2000. The stability of guar gum in an aqueous system under acidic conditions. *Food hydrocolloids*, *14*(2), pp.129-134.

254. Jo, S.H., Son, M.K., Koh, H.J., Lee, S.M., Song, I.H., Kim, Y.O., Lee, Y.S., Jeong, K.S., Kim, W.B., Park, J.W. and Song, B.J., 2001. Control of mitochondrial redox balance and cellular defense against oxidative damage by mitochondrial NADP+-dependent isocitrate dehydrogenase. *Journal of Biological chemistry*, *276*(19), pp.16168-16176.

255. Boni, R., Ali, A., Shavandi, A. and Clarkson, A.N., 2018. Current and novel polymeric biomaterials for neural tissue engineering. *Journal of biomedical science*, *25*, pp.1-21.

256. Ramakrishna, S., Mayer, J., Wintermantel, E. and Leong, K.W., 2001. Biomedical applications of polymer-composite materials: a review. *Composites science and technology*, *61*(9), pp.1189-1224.

257. Nair, L.S. and Laurencin, C.T., 2007. Biodegradable polymers as biomaterials. *Progress in polymer science*, *32*(8-9), pp.762-798.

258. Hamman, J.H., 2010. Chitosan based polyelectrolyte complexes as potential carrier materials in drug delivery systems. *Marine drugs*, *8*(4), pp.1305-1322.

259. Mohammadinejad, R., Maleki, H., Larrañeta, E., Fajardo, A.R., Nik, A.B., Shavandi, A., Sheikhi, A., Ghorbanpour, M., Farokhi, M., Govindh, P. and Cabane, E., 2019. Status and future scope of plant-based green hydrogels in biomedical engineering. *Applied Materials Today*, *16*, pp.213-246.

260. Luo, Y. and Wang, Q., 2014. Recent development of chitosan-based polyelectrolyte complexes with natural polysaccharides for drug delivery. *International journal of biological macromolecules*, *64*, pp.353-367.

261. Cheaburu, C.N., Ciocoiu, O.N., Staikos, G. and Vasile, C., 2013. Thermoresponsive sodium alginate-g-poly (N-isopropylacrylamide) copolymers III. Solution properties. *Journal of applied polymer science*, *127*(5), pp.3340-3348.

262. Sankalia, M.G., Mashru, R.C., Sankalia, J.M. and Sutariya, V.B., 2007. Reversed chitosan–alginate polyelectrolyte complex for stability improvement of alpha-amylase: Optimization and physicochemical characterization. *European journal of pharmaceutics and biopharmaceutics*, *65*(2), pp.215-232.

263. Beneke, C.E., Viljoen, A.M. and Hamman, J.H., 2009. Polymeric plant-derived excipients in drug delivery. *Molecules*, *14*(7), pp.2602-2620.

264. Rao, M.R., Warrier, D.U., Gaikwad, S.R. and Shevate, P.M., 2016. Phosphorylation of psyllium seed polysaccharide and its characterization. *International journal of biological macromolecules*, *85*, pp.317-326.

265. Bemiller, J.N., Whistler, R.L., Barkalow, D.G. and Chen, C.C., 1993. Aloe, chia, flaxseed, okra, psyllium seed, quince seed, and tamarind gums. In *Industrial gums* (pp. 227-256). Academic Press.

266. Kumar, D., Pandey, J., Kumar, P. and Raj, V., 2017. Psyllium mucilage and its use in pharmaceutical field: an overview. *Curr Synthetic Sys Biol*, *5*(134), pp.2332-0737.

267. Singh, B., 2007. Psyllium as therapeutic and drug delivery agent. *International journal of pharmaceutics*, *334*(1-2), pp.1-14.

268. Ahuja, M., Bhatia, M. and Saini, K., 2016. Sodium alginate–arabinoxylan composite microbeads: preparation and characterization. *Journal of Pharmaceutical Investigation*, *46*, pp.645-653.

269. Ali, A. and Ahmed, S., 2018. A review on chitosan and its nanocomposites in drug delivery. *International journal of biological macromolecules*, *109*, pp.273-286.

270. Desai, A., Shidhaye, S. and Kadam, V.J., 2007. Possible Use of Psyllium Husk as a Release Retardant. *Indian Journal of Pharmaceutical Sciences*, *69*(2).

271. Darakhshan, S., Pour, A.B., Colagar, A.H. and Sisakhtnezhad, S., 2015. Thymoquinone and its therapeutic potentials. *Pharmacological research*, *95*, pp.138-158.

272. Mahmoud, Y.K. and Abdelrazek, H.M., 2019. Cancer: Thymoquinone antioxidant/pro-oxidant effect as potential anticancer remedy. *Biomedicine & Pharmacotherapy*, *115*, p.108783.

273. Monge Neto, A.A., Bergamasco, R.D.C., de Moraes, F.F., Medina Neto, A. and Peralta, R.M., 2017. Development of a technique for psyllium husk mucilage purification with simultaneous microencapsulation of curcumin. *PloS one*, *12*(8), p.e0182948.

274. Konwar, A., Kalita, S., Kotoky, J. and Chowdhury, D., 2016. Chitosan–iron oxide coated graphene oxide nanocomposite hydrogel: a robust and soft antimicrobial biofilm. *ACS applied materials & interfaces*, *8*(32), pp.20625-20634.

275. Bhatia, M. and Ahuja, M., 2013. Thiol modification of psyllium husk mucilage and evaluation of its mucoadhesive applications. *The Scientific World Journal*, *2013*.

276. Pandima Devi, M., Sekar, M., Chamundeswari, M., Moorthy, A., Krithiga, G., Murugan, N.S. and Sastry, T.P., 2012. A novel wound dressing material—fibrin–chitosan–sodium alginate composite sheet. *Bulletin of Materials Science*, *35*, pp.1157-1163.

277. Aprilliza, M., 2017, April. Characterization and properties of sodium alginate from brown algae used as an ecofriendly superabsorbent. In *IOP conference series: materials science and engineering* (Vol. 188, No. 1, p. 012019). IOP Publishing.

278. Kulig, D., Zimoch-Korzycka, A., Jarmoluk, A. and Marycz, K., 2016. Study on alginate–chitosan complex formed with different polymers ratio. *Polymers*, *8*(5), p.167.

279. Yan, T., Feringa, B.L. and Barta, K., 2014. Iron catalysed direct alkylation of amines with alcohols. *Nature Communications*, *5*(1), p.5602.

280. Bates, S., Zografi, G., Engers, D., Morris, K., Crowley, K. and Newman, A., 2006. Analysis of amorphous and nanocrystalline solids from their X-ray diffraction patterns. *Pharmaceutical research*, *23*, pp.2333-2349.

281. Kumar, S. and Koh, J., 2012. Physiochemical, optical and biological activity of chitosan-chromone derivative for biomedical applications. *International journal of molecular sciences*, *13*(5), pp.6102-6116.

282. Kong, M., Chen, X.G., Xing, K. and Park, H.J., 2010. Antimicrobial properties of chitosan and mode of action: a state of the art review. *International journal of food microbiology*, *144*(1), pp.51-63.

283. Brynildsen, M.P., Winkler, J.A., Spina, C.S., MacDonald, I.C. and Collins, J.J., 2013. Potentiating antibacterial activity by predictably enhancing endogenous microbial ROS production. *Nature biotechnology*, *31*(2), pp.160-165.

284. Cabiscol Catalā, E., Tamarit Sumalla, J. and Ros Salvador, J., 2000. Oxidative stress in bacteria and protein damage by reactive oxygen species.

285. Sahu, T., Ratre, Y.K., Chauhan, S., Bhaskar, L.V.K.S., Nair, M.P. and Verma, H.K., 2021. Nanotechnology based drug delivery system: Current strategies and emerging therapeutic potential for medical science. *Journal of Drug Delivery Science and Technology*, *63*, p.102487.

286. Ezike, T.C., Okpala, U.S., Onoja, U.L., Nwike, P.C., Ezeako, E.C., Okpara, J.O., Okoroafor, C.C., Eze, S.C., Kalu, O.L., Odoh, E.C. and Nwadike, U., 2023. Advances in drug delivery systems, challenges and future directions. *Heliyon*.

287. Eldaw, G.E., 1998. A study of guar seed and guar gum properties (Cyamopsis tetragonolabous).

288. Maeda, H. and Khatami, M., 2018. Analyses of repeated failures in cancer therapy for solid tumors: poor tumor-selective drug delivery, low therapeutic efficacy and unsustainable costs. *Clinical and translational medicine*, *7*, pp.1-20.

289. Meybodi, N.M., Mortazavian, A.M., Monfared, A.B., Sohrabvandi, S. and Meybodi, F.A., 2017. Phytochemicals in cancer prevention: a review of the evidence. *Iranian Journal of Cancer Prevention*, *10*(1).

290. Upadhyay, S., Bhushan, R., Pandey, V., Tripathi, A., Sahu, A.N., Rani, A., Diwakar, A., Gupta, R. and Dubey, P.K., 2023. A comparative analysis of phytochemicals vs synthetic drugs/nanomedicines in the treatment of Uterine Fibroid: A Systematic Review.

291. Tatiraju, D.V., Bagade, V.B., Karambelkar, P.J., Jadhav, V.M. and Kadam, V., 2013. Natural bioenhancers: An overview. *Journal of Pharmacognosy and Phytochemistry*, *2*(3), pp.55-60.

292. Gunasekaran, V., Elangovan, K. and Devaraj, S.N., 2017. Targeting hepatocellular carcinoma with piperine by radical-mediated mitochondrial pathway of apoptosis: An in vitro and in vivo study. *Food and Chemical Toxicology*, *105*, pp.106-118.

293. Yaffe, P.B., Doucette, C.D., Walsh, M. and Hoskin, D.W., 2013. Piperine impairs cell cycle progression and causes reactive oxygen species-dependent apoptosis in rectal cancer cells. *Experimental and molecular pathology*, *94*(1), pp.109-114.

294. Das, S., Bera, D., De, D., Mondal, D., Karmakar, P., Das, S. and Dey, A., 2022. Thymoquinone incorporated chitosan-sodium alginate/psyllium husk derived biopolymeric composite films: A comparative antibacterial and anticancer profile. *European Polymer Journal*, *180*, p.111608.

295. Mudgil, D., Barak, S. and Khatkar, B.S., 2012. X-ray diffraction, IR spectroscopy and thermal characterization of partially hydrolyzed guar gum. *International Journal of Biological Macromolecules*, *50*(4), pp.1035-1039.

296. Malvern – Zetasizer Nano – User manual, Zeta potential theory, England, MAN0317, 2008, pp. 1–12 (Chapter 16).

297. Khalil, H.A., Yahya, E.B., Jummaat, F., Adnan, A.S., Olaiya, N.G., Rizal, S., Abdullah, C.K., Pasquini, D. and Thomas, S., 2023. Biopolymers based aerogels: A review on revolutionary solutions for smart therapeutics delivery. *Progress in Materials Science*, *131*, p.101014.

298. Negrini, R. and Mezzenga, R., 2011. pH-responsive lyotropic liquid crystals for controlled drug delivery. *Langmuir*, *27*(9), pp.5296-5303.

299. Davies, K.J., 2000. Oxidative stress, antioxidant defenses, and damage removal, repair, and replacement systems. *IUBMB life*, *50*(4-5), pp.279-289.

300. Pamplona, R., 2008. Membrane phospholipids, lipoxidative damage and molecular integrity: a causal role in aging and longevity. *Biochimica et Biophysica Acta (BBA)-Bioenergetics*, *1777*(10), pp.1249-1262.

301. Mukherjee, R., Patra, M., Dutta, D., Banik, M. and Basu, T., 2016. Tetracycline-loaded calcium phosphate nanoparticle (Tet-CPNP): rejuvenation of an obsolete antibiotic to further action. *Biochimica et Biophysica Acta (BBA)-General Subjects*, *1860*(9), pp.1929-1941.

302. Dassanayake, R.S., Acharya, S. and Abidi, N., 2018. Biopolymer-based materials from polysaccharides: Properties, processing, characterization and sorption applications. *Advanced sorption process applications*, pp.1-24.

303. Wang, R., Shou, D., Lv, O., Kong, Y., Deng, L. and Shen, J., 2017. pH-Controlled drug delivery with hybrid aerogel of chitosan, carboxymethyl cellulose and graphene oxide as the carrier. *International journal of biological macromolecules*, *103*, pp.248-253.

304. Dye, C., 2014. After 2015: infectious diseases in a new era of health and development. *Philosophical Transactions of the Royal Society B: Biological Sciences*, *369*(1645), p.20130426.

305. A.L. De Castilho, J.P.C. Da Silva, C.H.C. Saraceni, I.E.C. Diaz, M.L.B. Paciencia, A.D. Varella, I.B. Suffredini, In vitro activity of Amazon plant extracts against Enterococcus faecalis, Braz. J. Microbiol. 45 (3) (2014) 769–779.

306. Fyhrquist, P., Virjamo, V., Hiltunen, E. and Julkunen-Tiitto, R., 2019. Epidihydropinidine, the main piperidine alkaloid compound of Norway spruce (Picea abies) shows antibacterial and anti-Candida activity. *Fitoterapia*, *134*, pp.503-511.

307. Croxen, M.A. and Finlay, B.B., 2010. Molecular mechanisms of Escherichia coli pathogenicity. *Nature Reviews Microbiology*, *8*(1), pp.26-38.

308. Greenshields, A.L., Doucette, C.D., Sutton, K.M., Madera, L., Annan, H., Yaffe, P.B., Knickle, A.F., Dong, Z. and Hoskin, D.W., 2015. Piperine inhibits the growth and motility of triple-negative breast cancer cells. *Cancer letters*, *357*(1), pp.129-140

309. Sunila, E.S., Kuttan, G., Immunomodulatory and antitumor activity of *Piper longum* Linn. and piperine. J Ethnopharmacol 2004; 90(2-3): 339-46.

310. Habibi, N., 2014. Preparation of biocompatible magnetite-carboxymethyl cellulose nanocomposite: characterization of nanocomposite by FTIR, XRD, FESEM and TEM. *Spectrochimica Acta Part A: Molecular and Biomolecular Spectroscopy*, *131*, pp.55-58.

311. Saadiah, M.A., Zhang, D., Nagao, Y., Muzakir, S.K. and Samsudin, A.S., 2019. Reducing crystallinity on thin film based CMC/PVA hybrid polymer for application as a host in polymer electrolytes. *Journal of Non-Crystalline Solids*, *511*, pp.201-211.

312. Anitha, A., Deepagan, V.G., Rani, V.D., Menon, D., Nair, S.V. and Jayakumar, R., 2011. Preparation, characterization, in vitro drug release and biological studies of curcumin loaded dextran sulphate–chitosan nanoparticles. *Carbohydrate Polymers*, *84*(3), pp.1158-1164.

313. Li R, Jia Z, Trush MA (2016) Defning ROS in biology and medicine. React Oxyg Spec (apex, NC) 1(1):9

314. Mohler, H., P., firrmann, R., Frei, K., 2014. Redox-directed cancer therapeutics: taurolidine and Piperlongumine as broadly effective antineoplastic agents (Review). Int. J. Oncol. 1329e1336. http://dx.doi.org/10.3892/ijo.2014.2566.

315. Meeks, R.G. and Harrison, S., 1991. *Hepatotoxicology*. CRC press.

316. Valková, V., Ďúranová, H., Bilčíková, J. and Habán, M., 2020. Milk thistle (Silybum marianum): a valuable medicinal plant with several therapeutic purposes. *The Journal of Microbiology, Biotechnology and Food Sciences*, *9*(4), p.836.

317. Mukhtar, S., Xiaoxiong, Z., Qamer, S., Saad, M., Mubarik, M.S., Mahmoud, A.H. and Mohammed, O.B., 2021. Hepatoprotective activity of silymarin encapsulation against hepatic damage in albino rats. *Saudi Journal of Biological Sciences*, *28*(1), pp.717-723.

318. Vargas-Mendoza, N., Madrigal-Santillán, E., Morales-González, Á., Esquivel-Soto, J., Esquivel-Chirino, C., y González-Rubio, M.G.L., Gayosso-de-Lucio, J.A. and Morales-González, J.A., 2014. Hepatoprotective effect of silymarin. *World journal of hepatology*, *6*(3), p.144.

319. Gudin, J., Gonzalez, A. and Lee, J., 2010. Nonopioid analgesics. *LLIA TIVE MEDICINE*, *56*, p.198.

320. Grypioti, A.D., Theocharis, S.E., Demopoulos, C.A., Papadopoulou-Daifoti, Z., Basayiannis, A.C. and Mykoniatis, M.G., 2006. Effect of platelet-activating factor (PAF) receptor antagonist (BN52021) on acetaminophen-induced acute liver injury and regeneration in rats. *Liver International*, *26*(1), pp.97-105.

321. Bhattacharyya, S., Sinha, K. and C Sil, P., 2014. Cytochrome P450s: mechanisms and biological implications in drug metabolism and its interaction with oxidative stress. *Current drug metabolism*, *15*(7), pp.719-742.

322. David, S. and Hamilton, J.P., 2010. Drug-induced liver injury. *US gastroenterology & hepatology review*, *6*, p.73.

323. Clark, R., Borirakchanyavat, V., Davidson, A.R., Williams, R., Thompson, R.P.H., Widdop, B. and Goulding, R., 1973. Hepatic damage and death from overdose of paracetamol. *The Lancet*, *301*(7794), pp.66-70.

324. Newsome, P.N., Plevris, J.N., Nelson, L.J. and Hayes, P.C., 2000. Animal models of fulminant hepatic failure: a critical evaluation. *Liver Transplantation*, *6*(1), pp.21-31.

325. Jaeschke H, Knight TR, Bajt ML (2006) The role of oxidative stress and reactive nitrogen species in acetaminophen hepatotoxicity.Toxicol Lett 144:279–288

326. https://echa.europa.eu/registration-dossier/-/registered-dossier/12532/7/3/1

327. Dogra, R.K., Khanna, S. and Shanker, R., 2004. Immunotoxicological effects of piperine in mice. *Toxicology*, *196*(3), pp.229-236.

328. Faeez, M.A., 2013. *Haematological abnormalities in decompensated chronic liver disease* (Doctoral dissertation, Tirunelveli Medical College, Tirunelveli).

329. Draper, H.H., Polensek, L., Hadley, M. and McGirr, L.G., 1984. Urinary malondialdehyde as an indicator of lipid peroxidation in the diet and in the tissues. *Lipids*, *19*(11), p.836.

330. Mishra, P. and Sharma, P., 2019. Superoxide Dismutases (SODs) and their role in regulating abiotic stress induced oxidative stress in plants. *Reactive oxygen, nitrogen and sulfur species in plants: Production, metabolism, signaling and defense mechanisms*, pp.53-88.

331. Nandi, A., Yan, L.J., Jana, C.K. and Das, N., 2019. Role of catalase in oxidative stress- and age-associated degenerative diseases. *Oxidative medicine and cellular longevity*, *2019*.

332. Tomaro, M.L. and del C Batlle, A.M., 2002. Bilirubin: its role in cytoprotection against oxidative stress. *The international journal of biochemistry & cell biology*, *34*(3), pp.216-220.

333. Paik, J.M., Kabbara, K., Eberly, K.E., Younossi, Y., Henry, L. and Younossi, Z.M., 2022. Global burden of NAFLD and chronic liver disease among adolescents and young adults. *Hepatology*, *75*(5), pp.1204-1217.

334. Ekor, M., 2014. The growing use of herbal medicines: issues relating to adverse reactions and challenges in monitoring safety. *Frontiers in pharmacology*, *4*, p.66193.

335. Sabina, E.P., Souriyan, A.D.H., Jackline, D. and Rasool, M.K., 2010. Piperine, an active ingredient of black pepper attenuates acetaminophen–induced hepatotoxicity in mice. *Asian Pacific Journal of Tropical Medicine*, *3*(12), pp.971-976.

336. Nelson, S.D. and Pearson, P.G., 1990. Covalent and noncovalent interactions in acute lethal cell injury caused by chemicals. *Annual review of pharmacology and toxicology*, *30*(1), pp.169-195.

Publications

European Polymer Journal 180 (2022) 111608

Contents lists available at ScienceDirect

European Polymer Journal

journal homepage: www.elsevier.com/locate/europolj

Thymoquinone incorporated chitosan-sodium alginate/psyllium husk derived biopolymeric composite films: A comparative antibacterial and anticancer profile

Sanghita Das [a,b], Debbethi Bera [a,c], Debojyoti De [d], Dheeraj Mondal [a], Parimal Karmakar [d], Sukhen Das [a,*], Anindita Dey [b,c,*]

[a] Department of Physics, Jadavpur University, Kolkata 700032, India
[b] Department of Botany, Asutosh College, Kolkata 700026, India
[c] Centre for Interdisciplinary Research and Education, 404B, Jodhpur Park, Kolkata 700068, India
[d] Department of Life Science and Biotechnology, Jadavpur University, Kolkata 700032, India

ARTICLE INFO

Keywords:
Polymer composite
Psyllium husk
Thymoquinone
Sustained release
Antibacterial activity
Anticancer activity

ABSTRACT

The fabrication of biopolymeric film containing natural therapeutics envisioned to develop edible, nontoxic and biodegradable composite using polymers. Our study focused on extraction of psyllium husk mucilage, a medicinally acknowledged natural polysaccharide and develop a proper composite with chitosan. We combined chitosan with both alginate and husk mucilage separately to prepare two composite films. Drug release dynamics from the complex polymeric networks was evaluated where polymeric films showed sustained release of thymoquinone, a water-insoluble phytocomponent. Structural and physico-chemical properties of the films were confirmed by FTIR, XRD, FESEM, TGA analysis. Significant antimicrobial activities against both bacterial strains and strong anticancer activities against human prostate cancer cell line (PC3) and adenocarcinomic human alveolar basal epithelial cell line (A549) was observed. This biodegradable polymer combination suggests towards the possibility of potential applications for the food industry and variety of biomedical applications such as wound dressing, tissue scaffolding etc.

1. Introduction

Multifunctional biomaterials, polymer composite are extensively used in the field of pharmaceutical drug delivery because of their wide range of versatility, biocompatibility and stability to serve as a matrix or vehicle for drugs compared to synthetic or inorganic materials [1,2]. Polymer composites with proper ratio and modifications can be a better excipient constituent as sustained drug carrier with improved physical, mechanical, functional properties [3,4]. The stability of polymer composite could be affected by molecular weight, crystallinity, mixing ratio, presence of functional groups, pH of reaction medium, distribution of ionic groups, drying process, etc [5].

Chitosan has been used as a positively charged polymeric drug carrier due to its biocompatibility, biodegradability and relatively low production cost [6]. Alginate is a water soluble, unbranched, biodegradable polysaccharide consisting of alternating blocks of 1–4 linked -l-guluronic (G-block) and -d-mannuronic acid (M−block) residues [7]. Carboxylic acid groups of alginate is responsible for negative charges which attribute characteristic electrostatic interaction with the positively charged molecules [6]. Alginates are extracted from brown seaweeds and marine algae such as *Laminaria hyperborea*, *Ascophyllum nodosum* and *Macrocystis pyrifera* [4,8,9]. Since chitosan is positively charged at low pH values (below its pKa value), it spontaneously associates with negatively charged polyions like alginate in solution to form a special type of macromolecules, the polyelectrolyte complexes [4]. Psyllium mucilage obtained from the seed coat of *Plantago ovata* and *Plantago indica* belongs to the family Plantaginaceae which can be obtained by mechanical grinding of the outer layer of the seeds[10]. Psyllium mucilage is fibrous mucilaginous hydrocolloid used in treatment of intestinal inflammation, constipation, etc. [11]. Arabinoxylan, a complex heteroxylan of two pentose sugars i.e. arabinose and xylose is a highly branched hemicellulose [12–14]. Sodium alginate (Al) and

Abbreviations: Ch, Chitosan; Al, Sodium alginate; Ph, Psyllium husk mucilage; Tq, Thymoquinone.

* Corresponding authors.
E-mail addresses: sukhendas29@hotmail.com (S. Das), anindita.dey@asutoshcollege.in (A. Dey).

https://doi.org/10.1016/j.eurpolymj.2022.111608
Received 12 June 2022; Received in revised form 22 September 2022; Accepted 24 September 2022
Available online 28 September 2022

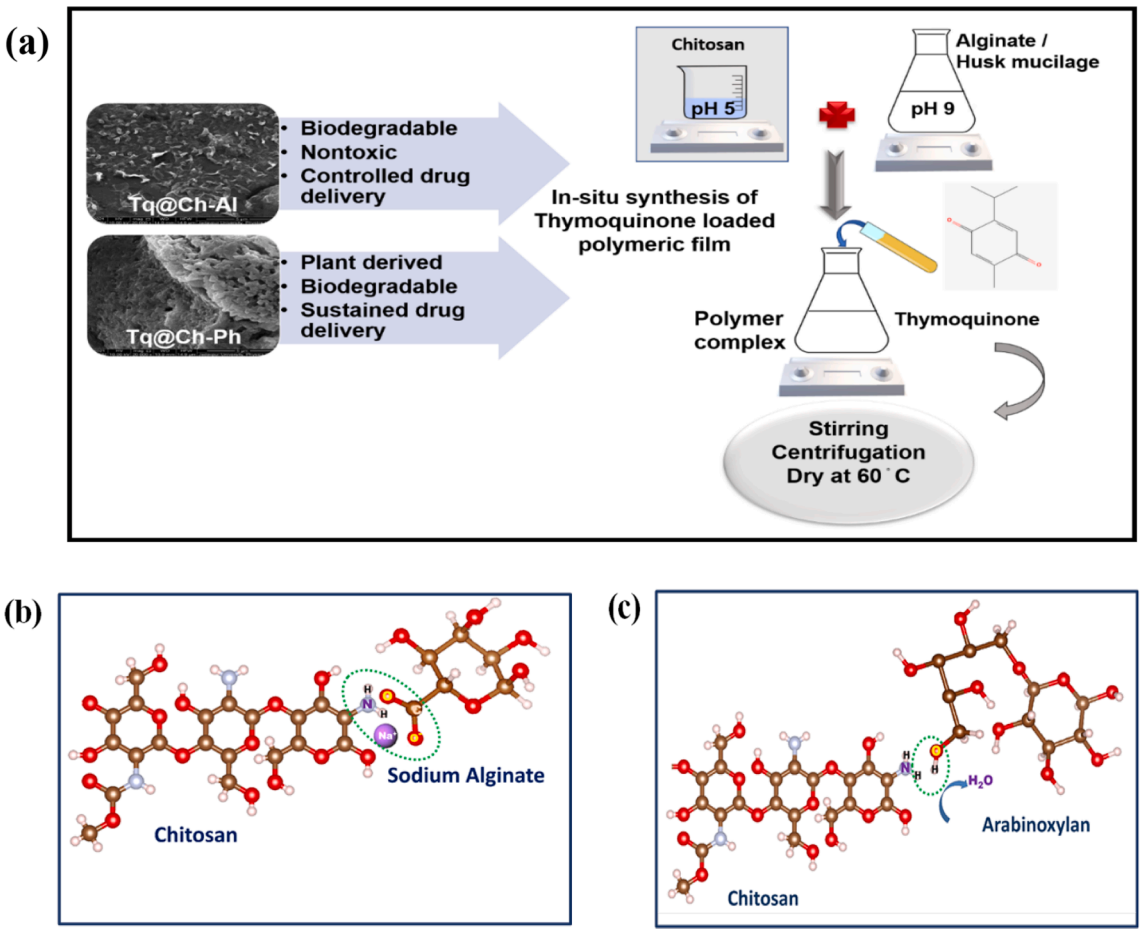

Fig. 1. (a) Schematic representation of synthesis procedure of polymeric films, Interaction pattern of chitosan with (b) sodium alginate and (c) arabinoxylan.

chitosan (Ch) are widely used as a matrix or hydrogel material to attain sustained drug release but still under widespread exploration [15,16]. Bindu et al. also reported that in combination with HPMC K4M, husk mucilage retarded the release of the drug which facilitate sustained release by reducing the instant swelling of the composite [17]. Psyllium husk mucilage (Ph) was chosen to interact with chitosan (Ch) to synthesis a stable complex to improve the drug loading efficiency when interacted with thymoquinone (Tq). The phyto-active component of the *Nigella sativa* essential oil (Tq) with cytotoxic, antimicrobial, antioxidant, antifungal properties is used to combine with each polymer separately (provided as supplementary data) as well as with polymer composites. Tq was able to induce apoptosis via p53-dependent as well as p53-independent pathways [18–20].

In this context, our present study is an effort toward the synthesis of high-performance composite polymer films to obtain good antibacterial as well as cytotoxic activity with minimal side effects followed by a discussion on their probable interaction with polymer composites. The paper describes a comparative structural characterization and clinical efficacy of chitosan-sodium alginate (Ch-Al), chitosan- Psyllium mucilage (Ch-Ph) films as well as Thymoquinone (Tq) loaded polymeric composites (Tq@Ch-Al and Tq@Ch-Ph).

2. Materials and methods

2.1. Materials and cultures

Na-Alginate with viscosity (25 °C): 5–40 cps and thymoquinone were procured from Sigma-Aldrich (Switzerland). Psyllium husk was acquired in local markets of Kolkata, India. Chitosan $(C_6H_{11}NO_4)_n$ (molecular weight: 100–300 kDa) was purchased from Acros organics. All other reagents were supplied by SRL Pvt. Lt. (India) and Merck ltd. Deionized (Millipore) water of 18 MΩ-cm was used in all experiments.

Test bacterial strains (*Enterococcus faecalis* 441 and *Pseudomonas aeruginosa* 1688) were purchased from Microbial Type Culture Collection, IMTECH (Chandigarh, India). Cell lines were procured from the National Centre for Cell Science (Pune, India).

2.2. Synthesis of Tq@Ch-Al/Ph

2.2.1. Extraction and purification of Ph

Ph was extracted by mixing with deionized water in a 1:100 (w/v) ratio, for 4 h, under constant agitation at 60℃. To prevent the water loss as a result of evaporation, water (60℃) was added at different intervals to the system. The insoluble non-carbohydrate fractions of psyllium seeds removed by filtration. Mucilage was stirred for 10 min with ethanol at a ratio of 100:50 (mucilage volume: ethanol volume). After centrifuging at 2000 rpm for 3 min the supernatant was used to quantify the non-precipitated carbohydrates. Ethanol was removed from the precipitate by using a rotary evaporator. Further, it was kept for drying in hot air oven after spreading on a glass plate at 50℃ temperature to dehydrate the carbohydrates [21].

2.2.2. Synthesis of composite films

Briefly, 50 mg Al was dissolved completely in 50 ml distilled water to form a 0.1% (w/v) Al solution at room temperature. The solution was adjusted to a pH of 9. 50 mg of Ch were dissolved in 50 ml of 1 % (v/v) acetic acid solution to obtain a 0.1 % (w/v) Ch solution. pH of the Ch solution was adjusted to 5. Both dispersions were homogenized with a

magnetic stirrer 4 h at room temperature. Then Al solution was added dropwise to Ch solution under constant magnetic stirring. The resulting opalescent suspension was cast on a glass petri dish and allowed to dry at 60°C for 24 hrs. Similar experimental procedure was followed in case of Ch-Ph synthesis.

2.2.3. Loading of Tq on Ch-Al/Ph film

Tq was added in lukewarm Millipore water (60℃), mixed with polymer solution and was allowed to stir for 24 hrs at room temperature. The obtained sample was centrifuged at 10,000 rpm for about 10 mins and washed three times and then dried at 60°C in a vacuum desiccator. A schematic representation of the synthesis procedure of therapeutic loaded polymeric film depicted in Fig. 1(a).

2.3. Apparatus and characterization of Tq@Ch-Al/Ph

The chemical interactions were confirmed by X-ray diffraction (XRD) spectra by using X-ray diffractometer (model-D8 Bruker AXS, Wisconsin, USA) and Fourier transform infrared spectroscopy (FTIR-8400S, Shimadzu, Tokyo) in the wavenumber range from 400 cm^{-1} to 4000 cm^{-1}. Field emission scanning electron microscope (FESEM) was conducted for the surface texture study employing INSPECT F50 (FEI, the Netherland) and EVO 18 Special edition, Carl Zeiss (Germany). The UV visible spectrophotometer (Epoch microplate reader, BioTek, USA) was used to estimate the absorbance intensity. Epoch Microplate Spectrophotometer, USA was used in natural therapeutics release study. Spectroscope (Hitachi, Japan) and fluorescence microscope (DM 2500, Leica, Germany) were used for the ROS detection. Ultrasonic bath sonicator is used for preparing all type of suspensions. All bacterial and cellular examinations were performed in a biosafety cabinet.

2.4. Antibacterial efficacy assessment

Antimicrobial properties of Tq loaded composite films were studied in respect of time by colony counting method on *P. aeruginosa* and *E. faecalis*. As because our samples are film matrix, we carried out an additional agar-diffusion method based on direct contact between the sample and the bacteria to examine their potential effectivity.

For agar-diffusion method, 100 μl of overnight grown bacterial culture (cell density 10^7 CFU ml^{-1}) was dispersed over the petri dish. The polymer films were positioned on the petri plate containing solid media with direct contact with the surface. Then the plates were incubated at 37°C for overnight [22].

For time dependent colony counting method a strip (weighted 3 mg) of Ch-Al, Ch-Ph, Tq@Ch-Al and Tq@Ch-Ph were added to bacterial culture (cell density 10^7 CFU ml^{-1}) containing 5 ml nutrient broth and incubated on a rotary shaker at 37°C. Finally microbial growth was assessed by plating treated culture on nutrient agar plates after 2, 4, 12 and 24 h. The microbial culture without polymer composite was considered as control. In case of control, after the incubation, inoculum was plated on nutrient agar plate and bacterial colonies were counted after 24 hrs. The antibacterial efficacy was calculated using the equation.

$$M(\%) = [(C - T)/C] \times 100$$

Where, M is the mortality percentage, C is the mean number of bacterial colonies on the control plate and T is the mean number of bacterial colonies on the treated plate [23].

To estimate intracellular ROS generation 2, 7 -dichlorodihydrofluorescein diacetate (DCFH2-DA) was used which can detect a broad range of reactive oxygen species after treatment. Finally, fluorescence intensity was measured spectroscopically at emission wavelengths 520 nm with an excitation wavelength of 485 nm [24]. To study bacterial cell morphology after treatment scanning electron microscopy (SEM) was performed for untreated *P. aeruginosa* and *E. faecalis* cells as well as treated (treated with Ch-Al, Ch-Ph, Tq@Ch-Al and Tq@Ch-Ph) for comparative study.

2.5. Evaluation of Tq loading and release

The Tq loading percentage within polymeric composite film was determined by calculating the concentration of the Tq using standard procedure. The drug loading content (DLC) and drug loading efficiency (DLE) were calculated using the following equations [25].

$$DLC(\%) = \frac{W_{total\ drug} - W_{free\ drug}}{W_{drug\ loaded\ vehicle}} \times 100 \quad (1)$$

$$\mathrm{DLE}\ (\%) = \frac{\mathrm{W_{total\ drug}} - \mathrm{W_{free\ drug}}}{\mathrm{W_{total\ drug}}} \times 100 \quad (2)$$

To determine the amount of Tq discharged from synthesized composite film, in vitro Tq release was calculated in a time dependent manner in physiological pH conditions (pH ~ 7.4) and intracellular pH conditions of cancer cells (pH ~ 5.5) at 37°C. The release percentage at different time intervals was calculated from a standard curve of Tq.

2.6. Anticancer activity assessment

2.6.1. Cytotoxicity study

In vitro cytotoxicity was evaluated with the help of the 3-(4, 5-dimethylthiazol-2-yl) − 2, 5-diphenyltetrazolium bromide (MTT) assay following a standard protocol against human lung fibroblasts i.e., WI38 cell line (provided as supplementary data), human prostate cancer cell line (PC3) and adenocarcinomic human alveolar basal epithelial cell line (A549). Cells were exposed to polymeric films (3 μg/μl each) for 24 hrs. After incubation, cells were washed with 1X PBS twice and further incubated for 4 h with MTT solution (450 μg/ml). After 4 hrs of incubation at 37°C the MTT solution was discarded and after addition of extraction buffer (Isopropanol, Tween 20, HCl), a crystal violet colour was observed. The absorbance the resulting formazan crystals was measured at 570 nm using a spectrophotometer, and the values were compared with untreated cells [26].

2.6.2. ROS estimation

To estimate intracellular ROS generation in PC3 and A549 cells DCFH2-DA assay was used. DCF-DA dye enters the cell and reacts with reactive oxygen to give a green fluorescent colour compound dichlorofluorescein (DCF). The absorbance was measured at excitation and emission wavelengths of 485 and 520 nm respectively using a spectrophotometer, and the values were compared with untreated cells to determine the fold change [27].

In separate experiments, cancer cells were seeded on coverslips placed on 35 mm cell culture plates and next day cells were treated with films for 24 hrs (3 μg/μl each). After incubation with 100 μM of DCF-DA for 30 mins at 37°C cells were observed under fluorescence microscope to observe and compare intensity of fluorescence.

2.7. Statistical analysis

All experiments were performed in triplicate and data were presented as mean ± standard deviation (SD) for each set of experiments. Single factor one-way statistical analysis was performed using ANOVA. To determine statistical significance, value of $p < 0.05$ was considered to indicate significance or otherwise mentioned.

3. Results and discussion

3.1. Formation of polymer composite

In case of Ch-Al the negatively charged carboxylic acid (–COO) groups of manuronic and guluronic acid units of Al interact electrostatically with the positively charged amino (–NH2) groups of Ch and

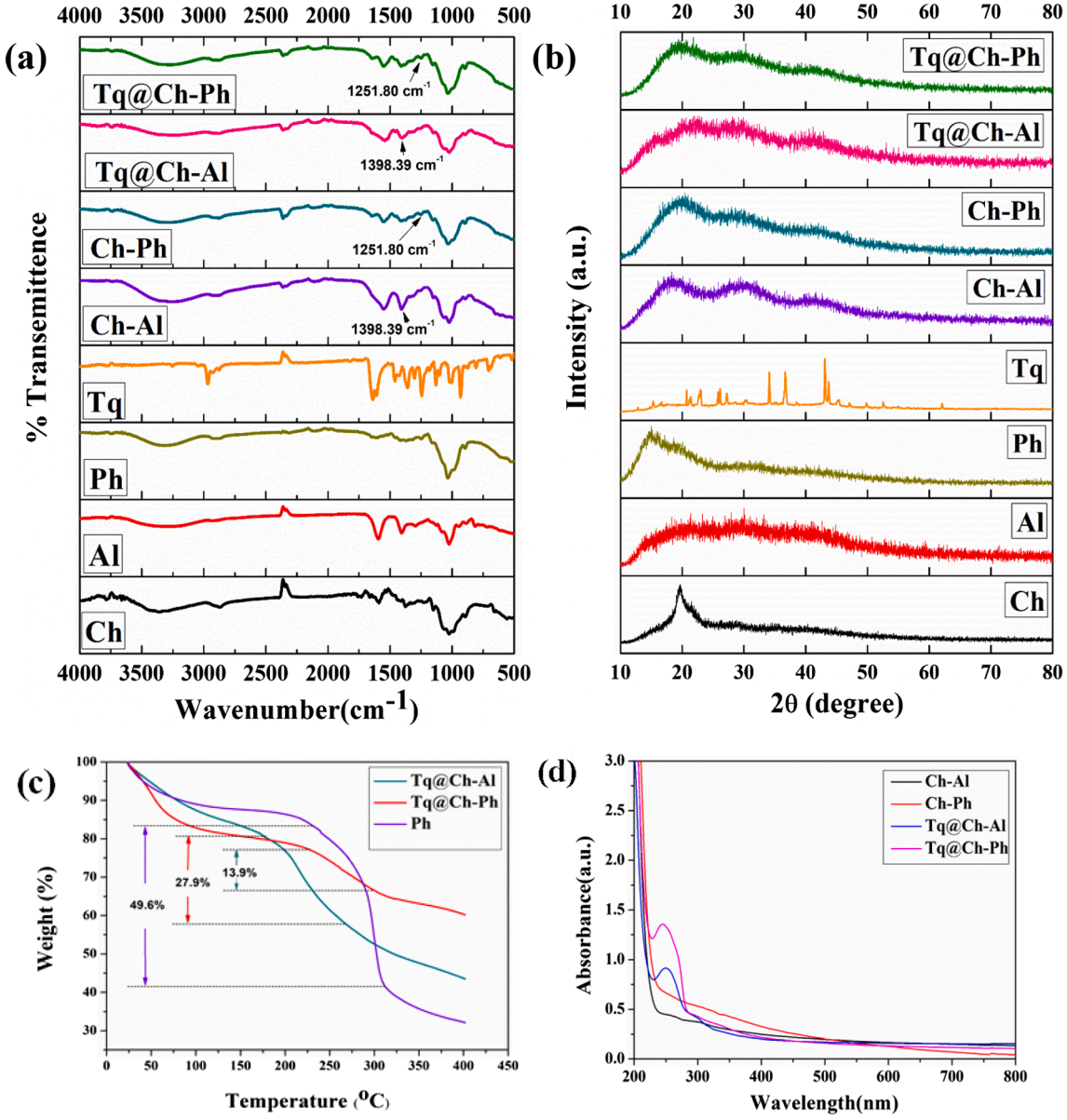

Fig. 2. (a) FT-IR spectra and (b) XRD pattern of synthesized polymer composites (c) TGA curve of Ph, Tq@Ch-Al and Tq@Ch-Ph (d) UV–vis spectra of polymer composites.

form a polyelectrolyte complex [4]. In acidic environment Ch becomes positively charged due the protonation of the –NH2 group results in formation NH3 + ions [28]. The Ch-Ph composite film is formed due to the interaction between the free amino (–NH2) group of Ch with the -hydroxyl (–OH) group present in arabinoxylan. Fig. 1(b) and 1(c) demonstrate the interaction patterns of Ch and Al/ Ph hydrocolloid.

3.2. Characterization of Tq@Ch-Al and Tq@Ch-Ph

3.2.1. FTIR analysis of Tq@Ch-Al/Ph

FT-IR analysis has been performed to determine the chemical structure and the presence of characteristic functional group. In Fig. 2(a) a broad absorption band at 3307.9 cm^{-1} is observed which may be due to –OH stretching of alcohols of Ph. A band appearing at 2891.2 cm^{-1} in Ph is due to –CH stretching of alkanes. Similar peaks are observed in Ch-Ph and in Tq@Ch-Ph [29]. The FTIR spectrum of Ph (arabinoxylan) shows a peak at 894.97 cm^{-1} which represent the bending of polymer backbone of arabinoxylan [15]. Similarly, Ch-Ph and Tq@Ch-Ph shows this characteristic peak at 891.11 cm^{-1} and 889.18 cm^{-1} respectively. The absorption band at 1529.55 cm^{-1} in Tq@Ch-Al and 1556.55 cm^{-1} in Tq@Ch-Ph corresponds to amide II groups present in Ch at 1589.34 cm^{-1} [30]. Peaks at 950.96 cm^{-1} and at 883.40 cm^{-1} are observed due to the presence of uronic acid group and mannuronic acid functional group in Al . Similar peaks are appearing at FTIR spectra of Ch-Al and Tq@Ch-Al ascribed the presence of Al [31]. A broad peak at 3342.63 cm^{-1} correspond to the hydroxyl group [29]. The recorded peaks at 1328.95 cm^{-1} in Tq@Ch-Al and 1369.46 cm^{-1} at Tq@Ch-Ph could be assigned the presence of Tq [32]. Further, the FTIR spectrum of Tq@Ch-Al and Tq@Ch-Ph respectively at 3329.13 cm^{-1} and 3304.07 cm^{-1} represent O—H stretch of Tq [32]. A peak at 1398.39 cm^{-1} in Ch-Al and Tq@Ch-Al possibly corresponded to electrostatic interaction between –COO groups of Al with the –NH2 groups of Ch [33]. In case of Ch-Ph and Tq@Ch-Ph, the direct C—N bond formation via coupling of –OH group present in arabinoxylan and –NH2 group of Ch is which confirmed by the peak at 1251.80 cm^{-1}(C—N—C asymmetric stretch) [34].

3.2.2. XRD study of Tq@Ch-Al/Ph

XRD study was performed to find out the phase and crystallinity of

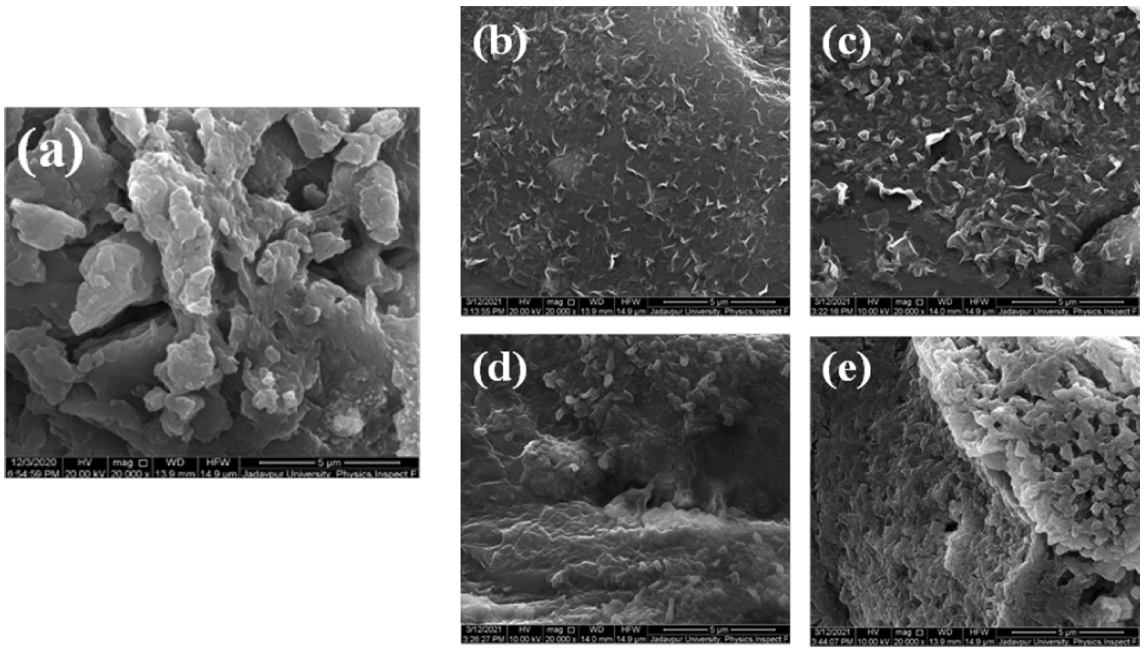

Fig. 3. (c) FESEM image of (a) Ph (b) Ch-Al, (c) Tq@Ch-Al, (d) Ch-Ph and (e) Tq@Ch-Ph.

the composite film. Fig. 2(b) demonstrates the XRD spectra of Ph, Ch-Al, Ch-Ph, Tq@Ch-Al and Tq@Ch-Ph. All four synthesized polymer film exhibited a broad hallow which indicates very low crystallinity due to amorphous nature. Amorphous forms consist of disordered arrangements of molecule which do not have a distinguishable crystal lattice [35]. Ch has very broad peaks at $2\theta = 20^{\circ}$ [36]. Al showed three broad humps at $2\theta = 20^{\circ}$, $2\theta = 30^{\circ}$, $2\theta = 40^{\circ}$. The XRD pattern of Ph also indicated an amorphous form with two humps at around 2θ of 15°and 20°. Ch-Al, Ch-Ph, Tq@Ch-Al and Tq@Ch-Ph displayed shifted hump at around 2θ of 20° and sharp peak of chitosan at $2\theta = 20^{\circ}$ became weak. These results confirmed good compatibility and the interaction between Ch with Al or Ph to form Ch-Al and Ch-Ph. The XRD pattern also suggested the amorphous form of composite film. The amorphous nature of polymer films were maintained after incorporation of Tq, which is beneficial for biomedical applications.

3.2.3. *Thermal stability of Tq@Ch-Al/Ph*

Thermo Gravimetric Analysis of Ph and Tq loaded composite was measured to determine the thermal stability and the decomposition temperature shown in Fig. 2(c). It was observed that the TGA of Ph, Tq@Ch-Al and Tq@Ch-Ph showed a two-step of weight loss. Initial weight loss may correspond to the evaporation of moisture or loss of adsorbed or bound water. In case of Ch and Al the initial degradation at around 30–100°C are almost 5% and 10% respectively [37,38]. The second weight loss of Ph is about 49.6% in the range 230–311°C was due to the complexity of the process, which led to the degradation of the sample. At the end of 400°C the total weight loss of sample was 56.36% in case of Tq@Ch-Al and 39.68% in case of Tq@Ch-Ph.

3.2.4. *UV–visible spectrophotometric analysis*

In our study, UV–visible spectroscopy was used to study the absorption spectra of films. The UV–vis spectra of Tq is characterized by the presence of one prominent peak (λ^{max}) at 254–257 nm regarded as a distinguishing peak for quinones [39]. As observed in Fig. 2(d), UV–vis absorbance spectrum of Tq@Ch-Al and Tq@Ch-Ph displayed a prominent peak at 248 nm and 252 nm respectively. The results ascertained the successful interaction with Tq.

3.2.5. *Morphology study of Tq@Ch-Al/Ph*

As observed in FESEM image (Fig. 3) the surface morphologies of all these five samples are porous in nature. The SEM image of Ph (Fig. 3(a) revealed discontinuous and irregular microporous surface which is also observed in image captured from Ch-Ph and Tq@Ch-Ph depicted in Fig. 3(d) and (e). Fig. 3. 3(a) and (b) shows flaky polymeric structure of Ch-Al and Tq@Ch-Al respectively. FESEM image clearly indicate the marked differences between Tq tagged polymer composites and bare polymer composites.

3.2.6. *Drug loading efficiency*

The loadings content and loading efficiencies of a wide range of natural therapeutics in polymer matrix are highly depend on the chemical nature and the interaction pattern between polymer and drug. Loading content is determined to be 36.15% in case of Tq@Ch-Al and 38.10% in case of Tq@Ch-Ph. We report higher loading efficiency of Tq when we replace alginate with Ph. Condensed porous surface of polymer composite restricted the leakage of drug from the films results in high loading efficiency of hydrophobic Tq. The loading efficiency of Tq@Ch-Al and Tq@Ch-Ph is 78.33% and 81.30% respectively. These results indicated that the incorporation capacity of Ch-Ph is higher than Ch-Al.

3.3. *Antimicrobial activity*

Fig. 4(a) represents the antibacterial potentials of four types of composite films (namely, Ch-Al, Ch-Ph, Tq@Ch-Al and Tq@Ch-Ph) against *P. aeruginosa* and *E. faecalis* as determined by the plate counting method. Percent of cell mortality was plotted in time dependent manner over a period of 24 hrs to determine the effect of the composite films which were found to display significant antibacterial activity against pathogenic bacteria. Agar plates of the control and treated bacteria after 24 hrs of incubation are displayed in Fig. 4(a). The differential antibacterial kinetics of test bacteria are checked against our four samples by time kill assay using colony count method. Fig. 4(c) demonstrate that within 24hrs of incubation period the mortality rate of *P. aeruginosa* for Tq@Ch-Al and Tq@Ch-Ph are 73.60% and 74.50% respectively. *E. faecalis* display 96.80% and 98.50% mortality rate when treated against Tq@Ch-Al and Tq@Ch-Ph during the same incubation period (Fig. 4b). The test result also demonstrates excessive colonies against composite without Tq i.e., Ch-Al, Ch-Ph. Bacteriostatic activities of Ch-Al and Ch-Ph occurred because of the antibacterial property of chitosan. Ph has no such antibacterial activity when we treated our test

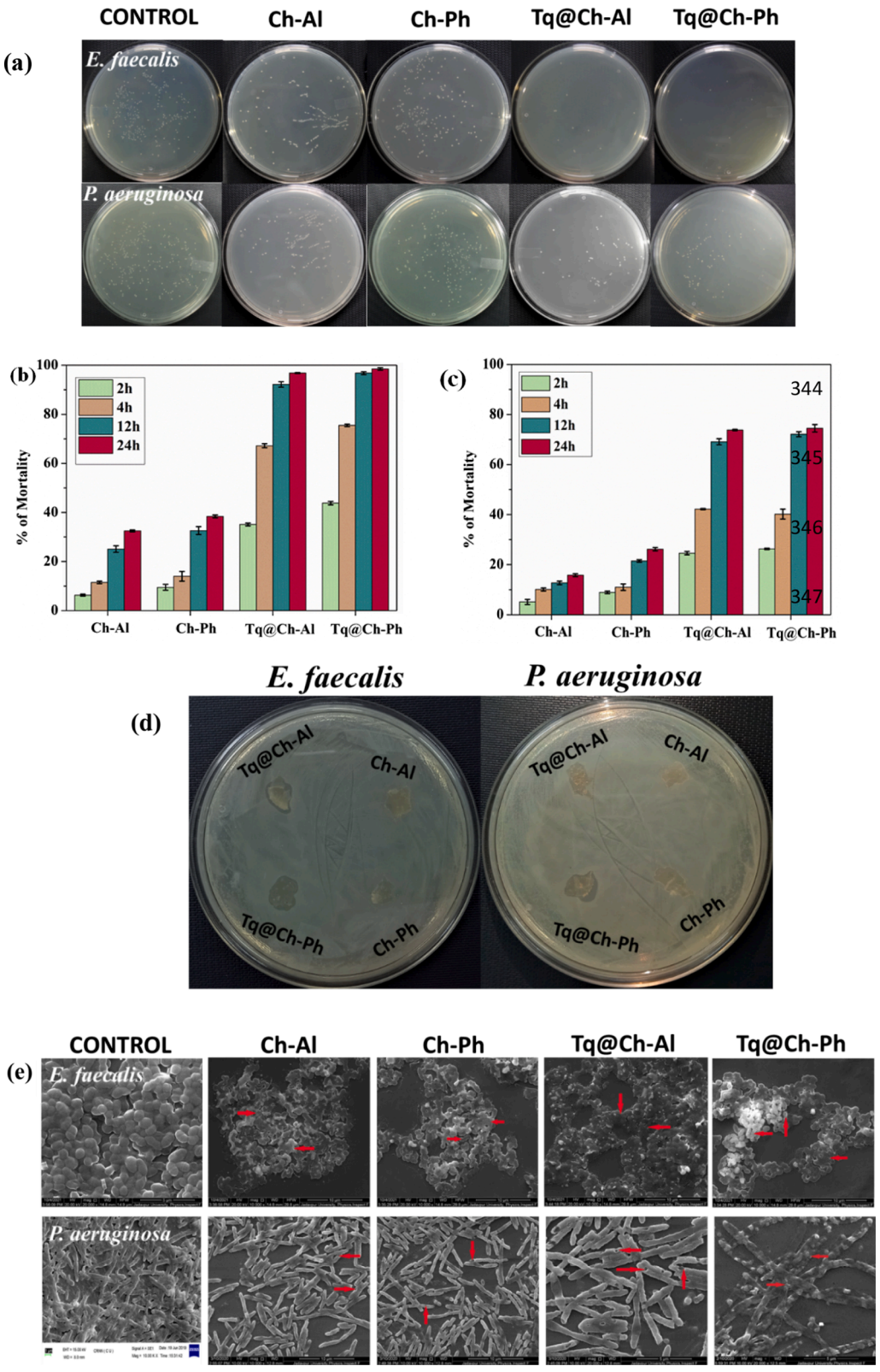

Fig. 4. (a) Plate count photograph showing the antibacterial efficacy of films after 24 h of incubation. Graphical representation of the percentage of cell mortality of (b) *Enterococcus faecalis* and (c) *Pseudomonas aeruginosa*. (d) Photographic images of the antimicrobial activity of films (e) FESEM micrographs showing morphological characteristics of bacterial cells. Graphical representation of bacterial ROS generation by DCFDA assay in case of (f) *Enterococcus faecalis* (g) *Pseudomonas aeruginosa.*

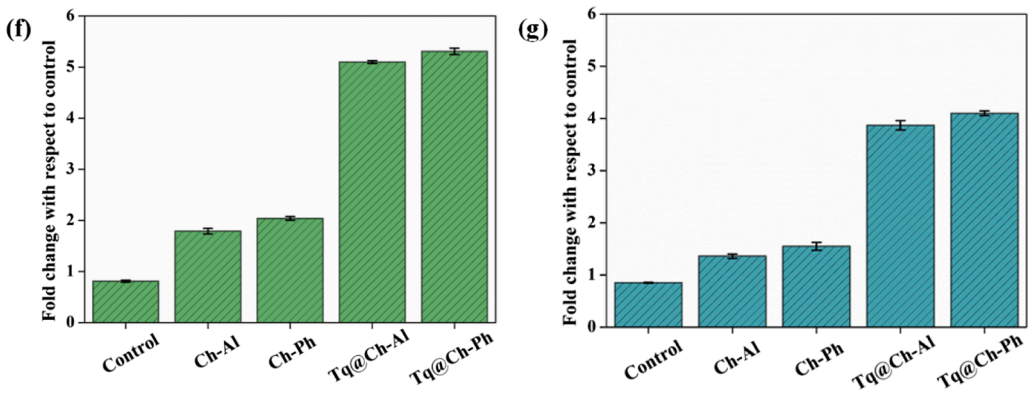

Fig. 4. (*continued*).

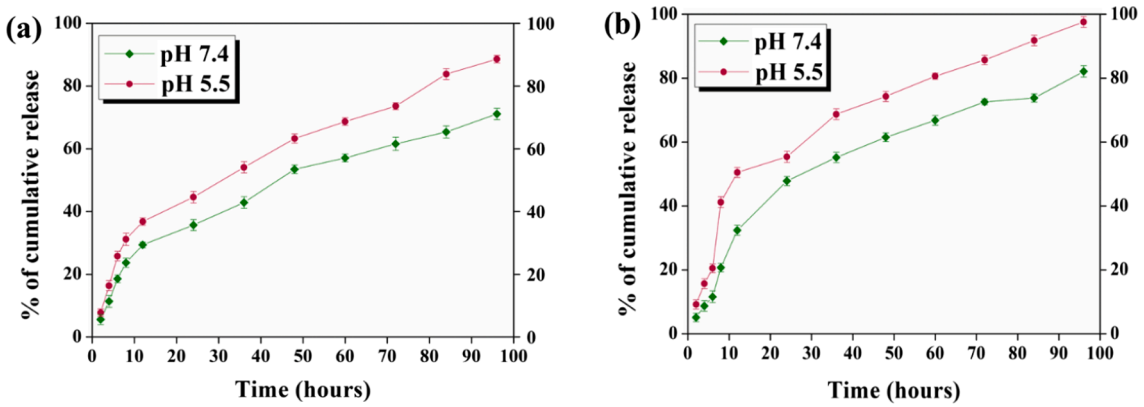

Fig. 5. Graphical representation of pH-responsive time-dependent release study of thymoquinone from (a)Tq@Ch-Al (b) Tq@Ch-Ph.

bacteria against Ph alone.

Fig. 4(d) showing agar diffusion method which revealed that Ch-Al, Ch-Ph, did not display any significant zone of inhibition but there is no trace of bacterial biofilms formation on film surface. On the other hand, the Tq encapsulated composite films revealed a zone of inhibition. Upon contact with the Tq loaded film, the ionic interactions may occur between positively charged amino groups present in Ch and negatively charged lipopolysaccharides of bacterial cell wall. The hydrophobic moieties of Tq possibly interact with the cell membrane lipopolysaccharides may results in destabilization in cellular membrane and altered permeability for Tq [40].

FESEM image of Fig. 4(e) confirmed the damaged bacterial membrane integrity upon interaction with Ch-Al, Ch-Ph, Tq@Ch-Ph and Tq@Ch-Al compared to the smooth and undamaged structure of control groups.

Oxidative stress can be a major cause of disruption of cellular integrity by damaging DNA, RNA, lipids and proteins [41]. Fig. 4(f) and 4(g) also stated the higher ROS generation in bacterial cell in case of Tq@Ch-Ph compared to Tq@Ch-Al which also correlate with the cell mortality study stated earlier. Due to ROS accumulation polyunsaturated fatty acids of bacterial membrane are attacked which initiate lipid peroxidation and alter the integrity of membrane-bound proteins [42].

3.4. Drug release

We verified whether these polymer complexes can achieve stability and controlled release of Tq in physiological conditions as well as acidic environment which is essential for clinical applications. The in vitro release behaviour of incorporated Tq from Tq@Ch-Al and Tq@Ch-Ph occurred in two steps, i.e., an initial rapid release within the first 12 h followed by a slow leaching over a period of 96 h (Fig. 5a and b). At pH 5.5 (acidic condition), after 24 hrs the estimated release percentage of Tq from Tq@Ch-Ph (approx. 55.40%) was found to be greater than Tq@Ch-Al (approx. 44.60%). Release behaviour depends on the nature of interaction of therapeutics with polymer mesh. Moreover, the release profile suggested sustained but faster release in acidic condition and thus it confirms the efficacy of polymer composite to release adequate amount Tq for its anticancer applications.

Table 1
Effective concentration of thymoquinone in bacterial broth during antibacterial assay.

TIME (hr)	Tq@Ch-Al (μg/ml)	Tq@Ch-Ph (μg/ml)
2	12.15	12.12
4	24.73	19.93
12	63.77	74.07
24	77.43	109.27

Table 1 demonstrate time and pH dependent effective concentration of Tq. If we compare the MIC value reported by Chaieb et al. it can be said that in case of *E. faecalis,* treatment with both Tq@Ch-Al and Tq@Ch-Ph showed high bacterial growth within 4 h even if the effective concentration of Tq is less than the MIC value [43]. However, in the 12–24 hrs range the effective concentration of Tq is more than MIC value which correspond to the observed antibacterial activity.

3.5. Assessment of anticancer properties

The in vitro cytotoxicity of synthesized films were assessed by MTT assay to human PC3 and A549 cell lines. In Fig. 6 we had observed that the cell treated with Tq@Ch-Ph and Tq@Ch-Al resulted in significant

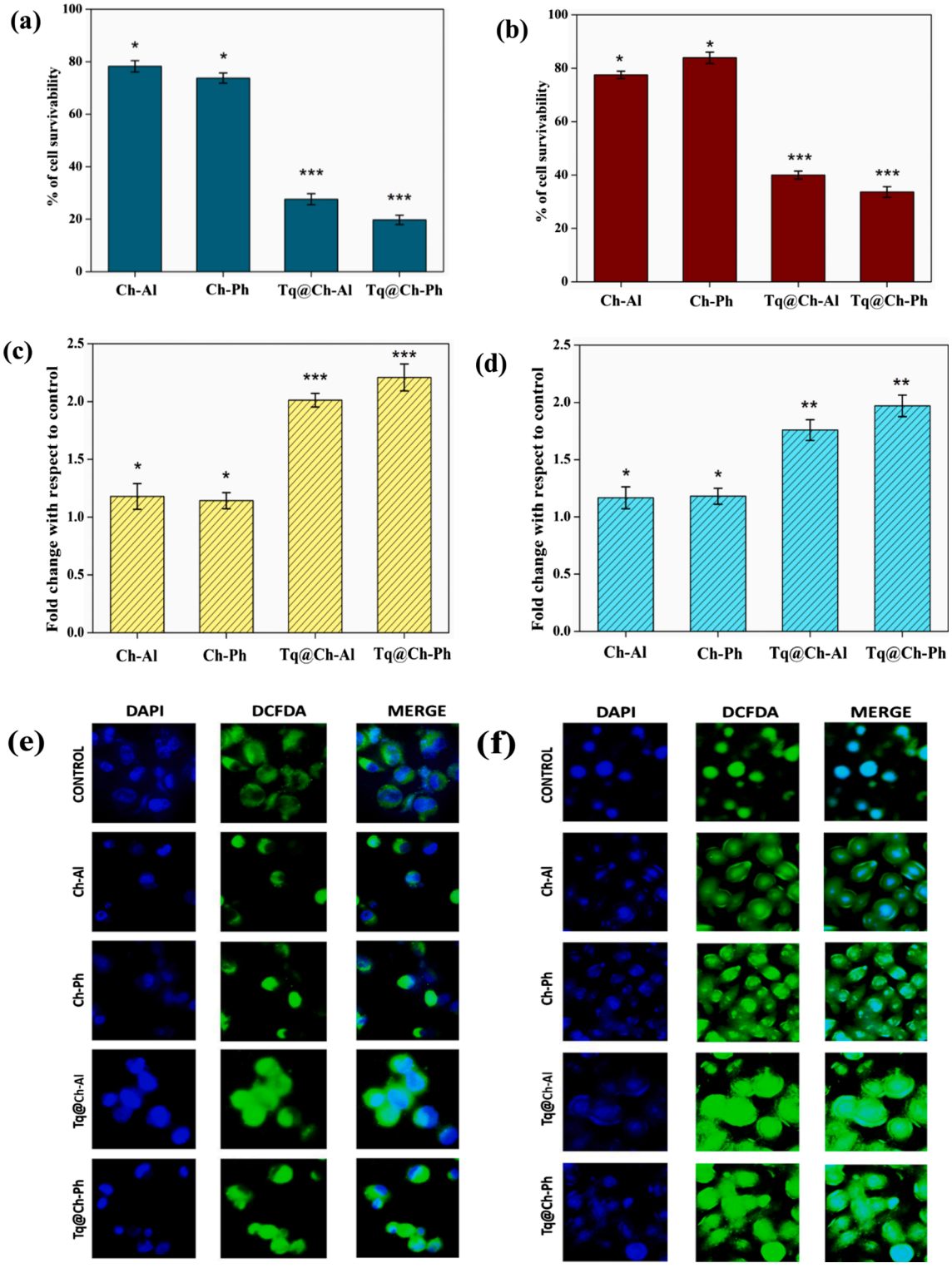

Fig. 6. MTT assay on (a)PC3 and (b)A549 cell line after treatment with films. The Cell Survivability Percentage was expressed as a mean ± SD of three independent experiments and significance was shown as *($P < 0.05$), **($P < 0.01$) and ***($P < 0.001$). Graphical representation of mean fluorescent intensity for ROS generation in (c)PC3 and (d)A549 cell line. The fold change with respect to control was expressed as a mean ± SD of three independent experiments and significance was shown as *($P < 0.05$), **($P < 0.01$) and ***($P < 0.001$). Fluorescence microscopic image of intracellular ROS generation for (e)PC3 and (f) A549 cell line.

cell death in case of both cell lines compared to Ch-Al and Ch-Ph which did not exhibit any marked cell death. In case of PC3 cell line Tq@Ch-Ph treated cell exhibited 19.73% cell survivability whereas 33.66% cell survivability is observed in case of A549 cells.

Monitoring intracellular ROS generated from the activity of polymer composites we found out that the fold change in case of Ch-Al, Ch-Ph both was almost similar to untreated cells whereas Tq@Ch-Ph and Tq@Ch-Al exhibited a marked increase in the production of ROS (Fig. 6). This was confirmed by both spectrophotometry as well as fluorescence microscopy.

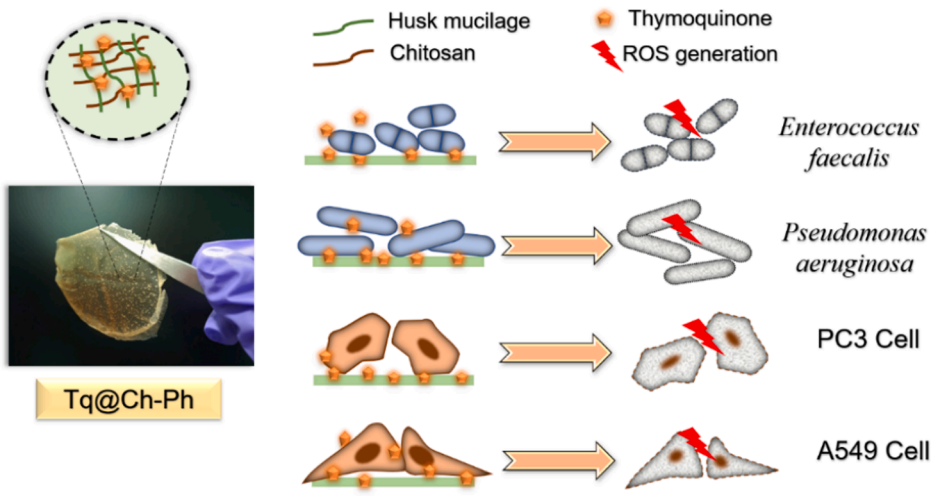

Fig. 7. Schematic representation showing the efficacy of polymeric film on pathogenic bacterial strains and carcinoma cells.

4. Conclusion

In this study, antimicrobial and anticancer composites were obtained by simply combining Ch with Ph or Al without the addition of any compatibilizer or chemical modification of film surfaces, thus providing a simple synthetic procedure to develop biopolymeric film with bactericidal as well as cytotoxic applications. The obtained polymer composites incorporating Tq were characterized regarding their morphology, physico-chemical properties and thermal stability by different techniques, from which we can confirm effective interactions and good compatibility between Ch and Ph / Al as well as between the polymer composites and the Tq. The incorporation efficiencies and release kinetics of Tq were also evaluated and contrasted with results attained for the antimicrobial activity against bacterial strains. Notably, compared to Tq@Ch-Al, Tq@Ch-Ph exhibited significantly improved in vitro Tq release as well as better antibacterial efficacy. In the FESEM study of bacterial cell, morphological changes induced by the Tq and Ch in polymeric films are evident due to cell damage. An in vitro cytotoxicity study revealed that the Tq-loaded polymeric films showed remarkable cell death against PC3 and A549 cell lines in a highly effective manner (Fig. 7). Moreover, experimental results confirmed that the broad-spectrum antibacterial and cytotoxic activity observed due to the chitosan and Tq released from polymer film. The prepared polymeric film either adhered to the bacterial cell wall or the released Tq interact with the bacterial membrane and promote ROS generation thus destabilized the cellular integrity and membrane permeability. Hence, from overall study it has been established that Ph mucilage can be used to develop effective polymeric film in combination with another polymer if properly standardised. Thus, in combination with therapeutic agents i.e., Tq, Tq@Ch-Ph is established as an excellent antibacterial as well as anticancer film which can be advantageous for further investigations. Thus, this type of film containing nontoxic plant derived materials has promising potential for therapeutic applications and in biomedical industry.

Funding

This research did not receive any specific grant from funding agencies in the public, commercial, or not-for-profit sectors.

Declaration of Competing Interest

The authors declare that they have no known competing financial interests or personal relationships that could have appeared to influence the work reported in this paper.

Data availability

Data will be made available on request.

Acknowledgements:

We are grateful to The Department of Biotechnology, Jadavpur University and CRNN, University of Calcutta for their support.

Appendix A. Supplementary material

Supplementary data to this article can be found online at https://doi.org/10.1016/j.eurpolymj.2022.111608.

References:

[1] R. Boni, A. Ali, A. Shavandi, N.A. Clarkson, Current and novel polymeric biomaterials for neural tissue engineering, J. Biomed. Sci., 25 (90) (2018). 10.1186/s12929-018-0491-8.
[2] S. Ramakrishna, J. Mayer, E. Wintermantel, K.W. Leong, Biomedical applications of polymer-composite materials: a review, Compos. Sci. Technol., 61 (9) (2001). pp. 1189-1224. 10.1016/S0266-3538(00)00241-4.
[3] L.S. Nair, C.T. Laurencin, Biodegradable polymers as biomaterials, Prog. Polym. Sci., 32 (8–9) (2007). Pp. 762-798. 10.1016/j.progpolymsci.2007.05.017.
[4] J.H. Hamman, Chitosan based polyelectrolyte complexes as potential carrier materials in drug delivery systems, Mar. Drugs, 8 (4), (2010). pp. 1305-22. 10.3390/md8041305.
[5] R. Mohammadinejad, H. Maleki, E. Larraneta, A. R. Fajardo, A.B. Nik, A. Shavandi, A.Sheikhi, M. Ghorbanpour, M. Farokhi, P. Govindh, E. Cabane, S. Azizi, A.R. Aref, M. Mozafari, M. Mehrali, S. Thomas, J.F. Mano, Y.K. Mishra, V.K. Thakur, Status and future scope of plant-based green hydrogels in biomedical engineering, Appl. Mater. Today, 16, (2019) pp. 213-246. 10.1016/j.apmt.2019.04.010.
[6] Y. Luo, Q. Wang, Recent development of chitosan-based polyelectrolyte complexes with natural polysaccharides for drug delivery. Int. J. Biol. Macromol., 64, (2014). pp. 353-367. 10.1016/j.ijbiomac.2013.12.017.
[7] C.N. Cheaburu, O.N. Ciocoiu, G. Staikos, C. Vasile, Thermoresponsive Sodium Alginate-g-Poly (N-Isopropylacrylamide) Copolymers III. Solution Properties, J. Appl. Polym. Sci., 127 (5) (2013). pp. 3340-3348. 10.1002/app.37789.
[8] M.G. Sankalia, R.C. Mashru, J.M. Sankalia, V.B. Sutariya, Reversed chitosan-alginate polyelectrolyte complex for stability improvement of alpha-amylase: Optimization and physicochemical characterization, Eur. J. Pharmaceut. Biopharmaceut., 65 (2) (2007). pp. 215–232. 10.1016/j.ejpb.2006.07.014.
[9] C.E. Beneke, A.M. Viljoen, J.H. Hamman, Polymeric plant-derived excipients in drug delivery, Molecules 14(7) (2009) pp. 2602–2620. 10.3390/molecules14072602.
[10] M.R.P. Rao, D.U. Warrier, S.R. Gaikwad, P.M. Shevate. Phosphorylation of psyllium seed polysaccharide and its characterization, Int. J. Biol. Macromol., 85 (2016). pp. 317-326. 10.1016/j.ijbiomac.2015.12.043.
[11] J.N. Bemiller, R.L. Whistler, D.G. Barkalow, C.C Chen, Aloe, chia, flaxseed, okra, psyllium seed, quince seed, and tamarind gums, Industrial Gums 9 (Third Edition), (1993). pp. 227-256. 10.1016/B978-0-08-092654-4.50013-9.
[12] D. Kumar, J.Pandey, P.Kumar, V. Raj, Psyllium Mucilage and Its Use in Pharmaceutical Field: An Overview, Curr. Synth. Syst. Biol., 5 (1), (2017). 10.4172/2332-0737.1000134.

[13] B. Singh, Psyllium as therapeutic and drug delivery agent, Int. J. Pharmaceut., 334 (1-2),(2007).pp. 1-14. 10.1016/j.ijpharm.2007.01.028.
[14] T.B. Qaisrani, M.M. Qaisrani, T.M. Qaisrani, Arabinoxylans from psyllium husk: A review 2016, J. Environ. Agric. Sci., 6(2016). pp. 33-39.
[15] M. Ahuja, M. Bhatia, K. Saini, Sodium alginate–arabinoxylan composite microbeads: preparation and characterization, J. Pharmaceut. Invest., 46 (2016). pp. 645-653. 10.1007/s40005-016-0244-1.
[16] A. Ali, S. Ahmed. A review on chitosan and its nanocomposites in drug delivery, Int. J. Biol. Macromol., 109 (2018). pp. 273-286. 10.1016/j.ijbiomac.2017.12.078.
[17] A. Desai, S. Shidhaye, V.J. Kadam, Possible Use of Psyllium Husk as a Release Retardant, Indian J. Pharmaceut. Sci. 69 (2), (2007) pp. 206-210. 10.4103/0250-474X.33144.
[18] S. Darakhshan, P.A. Bidmeshki, C.A. Hosseinzadeh, S. Sisakhtnezhad, Thymoquinone and its therapeutic potentials, Pharmacol. Res., Volumes 95–96, 2015, Pages 138-158, ISSN 1043-6618, 10.1016/j.phrs.2015.03.011.
[19] K.Y. Mahmoud, H.M.A. Abdelrazek, Cancer: Thymoquinone antioxidant/pro-oxidant effect as potential anticancer remedy, Biomed. Pharmacother., 115, 2019, pp. 108783. 10.1016/j.biopha.2019.108783.
[20] S. Das, D. Bera, K. Pal, P. Karmakar, S. Das, A. Dey, Guar gum micro-vehicle mediated delivery strategy and synergistic activity of thymoquinone and piperine: An in vitro study on bacterial and hepatocellular carcinoma cells, J. Drug Deliv. Sci. Technol., 60 (2020) pp. 101994. 10.1016/j.jddst.2020.101994.
[21] A.A.M. Neto, R.D.C. Bergamasco, F.F.D. Moraes, A.M. Neto, R.M. Peralta, Development of a technique for psyllium husk mucilage purification with simultaneous microencapsulation of curcumin, PLoS One, 12 (8), (2017). pp. e0182948. 10.1371/journal.pone.0182948.
[22] S. Banerjee, B. Bagchi, S. Bhandary, A. Kool, N.A. Hoque, P. Biswas, K. Pal, P. Thakur, K. Das, P. Karmakar, S. Das, Antimicrobial and biocompatible fluorescent hydroxyapatite-chitosan nanocomposite films for biomedical applications, Colloids and Surfaces B: Biointerfaces. 171 (2018). pp. 300-307. 10.1016/j.colsurfb.2018.07.028.
[23] B. Bagchi, S. Dey, S. Bhandary, S. Das, A. Bhattacharya, R. Basu, P. Nandy. Antimicrobial efficacy and biocompatibility study of copper nanoparticle adsorbed mullite aggregates, Mater. Sci. Eng.: C, 32 (7), (2012). pp. 1897-1905. 10.1016/j.msec.2012.05.011.
[24] K. Sawamura, Bacterial and H2O2 stress-induced apoptosis-like events in Cryptococcus neoformans. Res. Microbiol. 2008 Nov-Dec;159(9-10):628-34. 10.1016/j.resmic.2008.07.006. Epub 2008 Aug 29. PMID: 18793720.
[25] Y. Wang, Q. Luo, L. Gao, C. Gao, H. Du, G. Zha, X. Li, Z. Shen, W. Zhu, A Facile Strategy to Prepare Redox-Responsive Amphiphilic PEGylated Prodrug with High Drug Loading Content and Low Critical Micelle Concentration, Biomater. Sci., 2 (10), (2014). pp. 1367-1376. 10.1039/C4BM00065J.
[26] J.V. Meerloo, G.J.L. Kaspers, J. Cloos, Cell sensitivity assays: the MTT assay, Cancer Cell Culture: Methods Mol. Biol., 731, (2011). pp. 237-2045. 10.1007/978-1-61779-080-5_20.
[27] D. Wu, P. Yotnda, Production and detection of reactive oxygen species (ROS) in cancers, J. Visual. Exp., (57) (2011). pp. e3357. 10.3791/3357.
[28] S. Kalita, J. Kotoky, D. Chowdhury, Chitosan-Iron Oxide Coated Graphene Oxide Nanocomposite Hydrogel: A Robust and Soft Antimicrobial Biofilm. ACS Appl. Mater. Interfaces. 2016 Aug 17;8(32):20625-34. 10.1021/acsami.6b07510. Epub 2016 Aug 2. PMID: 27438339.
[29] M. Bhatia, M. Ahuja, Thiol modification of psyllium husk mucilage and evaluation of its mucoadhesive applications. Scient. World J., 2013 (284182), (2013). pp. 284182. 10.1155/2013/284182.
[30] M.P. Devi, M. Sekar, M. Chamundeswari, A. Moorthy, G. Krithiga, N.S. Murugan, T. P. Sastry, A novel wound dressing material-fibrin–chitosan–sodium alginate composite sheet, Bull. Mater. Sci., 35 (7), (2012). pp. 1157-1163. 10.1007/s12034-012-0404-5.
[31] Helmiyati et al. M. Aprilliza, Characterization and properties of sodium alginate from brown algae used as an ecofriendly superabsorbent, IOP Publish. IOP Conf. Series: Mater. Sci. Eng. 188 (2017) 012019 10.1088/1757-899X/188/1/012019.
[32] R. Surekha, T. Sumathi, An Efficient Encapsulation of Thymoquinone Using Solid Lipid Nanoparticle for Brain Targeted Drug Delivery: Physicochemical Characterization, Pharmacokinetics and Bio-Distribution Studies, Int. J. Pharmaceut. Clin. Res., 8 (12), (2016) pp. 1616-1624.
[33] D. Kulig, A. Zimoch-Korzycka, A. Jarmoluk, K. Marycz, Study on Alginate˙Chitosan Complex Formed with Different Polymers Ratio, Polymers (Basel). 8 (5) (2016) 167, https://doi.org/10.3390/polym8050167. PMID: 30979272; PMCID: PMC6432350.
[34] T. Yan, B.L. Feringa, K. Barta, Iron catalysed direct alkylation of amines with alcohols, Nat. Commun. 26 (5) (2014) 5602, https://doi.org/10.1038/ncomms6602. PMID: 25424885.
[35] S. Bates, G. Zografi, D. Engers, M. Kenneth, K. Crowley, A. Newman, Analysis of Amorphous and Nanocrystalline Solids from Their X-Ray Diffraction Patterns, Pharm. Res., 23, (2006). pp. 2333-2349. 10.1007/s11095-006-9086-2.
[36] S. Kumar, J. Koh, Physiochemical, Optical and Biological Activity of Chitosan-Chromone Derivative for Biomedical Applications, Int. J. Mol. Sci. 13 (5), (2012) pp. 6102-6116. 10.3390/ijms13056102.
[37] A.H. Gedam, R.S. Dongre, Adsorption characterization of Pb (II) ions onto iodate doped chitosan composite: equilibrium and kinetic studies. RSC Adv., 5 (67), (2015). pp. 54188-54201. 10.1039/c5ra09899h.
[38] A. Salisu, M.M. Sanagi, A.A. Naim, K.J.A. Karim, W.A.W. Ibrahim, U. Abdulganiyu, Alginate graft polyacrylonitrile beads for the removal of lead from aqueous solutions. Polym. Bull., 73 (2), (2016). pp. 519-537. 10.1007/s00289-015-1504-3.
[39] M.J.M. Salmani, S. Asghar, L. Huixia, J. Zhou, Aqueous Solubility and Degradation Kinetics of the Phytochemical Anticancer Thymoquinone; Probing the Effects of Solvents, pH and Light, Molecules, 19 (5), (2014), pp. 5925-5939. 10.3390/molecules19055925.
[40] M. Kong, X.G. Chen, K. Xing, H.J. Park, Antimicrobial Properties of Chitosan and Mode of Action: A State of the Art Review, Int. J. Food Microbiol., 144 (1), (2010) pp. 51-63. 10.1016/j.ijfoodmicro.2010.09.012.
[41] M. Brynildsen, J.A. Winkler, C.S. Spina, C. MacDonald, J.J. Collins, Potentiating antibacterial activity by predictably enhancing endogenous microbial ROS production. Nat. Biotechnol., 31, (2013). pp. 160-165. 10.1038/nbt.2458.
[42] C.C. Elisa, T.S. Jordi, R.S. Joaquim, Oxidative stress in bacteria and protein damage by reactive oxygen species, Int. Microbiol., 3 (1), (2000). pp. 3-8. http://hdl.handle.net/10459.1/56751.
[43] K. Chaieb, B. Kouidhi, H. Jrah, K. Mahdouani, A. Bakhrouf. Antibacterial activity of Thymoquinone, an active principle of Nigella sativa and its potency to prevent bacterial biofilm formation, BMC Complement. Alternat. Med., 11 (29), (2011). 10.1186/1472-6882-11-29.

Journal of Drug Delivery Science and Technology 60 (2020) 101994

Contents lists available at ScienceDirect

Journal of Drug Delivery Science and Technology

journal homepage: www.elsevier.com/locate/jddst

Research paper

Guar gum micro-vehicle mediated delivery strategy and synergistic activity of thymoquinone and piperine: An in vitro study on bacterial and hepatocellular carcinoma cells

Sanghita Das [a,b], Debbethi Bera [a,c], Kunal Pal [d,e], Dheeraj Mondal [a], Parimal Karmakar [d], Sukhen Das [a], Anindita Dey [b,*]

[a] Department of Physics, Jadavpur University, Kolkata, 700032, India
[b] Department of Botany, Asutosh College, Kolkata, 700026, India
[c] Centre for Interdisciplinary Research and Education, 404B, Jodhpur Park, Kolkata, 700068, India
[d] Department of Life Science and Biotechnology, Jadavpur University, Kolkata, 700032, India
[e] Division of Molecular Medicine and Centre for Translational Research, Bose Institute, Kolkata, 700056, India

ARTICLE INFO

Keywords:
Thymoquinone
Piperine
Guar gum micro-vehicle
Biopolymer
Antibacterial activity
Anticancer activity

ABSTRACT

This study reports the observed synergy in antimicrobial and anticancer activity of thymoquinone and piperine, encapsulated in porous guar gum micro-vehicle. Natural therapeutics like piperine and thymoquinone showed less effectivity in human medical trials due to their hydrophobicity leading to poor clinical efficacy. To overcome this problem, we have developed a delivery strategy by using guar gum, a natural biodegradable biopolymer. The successful encapsulation of phytochemicals and the microstructures of gum micro-vehicles were confirmed by Fourier transform infrared spectroscopy (FTIR), x-ray diffraction (XRD), Field emission scanning electron microscopy (FESEM) and UV–Vis spectra analysis. We also report here a significant decrease in minimum inhibitory concentration (MIC) value and synergistic bactericidal activity against four different bacterial strains and observed remarkably low median lethal dose (LD50) value against human hepatocellular carcinoma cell lines along with pH-responsive delivery of therapeutic in the case of combinatorial therapy. In our overall study, we analyze and discuss the structure, efficacy, and delivery of our designed natural therapeutic amalgamation to pave the way for augmenting the use of phytochemicals in medical applications.

1. Introduction

Natural therapeutic components have been very much popular in revolutionizing different antimicrobial, anti-inflammatory, and anticancer treatments because of their effective outcomes and almost no side effects [1–6]. Pathogens have acquired varied mechanisms to combat the currently available conventional antibiotics and expand as multi-drug therapeutics resistant forms [7]. Therefore, combinational therapy of these phytochemicals can be an intelligent therapeutic strategy in the field of applied and therapeutic sciences [8,9]. Thymoquinone (IUPAC name: 2-isopropyl-5-methyl 1,4-benzoquinone), a major bioactive component of *Nigella sativa, a* plant of Ranunculaceae family is also known as black cumin (kala jeera) [10]. Piperine is extracted as a bioactive amide alkaloid constituent from *the Piper nigram* plant of the Piperaceae family [11]. Thymoquinone and piperine exhibit potent activity against a wide range of microorganisms and play an important subject in the fields of antimicrobial treatment like other therapeutic modalities [11,12]. The present experiment was aimed to study the synergistic combinational therapeutic potency of thymoquinone and piperine and their biomedical application. Studies revealed that the mode of action of a single antimicrobial drug differs from that of the same drugs when applied in combination with others [13].

It has been reported that thymoquinone possesses hepatoprotective, antidiabetic, antifungal, anticancer, and neuroprotective properties [10,14,15]. It is well established that the functional mechanism of thymoquinone is to alter the biochemical reactions associated with the reactive oxygen species (ROS) generation [10]. Cellular In vivo studies revealed that thymoquinone induces activities of certain antioxidant enzymes glutathione transferase, superoxide dismutase (SOD), quinone reductase, glutathione (GSH). Thus, thymoquinone has a potent antioxidant

* Corresponding author.
E-mail address: sunimondal@yahoo.com (A. Dey).

https://doi.org/10.1016/j.jddst.2020.101994
Received 23 June 2020; Received in revised form 21 July 2020; Accepted 31 July 2020
Available online 14 August 2020
1773-2247/

property by inhibiting lipid peroxidation and preventing the generation of ROS [10,16]. Therefore, thymoquinone exerts a dual function, both antioxidant and pro-oxidant. Piperine is used as a remedy to cure inflammation, diarrhea, fungal infections, etc. The IUPAC name of piperine ($C_{17}H_{19}NO_3$) is 1-(5-[1,3-benzodioxol-5-yl]-1-oxo-2,4-pentadienyl) piperidine which is bestowed with extensive pharmacological outputs including analgesic activity, antithyroid activity, antimutagenic activity, antimetastatic activity, hepatoprotective, diuretic and anti-asthmatic activity, etc. [17,18]. The important phytochemicals present in piperine are some flavonoids and phenolic contents that inhibit reactive oxygen species, lipid peroxidation, and free radicals [19].

Despite all these promising biomedical properties, the application of thymoquinone and piperine is arrested due to several difficulties [20–22]. These two natural therapeutics have been proven to be lipophilic, thus very poorly soluble in aqueous media, restricting its therapeutic and biomedical applications [21–23]. This hydrophobic nature causes hindrance in the effective formulation may lead to unstable end products. Generally, hydrophobic components with poor bioavailability result in lowering the amounts of therapeutics in the target site when used in clinical trials [13,24]. To increase the stability of drugs, it can be encapsulated within a biopolymeric carrier system which is capable of delivering the therapeutics to the target cells effectively [25–29]. One of the most stable carrier protocols, used to encapsulate both hydrophilic and hydrophobic agents, is micro or nano-particle [30–33]. In our study, we used guar gum micro-vehicle loaded with piperine and thymoquinone individually and in combination. Guar gum, a natural hydrophilic nonionic polysaccharide derived from the seeds of *Cymompsis tetraganolobus* of the Leguminaceae family [34]. Micro-vehicles formed of biopolymers have long been employed as vehicles in natural therapeutic delivery due to their unique non-toxic, non-immunogenic, biocompatible, biodegradable, and rapid hydration properties [35,36]. Due to very high molecular weight, which ranges from 200,000–300,000 Da, guar gum can form highly viscous aqueous colloidal dispersion even in cold water [34,37]. The guar galactomannan has a distinctive character of imbibing a large quantity of water which makes a highly viscous solution of guar polysaccharide [36,38]. Being a natural polymer guar gum is appealing for use in natural therapeutic delivery because of its biocompatibility, nontoxicity, and biodegradability [39].

Our present experiments with the combinations of natural therapeutics lead to damage in bacterial cell wall integration which might have caused due to excessive ROS generation or altered signaling pathway results in improper cell wall synthesis in both Gram + ve and Gram − ve bacterial strains. Thymoquinone and piperine have an impact on altered cellular metabolism inhibiting proliferation and metastasis of cancer cells. Reactive oxygen species (ROS) generation plays a crucial role in the maintenance of the redox balance in most cancer cells and an elevated ROS level may promote oxidative damage leading to cellular abnormalities or death [40]. Thymoquinone had been proven to induce cell apoptosis by increasing caspase-3 activity [41]. Caspases are one type of protease enzymes that amplify the apoptotic signaling pathway which results in cell death due to their proteolytic activity [42,43]. Induced by some initiator caspases (caspase-8, caspase-9, or caspase-10), caspase-3 mediates fragmentation of DNA within the nuclei and cytoskeletal protein degradation [44]. It has been postulated that in anticancer treatment, the activity of some drugs and bioactive compounds is enhanced by the use of piperine [45,46]. Plant-derived bio--enhancers are responsible for enhancing the efficiency of some drugs having less bio-availability or in the case of long-term drug administration [46]. In the current study, we investigated the combinatorial effect of thymoquinone and piperine on bacterial cells as well as HepG2 cells.

Here we have studied the effect of thymoquinone (TQ) and piperine (PIP) loaded guar gum micro-vehicle (GG) on the prokaryotic and eukaryotic systems. The guar gum capped TQ and PIP (GG-PIP-TQ) has a promising synergistic effect against Gram + ve (*E.faecalis, S. aureus*) and Gram −ve (*P.aeruginosa, E. coli*) pathogenic bacterial species. In this study, we investigated the antimicrobial as well as anticancer activities of these two therapeutics against human hepatocellular carcinoma cell lines. Thus, the development of these natural therapeutics has the potential to emerge as an effective dual therapeutic agent.

2. Experimental details

2.1. Materials

TQ and PIP were procured from Sigma-Aldrich (Switzerland). Guar gum was obtained from Hi-Media chemicals. All other reagents including fluorescence stains, MTT reagent, glutaraldehyde were purchased from Merck Ltd. and SRL Pvt. Lt. (India). Deionized (Millipore) water of 18 MΩ-cm was used in all experiments. For antibacterial experiments, all therapeutics loaded gum micro-vehicles were sterilized under UV radiation.

2.2. Microbial cultures

In this study, the antibacterial property of our designed natural therapeutics was tested on four pathogenic bacterial strains. These are Gram + ve (*Staphylococcus aureus*740 and *Enterococcus faecalis*441) and Gram−ve (*Escherichia coli* 443 and *Pseudomonas aeruginosa* 1688) obtained from Microbial Type Culture Collection, IMTECH (Chandigarh, India).

2.3. HepG2 cell lines

Human hepatocellular carcinoma cell lines (HepG2) were obtained from National Center for Cell Science (NCCS) Pune, India. These cells were allowed to grow in DMEM/RPMI 1640 with 10% Fetal Bovine Serum, penicillin/streptomycin (100 units/ml), amphotericin-B (antifungal) at 37 °C and 5% $C0_2$ respectively. All the treatments were performed with their respective LD_{50} doses. All the experiments were done at 37 °C allowing to grow exponentially.

2.4. Synthesis

2.4.1. Preparation of GG

GG was carried out by a simple procedure in aqueous media. Initially, powdered GG was dissolved in lukewarm Millipore water and was vigorously stirred for 24 h. The solution became thick after the complete dissolution of the gum which was then dried in a desiccator at 60 °C temperature. The dried sample was then collected and after cooling mortared for finer grains. The sample was then named as GG and sent for characterizations.

2.4.2. Synthesis of TQ/PIP loaded GG

First, GG was dissolved in lukewarm Millipore water allowed for stirring under vigorous stirring conditions for about 24 h. TQ was measured and added to gum solutions and was allowed to stir for 24 h. The obtained sample was centrifuged at 10,000 rpm for about 10 min and washed three times. These solutions were then dried at 60 °C in a vacuum desiccator. Finally, the dried sample was mortared in an agate mortar to obtain finer grains. The same procedure was followed to prepare PIP tagged gum vehicle. Finally, we got GG-TQ, GG-PIP for further characterizations. We combined GG with TQ/PIP in different ratios, but the best solubility as well as the best results were observed in the ratio of 6:4 which was carried by our overall study ignoring other ratios.

2.4.3. Synthesis of both TQ-PIP loaded GG

The same procedure was followed except that TQ and PIP both were added to the GG solution randomly in different ratios. Since solubility in water is regarded as an important criterion of biological samples, the

solubility of all the samples was measured in water. The results suggested that the ratio of 6:2:2 showed the best solubility in water. Hence this ratio was chosen and the sample was named as GG-PIP-TQ.

2.5. Characterization

The interactions between GG and bioactive therapeutics were studied by Fourier transform infrared spectroscopy (FTIR), FTIR-8400S, Shimadzu, Tokyo in the wavenumber range from 400 cm^{-1} to 4000 cm^{-1}, x-ray diffraction (XRD) spectra by using x-ray diffractometer model-D8 Bruker AXS (Wisconsin, USA) employing Cu-Kα radiation. Field emission scanning electron microscope (FESEM) was conducted for the surface texture study of our therapeutics as well as bacterial strains employing INSPECT F50 (FEI, the Netherland) and EVO 18 Special edition, Carl Zeiss (Germany). The UV visible spectrophotometer (Epoch microplate reader, BioTek, USA) was used to estimate the absorbance intensity of solubilized MTT formazan product and the natural therapeutics after being dispersed completely in MilliQ water. The average particle diameter and the zeta potential of samples were measured by Zetasizer (NANO ZS90, Malvern Instruments Ltd, UK). Epoch Microplate Spectrophotometer, USA was used in natural therapeutics release study. During the ROS estimation spectroscope (Hitachi, Japan) and fluorescence microscope (DM 2500, Leica, Germany) were used. GSH-Glo™ is used to record the experimental data. Glutathione Assay kit (Promega) for GSH measurement and Amplite™ Fluorometric NADPH Assay kit (Advancing Assay & Test technologies [AAT] Bioquest, USA) for NADPH measurement with the aid of Microplate reader (BioTek) were used. All suspensions were prepared by using an ultrasonic bath sonicator. All bacterial and cellular examinations were methodically done in a biosafety cabinet.

2.6. Antibacterial activity assessment

2.6.1. MIC and MBC

The microdilution method was chosen to assess the minimum inhibitory concentration (MIC) and minimum bactericidal concentration (MBC) values [47]. Different concentrations (50 μg/ml, 100 μg/ml, 200 μg/ml, 400 μg/ml, 600 μg/ml) of our synthesized natural therapeutics were added to 1 ml nutrient broths containing 10 μl of bacterial culture (2.5×10^5 CFU/ml bacteria) and were incubated for 24 h at 37 °C in an incubator shaker. The MIC was performed by measuring the turbidity of bacterial growth, which implies nearly 99% growth inhibition. Each experiment was done thrice. The MBC was measured using the MIC dilutions of bacterial cultures and incubated for 24 h at a temperature of 37 °C. MBC value signifies the lowest concentration of synthesized therapeutics required for the complete killing of the bacteria.

The tolerance levels of each bacterial strain against TQ and PIP loaded GG were determined by MBC and MIC values of our experiments. Tolerance level (MBC)/(MIC) gives a clear indication of the antimicrobial activity of our natural therapeutics loaded gum [48].

2.6.2. Agar well diffusion method

The antimicrobial activities of GG-TQ, GG-PIP, GG-PIP-TQ were also measured by using the agar well diffusion method. Antibacterial activity against four pathogenic bacterial strains was measured by adding each GG, GG-PIP, GG-TQ, GG-PIP-TQ at their respective MBC concentration into the wells separately for comparative study and left them to grow on the Mueller Hinton agar overnight at a temperature of 37 °C. At the end of the incubation, the zone of inhibition surrounding the disc was measured and recorded [47,49].

2.6.3. Bacterial ROS estimation

To detect intracellular ROS generation 2, 7-dichlorofluorescein diacetate (DCFH2-DA) assay was used [50]. Bacterial cells were treated with different concentrations (50 μg/ml, 100 μg/ml, 200 μg/ml, 400 μg/ml, 600 μg/ml) GG, GG-TQ, GG-PIP, GG-PIP-TQ and cultured for overnight. Afterward, the culture was washed by centrifugation at 5000 rpm for 5 min by using PBS solutions. Then the cells were allowed to incubate for 30 min with DCFH2-DA in the dark conditions at 37 °C. Finally, the images of bacteria cells were measured both spectroscopically and with a fluorescence microscope at excitation and emission wavelengths of 485 and 520 nm, respectively.

2.7. Evaluation of release of natural therapeutic

The natural therapeutics loading percentage within the polymeric GG was determined by calculating the concentration of the TQ by obtaining the absorbance of the solution using standard procedure. The absorbance of the bare micro-vehicle (GG) was considered as the baseline. The drug loading content (DLC) and drug loading efficiency (DLE) were determined by the following equations [51].

$$\text{DLC (\%)} = \{(\text{Weight of natural therapeutics encapsulated in micro-vehicles}/\text{Weight of micro-vehicles taken})\} \text{ X } 100 \quad (1)$$

$$\text{DLE (\%)} = \{(\text{Weight of natural therapeutics in micro-vehicles}) / (\text{Weight of natural therapeutics injected})\} \text{ X } 100 \quad (2)$$

To determine the amount of TQ discharged from the micro-vehicle in respect of time interval, in vitro TQ release was calculated. The cumulative natural therapeutics release study was carried out in physiological pH conditions (pH ~7.4) and intracellular pH conditions of cancer cells (pH ~ 5.5) at 37 °C. The percentage of TQ released at different time intervals was calculated from a standard curve of TQ by measuring the absorbance of the supernatant solution at 340 nm.

2.8. Anticancer activity assessment

2.8.1. MTT assay

The HepG2 cell viability was assayed with the help of the 3-(4, 5-dimethylthiazol-2-yl) −2, 5-diphenyltetrazolium bromide (MTT) assay following a standard protocol [50]. The cell viability was examined after exposure to GG, GG-TQ, GG-PIP, GG-PIP-TQ respectively at the concentrations of untreated as a control and 20 μg/ml, 40 μg/ml, 60 μg/ml, 80 μg/ml, 100 μg/ml. In this method, the absorbance of solubilized MTT formazan product was estimated by a UV–vis spectrophotometer at a wavelength of 570 nm.

2.8.2. ROS estimation

Reactive oxygen species are induced by some stressful conditions like exposure to different concentrations of therapeutics (40 μg/ml, 80 μg/ml, 100 μg/ml) which leads to oxidative stress. To monitor intracellular ROS generation in HepG2 cells DCFH2-DA assay was used.

2.8.3. NADPH and GSH assessment

In order to examine the intracellular antioxidant level in HepG2 cells on treatment with different concentrations (i.e. 20 μg/ml, 40 μg/ml, 60 μg/ml, 80 μg/ml, 100 μg/ml) of GG, GG-PIP, GG-TQ, GG-PIP-TQ the intracellular GSH and NADPH sensing luminescence was performed using standard protocols.

3. Results

3.1. Characterization of the micro-vehicle

The incorporation of natural therapeutics in the gum micro-vehicle was confirmed by XRD spectra are shown in Fig. 1a. The diffraction patterns of four samples (GG, GG-TQ, GG-PIP, GG-PIP-TQ) confirmed the incorporation of natural therapeutics in gum micro-vehicle. GG exhibited a broad hallow which indicates very small crystallinity while on GG-TQ also depicted low intensity broader peak revealing its incorporation into the polymer matrix in the amorphous state [52,53]. The

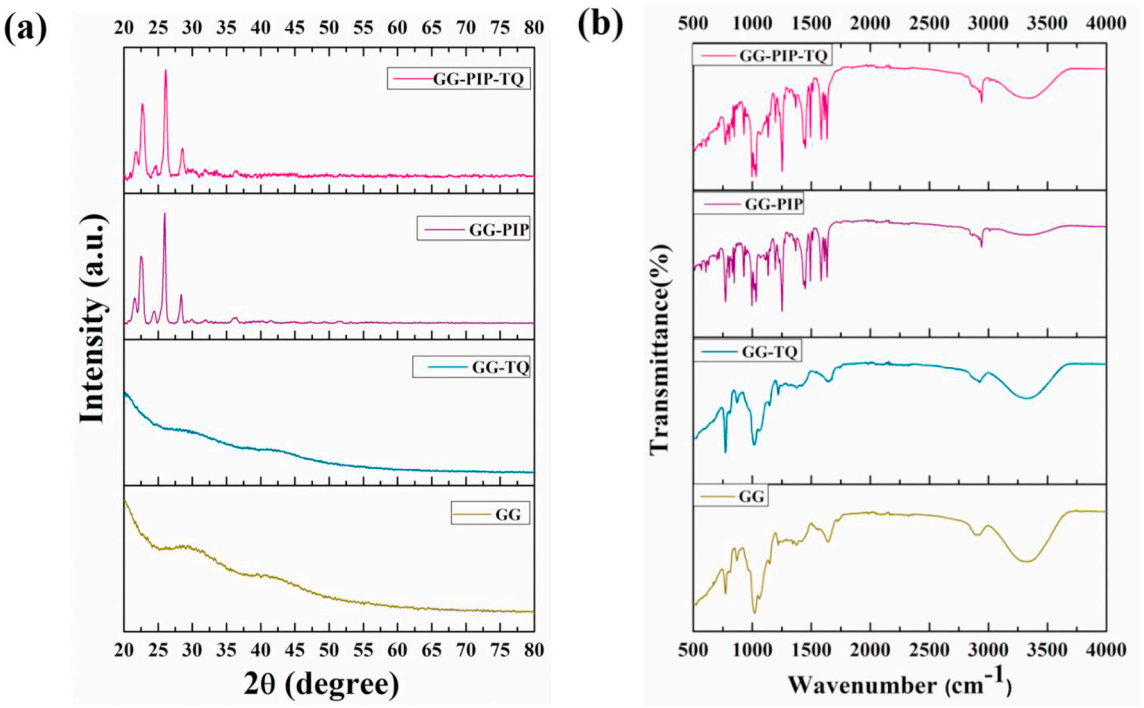

Fig. 1. Characterization of Guar Gum Micro-vehicles (a) XRD patterns of GG, GG-TQ, GG-PIP, GG-PIP-TQ, (b) FTIR analysis of GG, GG-TQ, GG-PIP, GG-PIP-TQ.

XRD pattern of GG-PIP, as well as GG-PIP-TQ, indicated the similarity with the typical pattern of PIP (JCPDS Card no: 00-043-1627) [54].

The FTIR spectrum (Fig. 1b) revealed GG absorption peak, spectra around 3328 cm^{-1} is due to O–H stretching vibration of water and gum (polymer) and 772 cm^{-1} is attributed to (1–4), (1–6) linkage of galactose and mannose respectively, the absorption bands at 2922 cm^{-1} (C–H stretching of CH_2group), 1644 cm^{-1} (ring stretching of mannose) and 1020 cm^{-1} (-CH_2 twisting vibration) [52,55,56]. The presence of the characteristic peaks of TQ at about 1654 cm^{-1} (C══O stretch) and 1376 cm^{-1} (C–H methyl rock) established that TQ is successfully attached to the GG [57]. The presence of absorption peak due to aliphatic C–H stretching around 2942 cm^{-1} (GG-PIP) and 2942 cm^{-1} (GG-PIP-TQ) are attributed to the presence of PIP [20]. When we analyzed and compared the FTIR spectrum of GG-PIP, GG-TQ, and GG-PIP-TQ we found that they show similarities to their corresponding therapeutics indicating that they successfully attached to the polymer without any change of their chemical properties.

The optical behaviour of our formulated therapeutics was characterized by UV–vis spectroscopy stated in Fig. 2a [58]. UV–vis absorbance spectrum of GG, GG-PIP did not show any sharp peak in its spectrum due to its UV inactiveness whereas the GG-TQ, GG-PIP-TQ sample exhibited a prominent peak at 340 nm and 335 nm which ascertained the successful incorporation of TQ.

The surface morphology of GG and GG-PIP-TQ are determined by the FESEM study. Fig. 2b and c showed FESEM image of GG which indicated a discontinuous and irregular structure of gum micro-vehicles whereas a noticeable change is observed in the case of GG-PIP-TQ indicating a clear attachment of natural therapeutics (PIP and TQ) with GG which confirmed by the reduction of porosity of micro-vehicles.

GG-TIQ-PIP showed a zeta potential of 13.27 ± 4.4 mV (Table 1). TQ loading does not alter the zeta potential, but increases the hydrodynamic diameter. The presence of TQ inside the matrix also increases the size of the micro-vehicle than the bare ones. The corresponding polydispersity index (PDI) values of the samples are a quite low, suggesting that they form a homogenous solution that is desirable for any biological application.

3.2. Synergistic antibacterial activity of GG-PIP-TQ

MIC values were decreased in case of a combination between TQ and PIP against all four pathogenic bacterial strains which depicted in Table 2. To estimate an alternative way to combat bacterial pathogens and to minimize the adversity associated with the conventional antibiotics, PIP and TQ encapsulated GG were screened singly and in combination with each other to determine their synergistic, additive, or antagonist interactions against *S. aureus, P. aeruginosa, E. faecalis* and *E. coli* (Fig. 3). This decrease is more significant in the case of Gram + ve bacteria.

Tolerance is an important parameter which reflects the bactericidal capacity of natural therapeutics. For a particular bacterium, if the MBC/MIC ratio is greater than or equal to 16, the antibacterial agents are considered as a bacteriostatic type, and while less than or equal to 4, then are considered as a bactericidal agent. Table 2 stated that GG-PIP, GG-TQ, GG-PIP-TQ shows bactericidal activity. In a well diffusion study (Fig. 3e), GG-PIP-TQ exhibits synergistic bactericidal activity against all four pathogenic strains, especially against Gram + ve bacteria (*S.aureus, E. faecalis*).

Our study indicated the efficacy of GG-PIP-TQ which significantly increase intracellular ROS generation compared to GG-PIP and GG-TQ in the case of all the four pathogenic strains as shown in Fig. 4.

Scanning electron microscopy (SEM) detected ultrastructural morphological changes in bacteria as shown in Fig. 5. All untreated strains looked undamaged with a smooth and intact surface. GG-PIP-TQ treated bacterial cells become uneven and distorted. Perforated membranes indicate GG-PIP-TQ induced membrane damage.

3.3. A pH-responsive release of natural therapeutic from GG

The natural therapeutic release profile showed in Fig. 6 stated that in GG, DLC and DEE are 58% and 79%, respectively. The high natural therapeutics loading content is due to the extensive large surface area of the micro-vehicle. Approximately 28% and 34% TQ release was observed from GG-TQ after 12 h and 24 h, respectively at pH 7.4. This controlled release of natural therapeutics is very much effective to

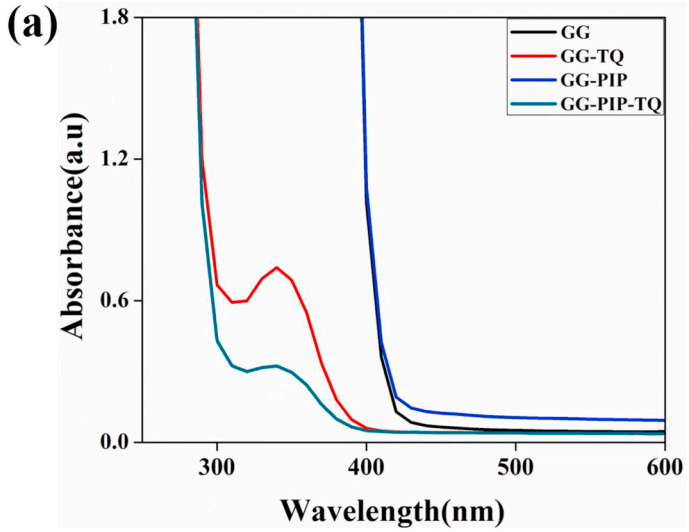

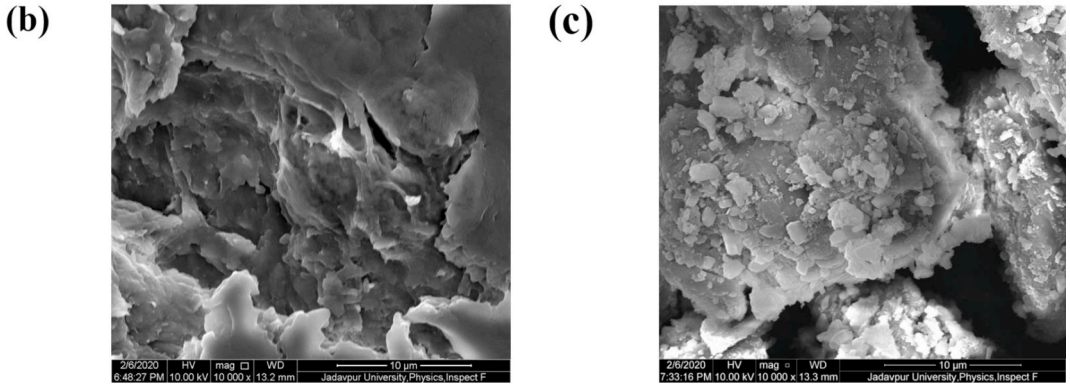

Fig. 2. (a) UV–Vis spectra of GG, GG-TQ, GG-PIP, GG-PIP-TQ, FESEM analysis of (b) GG and (c) GG-PIP-TQ.

Table 1
Represents the DLS and Zeta potential of the samples.

SAMPLE	DLS SIZE (d.nm)	P.D.I	Zeta potential
GG	176 ± 3.4	0.16	12.34 ± 2.8
GG-PIP	197 ± 3.8	0.24	14.54 ± 1.4
GG-TQ	204 ± 2.2	0.27	11.34 ± 2.4
GG-PIP-TQ	215 ± 2.5	0.29	13.27 ± 4.4

combat the problem of rapid elimination from the system as well as an increase in therapeutic efficiency [59]. On the other hand, in the case of pH 5.5, the corresponding release was 44% and 58% respectively.

3.4. Remarkable anticancer activity observed in HepG2 cell lines

3.4.1. Cytotoxicity study

In-vitro cytotoxicity of the therapeutics is evaluated for determining the cytotoxic effects on HepG2 cell line. The cells were treated with various concentrations of GG, GG-TQ, GG-PIP, GG-PIP-TQ (0–100 μg/ml) for a time span of 24 h and were afterward followed by MTT assay. Fig. 7a exhibited that GG-PIP, GG-TQ, GG-PIP-TQ exerted a decrease in the cell survivability in a dose-dependent manner whereas bare GG showed no such activity. Table 3 stated the LD_{50} values against HepG2 cells.

3.4.2. ROS generation study

The generation of reactive oxygen species was evaluated in case of treatment of HepG2 with GG, GG-PIP, GG-TQ, GG-PIP-TQ at concentrations of 40 μg/ml, 80 μg/ml, 100 μg/ml for 12 h and was then incubated with DCFDA for 30 min. The treated cells were evaluated with

Table 2
Represents MIC, MBC and Tolerance level of bacterial strains against GG, GG-PIP, GG-TQ, GG-PIP-TQ.

BACTERIA	SAMPLE	MIC	MBC	TOLERANCE LEVEL
Pseudomonas aeruginosa	GG	–	–	–
	GG-PIP	331.55	1160.43	3.5
	GG-TQ	281.82	1018.55	3.61
	GG-PIP-TQ	259.37	907.8	3.5
Escherichia coli	GG	–	–	–
	GG-PIP	397.65	1391.76	3.5
	GG-TQ	309.66	1052.85	3.4
	GG-PIP-TQ	244.88	883.57	3.6
Enterococcus feacalis	GG	–	–	–
	GG-PIP	253.73	867.76	3.42
	GG-TQ	202.38	684.04	3.38
	GG-PIP-TQ	184.71	600.30	3.25
Staphylococcus aureus	GG	–	–	–
	GG-PIP	245.1	808.83	3.3
	GG-TQ	196.72	674.75	3.43
	GG-PIP-TQ	178.89	572.45	3.2

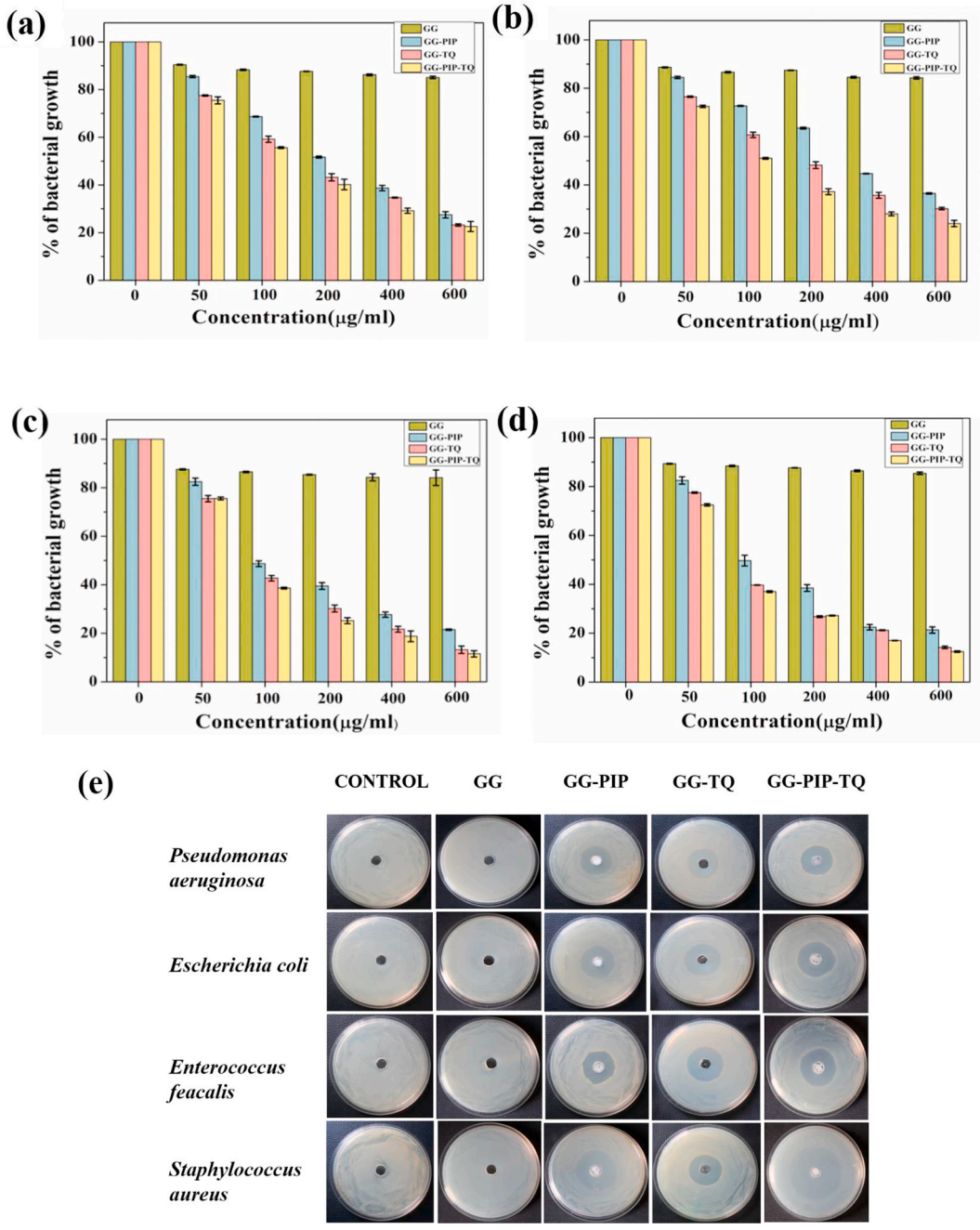

Fig. 3. (a)Analysis of activity of GG, GG-PIP, GG-TQ, GG-PIP-TQ by MIC method in *Pseudomonas aeruginosa* (b) *Escherichia coli* (c) *Enterococcus faecalis* (d) *Staphylococcus aureus*; (e) Well diffusion method indicating synergistic activity of GG-PIP-TQ.

the help of the UV–Vis spectrophotometer which stated in Fig. 7b. Furthermore, the fluorescence microscopic images clearly depicted the gradually enhanced green fluorescence intensity after 12 h when treated with a dose of 100 μg/ml (Fig. 7c).

3.4.3. NADPH and GSH level determination

In this experiment, the results (Fig. 8) exhibit a drastic dose-dependent diminish in the percentage of GSH and NADPH level on the exposure of HepG2 cells to GG-PIP, GG-TQ, GG-PIP-TQ treatment where treatment with GG showed no such decrease in GSH and NADH level while GG-PIP-TQ exhibited a maximum decrease.

4. Discussion

Several studies have been carried out to combat cancer progression and various infectious diseases without any detrimental side effects. In this regard, GG-PIP, GG-TQ, GG-PIP-TQ have been assessed on four bacterial strains which are capable of causing systemic infections in human as well as HepG2 cells. FTIR and XRD data clearly demonstrated efficient interaction as well as successful encapsulation of therapeutics. The solubility of hydrophobic TQ and PIP can be increased and optimum delivery can be achieved by an appropriate combination of GG. Encapsulation of gum by TQ and PIP cannot affect their antibacterial or anticancer property. Bare GG exhibited no such activity against bacterial and cancer cells which was established by ROS estimation studies. We observed a remarkable synergistic antibacterial activity by MIC, MBC,

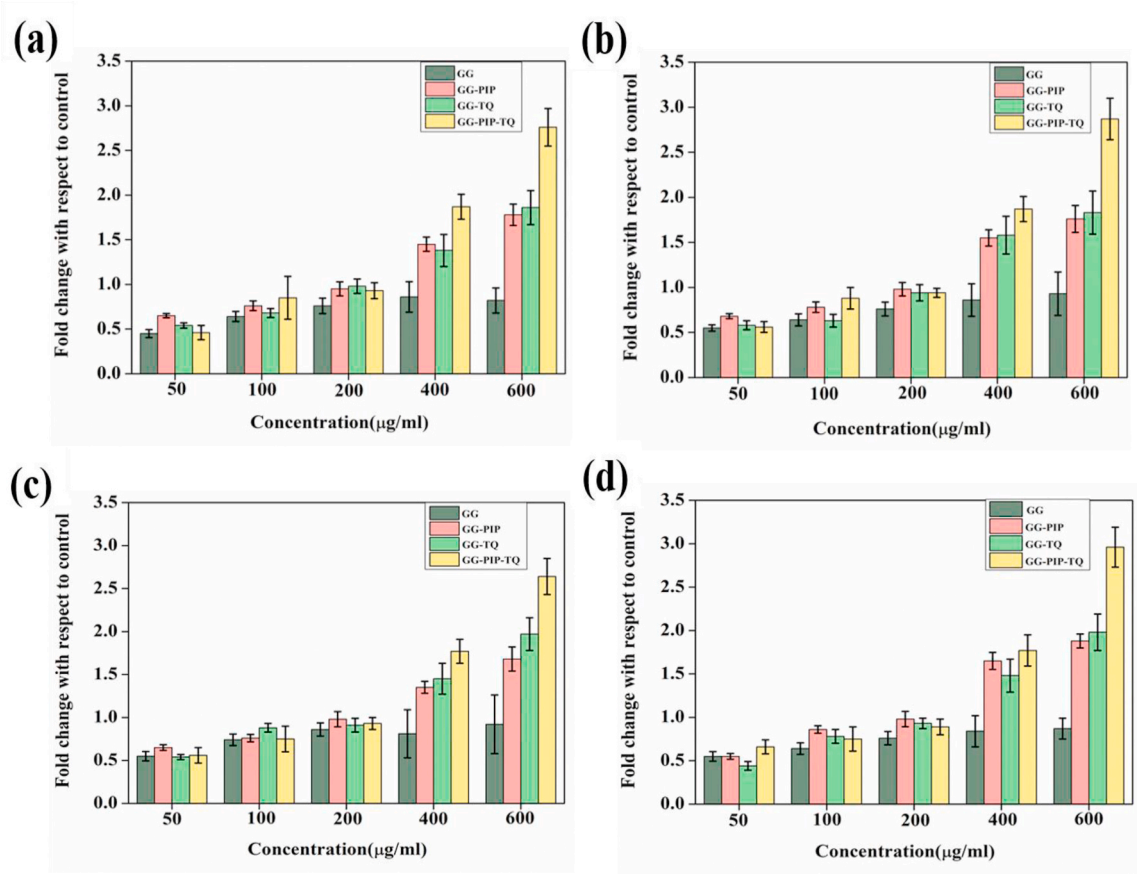

Fig. 4. Determination of bacterial ROS by DCFDA assay (a)*Pseudomonas aeruginosa* (b)*Escherichia coli* (c) *Enterococcus faecalis* (d)*Staphylococcus aureus*.

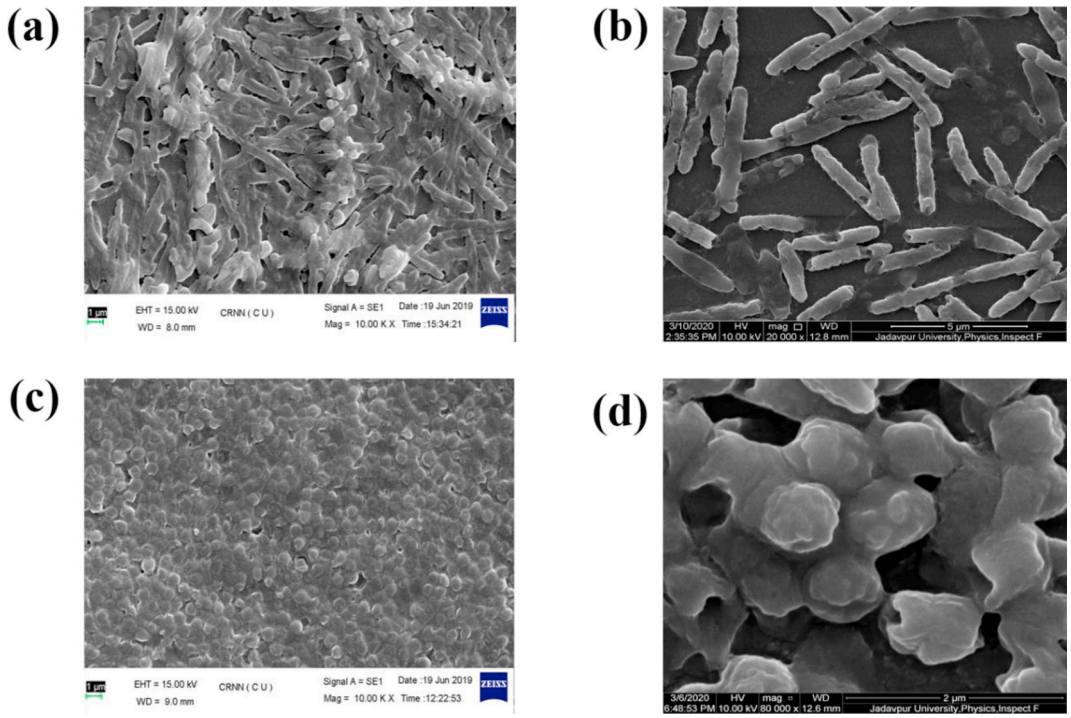

Fig. 5. FESEM micrographs showing morphological characteristics of (a) untreated *P. aeruginosa* cells, (b) *P. aeruginosa* cells after treatment with GG-PIP-TQ, (c) untreated *S. aureus* cells, (d) *S.aureus* cells after treatment with GG-PIP-TQ.

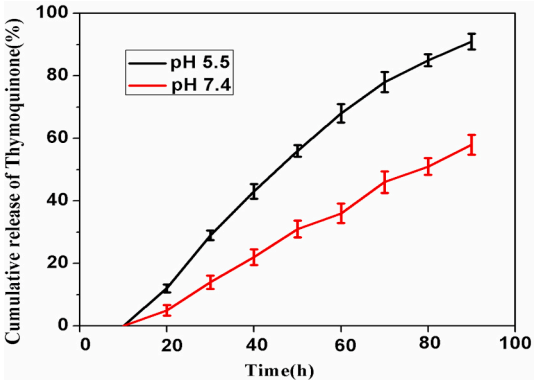

Fig. 6. Graphical representation of pH-responsive time-dependent release study of thymoquinone.

ager well diffusion and tolerance level study on four bacterial strains specially against Gram + ve bacteria. An effective permeability barrier of Gram -ve bacteria results in the restriction of proper penetration of bioactive phytochemicals through it. The tolerance level reflects the bactericidal capacity of natural therapeutics as obtained from MBC/MIC ratio which is less than 4. Increased level of bacterial ROS is may be due to the effective penetration of natural therapeutics into the bacterial cells that causes oxidative stress and acts as an ideal bactericidal agent following bacteriostatic activity.

Additionally, the pH-responsive release of natural therapeutic from porous GG suggested that the TQ release in intracellular acidic pH of cancer cell (~ 5.5) is faster than that of the normal physiological pH (~7.4). Previous study suggested that also at acidic pH guar gum could retain stability [60]. During the encapsulation of natural therapeutics within gum, they form a covalent linkage between them. The possible reason behind the faster release of therapeutic may be the breakage of the interlinking bonds at acidic pH, followed by the release of TQ gradually.

In case of HepG2 cells, increased ROS generation and cytotoxic activity observed in MTT assay suggested that the natural therapeutics loaded micro-vehicles could exert encouraging anticancer activity. The homeostasis of the ROS level is critically maintained inside the cell and solely regulated by intracellular antioxidant levels (NADPH and GSH) in mitochondria and cytosol [61]. Therefore, the elimination of NADPH and GSH levels leads to oxidative stress-mediated cell death [62]. Estimated ROS, GSH and NADPH content within the cells after treatment with GG-PIP, GG-TQ, GG-PIP-TQ indicated towards the synergistic activity of TQ and PIP. GSH and NADPH levels were significantly decreased when treated with GG-PIP-TQ indicating ROS liberation.

Both antibacterial and anticancer activities of GG-PIP-TQ implied that these two phytochemicals may activate each other's mode of action. Otherwise one of them followed a mechanism that enhanced the activity of the other natural therapeutics. The bio enhancing activity of PIP was proven to be effective in synergism assay [45]. The synergistic interaction between two drugs may lead to modified and more effective binding mechanism for the active site or it may result in delayed efflux of accumulated therapeutic complex out of the cell. Thus, combination of drugs often exerts their synergistic effect in a particular species of

Table 3
Represents LD_{50} values of GG, GG-PIP, GG-TQ, GG-PIP-TQ.

SAMPLE	LD_{50} VALUE
GG	–
GG-PIP	61.24
GG-TQ	59.46
GG-PIP-TQ	48.03

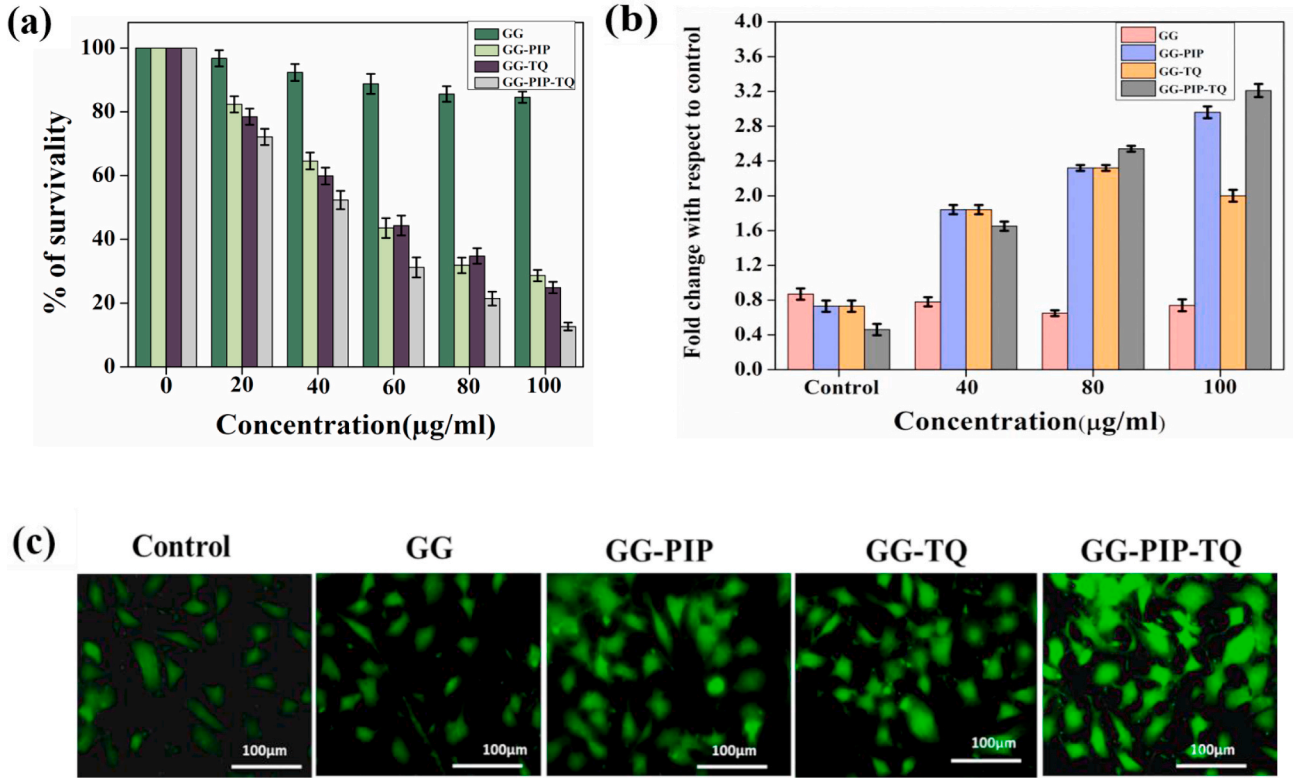

Fig. 7. (a) MTT assay on HepG2 cell line after treatment with GG, GG-PIP, GG-TQ, GG-PIP-TQ. (b)Graphical representation of mean fluorescent intensity for ROS generation in HepG2 cells (c)Fluorescence microscopic image of intracellular ROS generation for HepG2 cells control, treated with GG, GG-PIP, GG-TQ, GG-PIP-TQ at their respective LD_{50} dose measurement which indicates the enhancement of ROS.

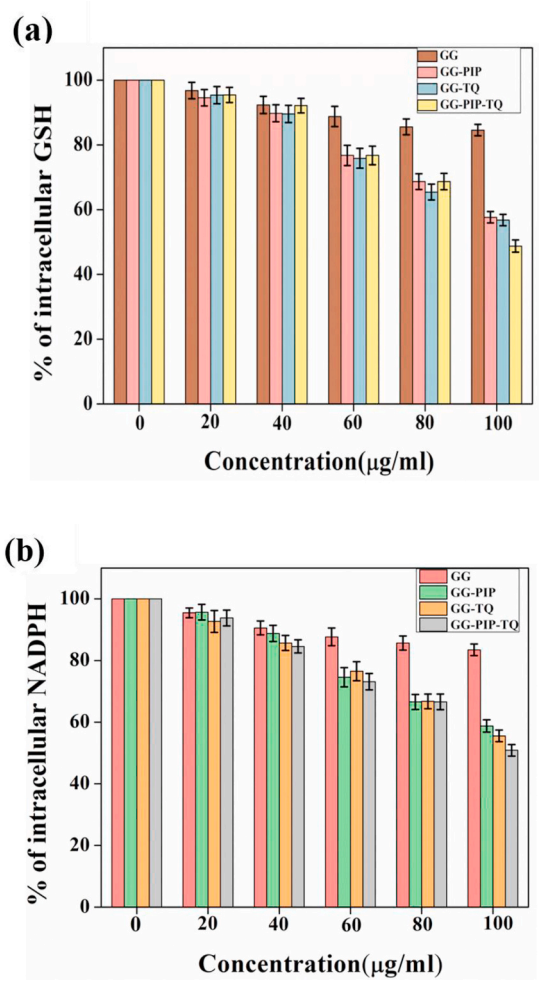

Fig. 8. (a)Graphical representation of Intracellular depletion of GSH after treatment with GG, GG-PIP, GG-TQ, GG-PIP-TQ. (b) Graphical representation of Intracellular NADPH level after treatment with GG, GG-PIP, GG-TQ, GG-PIP-TQ.

microorganisms either by inhibiting the cell wall synthesis or by triggering its lysis. By calculating the tolerance level of bacteria and the LD_{50} value in case of HepG2 cells, this new amalgamation of TQ and PIP with biopolymer GG suggested a remarkable synergistic effect.

5. Conclusion

Our study is aimed at using phytochemicals having potent antibacterial and anti-cancer properties individually or in combination. We used an inexpensive, abundantly available natural biopolymer and assembled TQ and PIP with this polymer for synergism assay, which overcomes the poor aqueous solubility of these natural bioactive compounds. Novel amalgamation with porous polymeric substances can improve the efficacy of natural therapeutic delivery as well as give a new perspective on polymeric technology. The pH-responsive release of TQ is advantageous for cancer therapy and also required for the survivability of normal healthy cells. The result of the study demonstrates that GG-PIP-TQ exerts more effect on Gram + ve than Gram −ve bacteria. Thus, the therapeutic application of our combined amalgamation can be a suitable alternative of conventional drugs to overcome the problem of side effects and antibiotic resistivity. In conclusion, we have established that the hydrophilic biocompatible GG-PIP-TQ can emerge as an ideal platform for multiple therapeutic applications.

Author's statement

The authors have approved the submission of the manuscript having the manuscript number of JDDST-D-20-00268 with all the corrections needed as per the reviewer's suggestion.

The authors have not submitted the article to any other journal for consideration.

Declaration of competing interest

The authors have no conflicts to declare.

Acknowledgements

The authors would like to thank to CRNN, University of Calcutta, India for their support. We are also grateful to Biplab Kumar Paul and Nur Amin Hoque for their expert suggestion.

References

[1] H.E. Thu, Z. Hussain, I.N. Mohamed, A.N. Shuid, Recent advances in antibacterial, antiprotozoal and antifungal trends of Eurycoma longifolia: a review of therapeutic implications and future prospects, Curr. Drug Targets 19 (14) (2018) 1657–1671, https://doi.org/10.2174/1389450119666180219123815.

[2] L.H. Chen, J.F. Xue, Z.Y. Zheng, M. Shuhaidi, H.E. Thu, Z. Hussain, Hyaluronic acid, an efficient biomacromolecule for treatment of inflammatory skin and joint diseases: a review of recent developments and critical appraisal of preclinical and clinical investigations, Int. J. Biol. Macromol. 116 (2018) 572–584, https://doi.org/10.1016/j.ijbiomac.2018.05.068.

[3] M.A. Tumpang, N.A. Ramli, Z. Hussain, Phytomedicines are efficient complementary therapies for the treatment of atopic dermatitis: a review of mechanistic insight and recent updates, Curr. Drug Targets 18 (15) (2017), https://doi.org/10.2174/1389450118666170913162147.

[4] F. Hussain, A. Malik, U. Ayyaz, H. Shafique, Z. Rana, Z. Hussain, Efficient hepatoprotective activity of cranberry extract against CCl4-induced hepatotoxicity in wistar albino rat model: down-regulation of liver enzymes and strong antioxidant activity, Asian Pacific J. Trop. Med. 10 (11) (2017) 1054–1058, https://doi.org/10.1016/j.apjtm.2017.10.008.

[5] S. Khan, M. Imran, T.T. Butt, S.W.A. Shah, M. Sohail, A. Malik, S. Das, H.E. Thu, A. Adam, Z. Hussain, Curcumin based nanomedicines as efficient nanoplatform for treatment of cancer: new developments in reversing cancer drug resistance, rapid internalization, and improved anticancer efficacy, Trends Food Sci. Technol. 80 (2018) 8–22, https://doi.org/10.1016/j.tifs.2018.07.026.

[6] J.T. Thornthwaite, H.R. Shah, P. Shah, W.C. Peeples, H. Respess, The formulation for cancer prevention & therapy, Adv. Biol. Chem. 3 (2013) 356–387.

[7] B. D. Brooks, A. E. Brooks, Therapeutic strategies to combat antibiotic resistance, https://doi.org/10.1016/j.addr.2014.10.027.

[8] S. N. A. Bukhari, F. Hussain, H. E. Thu, Z. Hussain, Synergistic effects of combined therapy with curcumin and fructus ligustri lucidi for the treatment of osteoporosis: cellular and molecular evidence of enhanced bone formation. J. Integr. Med. 17(1): 38-45, https://doi.org/10.1016/j.joim.2018.08.003.

[9] M.M. Chan, R. Chena, D. Fong, Targeting cancer stem cells with dietary phytochemical - repositioned drug combinations, Canc. Lett. 433 (2018) 53–64, https://doi.org/10.1016/j.canlet.2018.06.034.

[10] M.R. Mohammadabadi, M.R. Mozafari, Enhanced efficacy and bioavailability of thymoquinone using nanoliposomal dosage form, J. Drug Deliv. Sci. Technol. 47 (2018) 445–453.

[11] D.M. Hikal, Antibacterial activity of piperine and black pepper oil, biosciences biotechnology research Asia, December 15 (4) (2018) 877–880.

[12] E. Halawani, Antibacterial activity of thymoquinone and thymohydroquinone of nigella sativa L. And their interaction with some antibiotics, Adv. Biol. Res. 3 (5–6) (2009) 148–152.

[13] S. Chanda and K. Rakholiya, Combination Therapy: Synergism between Natural Plant Extracts and Antibiotics against Infectious Diseases, Science against Microbial Pathogens: Communicating Current Research and Technological Advances - A. Méndez-Vilas (Ed.). .

[14] Z. Ahmad, T.F. Laughlin, I.O. Kady, Thymoquinone Inhibits Escherichia coli ATP Synthase and Cell Growth, 2015, https://doi.org/10.1371/journal.pone.0127802. May21.

[15] A.R. Farrag, K.A. Mahdy, G.H. Abdel Rahman, M.M. Osfor, Protective effect of nigella sativa seeds against lead-induced hepatorenal damage in male rats, Pakistan J. Biol. Sci. 10 (2007) 2809–2816 [PubMed: 19090181].

[16] I. Nallamuthu, A. Parthasarathi, F. Khanum, Nallamuthu, et al., Thymoquinone-loaded PLGA nanoparticles: antioxidant and anti-microbial properties, International Current Pharmaceutical Journal, November 2 (12) (2013) 202–207.

[17] L. Gorgani, M. Mohammadi, G.D. Najafpour, M. Nikzad, Piperine the bioactive compound of black pepper: from isolation to medicinal formulations, Compr. Rev. Food Sci. Food Saf. 16 (2017).

[18] K. Srinivasan, Black Pepper (Piper Nigrum) and its Bioactive Compound, Piperine, May 2009. https://www.researchgate.net/publication/279408516.

[19] C.G. Kalunta, Antimicrobial effect of different seed extracts of Piper nigrum against Escherichia coli, Staphylococcus aureus and Candida albican, Biotechnol. Res. 3 (3) (2017) 71–76, e ISSN 2395-6763.
[20] A. Laha, S. Yadav, S. Majumdar, C.S. Sharma, In-vitro Release study of hydrophobic drug using electrospun cross-linked gelatin nanofibers, Biochem. Eng. J. 105 (2016) 481–488.
[21] S.N. Goyal, C.P. Prajapati, P.R. Gore, C.R. Patil, U.B. Mahajan, C. Sharma, S. P. Talla, S.K. Ojha, Therapeutic potential and pharmaceutical development of thymoquinone: a multitargeted molecule of natural origin, Front. Pharmacol. (21 September 2017), https://doi.org/10.3389/fphar.2017.00656.
[22] S. Shityakov, E. Bigdelian, A. A. Hussein , M. B. Hussain, Y. C. Tripathi, M. U. Khan, M. Ali Shariati Phytochemical and pharmacological attributes of piperine: a bioactive ingredient of blackpepper, https://doi.org/10.1016/j.ejmech.2019.04.002 0223-5234/©2019.
[23] M. Alam Khan, Antimicrobial action of Thymoquinone, DOI: 10.1007/978-981-10-8800-1_5.
[24] S. Alam, Dr G. Mustafa, Z. Iqbal, Development and evaluation of thymoquinone encapsulated chitosan nanoparticles for nose-to-brain targeting: a pharmacoscintigraphic study, Int. J. Nanomed. (2012), https://doi.org/10.2147/IJN.S35329. November.
[25] Z. Hussain, Nanotechnology guided newer intervention for treatment of osteoporosis: efficient bone regeneration by up-regulation of proliferation, differentiation and mineralization of osteoblasts, Int. J. Polym. mater. Polym. Biomat. (2020), https://doi.org/10.1080/00914037.2019.1683558.
[26] G. Fang, Q. Zhang, Y. Pang, H.E. Thu, Z. Hussain, Nanomedicines for improved targetability to inflamed synovium for treatment of rheumatoid arthritis: multi-functionalization as an emerging strategy to optimize therapeutic efficacy, J. Contr. Release 303 (2019) 181–208, https://doi.org/10.1016/j.jconrel.2019.04.027.
[27] S. Md, J. Kaur, K. Singh, M. Waqas, M. Pandey, H. Choudhury, H. Habib, F. Hussain, Z. Hussain, Nanoencapsulation of betamethasone valerate using high pressure homogenization-solvent evaporation technique: optimisation of formulation and process parameters for efficient dermal targeting, Drug Dev. Ind. Pharm. 45 (NO. 2) (2019) 323–332, https://doi.org/10.1080/03639045.2018.1542704.
[28] Z. Hussain, H.E. Thu, S. Ng, S. Khand, H. Katas, Nanoencapsulation, an efficient and promising approach to maximize wound healing efficacy of curcumin: a review of new trends and state-of-the-art, Colloids Surf. B Biointerfaces 150 (2017) 223–241, https://doi.org/10.1016/j.colsurfb.2016.11.036.
[29] S.K. Nitta, K. Numata, Biopolymer-based nanoparticles for drug/gene delivery and tissue engineering, Int. J. Mol. Sci. 14 (2013) 1629–1654, https://doi.org/10.3390/ijms14011629.
[30] Z. Hussain, M. Pandey, H. Choudhury, P.C. Ying, T.M. Xian, T. Kaur, G.W. Jia, B. Gorain, Hyaluronic acid functionalized nanoparticles for simultaneous delivery of curcumin and resveratrol for management of chronic diabetic wounds: fabrication, characterization, stability and in vitro release kinetics, J. Drug Deliv. Sci. Technol. 57 (2020) 101747, https://doi.org/10.1016/j.jddst.2020.101747.
[31] F. Zhuo, M.A.S. Abourehab, Z. Hussain, Hyaluronic acid decorated tacrolimus-loaded nanoparticles: efficient approach to maximize dermal targeting and anti-dermatitis efficacy, Carbohydr. Polym. 197 (2018) 478–489, https://doi.org/10.1016/j.carbpol.2018.06.023.
[32] M. Shao, Z. Hussain, H.E. Thu, S. Khan, H. Katas, T.A. Ahmed, M. Tripathy, J. Leng, H. Qin, S.N.A. Bukhari, Drug nanocarrier, the future of atopic diseases: advanced drug delivery systems and smart management of disease, Colloids Surf. B Biointerfaces 147 (2016) 475–491, https://doi.org/10.1016/j.colsurfb.2016.08.027, 2016.
[33] K.A. Janes, P. Calvo, M.J. Alonso, Polysaccharide colloidal particles as delivery systems for macromolecules, Adv. Drug Deliv. Rev. 47 (2001) 83–97.
[34] Jay J. Patel, Mander Karve, Nirmal K. Patel, Guar gum: a versatile material for pharmaceutical industries, Int. J. Pharm. Pharmaceut. Sci. 6 (8) (2014), 0975-1491.
[35] D. Mudgil, S. Barak, B.S. Khatkar, Guar gum: processing, properties and food applications—a Review, Food Sci. Technol. 51 (3) (2014 Mar) 409–418.
[36] B. Goudoulas Thomas, Polymers and Biopolymers as Drug Delivery Systems in Nanomedicine, 2012, https://doi.org/10.2174/1877913111202010052.
[37] N. Thombarea, U. Jha, S. Mishra, M.Z. Siddiqui, Guar gum as a promising starting material for diverse applications: a Review, Int. J. Biol. Macromol. 88 (2016) 361–372.
[38] V. Singh, A. Tiwari, D.N. Tripathi, R. Sanghi, Grafting of polyacrylonitrile onto guar gum under microwave irradiation, J. Appl. Polym. Sci. (May 2004), https://doi.org/10.1002/app.20099.
[39] M. Chaurasia, M.K. Chourasia, N.K. Jain, A. Jain, V. Soni, Y. Gupta, S.K. Jain, Cross-Linked Guar Gum Microspheres: A Viable Approach for Improved Delivery of Anticancer Drugs for the Treatment of Colorectal Cancer, AAPS PharmSciTech, 2006, https://doi.org/10.1208/pt070374.
[40] L. Khandrika, B. Kumar, S. Koul, P. Maroni, and H. K. Koul, Role of Oxidative Stress in Prostate Cancer, doi: 10.1016/j.canlet.2008.12.011.
[41] N. Ismail, Y.A. Mottaleb, A. Ali E. Ahmed, Nabila N. El-Maraghy, Novel combination of thymoquinone and resveratrol enhances anticancer effect on hepatocellular carcinoma cell line, Future J. Pharmaceut. Sci. 4 (2018) 41e46.
[42] N.N. Danial, S.J. Korsmeyer, Cell death: critical control points, Cell 116 (2) (2004 Jan 23) 205e219.
[43] E. Behzadi, P. Behzadi, An in vitro study on the apoptosis inducing effects of ultraviolet Blight in Staphylococcus aureus, Méd. 7 (1) (2012 Jan) 54e57.
[44] H. Sakahira, M. Enari, S. Nagata, Cleavage of CAD inhibitor in CAD activation and DNA degradation during apoptosis, Nature 391 (6662) (1998 Jan 1) 96e99.
[45] R.P. Singh, S. Devi, J.H. Patel, U.D. Patel, S.K. Bhavsar, A.M. Thaker, Indian herbal bioenhancers: a review, Phcog. Rev. 3 (Issue 5) (2009) 90–92.
[46] G. Chinta, S.B. Syed, M.S. Coumar, L. Periyasamy, Piperine: a comprehensive review of pre-clinical and clinical investigations, Curr. Bioact. Compd. 11 (2015) 156–169.
[47] D. Bera, K. Pal, S. Bardhan, S. Roy, R. Parvin, P. Karmakar, P. Nandy and S. Das, Functionalised biomimetic hydroxyapatite NPs as potential agent against pathogenic multidrug-resistant bacteria, https://doi.org/10.1088/2043-6254/ab5104.
[48] J. May, K. Shannon, A. King, Glycopeptide tolerance of Staphylococcus aureus, J. Antimicrob. Chemother. (1998) 42.
[49] D. Bhattacharya, B. Saha, A. Mukherjee, C.R. Santra, P. Karmakar, Nanosci. Nanotechnol. 2 (2012) 14–21.
[50] S. Bardhan, K. Pal, S. Roy, S. Das, A. Chakraborty, P. Karmakar, R. Basu, S. Das, J. Nanosci. Nanotechnol. 19 (2019) 1–11.
[51] Y. Wang, Q. Luo, L. Gao, C. Gao, H. Du, G. Zha, X. Li, Z. Shena and W. Zhu, A Facile Strategy to Prepare Redox-Responsive Amphiphilic PEGylated Prodrug with High Drug Loading Content and Low Critical Micelle Concentration, Biomaterials Science.
[52] H. Gong, M. Liu, J. Chen, F. Han, C. Gao, B. Jhang, Synthesis and Characterization of Carboxymethyl Guar Gum and Rheological Properties of its Solutions, doi: 10.1016/j.carbpol.2012.01.057.
[53] V. Sing, P. Kumari, S. Panday, T. Narayan, Removal of chromium (VI) using poly (methylacrylate) functionalized guar gum, Bioresour. Technol. 100 (2009) 1977–1982.
[54] Z.R. Khan, F. Moni, S. Sharmin, M.A. Al-Mansur, A. Gafur, O. Rahman, F. Afroz, Isolation of bulk amount of piperine as active pharmaceutical ingredient (API) from black pepper and white pepper (piper nigrum L.), Pharmacol. Pharm. 8 (2017) 253–262.
[55] D. Mudgil, B. Khatkar, S. Barak, X-ray diffraction, IR spectroscopy and thermal characterization of partially hydrolyzed guar gum, Int. J. Biol. Macromol. 50 (2012) 1035–1039.
[56] V.K. Gupta, D. Pathania, P. Singh, A. Kumar, B.S. Rathore, Absorptional removal of methylene blue by guar gum-cerium (IV)tungstate hybrid cataionic exchanger, Carbohydr. Polym. 101 (2014) 684–691.
[57] R. Surekha, T. Sumathi, An efficient encapsulation of thymoquinone using solid lipid nanoparticle for brain targeted drug delivery: physicochemical characterization, pharmacokinetics and bio-distribution studies, Int. J. Pharmaceut. Chem. Res. 8 (12) (2016) 1616–1624.
[58] I.J. Bigio, J.R. Mourant, Ultraviolet and visible spectroscopies for tissue diagnostics: fluorescence spectroscopy and elastic-scattering spectroscopy, Phys. Med. Biol. 42 (1997) 803–814.
[59] K.E. Uhrich, S.M. Cannizzaro, R.S. Langer, K.M. Shakesheff, Polymeric Systems for Controlled Drug Release, American Chemical Society, 1999.
[60] Q. Wang, P. R Ellis, S.B. Ross-Murphy, The stability of guar gum in an aqueous system under acidic conditions, Food Hydrocolloids 14 (2) (March 2000) 129–134, https://doi.org/10.1016/S0268-005X(99)00058-2.
[61] M. Ott, V. Gogvadze, S. Orrenius, B. Zhivotovsky, Mitochondria, oxidative stress and cell death, Apoptosis 12 (2007) 913–922.
[62] S. Jo, M. Son, H. Koh, S. Lee, I. Song, Y. Kim, Y. Leei, K. Jeong, W.B. Kim, J. Parki, B.J. Song, T. Huhe, Control of mitochondrial redox balance and cellular defence against oxidative damage by mitochondrial NADP1-dependent isocitrate dehydrogenase, J. Biol. Chem. 276 (19) (2001) 16168–16176. Issue of May 11.

MATHEWS JOURNAL OF PHARMACEUTICAL SCIENCE

MATHEWS Open Access Journals

Review Article

ISSN :2474-753X

Vol No: 04, Issue: 02

Received Date: November 07, 2020

Published Date: December 09, 2020

Sanghita Das1,2

Anindita Dey2,3*

Sukhen Das1

Papiya Nandy3

[1]Department of Physics, Jadavpur University, Kolkata-700032, India

[2]Department of Botany, Asutosh College, Kolkata-700026, India

[3]Centre for Interdisciplinary Research and Education, 404B, Jodhpur Park, Kolkata-700068, India

***Corresponding Author:**

Anindita Dey

Department of Botany, Asutosh College, Kolkata-700026, India

E-mail: sunimondal@yahoo.com

An Overview on Cancer-Fighting Phytochemicals from Selected Medicinal Plants in Bengal

ABSTRACT

Bengal possesses a diverse gene pool of ethno-botanically important plant species for alternative medicinal agents. Herbal remedies, also known as botanical medicine, have been recognized as a promising complementary treatment for cancer. In this article, we have methodically highlighted and summarized most popular and effective Bengal plants which possess phytocomponents with anti-cancer properties. Several in vitro as well as in vivo studies demonstrated the details of plant derived metabolites and their promising efficacy against different cancer cell lines. Therefore, recapitulated data about the bioactivity of these phytochemicals, with special emphasis on Bengal medicinal plants will enrich our knowledge about developing carefully designed standardized drug in controlling the carcinogenic processes traditionally over conventional therapies to prevent this global health crisis.

KEYWORDS: Phytochemicals; Anti-cancer; Medicinal plant; Traditional medicine

INTRODUCTION

Cancer remains to be one of the leading causes of mortality worldwide. Though the modern conventional therapeutic approach has indisputably enhanced survival rate, metastasized cancer remains untreatable. Hence, continued searching for more efficient and effective chemoprevention is clearly desirable to improve the treatment [1]. According to an estimation of World Health Organization, 80 % of rural population rely chiefly on medicinal herbs and traditional medicine as a primary healthcare system [2]. In the Ayurveda, numerous plants with medicinal properties are documented in various texts but it requires newer guidelines of standardization, production and quality control. It has been reported that approximately 50% of all modern pharmaceutic in clinical use are plant derived [3]. Many of these have been recognized to have apoptotic activity in various cancer cells of human origin [1]. Any part of a medicinal plant such as seeds, bark, leaves, roots, flowers, fruits can contain some bioactive substances that can be used for therapeutic or medicinal purposes. Phytochemicals are the secondary metabolites that are taxonomically extremely diverse in nature and an excellent reservoir of potential precursors of new drugs based on their modes of pharmacological action [4,5]. Moreover, these bioactive compounds such as flavonoids, terpenoids and alkaloids have received considerable attention for their anti-mutagenic, anti-malignant, antineoplastic and potential chemo preventive

DOI: https://doi.org/10.30654/MJPS.10005

properties through their effects on signal transduction in cell proliferation and angiogenesis [5].

India is a heritage country in term of natural resources and biodiversity. West Bengal (a state occupies only 2.7% of India's land area) possesses an enormous number of medicinal plants [6]. The tropic of cancer passes almost through the middle of the state. Diverse climatic conditions of West Bengal include a tropical wet-dry climate in the southern part and a humid subtropical climate in the north (http://www.westbengalforest.gov.in). The total forested area of West Bengal is 11879 sq. km. which is 13.38% of the total geographic area of the state (http://www.westbengalforest.gov.in/history.php). At present West Bengal has 23 districts which are distributed in five agro-climatic zones i.e. Darjeeling Himalayan hill region, Tarai – Dooars region, western undulating high land and plateau, north and southern plains of Bengal and Gangetic deltaic regions are favourable to establish the diversity of plants [7]. But unscientific and unorganized harvesting and production of raw materials, lesser concern about quality control, fluctuation in demand and supply, lack of coordination, research and inefficient marketing infrastructure are the main difficulties to promote these therapeutic plants effectively. As per recommendations of the National Medicinal Plant Board (NMPB) as well as West Bengal State Medicinal Plant Board (WBSMPB) some medicinal plant species are recognized for the scientific cultivation in West Bengal. These herbal plants are prioritized because of its vast uses in Indian System of Medicine and Homeopathy (ISM & H). Department of AYUSH (Ayurveda, Yoga, Unani, Siddha and Homeopathy systems) of the Government of India regulates researches on indigenous alternative medicines and their quality control and practices (https://www.ayush.gov.in/). Therefore, scientific cultivation, conservation, suitable maintenance measures regarding harvesting and marketing of medicinal plants may lead to greater success in cancer prevention.

PLANTS WITH ANTICANCER ACTIVITY

According to previous reports, these medicinal plants contain some important active components i.e. vitamins, carotene, enzymes, minerals, polysaccharides, polyphenols, flavonoids, lignin, xanthones, etc. [Figure 1] which exert potent anticarcinogenic and antimetastatic activities [1]. Plants described in this study are endemic in West Bengal state and also well acknowledged possessing several antioxidants. A significant number of research work has been done about the anticancer efficacy of these plants. Thus, the various combinations of the phytochemicals extracted from these plants may undergo further assessment for their synergistic activity after identification. With the above background, this review article enumerates 20 medicinal plants from West Bengal, according to their suppressive and antiproliferative effect on specific cancer types as well as anti-tumor, antimetastatic and antioxidant properties [Table 1]. We have chosen these plant species based on their availability throughout the state, their popularity among people and last but not the least their significant ability to cure the deadly disease cancer to some extent.

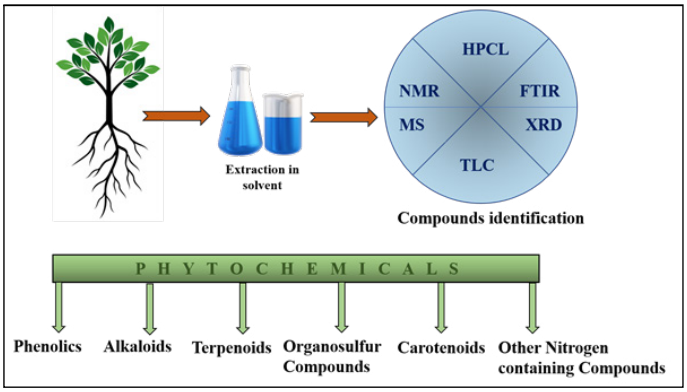

Figure 1: Schematic representation of isolation techniques and types of phytochemicals.

Serial No.	Scientific Name with Family	Active Components	Effect in Cancer
1	***Achyranthes aspera*** (Amaranthaceae)	Achyranthine, phenolic compounds	• cytotoxic activity against pancreatic cancer • antiproliferative activity against breast and cervix cancer
2	***Aerva lanata*** (Amaranthaceae)	Aervitrin, aervolanine, campesterol, kaempferol	• antiproliferative activity against hepatic cancer cells (Hep3B) • induce apoptosis of MCF – 7 cells

DOI: https://doi.org/10.30654/MJPS.10005

3	***Allium sativum*** (Liliaceae)	Allicin, alliin, allixin, Z-again	• suppress colorectal, lung and esophageal cancers • anti-proliferative effects on cancer stem cells of brain malignancies (Glioblastoma multiforme)
4	***Alstonia scholaris*** (Apocynaceae)	Echitamine, alstonidine, alstonin	• cytotoxic activity against human lung cancer cell lines, adenocarcinoma (MOR-P) • cytotoxicity against HepG2, HL60, HeLa, KB, MCF-7 cells, Vero cells, fibrosarcoma
5	***Andrographis paniculate*** (Acanthaceae)	Andrographolide, xanthones, stigmasterols	• anti-proliferative activity against HT-29 (colon cancer), KB (human epidermoid carcinoma) cells and P388 (lymphocytic leukaemia) • antitumor activity against breast cancer cell lines
6	***Artemisia indica*** (Asteraceae)	Ludartin, lupeol	• strong inhibitory activity against cultured MCF-7, BHY, Miapaca-2, Colo-205 and A-549 cell lines • toxic effects on liver cancer cells (HepG2)
7	***Azadirachta indica*** (Meliaceae)	Nimbolide,azadirachtins, nimocinol, isomeldenin, azadirachtol,	• anticancer activity in lung cancer, osteosarcoma, neuroblastoma, choriocarcinoma, leukemia and melanoma • suppress viability of HeLa cervical cancer cells and breast cancer cells
8	***Bauhinia variegata*** (Fabaceae)	Flavonoids, anthraquinones, saponins	• cytotoxic activity against ovarian cancer cell lines • chemo-preventive against human epithelial larynx cancer (HEp2) and human breast cancer (HBL-100) cell lines
9	***Butea monosperma*** (Fabaceae)	Butrin, butein, butin, isobutrin, isocoreopsin	• isocoreopsin exhibits remarkable efficacy in cell mortality on human colon and liver cancer cell lines • floral extracts exhibit strong inhibitory activity on HCT-116 cells
10	***Calotrophis gigantea*** (Asclepiadaceae)	Pregnanes, terols, flavonol glycosides, usharin, gigantin, giganteol, giganteol	• antitumor activityof methanol extract • anticancer effect against human epidermal carcinoma of the nasopharynx tissue
11	***Camellia sinensis*** (Theaceae)	Epigallocatechin-3-gallate, epigallocatechin, epicatechin-3-gallate, epicatechin	• inhibit tumour cell proliferation of leukaemia cells and hepatocellular carcinoma cell • prevent growth of skin tumors
12	***Cassia fistula*** (Leguminosae)	Rhein, emodine, physion, chrysophanol, Obtusin, chrysoobtusin	• remarkable chemopreventive ability • tumour inhibitory activity of methanolic extract of seed on the growth of Ehrlich ascites carcinoma

DOI: https://doi.org/10.30654/MJPS.10005

13	***Centella asiatica*** (Apiaceae)	Asiatic acid, kaempferol, asiaticosside	• induce apoptosis of MCF-7 breast cancer cells, human melanoma SK-MEL-2 cells and human HepG2 cell line • effective antiproliferative activity on skin and lung cancer cells
14	***Curcuma longa L.*** (Zingiberaceae)	Curcumin, demethoxycurcumin, bisdemethoxycurcumin	• activity against melanoma, leukemia, colon, CNS, renal, and breast cancer cell lines • inhibits the proliferation of several tumour cells
15	***Emblica officinalis*** (Euphorbiaceae)	Pyrogallol, gallic acid	• cause decrease in the HepG2 and H520 cell viability • induce apoptosis in Hela (cervical), A549 (lung), MDA MB 231 (breast), SK OV3 (ovarian) and SW620 (colorectal) cell lines
16	***Oroxylum indicum*** (Bignoniaceae)	Baicalein, oroxylin A	• cytotoxic activity in MDA-MB-435S and Hep3B cell lines • anticancer activity when treated against CT-26 colon carcinoma and human breast cancer cells
17	***Semecarpus anacardium*** (Anacardiaceae)	Galluflavanone, phenolic compounds	• cytotoxic effects against acute myeloblastic leukemia (HL-60), chronic myelogeincleukemia (K-562), • anticancer activity against breast adenocarcinoma (MCF-7) and cervical epithelial carcinoma (HeLa) cell lines
18	***Syzygium cumini*** (Myrtaceae)	Betulinic acid, Kaempferol 7-O-methylether isoquercitin, quercetin	• induce apoptosis in human cervical cancer cell lines HeLa, A2780, MCF7, PC-3, H460 and SiHa cell lines • pro-apoptotic properties against breast cancer cells
19	***Vitex negundo*** (Verbenaceae)	Evn-50	• cytotoxic effect on breast cancer, prostate cancer and ovarian cancer • broad spectrum cytotoxic activity on hormone dependent as well as hormone independent cancers
20	***Withania somnifera*** (Solanaceae)	Withaferin A	• *in-vitro* cytotoxicity against A-549 (lung), PC-3 (prostrate), HCT-15 (colon), and IMR-32 (neuroblastoma) cell lines. • efficient cytotoxicity on MCF-7, A549 and PA-1 cancer cell line

Table 1: Name of the selected Bengal plants, active components and their role in anticancer studies.

DOI: https://doi.org/10.30654/MJPS.10005

Achyranthes aspera

Family: Amaranthaceae **Parts Used:** Leaf, stem, seed

Activity: In traditional medicinal system of Ayurveda *A. aspera* (local name: Apang) is well known for hepatoprotective, diuretic, immunostimulatory and anti-cancer properties [8,9]. *A. aspera*, an annual shrub frequently found in tropical and warmer regions in India reportedly contains fatty acids, oleonic acid, triterpenoid based saponins, oleanolic acid, triacontanol, dihydroxy ketones, betaine, achyranthine and various amino acids [10]. The methanol extract of *A. aspera* shows higher quantity of phenolic compounds compared to aqueous extract [9]. It has been reported that leaf extract is used to treat cancer, particularly breast and cervix cancer [10]. Alkaloid extract of leaf induced apoptosis in breast cancer cell through p53 pathways [11]. Several studies demonstrated that the methanolic extract of leaves contains potent antiproliferative and cytotoxic activity against pancreatic cancer cell lines through the inhibition in the expression of pro metastatic and angiogenic genes [8].

Aerva lanata

Family: Amaranthaceae **Parts Used:** Aerial parts

Activity: In traditional Ayurvedic medicines, *A. lanata* (local name: Chaya) was found to be effective against several medical conditions for its antihyperglycemic, hepatoprotective, anti-diabetic, anti-urolithiasis, immunomodulatory properties [12]. *A. lanata* extracts have significant amount of biologically active secondary metabolites like polyphenols, flavanoid glycosides, aervitrin, aervolanine, aervoside, kaempferol, amyrin betulin, campesterol [12]. Some previous studies proved free radical scavenging activity of ethanol, chloroform and hexane extracts of *A. lanata* leaves [13]. *A. lanata* displays strong antiproliferative activity and induced apoptosis of Hep3B (hepatic cancer cells) cell lines [14]. Previous studies showed that p53 mRNA expression was found to decrease Hep3B cells in a dose dependent manner and induced apoptotic activity when treated with petroleum ether extract of A. lanata [14]. The methanolic callus extract of this plant contains potential anticancer property on MCF – 7 cell lines for its significant anti- proliferative activity by induction of the apoptosis in cancer cells. Also the methanol extract of the aerial parts of *A. lanata* has proven to be a source of potent anticancer and antioxidant compounds when treated on Ehrlich Ascites Carcinoma (EAC) cells in Swiss albino mice by monitoring inhibition of tumor cell growth , measurement of tumor weight and survival time of mice [15].

Allium sativum

Family: Liliaceae **Parts Used:** Bulb

Activity: *A. sativum* (local name: Rasun) has been attributed in the Indian medicinal system to possess several medicinal effects. The consumption of garlic offers multiple beneficial properties for its chemo-preventive as well as anti-tumor activity [16]. It has been reported that garlic extract contains some organosulfur phytochemicals like diallylthiosulfinate (allicin), S-allylcysteine sulfoxide (alliin), allixin, adenosine, allyl1,5-hexadienyl trisulphide, allyl methyl trisulphide and eight vital amino acids [17]. There is convincing evidence that the consumption of garlic bulb extract reduces the risk of colorectal, lung and esophageal cancers [16]. Studies showed that garlic can also act against stomach cancer by repressing *Helicobacter pylori* [18]. Its organosulfur components which have free radical scavenging activity also cause cell cycle arrest [17]. It has been found from studies that garlic in several forms can change carcinogen metabolism, reduce formation of carcinogenic products, induce phase II detoxification enzymes including glutathione transferases, quinone reductase, promote apoptosis in cancer cells and inhibit tumour initiation [16]. Several studies demonstrated that the bioactive phytochemicals of garlic modifying the cytokine pattern which leads to an inhibition of a NFκB, a prime regulator of pro-inflammatory gene expression [19]. The immune modulatory activity of garlic shifts a proinflammatory and immunosuppressive cellular environment to an enhanced anti-tumor response which helps in tumorsuppression. Garlic contains two very effective trace metals, germanium and selenium, which have potential therapeutic value in cancer treatment [17]. Researchers hypothesized that the phytocomponents present in garlic evokes anti oxidative, immune-modulating and anti-inflammatory responses which suppress a developing malignancy [18]. Z-again, a component derived from garlic reportedly has a range of biological properties like anti proliferative effects on cancer stem cells (CSC) of brain malignancies like Glioblastoma multiforme (GBM) [18].

Alstonia scholaris

Family: Apocynaceae **Parts Used:** Bark

Activity: *A. scholaris* (local name: Saptaparni) is a medicinal plant, whose bark have been pharmacologically proven to possess anticancer properties [20]. It is most extensively used in different cultures and civilizations such as India, in herbal formulations for many years [20]. The bark of this species are rich in alkaloids, steroids, triterpenoids, and flavonoids but it is valued for its alkaloids such as echitamine, alstonidine, alstonin, ditain, ditainealstovenine, echicaoutchin, echicerin, echiretin, porphyrine, echaitein, chlorogenine, porphyrosine, and reserpine [21]. The powerful alkaloids of *A. scholaris* protect cells

DOI: https://doi.org/10.30654/MJPS.10005

from the damage by free radicals [21]. From earlier researches it has been revealed that the methanolic extracts of the root bark possess cytotoxic activity against human lung cancer cell lines, adenocarcinoma (MOR-P), and large cell carcinoma (COR-L23). Studies showed that a hydroalcoholic extract of *A. scholaris* also has promising antineoplastic effects [22]. The antineoplastic activity of this bark extract from the same tree in vitro study against HeLa cells (cultured human cervical neoplastic cells) showed that the rate of cell mortality was dependent on the season when the plant bark was harvested and the cytotoxic effects were highest in summer (IC50 of 30 µg/ml) [22]. Echitamine, a bioactive phytochemical of bark extract also has cytotoxicity against HepG2, HL60, HeLa, KB, MCF-7 cells, Vero cells, fibrosarcoma, and Ehrlich ascites carcinoma *in vitro* [23]. Alstonine, another indole alkaloid present in *A scholaris*, is reported to possess antineoplastic effect [24]. Multiple reports also demonstrated that the triterpenoid lupeol present in *A. scholaris* induced cell cycle arrests at G1-S phase and is responsible for increase in the expression of p21 protein in PC-3 cells as well as decrease in cyclin D1, cyclin D2, and cdk2 expressions. It has been reported that bioactive bark components reduce the expression of Ras oncoprotein [22]. Additionally, studies revealed that bark extracts downregulate Bcl2, upregulate Bax, activate caspase-3, and induce poly(ADP) ribose polymerase cleavage, and activate caspase-3, -9, and apaf1 genes in CWR22Rnu1 and PC-3 neoplastic cells which lead to apoptosis [22].

Andrographis paniculate

Family: Acanthaceae **Parts Used:** Aerial part

Activity: *A. paniculate* (local name: kalmegh) has been widely recognized as a natural remedy for various physiological disorders. Diversified medicinally active phytochemicals like flavonoids,diterpenoid lactone, xanthones, stigmasterols have been isolated from the extract of *A. paniculate* [25]. The methanol extract (concentration of 10 µg/mL) of aerial part displays the anti-proliferative activity against HT-29 (colon cancer) cells by 50% but the aqueous extract did not inhibit the proliferation of HT-29 cells [26]. Andrographolide, a diterpenoid, repressed the proliferation of cancer cells promisingly. Previous studies demonstrated that andrographolide exhibited cytotoxic activity against KB (human epidermoid carcinoma) cells and P388 (lymphocytic leukaemia) [26]. Andrographolide 1 (diterpene lactone) of *A. paniculate* extract also has antitumor activity against breast cancer cell lines and mouse myeloid leukaemia cells [27]. Some recent reports displayed the potential of andrographolide (1) to act as a promising anticancer chemotherapeutic compound as it blocks cell cycle progression by decreasing cyclin-dependant kinase (CDK4) expression [27].

Artemisia indica

Family: Asteraceae **Parts Used:** Leaves, flowering stems

Activity: Aerial parts of *A. indica* (local name: Naagdana) has been reported to have anti-parasitic, hepato-protective, anti-helminthic and antiseptic properties [28]. It deserves further research into the chemoprevention and anticancer activity [28]. Among the 43 compounds isolated from extracted essential oils (representing 96.6% of the oil), artemisia ketone (42.1%), germacrene B (8.6%), borneol (6.1%) and cis-chrysanthenyl acetate (4.8%) are some major phytoconstituents exhibiting significant cytotoxic and antioxidant activities [29]. Some biological evaluation demonstrated that the essential oil from *A. indica* leaves have strong toxic effects on liver cancer cells HepG2 [30]. Essential oil extracted from *A. indica* exhibited significant reduction of cell viability against the HT-29 cells of colon cancer, THP-1 cells of leukaemia, A-549 cell of lung cancer [30]. A strong inhibitory activity of the ethyl acetate extraction of *A. indica* (having ludartin and lupeol) was reported against cultured human tumor cell lines MCF-7, BHY, Miapaca-2, Colo-205 and A-549. Researchers also revealed that the anti-proliferative effects of ludartin and lupeol as anticancer agents may be due to the significant DNA damage and loss of mitochondrial membrane potential. However, a favourable interaction between the chemicals may be responsible for the overall antiproliferative action of the extract [28].

Azadirachta indica

Family: Meliaceae **Parts Used:** Leaf, seed, bark

Activity: *A. indica* (local name: Neem), a plant containing are markably diverse array of phytochemicals like terpenoids, flavonoids,coumarins,carbohydrates,proteinswerefoundtocure different ailments due to its anti-plasmodial, antioxidant, anti-angiogenic, anti-cancer, anti-bacterial, antiviral, and fungicidal activities [31]. Its varied pharmacological properties attributed to extractions of different parts of these plants containing phytocompounds like azadirachtins, nimocinol, isomeldenin, azadirachtol (a tetranortriterpernoid), 2,3′ -dehydrosalanol gedunin, nimbin, nimolicinol, odoratone, azadironolide, isoazadironolide [31]. The chemo-preventive effects of dietary doses of aqueous neem leaf extract are useful for its anticancer activity [32]. Leaf and seed extract have potential antioxidant activity. Previous studies demonstrated that polysaccharides and limonoids present in the neem bark, leaves and seed oil reduced tumors and exhibited efficacy against lymphocytic leukemia

[33]. Researchers revealed that nimbolide, a triterpenoid present in the extract, arrested the HT-29 (human colon carcinoma cells) in G2 /M and G0 /G1 stages apparently through upregulation of p21 thereby inhibit tumorigenesis [33]. Nimbolide has also exhibited anticancer activity in numerous cancer types such as lung cancer, osteosarcoma, neuroblastoma, choriocarcinoma, leukemia and melanoma. Also, Azadirachtin and nimbolide of neem suppressed the viability and increase in apoptosis of HeLa cervical cancer cells [34]. The neem extracts also exhibit anti-proliferative effects in both estrogen-dependent as well as independent breast cancer cells and the neem seed oil can inhibit the growth of HeLa cervical cancer cells [34].

Bauhinia variegate

Family: Fabaceae **Parts Used:** Leaf

Activity: *B. variegate* (local name: Raktakanchan) is reported to have different phytochemicals, which possess a wide range of activities and give protection against some skin diseases, stomatitis and chronic diseases reported in Indian Ayurvedic medicine [35]. The study revealed the presence of secondary metabolites such as terpenoids, phenolics, flavonoids, anthraquinones, saponins, tannins, and alkaloids in *B. variegata* leaf extract [35]. Flavonoids extracted from *B. variegata* stem have been shown to possess cytotoxic activity against Dalton's ascetic lymphoma, leukemia, and many more cancer cell lines [36]. *B. variegata* leaf extracts have capability to combat oxidative damage because of its iron binding, radical neutralization ability. It has been reported that extracted flavones are more selective against ovarian cancer cell lines and the presence of flavonoids, anthraquinones, and saponins are responsible for its promising anticancer activity [36]. Ethanol extract of *B. variegata* showed a significant chemo-preventive and cytotoxic effect against human epithelial larynx cancer (HEp2) and human breast cancer (HBL-100) cell lines [37].

Butea monosperma

Family: Fabaceae **Parts Used:** Flower

Activity: *B. monosperma* (local name: Palash) is widely known in the traditional Indian Ayurvedic system for the treatment of a variety of ailments including cancer and liver disorders [38]. The main constituent of the flower is butrin, butein, butin, isobutrin, plastron, and isocoreopsin [39]. The ability of aqueous extract of *B. monosperma* flowers to impose growth arrest, alter mitogenic signalling and trigger pro-apoptotic death in hepatoma cells associated with its strong chemo-preventive effect in vivo with almost zero cytotoxic effect [38]. Isocoreopsin, a purified flavonoid isolated from flower extract possess significant free radical scavenging activity, showed remarkable efficacy in cell mortality on human colon and liver cancer cell lines (50 µg/ml in HT-29 and 100 µg/ml in HepG2) [40]. Intraperitonial administration of the aqueous extract of flowers of *B. monosperma* in the X-15-myc onco mice showed antitumorgenic activity [39]. Ethyl acetate, butanol and aqueous solutions derived from total methanol extract of *B. monosperma* flowers have effective free radical scavenging activities due to the higher phenolic content [39]. Cytotoxic property of *B. monosperma* floral extracts revealed significant inhibitory effect on HCT-116 cells [41].

Calotrophis gigantea

Family: Asclepiadaceae **Parts Used:** Leaf, root

Activity: Traditionally extracts and preparations from roots and leaves of C. gigantean (local name: Akanda) are used against abdominal tumours, syphilis, tuberculous, leprosy, skin diseases, piles, wounds, and insect-bites [42]. Several phytochemicals have been isolated from *C. gigantea* and they include cytotoxic cardenolides, antifeedant nonprotein amino acid, a mixture of tetracyclic triterpene compounds, pregnanes, ursane-type triterpenoids, terols, flavonol glycosides, usharin, gigantin, calcium oxalate, alpha and beta-calotropeol, beta-amyrin., fatty acids (both saturated and unsaturated), giganteol and giganteol [43]. Some experiments explore antitumor activity of methanol extract of *C. gigantea* root [42]. The plant has been reported to have cytotoxic potentials besides pharmacological properties such as cardiotonic, antimicrobial and many more [44]. Study also revealed that the plant *C. gigantea* possess anti-oxidant activity and alcoholic extracts of the root and the leaves were found to have anticancer activity against human epidermal carcinoma of the nasopharynx tissue [45].

Camellia sinensis

Family: Theaceae **Parts Used:** Leaf

Activity: *C. sinensis* (local name: Cha) is one of the most common drinks consumed worldwide as green tea, a rich source of nutritional flavonoids like epigallocatechin-3-gallate, epigallocatechin, epicatechin-3-gallate and epicatechin [46]. Studies have shown that green tea has a potential to inhibit tumour cell proliferation and induce mortality of leukaemia cells [46]. Some previous research demonstrated that epigallocatechin-3-gallate has free radicals scavenging activity and by arresting cell cycle it suppresses the proliferation of hepatocellular carcinoma cell [47]. Several investigations have suggested that epigallocatechin gallate (EGCG), the major tea polyphenol along with other polyphenols have

DOI: https://doi.org/10.30654/MJPS.10005

anti-inflammatory and anti-cancer properties that may help prevent the onset and growth of skin tumors [48]. *C. sinensis* is a potent anti-carcinogen with no side effects [47]. The antioxidant activity of tea polyphenols is not only due to their ability to scavenge superoxide but also due to increased activity of some detoxifying enzymes such as glutathione peroxidase, glutathione reductase, glutathione-S-transferase, catalase and quinine reductase in small intestine, liver and lungs [49]. Moreover, researchers found that people who drank tea were less susceptible to develop stomach cancer, colorectal cancer, esophageal cancer, pancreatic cancer and lung cancer than those who did not drink green tea [47].

Cassia fistula

Family: Leguminosae **Parts Used:** Flower, seed, leaf, bark

Activity: *C. fistula* (local name: Amaltaas), a well-known Indian medicinal plant possesses significant antimicrobial, anti-inflammatory, hepatoprotective, wound healing and hypoglycemic activity [50]. It has been reported that *C. fistula* leaf extract have a rich amount of anthraquinone glycosides, flavonoids and phenolic compounds [50]. It is also suggested that anthraquinone glycoside (rhein, emodine, physion, chrysophanol, Obtusin, chrysoobtusin etc) have an anticancer activity. *C. fistula* extracts are high in total phenolics and proanthocyanidin content which are responsible for the synergistic oxidative potency of the extracts [51]. The results of some studies revealed that methanol extract of *C. fistula* seed has an antitumor activity [52]. Researchers demonstrated the tumour inhibitory activity of methanolic extract of *C. fistula* seed on the growth of Ehrlich ascites carcinoma [53]. Oral administration of bark extracts in 7, 12-dimethyl benz(a) anthracene (DMBA) induced oral squamous cell carcinoma in hamster showed complete prevention of carcinogenesis due to its remarkable chemopreventive ability [54].

Centella asiatica

Family: Apiaceae **Parts Used:** leaf

Activity: *C. asiatica* (local name: Thankuni) is valued in traditional Ayurveda medicine for treating a variety of diseases like skin problems, wound healing, mental fatigue, stomach ulcers, diarrhea, epilepsy, and for revitalizing the nerves and brain cells. The scientific studies have demonstrated a variety of biochemical components i.e. amino acids (mainly Alanine and serine), flavonoids, terpenoids, essential oils, alkaloids present in aerial parts of this herb [55]. The flavonoids of leaf extract include kaempferol, kaempferol-3-o-β-d-glucuronide, quercetin, quercetin-3-o-β-d-glucuronide, castillicetin, castilliferol, apigenin, rutin, luteolin etc and the triterpenes are composed of asiatic acid, madecassic acid, asiaticosside, madecassoside, centelloside, madasiatic acid, brahminoside, brahmoside, brahmic acid, thankiniside, isothankunisode, centic acid, and cenellicacid [55]. *C. asiatica* methanolic extract showed concentration dependent inhibition of cell proliferation and induction of apoptosis in MCF-7 breast cancer cells [56]. At a concentration above 0.1% of *C. asiatica* juice, an increased DNA damage and apoptotic cell death was noticed on human HepG2 cell line [57]. Asiatic acid, a phytocompound from *C. asiatica* showed effective antiproliferative activity on skin and lung cancer cells and also responsible for induction of apoptosis and lowering viability in human melanoma SK-MEL-2 cells [56]. When treated with 40 µg/ml concentration of asiatic acid, a reduction up to 50% in viability in ovarian cancer cells was observed and it also showed cell cycle arrest at the G0/G1 phase followed by increased apoptosis by 7-10 folds [58]. A partially purified fraction of methanol extract of *C. asiatica* inhibited the tumour growth with no toxic effects on lymphocytes and leaf water extract has a chemo preventive effect on colon tumorigenesis [59].

Curcuma longa L.

Family: Zingiberaceae **Parts Used:** Root, stem and leaves

Activity: Curcumin, a phenolic compound from the plant *Curcuma longa L.* (local name: Haldi) has shown a wide-spectrum chemo-preventive, antioxidant and antitumor activities. Curcumin is the natural yellow pigment in turmeric isolated from the rhizome of the plant *C. longa* [60]. Curcumin was found to inhibit the generation of ROS including superoxide dismutase and hydrogen peroxide in peritoneal macrophages. Curcumin as an anti-inflammatory agent, inhibits the proliferation of several tumour cells [60]. Recently, curcumin has been listed as the third generation of antitumor drug by the US National Cancer Institute (NCI) [61]. Curcumin, demethoxycurcumin and bisdemethoxy curcumin are the most common antitumor constituents in the curcuminoids of turmeric [62]. Curcumin I, curcumin II (monodemethoxycurcumin) and curcumin III (bisdemethoxycurcumin) from *C. longa* was assayed for their cytotoxicity, antioxidant and anti-inflammatory activities [63]. These compounds showed activity against melanoma, leukemia, colon, CNS, renal, and breast cancer cell lines [63]. Cell viability assays demonstrated the efficacy of rubusoside-solubilized curcumin against human colon, breast, and pancreatic cancer cell lines. Multiple mechanisms of action of curcumin are responsible for various effects on cancer cells including cell cycle arrest at G1/S stage, apoptosis induction which has been

observed in different tumor cell lines [64].

Emblica officinalis

Family: Euphorbiaceae **Parts Used:** Fruit pulp

Activity: *E. officinalis* (local name: Amlaki) has been used in Asian herbal pharmaceuticals for treatment of various illnesses specially in case of gastrointestinal problems [65]. It has been reported that the medicinal fruit of *E. officinalis* contains unique biologically active ingredients tannoids and flavanoids, having powerful antioxidant properties and high content of the antioxidant vitamin C, gallic acid [65]. The isolated ingredients from fruit extract have shown their protective effect against lipid peroxidation [66]. From previous studies, it has been proven that fruit extract act as an antimutagen directly as well as against mutagens that need metabolic activation and it also showed anticarcinogenic activity against methylcholanthrene-induced sarcoma formation [67]. The anticancer properties of the bioactive components of fruit extract is exerted through the removal of free radicals and by inhibiting Phase-I enzymes which are required for the activation of carcinogen and activation Phase-II enzymes (antagonist of Phase-I enzyme) [67]. It has been proven that aqueous extracts of *E. officinalis* cause decrease in the HepG2 cell viability by reducing ROS generation as well as improving reduced intracellular GSH levels. *E. officinalis* aqueous extracts also induce apoptosis in several cancer cell lines i.e. Hela (cervical), A549 (lung), MDA MB 231 (breast), SK OV3 (ovarian) and SW620 (colorectal) [68]. Pyrogallol, a bioactive catechin compound of *E. officinalis* fruit extracts showed significant anti proliferative activity against H520 (lung squamous cell carcinoma) and human lung cancer cell lines H441 (lung adenocarcinoma) [69]. Development of pyrogallol based high potency anti lung cancer drug needs to be supported by further researches.

Oroxylum indicum

Family: Bignoniaceae **Parts Used:** bark

Activity: The medicinally active plant *O. indicum* (local name: Sonapatha) has drawn considerable attention in research because of wide nutritional and medicinal properties to treat biliousness, fevers, intestinal worms, leucoderma, inflammation, diarrhoea, dysentery, diaphoretic, bronchitis pneumonia and respiratory troubles etc [70]. Bioactive phenolic compounds present in *O. indicum* extract are baicalein, oroxylin A, chrysin and its variety of derivatives. [70]. *O. indicum* in its methanol and aqueous extracts have previously been reported for its cytotoxicity in MDA-MB-435S and Hep3B cell lines [71]. The bark decoction of O. indicum has also been reported for its use in treating cancer, despite the lack of mechanistic evidence about this therapeutic function [72]. *O. indicum* bark extracts were furthermore reported to possess anti-proliferative property on human breast cancer cells [73]. The stem bark extract of *O. indicum* showed effectual cytotoxicity, apoptosis-inducing abilities and distinctive anti-metastatic potentials against estrogen receptor-negative breast cancer [71]. Baicalein, a naturally occurring flavonoid compound isolated from *O. indicum* possesses effectual anticancer activity when treated against CT-26 colon carcinoma [70].

Semecarpus anacardium

Family: Anacardiaceae **Parts Used:** Nut

Activity: The fruits of *S. anacardium* (local name: Bhallatak), a tropical tree growing wild in the Indian subcontinent, are used extensively for the treatment of human cancers in the Ayurvedic medicine [74]. The nut milk extract of this plant exhibits anti-tumor activity by inducing the in vivo antioxidant system or by suppressing hypoxic and angiogenic factors (hypoxia inducible factor-1 alpha), vascular endothelial growth factor, and inducible nitric oxide synthase [74]. The oil extracted from *S. anacardium* nut is reported to have cytotoxic effects against acute myeloblastic leukemia (HL-60), chronic myelogeincleukemia (K-562), breast adenocarcinoma (MCF-7) and cervical epithelial carcinoma (HeLa) cell lines [75]. Phytochemical analysis of the nut reveals the presence of bioflavonoids (galluflavanone), bhilawanols, phenolic compounds, glycosides and sterols [76]. *S. anacardium* oil having strong antioxidant capacity showed its anti-tumour activity through a mechanism which does not cause any acute physiological disturbance [77]. Reports have also established that a single injection of nut extract could bring complete inhibition of tumour growth in rats. *S. anacardium* nut extract may be a potential antineoplastic agent against mammary carcinoma cell [78].

Syzygium cumini

Family: Myrtaceae **Parts Used:** Fruit, seed

Activity: *S. cumini* (local name: Kaalojaam), a large evergreen tree native to India has been valued in traditional Ayurveda and Unani medication for its therapeutic potentials [79]. The various parts of the plant (bark, leaf, fruit and seed) is reported to possess antioxidant, anti-inflammatory, anti-microbial, anti-bacterial, anti-HIV, anti-leishmanial, anti-fungal, nitric oxide scavenging, free radical scavenging, anticancer, anti-clastogenic, anti-diarrheal, gastroprotective, anti-ulcerogenic and chemotherapeutic activities [80]. These parts have been extensively investigated for their bioactive phytochemical

constituents like maleic acid, oxalic acid, gallic acid, ellagic acid, oleanolic acid, betulinic acid, isoquercitin, quercetin, myricetin, kaempferol, cynidin glycoside, flavonoids, tannins, essential oils and triterpenoids [81]. Some of these components may be collectively responsible for the antineoplastic, radioprotective, chemopreventive properties of such plant extract [81]. Anthocyanins and Betulinic acid, Cyanidin diglycoside, Ferulic acid were reported for their potent anticancer activity. Study showed that ethanol extract of fruit containing Kaempferol 7-O-methylether and Y-Sitosterol is responsible for their antioxidant and anti- leukemia activities [79]. The crude extract of *S. cumini* fruits inhibited growth and induced apoptosis in human cervical cancer cell lines HeLa and SiHa in a dose and time-dependent manner [82]. *S. cumini* fruit extract has been further observed to have anti-tumor and anti-oxidative potential against chemically induced stomach carcinogenesis [80]. Some studies also revealed the significant cytotoxic activity of the seed extract of *S. cumini* on various cancer cell lines (A2780, MCF7, PC-3, H460) [82]. Previous experiments have shown that the standardized fruit extract of this plant possesses antiproliferative as well as pro-apoptotic properties against breast cancer cells.

Vitex negundo

Family: Verbenaceae **Parts Used:** Leaves, seed

Activity: Traditionally, plant parts of *V. negundo* (local name: Nishinda) are used for the treatment of skin-ulcers, leukoderma, rheumatoid arthritis, bronchitis, leucoderma, gonorrhea, bronchitis etc. *V. negundo* also exhibits anti-bacterial, anti-fungal, anti-inflammatory, anti-tumor activity [83]. The phytochemical study of ethanolic extract of leaves of *V. nigundo* indicated the presence of flavonoids, Alkaloids and terpenoids [84]. The anti-tumour effect shown by the ethanolic extract may be due to antioxidant potential of flavonoids [84]. Evn-50 is a mixture of lignan compounds extracted from V. negundo possesses a broad spectrum of cytotoxic activity for various cancers including hormone dependent and hormone independent cancers ranging from pancreatic cancer, liver cancer, kidney cancer, lung cancer, gastric cancer, and colon cancer [85]. This cytotoxicity of EVn-50 may be due to cell cycle arrest at G2/M phase as observed by flow cytometric study, followed by apoptosis of cancer cells. EVn-50 exerts cytotoxic effect on some hormone related cancers including breast cancer, choriocarcinoma, prostate cancer and ovarian cancer, possibly via apoptosis inducing mechanism and so acknowledged as potential anticancer compound [85].

Withania somnifera

Family: Solanaceae **Parts Used:** Root, stem and leaves

Activity: In Indian traditional Ayurvedic medicine *W. somnifera* (local name: Ashwagandha) is well proven as a potential source of various anticancer components due to the presence of several bioactive components acting as free radical scavengers, reducing agents and quenchers of singlet oxygen [86]. Some recent studies using 50% ethanol extract of root, stem and leaves of *W. somnifera* exhibited in-vitro cytotoxicity against five human cancer cell lines of four different tissues i.e. A-549 (lung), PC-3(prostrate), DU-145 (prostrate), HCT-15 (colon), and IMR-32 (neuroblastoma) [87]. *W. somnifera* also has anti-inflammatory, anti-tumour and radio-sensitizing actions and analgesic activity [87]. Studies on *W. somnifera* suggest that it decreases tumour cell proliferation and boosts the efficiency of radiation therapy while potentially mitigating unwanted side effects. Hydro alcoholic (1:1) sample of *W. somnifera* (leaves) shows efficient cytotoxicity on MCF-7, A549 and PA-1 cancer cell line (breast, lung and ovary respectively) [86]. In a study, *W. somnifera* was suggested as an alternative long-term therapy to prevent the spread of cancer cells. In this case, the root extracts were tested against vimentin pro-metastatic protein. Thus, different formulations of *W. somnifera* were used to establish as cell motility inhibitor in case of breast tumours [88]. Withaferin A, an active anticancer agent extracted from the leaf of the plant [89]. Moreover, some experiments proved that the lower concentrations of root extract of *W. somnifera* can constrain breast cancer metastasis with negligible adverse effects in rat model [88,89]. These findings paved the way for researchers to focus on the bioactivities of this plant and to formulate the composition for medicinal use.

ANTICANCER APPLICATIONS OF PHYTOCHEMICALS

The curative properties of these plants are due to the presence of complex phytochemical constituents of diverse compositions grouped alkaloids, glycosides, corticosteroids, essential oils etc. [Figure 2]. Plant derived medicines are basically multi-compounds extract with complicated compositions in which fractional components possess chemo preventive activity.

DOI: https://doi.org/10.30654/MJPS.10005

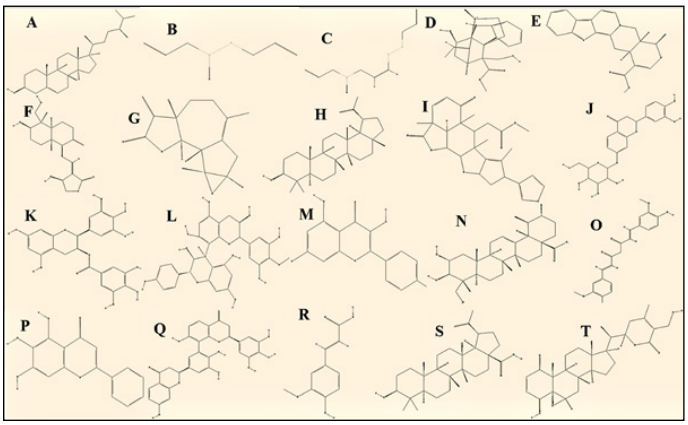

Figure 2: Structural representation of phytochemicals having cytotoxic or anticancer properties. The structures and Compound identification number (CID) are taken from PubChem Database of National Centre for Biotechnology Information (NCBI). (A) campesterol, CID: 173183 ; (B) allicin, CID: 65036 (C) Z-ajoene, CID: 9881148 (D) echitamine, CID: 5364099 (E) alstonine CID: 24188474 (F) andrographolide, CID: 5318517; (G) ludartin, CID: 14355826; (H) lupeol, CID: 259846; (I) nimbolide, CID: 100017; (J) isocoreopsin, CID: 12309899; (K) epigallocatechin gallate, CID: 65064; (L) proanthocyanidin, CID: 108065 (M) kaempferol, CID: 5280863 (N) asiatic acid, CID: 119034 (O) curcumin, CID :969516 (P) baicalein, CID : 5281605; (Q) galluflavanone, CID: 101326873 (R) ferulic acid, CID: 445858 (S) betulinic acid, CID: 64971 (T) withaferin A, CID: 265237 (accessed on 19th July 2020).

Several emerging analytical separation methods are reported to have more advantages over conventional procedures to separate and screen the phytochemical constituents of certain medicinal activities. But it is still a challenge to formulate an ideal phytochemical-based medicine containing isolated bioactive anticancer agents. Phytochemical studies revealed that *A. aspera, A. scholaris, B. variegate, C. asiatica, V. negundo* possess alkaloid compounds with chemo preventive effects. *A. scholaris* from (Apocynaceae) has been reported to have an alkaloid derivative antineoplastic agent, Alstonine [24]. Manyphenolic compounds are isolated from *A. aspera, A. lanata, B. variegate, B. monosperma, C. sinensis, C. longa, O. indicum, S. anacardium*. Epigallocatechin gallate, a polyphenol isolated from *C. sinensis* (Theaceae) leaf reported to have broad chemopreventive efficacy [47]. Proanthocyanidin is another polyphenol (oligomeric flavonoid) identified in *C. fistula* (Leguminosae) extract has potent anti-carcinogenic activity [51].Curcumin, a natural polyphenol present in *C. longa* (Zingiberaceae) modulates cell signalling thus interfering cancer cell proliferation and angiogenesis [60]. *E. officinalis* (Euphorbiaceae) fruit extracts contain a bioactive polyphenol called pyrogallol that exhibited significant anti-proliferative activity [69]. Ferulic acid, a phenolic compound present in *S. cumini* (Myrtaceae) extract has promising chemo preventive as well as anti-neoplastic activity against various cancer cell lines [80,81]. Campesterol, a phytosterol possessing radical scavenging activity have been isolated from *A. lanata* (Amaranthaceae) [12,13]. Some organosulfur phytochemicals like allicin from *A. sativum* (Liliaceae) have promising repressing properties against numerous cancer cell lines [17]. Various bioactive flavonoid compounds are isolated from *A. paniculate, A. indica, B. variegate, B. monosperma, C. asiatica, C. gigantea, C. sinensis, C. fistula, S. anacardium and V. negundo*. Isocoreopsin, a flavonoid extract of butanol *B. monosperma* flower showed excellent efficacy against human liver and colon cancer cell lines [40]. Kaempferol, a flavonol present in *C. asiatica* (Apiaceae) extract was reported to have metastasis and angiogenesis repressing capacity [55]. Baicalein, a flavonoid extracted from *O. indicum* (Bignoniaceae) was known to suppress invasiveness of colorectal cancer [70]. Galluflavanone, a new biflavonone isolated from *S. anacardium* nut shells are known to possess cancer preventive potential [76]. Extracts of *A. aspera, A. scholaris, A. paniculate, A. indica, B. variegate, C. gigantea, C. asiatica, S. cumini, V. negundo* have been reported to contain terpenoid compounds. Andrographolide, a diterpenoid from *A. paniculate* (Acanthaceae) exhibited cytotoxic activity against human epidermoid carcinoma cells, breast cancer cell lines and lymphocytic leukaemia [26]. Nimbolide, a tetranortriterpernoid isolated from *A. indica* (Meliaceae) leaf involved in modulating multiple signalling pathways in malignant cells which showed potent chemopreventive activity [33]. Asiatic acid, a pentacyclic triterpenoid extracted from *C. asiatica* (Apiaceae) possesses excellent anti-proliferative efficacy against various cancer cell lines including human lung cancer [58]. Evn-50, a lignan compounds mixture of *V. negundo* (Verbenaceae) has excellent broad-spectrum cytotoxic activity specially against SMMC-7721 (liver cancer) and MDA-MB-435 (breast cancer) cell lines [85].

There are some trademarks common in every type of cancer i.e. self-sufficiency in growth signals and uncontrolled cell proliferations, growth inhibitory signal resistance capability, evasion of apoptosis, unrestricted replication capacity, sustained angiogenesis, metastatic activity and invasion. The complicated mechanism of actions requires strong multi-targeted treatment [90]. Bioactive multi-components plant extract involves in modulating various mechanism by interfering cellular transportations, activating pro-drugs to alter metabolites, inhibiting binding to target proteins etc. It has been observed that natural therapeutics exert significant additive or synergistic mode of action at the signalling cascade by which severe toxic side effects associated with conventional cancer therapies can be avoided. In this scenario, we should

focus on preclinical studies i.e. quality control, drug designing, delivery strategy, drug safety and therapeutic efficacy as well as clinical studies to overcome the problem of data insufficiency about majority of plant derived drugs. Considering the findings of these ethnopharmacological researches on medicinal plants of Bengal, it is possible to formulate effective anticancer drugs either using single or in combination with other phytochemicals through an extensive scientific analysis.

CONCLUDING REMARKS

Science has long acknowledged the value of natural phytochemical based remedies. These traditional therapeutic-inspired approaches to drug discovery attract considerable attention in cancer therapy due to presence of diverse range of active ingredients. But the effectiveness of any herbal product is dependent upon molecular recognition, rational designing, proper standardization, smart delivery strategy during clinical trials. While some natural formulations have shown to exert promising cytotoxicity against cancer cell lines, many remedies aren't supported by research. Our article highlighted twenty most common Bengal plants having strong anti-cancer properties by promoting anti-tumour or anti carcinogenic activities and boosting up the immunity machineries. Our review helps to make a potent data base on those medicinal plants from different plant families with antiproliferative and anti-carcinogenic effect on some specific cancer types and pave the way for the development and utilization of new phytotherapeutic agents in medical applications.

DECLARATION OF INTEREST

There are no conflicts to declare.

Funding

The research work is not assisted by any kind of funding agencies or research fund.

ACKNOWLEDGEMENTS

The authors would like to thank Biophysics department of Jadavpur University, National Medicinal Plant Board (NMPB), West Bengal State Medicinal Plant Board (WBSMPB) Government of India's Department of AYUSH. We are thankful to everyone who provided valuable information and guidance during research of this review. We are also grateful to Dr. Ashesh Nandy for careful reading of our article.

REFERENCES

1. Pandey G, Sharma M. (2009). Some medicinal plants as natural anticancer agents. Phcog Rev. 3(6):259-263.
2. Andualem G, Umar S, Getnet F, Tekewe A, Alemayehu H, et al. (2014). Antimicrobial and Phytochemical Screening of Methanol Extracts of Three Medicinal Plants in Ethiopia. Advances in Biological Research. 8(3):101-106.
3. Rosangkima G, Prasad SB. (2004). Antitumour activity of some plants from Meghalaya and Mizoram against murine ascites Dolton's lymphoma. Indian J Exp Biol. 42:981-988.
4. Perumal SR, Gopalakrishnakone P. (2010). Therapeutic Potential of Plants as Anti-microbials for Drug Discovery. Advance Access Publication. 7(3):283–294. doi:10.1093/ecam/nen036.
5. Hassan W, Nida S, Kazmi Z, Noreen H, Riaz A, et al. (2016). Antimicrobial Activity of *Cinnamomum tamala* Leaves. J Nutr Disorders Ther. 6:2. http://dx.doi.org/10.4172/2161-0509.1000190.
6. Sen R. (2009). The Evolution of Industrial Relations in West Bengal, Cornell University ILR School Digital Commons@ ILR, 2009 International Labour Organization.
7. De B. (1990). West Bengal: A Geographical Introduction, Economic and Political Weekly, May 5-12, 1990. 25:995+997+999-1000.
8. Subbarayana PR, Sarkar M, Impellizzeri S, Raymo F, Lokeshwar BL, et al. (2010). Anti-proliferative and anti-cancer properties of *Achyranthes aspera*: Specific inhibitory activity against pancreatic cancer cells, Journal of Ethnopharmacology. 131;78–82. doi:10.1016/j.jep.2010.06.002.
9. Priya CL, Kumar G, Karthik L, Rao KVB. (2012). Phytochemical composition and in vitro antioxidant activity of *Achyranthes aspera* Linn (Amaranthaceae) leaf extracts. Journal of Agricultural Technology. 8(1):143-156.
10. Srivastava PK. (2014). *Achyranthes aspera*: A potent immunostimulating plant for traditional medicine; IJPSR. 5(5):1601-1611. DOI: 10.13040/IJPSR.0975-8232.5(5).1601-11.
11. Adnyana DPA, Meles IDK, Meles W. (2008). Alkaloid Fraction of Jarong (*Achyranthes Aspera* Linn) Leaf Induced apoptosis breast cancer cell through p53 pathways. The Open Natural Products Journal. 1:44-49.
12. Bitasta M, Madan S. (2016). *Aervalanata*: A blessing of Mother Nature. Journal of Phar macog nosy and Phytoc he mistry. 5(1):92-101.
13. Battu GR, Kumar BM. (2012). Invitro antioxidant activity of A. lanata Linn. Int J Pharm Sci. 2:74-8.

14. Govindan NK. Antioxidant *Aervalanata* Extract Supresses Proliferation and Induce Mitochondria Mediated Apoptosis in Human Hepatocelluar carcinoma cell line A. J Exp Integr Med. 6(2). DOI: 10.5455/jeim. 270616.or.153.

15. Raihan O, Brishti A, Bahar E, Islam F, Rahman M, et al. (2012). Antioxidant and anticancer effect of methanolic extract of *Aervalanata* Linn. against Ehrlich Ascites Carcinoma (EAC) in vivo. Orient Pharm Exp Med. 12:219–225. DOI 10.1007/s13596-012-0073-3.

16. Thomson M, Ali M. (2003). Garlic [*Allium sativum*]: A Review of its Potential Use as an Anti-Cancer Agent. Current Cancer Drug Targets. 3:67-81.

17. Singh VK, Singh DK. (2008). Pharmacological Effects of Garlic (*Allium sativum L.*). ARBS Annual Review of Biomedical Sciences. 10:6-26.

18. Nouroz F, Mehboob M, Noreen S, Zaidi F, Mobin T. (2015). A Review on Anticancer Activities of Garlic (*Allium sativum L.*) Middle-East Journal of Scientific Research. 23(6):1145-1151.

19. Keiss HP, Dirsch VM, Hartung T, Haffner T, Trueman L, et al. (2003). Garlic (*Allium sativum L.*) modulates cytokine expression in lipopolysaccharide-activated human blood thereby inhibiting NF-kappa B activity. J Nutr. 133(7):2171-2175.

20. Jagetia GC, Baliga MS. (2006). Evaluation of Anticancer Activity of the Alkaloid Fraction of *Alstoniascholaris* (Sapthaparna) In vitro and In vivo. Phytother Res. 20:103–109. DOI: 10.1002/ptr.1810.

21. Jahan S, Chaudhary R, Goyal PK. (2009). Anticancer Activity of an Indian Medicinal Plant, *Alstoniascholaris*, on Skin Carcinogenesis in Mice. Integrative Cancer Therapies. 8(3):273–279.

22. Baliga MS. (2010). *Alstoniascholaris* Linn R Br in the Treatment and Prevention of Cancer: Past, Present, and Future. Integrative Cancer Therapies. 9(3):261–269.

23. Rastogi RM, Mehrotra BN. (1990). Compendium of Indian Medicinal Plants. Lucknow, India: Central Drug Research Institute.

24. Beljanski M, Beljanski MS. (1982). Selective inhibition of in vitro synthesis of cancer DNA by alkaloids of beta-carboline class. Exp Cell Biol. 50:79-87.

25. Mishra SK, Sangwan NS, Sangwan RS. (2007). *Andrographis paniculata* (Kalmegh): a review. Pharmacognosy Rev. 1:283-298.

26. Okhuarobo A, Falodun JE, Erharuyi O, Imieje V, Falodun A, et al. (2014). Harnessing the medicinal properties of *Andrographis paniculata* for diseases and beyond: a review of its phytochemistry and pharmacology. Asian Pac J Trop Dis. 4(3):213-222.

27. Menon V, Bhat S. (2010). Anticancer Activity of Andrographolide Semisynthetic Derivatives. Natural Product Communications. 5(5):717–720.

28. Zeng Y, Jiang J, Lao H, Guo J, Lun Y, et al. (2015). Antitumor and apoptotic activities of the chemical constituents from the ethyl acetate extract of *Artemisia indica*. Molecular medicine reports. 11:2234-2240.

29. Rashid S, Rather MA, Shah WA, Bhat BA. (2013). Chemical composition, antimicrobial, cytotoxic and antioxidant activities of the essential oil of *Artemisia indica* Willd. Food Chemistry. 138:693–700.

30. Bayala B, Bassole HN, Scifo R, Gnoula C, More L, et al. (2014). Anticancer activity of essential oils and their chemical components - a review. Am J Cancer Res. 4(6):591-607.

31. Attwood E , Joy C. (2009). *Azadirachta indica* (neem): a plant of multiple biological and pharmacological activities. Phytochemistry. 8:601–620.

32. Kumar GH, Mohan CKV, Rao JA, Nagini S. (2009). Nimbolide a limonoid from *Azadirachta indica* inhibits proliferation and induces apoptosis of human choriocarcinoma (BeWo) cells. Invest New Drugs. 27:246-52. DOI: 10.1007/s10637-008-9170-z.

33. Paul R, Prasad M, Sah NK. (2011). Anticancer biology of *Azadirachta indica L* (neem): A mini review. Cancer Biology & Therapy. 12(6):467-476.

34. Gupta SC, Prasad S, Tyagi AK, Kunnumakkar AB, Aggarwal BB. (2017). Neem (*Azadirachta indica*): An indian traditional panacea with modern molecular basis. Phytomedicine. 34:14–20.

35. Gunalan G, Krishnamurthy V, Saraswathy A. (2016). GC-MS and HPTLC fingerprinting of *Bauhinia variegata* leaves for anticancer activity. World Journal of Pharmaceutical Research. 3(9):1313-1336.

36. Mishra A, Sharma AK, Kumar S, Saxena AK, Pandey AK. (2013). *Bauhinia variegata* Leaf Extracts Exhibit Considerable Antibacterial, Antioxidant, and Anticancer Activities. BioMed Research International. Article ID 915436.

37. Mali RG, Mahajan SG, Mehta AA. (2007). Plant Review Rakta

Kanchan (*Bauhinia variegata*): Chemistry, Traditional and Medicinal uses- a review. Pharmacognosy Reviews. 1(2).

38. Choedon T, Shukla SK, Kumar V. (2010). Chemopreventive and anti-cancer properties of the aqueous extract of flowers of *Butea monosperma*, Journal of Ethnopharmacology. 129:208–213.

39. Sharma AK, Deshwal N. (2011). *Butea monosperma* A traditional medicinal plant; an overview. International Journal of Pharm Tech Research. 3:867-868.

40. Subramaniyan B, Polachi N, Mathan G. (2016). Isocoreopsin: An active constituent of n-butanol extract of Butea monosperma flowers against colorectal cancer (CRC). Journal of Pharmaceutical Analysis. 6:318–325.

41. Polachi N, Nagaraja P, Subramaniyan B, Mathan G. (2015). Antiproliferative activity of n-butanol floral extract from *Butea monosperma* against hct 116 colon cancer cells; drug likeness properties and in silico evaluation of their active compounds toward glycogen synthase kinase-3β/axin and β-catenin/t-cell factor-4 protein complex. Asian J Pharm Clin Res. 8(1):134-141.

42. Habib MR, Karim MR. (2011). Evaluation of antitumour activity of *Calotropis gigantea L*. root bark against Ehrlich ascites carcinoma in Swiss albino mice. Asian Pacific Journal of Tropical Medicine. 786-790.

43. Kumar PS, Kalavathy S. (2013). Review on a potential herb Calotropis gigantea (L.) R Br Sch Acad J Pharm. 2(2):135-143.

44. Pardesi GS, Chhaya G, Madhav VD, Hamid YH, Babita H, (2008). Preliminary studies on antimitotic and anticancer activity of Calotropis gigantean. Pharmacology online. 1:38-47.

45. Ahmed KKM, Rana AC, Dixit VK. (2005). Calotropis Species (Ascelpediaceae) – A Comprehensive Review. Phcog Mag. 2(1):48.

46. Parmar N, Rawat M, Vijay KJ. (2012). *Camellia Sinensis* (Green Tea): A Review, Global Journal of Pharmacology. 6(2):52-59.

47. Sharangi AB. (2009). Medicinal and therapeutic potentialities of tea (*Camellia sinensis L*.) – A review. Food Research International. 42:529–535.

48. Katiyar SK, Ahmad N, Mukhtar H, (2000). Green tea and skin. Archives of Dermatology. 136:989–994.

49. Frei B, Higdon JV. (2003). Antioxidant activity of tea polyphenols in vivo: Evidence from animal studies. Journal of Nutrition. 133(10):3275S–3284S.

50. Singh VK, Khan AM. (1990). Medicinal Plants and Folklores - A Strategy towards Conquest of Human Ailments. 9:67.

51. Ramma AL, Bahorun T, Mohammed A, Soobrattee, O, Aruoma I. (2002). Antioxidant Activities of Phenolic, Proanthocyanidin, and Flavonoid Components in Extracts of Cassia fistula. J Agric Food Chem. 50:5042–5047

52. Sen AB, Shukia YN. (1968). Chemical examination of Cassia fistula. J Indian Chem Soc. 45:744.

53. Gupta M, Mazumder UK, Rath N, Mukhopadhyay DK. (2000). Antitumor activity of methanolic extract of Cassia fistula L. seed against Ehrlich Ascites Carcinoma. Journal of Ethnopharmacology. 72:151–156.

54. Md. Danish, Singh P, Mishra G, Srivastava S, Jha KK, et al. (2011). *Cassia fistula* Linn. (Amulthus)- An Important Medicinal Plant: A Review of Its Traditional Uses. Phytochemistry and Pharmacological Properties. J Nat Prod Plant Resour. 1(1):101-118.

55. Zheng CJ, Qin LP. (2007). Chemical components of *Centella asiatica* and their bioactives. Journal of Chinese Integrative Medicine. 5:348-351.

56. Prakash V, Jaiswal N, Srivastava M. (2017). A review on medicinal properties of *Centella asiatica*. Asian J Pharm Clin Res. 10(10):69-74.

57. Hussin F, Eshkoor SA, Rahmat A, Othman F, Akim A. (2014). The *Centella asiatica* juice effects on DNA damage, apoptosis and gene expression in hepatocellular carcinoma (HCC). BMC Complement Altern Med. 14:32.

58. Ren L, Cao QX, Zhai FR, Yang SQ. Zhang HX. (2016). Asiatic acid exerts anticancer potential in human ovarian cancer cells via suppression of PI3K/Akt/mTOR signalling. Pharm Biol. 54(11):2377-82.

59. Jamil SS, Nizami Q, Salam M. (2007). *Centella asiatica* (Linn.) Urban óA review. Natural Product Radiance. 6(2):158-170.

60. Dorai T, Cao YC, Dorai B, Buttyan R, Katz AE. (2001). Therapeutic potential of curcumin in human prostate cancer. III. Curcumin inhibits proliferation, induces apoptosis and inhibits angiogenesis of LNCaP.

61. Jiang J, Jin X, Zhang H, Su X, QiaoB, et al. (2012). Identification of antitumor constituents in curcuminoids from Curcuma longa L. based on the composition–activity relationship. Journal of Pharmaceutical and Biomedical Analysis. 70;664–

670.

62. Liang G, Tian JL, Shao LL, Yang SL, Li XK. (2008). Progress in the research on SAR and development of antitumor curcuminoids. Chem Bull. 2:110–111.

63. Rarnsewak RS, DeWitt DL, Nair MG. (2000). Cytotoxicity, antioxidant and anti-inflammatory activities of Curcumins I-III from Curcuma longa. Phytomedicine. 7(4):303-308.

64. Srivastava RK, Chen Q, Siddiqui I, Sarva K, Shankar L. Linkage of curcumin induced cell cycle arrest and apoptosis by cyclin-dependent kinase inhibitor p21(/WAF1/CIP1). Cell Cycle 2007; 6:2953–61.

65. Reddy VD, Padmavathi P, Paramahamsa M, Varadacharyulu NC. (2010). Amelioration of alcohol induced oxidative stress by *Emblica officinalis* (amla) in rats. Indian J Biochem Biophys. 47:20 5.

66. Haque R, Bin-Hafeez B, Ahmad I, Parvez S, Pandey S, et al. (2001). Protective effects of *Emblica officinalis* Gaertn. in cyclophosphamide-treated mice. Human & Experimental Toxicology. 20:643–650.

67. Jose JK, Kuttan G, George J, Kutta R. (1997). Antimutagenic and Anticarcinogenic Activity of *Emblicaoficinalis.* J Clin Biochem Nutr. 22:171-176.

68. Ngamkitidechakul C, Jaijoy K, Hansakul P, Soonthornchareonnon N, Sireeratawong S. (2010). Antitumour effects of *Phyllanthus emblica* L.: induction of cancer cell apoptosis and inhibition of in vivo tumour promotion and in vitro invasion of human cancer cells. Phytother Res. 24:1405–1413.

69. Yang CJ, Wang CS, Hung JY, Huang HW, Chia YC, et al. (2009). Pyrogallol induces G2 M arrest in human lung cancer cells and inhibits tumor growth in an animal model. Lung Cancer. 66:162 8.

70. Laloua C, Basak A, Mishra P, Mohanta BC, Banik R, et al. (2013). Inhibition of Tumor Cells Proliferation and Migration by the Flavonoid Furin Inhibitor Isolated from *Oroxylum indicum*. Current Medicinal Chemistry. 20:583-591.

71. Kumar DRN, George VC, Suresh PK, Kumar RA. Cytotoxicity, Apoptosis Induction and Anti-Metastatic Potential of *Oroxylum indicum* in Human Breast Cancer Cells, DOI: http://dx.doi.org/10.7314/APJCP.2012.13.6.2729.

72. Mao *AA. Oroxylum* indicum vent. A potential anticancer medicinal plant. Ind J Trad Know, 2002; 1, 17-21.

73. Lambertini E, Piva R, Khan MT. (2004). Effects of extracts from bangladeshi medicinal plants on in vitro proliferation of human breast cancer cell lines and expression of estrogen receptor α gene. Int J Oncol. 24:419-23.

74. Premalatha B. (1999). Sachdanandam *P. Semecarpus* anacardium L. nut extract administration induces the in vivo antioxidant defence system in aflatoxin B1 mediated hepatocellular carcinoma. Journal of Ethnopharmacology. 66:131–139.

75. Chakraborthy S, Roy M, Taraphdar AK, Bhattacharya RK. (2004). Cytotoxic effect of root extract of *Tiliacororacemosa* and oil of *Semecarpus* anacardium nut in human tumor cells. Phytotherapy Research. 18:595–600.

76. Premalatha B. (2000). *Semecarpus anacardium* Linn. Nut- A boon in alternative medicine, Indian journal of experimental biology. 38:1177-1182.

77. Indap FMA, Ambaye RY, Gokhale SV. (1983). Antitumour and pharmacological effects of the oil from Semecarpus anacardium Linn. Ind J Physio Pharmac.

78. Sujatha V, Sachdanandam P. (2002). Recuperative Effect of *Semecarpus anacardium* Linn. Nut Milk Extract on Carbohydrate Metabolizing Enzymes in Experimental Mammary Carcinoma-bearing Rats Phytother. Res. 16:S14–S18. DOI: 10.1002/ptr.777.

79. Choi EJ, Ahn WS. (2008). Kaempferol induced the apoptosis via cell cycle arrest in human breast cancer MDA-MB-453 cells. Nutrition Res Practice. 2(4):322-325.

80. Goyal PK, Verma P, Sharma P, Parmar J, Agarwal A. (2010). Evaluation of Anti-Cancer and Anti-Oxidative Potential of *SyzygiumCumini* Against Benzo[a]pyrene (BaP) Induced Gastric Carcinogenesis in Mice. Asian Pacific J Cancer Prev. 11:753-758.

81. Swami SB, Singh N, Thakor J, Patil MM, Haldankar PM. (2012). Jamun (*Syzygiumcumini* (L.)): A Review of Its Food and Medicinal Uses Food and Nutrition Sciences. 3:1100-1117.

82. Yadav SS, Meshram GA, Shinde D, Patil RC, Manohar SM, et al. (2011). Antibacterial and Anticancer Activity of Bioactive Fraction of *Syzygiumcumini* L. Seeds. Journal of Biosciences. 18(3):118-122.

83. Md. Islam S, Most. Akhtar M, Md. Parvez S, Md. Alam J, Alam MF. (2013). Antitumor and antibacterial activity of a crude methanol leaf extract of *Vitex negundo*. Arch Biol Sci. 65(1):229-238.

84. Chitra V, Sharma S, Kayande N. (2009). Evaluation of Anticancer Activity of Vitex negundo in Experimental Animals: An In Vitro & In Vivo Study. Int J Pharm Tech Res. 1(4).

85. Xin H, Kong Y, Wang Y, Zhou Y, Zhu Y, et al. (2013). Lignans extracted from *Vitex negundo* possess cytotoxic activity by G2/M phase cell cycle arrest and apoptosis induction. Phytomedicine. 20:640–647.

86. Nema R, Khare S, Jain P, Pradhan A. (2013). Anticancer Activity of *Withania Somnifera* (Leaves) Flavonoids Compound. Int J Pharm Sci Rev Res. 19(1):103-106.

87. Yadav B, Bajaj A, Saxena M, Saxena AK. (2010). In Vitro Anticancer Activity of the Root, Stem and Leaves of *Withania Somnifera* against Various Human Cancer Cell Lines. Indian J Pharm Sci. 72(5):659–663.

88. Yang Z, Garcia A, Xu S. (2013). *Withania somnifera* root extract inhibits mammary cancer metastasis and epithelial to mesenchymal transition. PLoS One 8: e75069.

89. Rai M, Jogee PS, Agarkar G, dos Santos CA. (2016). Anticancer activities of *Withania somnifera*: Current research, formulations, and future perspectives. Pharm Biol. 54(2):189–197.

90. Hanahan D, Weinberg RA. (2000). The hallmarks of cancer. Cell. 100:57-70.

DOI: https://doi.org/10.30654/MJPS.10005

Spectrochimica Acta Part A: Molecular and Biomolecular Spectroscopy 273 (2022) 121061

Contents lists available at ScienceDirect

Spectrochimica Acta Part A: Molecular and Biomolecular Spectroscopy

journal homepage: www.elsevier.com/locate/saa

Real-time sensitive detection of Cr (VI) in industrial wastewater and living cells using carbon dot decorated natural kyanite nanoparticles

Souravi Bardhan [a], Shubham Roy [a], Sanghita Das [a], Ishita Saha [b], Dhananjoy Mondal [a], Jhilik Roy [a], Dipak Kr. Chanda [c], Solanky Das [d], Parimal Karmakar [b], Sukhen Das [a,*]

[a] Department of Physics, Jadavpur University, Kolkata 700032, India
[b] Department of Life Science and Biotechnology, Jadavpur University, Kolkata 700032, India
[c] School of Materials Science and Nano-Technology, Jadavpur University, Kolkata 700032, India
[d] Department of Geology, Jadavpur University, Kolkata 700032, India

HIGHLIGHTS

- Synthesis of carbon dot doped natural kyanite nanostructure has been reported.
- Selective detection of Cr (VI) in industrial wastewater and live cells is found.
- Limit of detection is found to be ~ 0. 11 μM against hexavalent chromium.
- Theoretical and experimental validation of the detection mechanism is reported.

GRAPHICAL ABSTRACT

Cost-effective and time-efficient synthesis of natural mineral (kyanite) based biocompatible, fluorometric sensor for highly selective and sensitive detection of Cr (VI) in aqueous media, industrial wastewater and living cells.

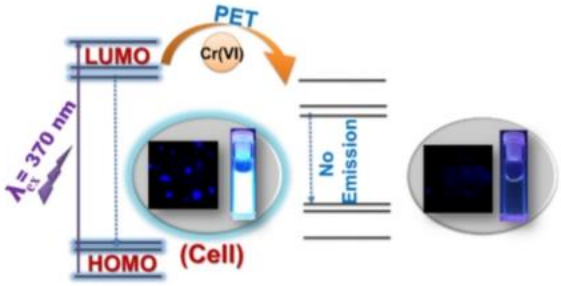

ARTICLE INFO

Article history:
Received 24 October 2021
Received in revised form 30 January 2022
Accepted 16 February 2022
Available online 19 February 2022

Keywords:
Natural mineral
Rietveld refinement
TDDFT
Molecular docking
Hexavalent chromium

ABSTRACT

This article reports a facile strategy to detect hexavalent chromium (Cr (VI)) using a naturally formed mineral (kyanite) based fluorometric sensor. Nitrogenous carbon dots have been incorporated into natural kyanite (KYCD) nanoparticles causing a stable bright blue fluorescence compared to its pristine counterpart. This sensing probe structurally stabilizes and resists the agglomeration of carbon dots, thus retaining fluorescence quality for a longer period. The promising bright blue fluorescence has been utilized further to detect Cr (VI) in wastewater and living cells. Ease of synthesis, low cost, and stability of the system offers the benefit for large-scale production, which is convenient for industrial production the sensing probe. The sensor shows high selectivity and sensitivity (LOD and LOQ of 0.11 μM and 0.36 μM respectively in case of linear fitting, whereas 0.26 μM and 0.88 μM respectively for full range plot) towards hexavalent chromium in presence of other interfering elements. A detailed study of photoinduced electron transfer (PET) mediated rapid 'turn off' sensing mechanism was carried out using Time-Dependent Density functional (TDDFT) calculations. The sensing efficacy of the probe remains unaltered under a wide range of pH and can be effective in various water types. Onsite sampling and probing of Cr (VI) in tannery wastewater has been performed to validate its real-life efficiency that yields excellent results. The sensor can effectively detect chromium at a cellular level (HeLa cells) in a similar way as the bright blue fluorescence diminishes in presence of the quenching ion. Experimental in vitro studies along with theoretical docking analysis has been conducted to substantiate such issues and a higher

* Corresponding authors.
E-mail address: sdasphysics@gmail.com (S. Das).

https://doi.org/10.1016/j.saa.2022.121061

Natural Products in Vector-Borne Disease Management

Edited by

Nagendra Singh Chauhan
Drugs Testing Laboratory Avam Anusandhan Kendra, Raipur, Chhattisgarh, India

Durgesh Nandini Chauhan
Columbia Institute of Pharmacy, Raipur, Chhattisgarh, India

ACADEMIC PRESS
An imprint of Elsevier

Chapter 5

Combating the vectors and management of vector-borne diseases with essential oil nanoemulsions

Anindita Dey[a,b], Sumanta Dey[b], Sanghita Das[c], Madhumita Majumder[d], Papiya Nandy[b], and Ashesh Nandy[b]

[a]*Department of Botany, Asutosh College, Kolkata, West Bengal, India,* [b]*Centre for Interdisciplinary Research and Education, Kolkata, West Bengal, India,* [c]*Department of Physics, Jadavpur University, Kolkata, West Bengal, India,* [d]*Department of Botany, Raidighi College, Raidighi, West Bengal, India*

Abbreviations

AChE	acetylcholinesterase
CHIKV	Chikungunya virus
DDT	dichlorodiphenyltrichloroethane
DENV	Dengue virus
EONEms	essential oil nanoemulsion
EOs	essential oils
GABA	gamma-aminobutyric acid
IVM	integrated vector management
JEV	Japanese encephalitis virus
LC_{50}	lethal concentration 50
O/W	oil in water
O/W/O	oil-in-water-in-oil emulsion
ONNV	O'nyong'nyong virus
PIC	phase inversion composition
PIT	phase inversion temperature
RFV	Rift Valley fever virus
SDM	solvent diffusion method
TBE	tick-borne encephalitis
W/O	water in oil

Natural Products in Vector-Borne Disease Management. https://doi.org/10.1016/B978-0-323-91942-5.00006-9

Materials science is an interdisciplinary field of researching and discovering materials. It is the study of the properties of solid materials and how those properties are determined by a material's composition and structure. This book contains five chapters. The first chapter demonstrates the importance of nano-fertilizer. The second chapter briefly tells about 3D printing. The third chapter shows polymer perovskites composites for energy applications. The fourth chapter demonstrates the novelty of antimicrobial peptides as an emerging materials for antibiotics. The fifth chapter describes about aluminium along with its novel properties and applications.

Dr. Ujjal Kumar Sur works as Associate Professor in the Department of Chemistry, Behala College, University of Calcutta, Kolkata, West Bengal, India. His research interests are electrochemistry, self-assembled monolayers of organic molecules, microwave chemistry, nanotechnology and surface-enhanced Raman spectroscopy, materials science.

9 786207 472604

Novel Materials

Ujjal Kumar Sur

Modern Trends in Materials Science Research

LAP LAMBERT Academic Publishing

Ujjal Kumar Sur

Contents

Chapter 1

Nano-fertilizer: A distinctive entreaty of nanomaterials to crop field

Abstract:

Fertilizers are very important for plant growth and development. However, most of the applied fertilizers are rendered unavailable to plants due to many factors, such as leaching, degradation by photolysis, hydrolysis, and decomposition. Hence, it is necessary to minimize nutrient losses through fertilization and to increase crop yield through the exploitation of new applications with the help of nanotechnology and nanomaterials. Higher plants, as sessile organisms and as the best ecological receptors of our environment, have an amazing capability to develop versatile mechanisms to perform better under suitable as well as adverse conditions.

Interactions of plants with nano-fertilizers include uptake, translocation, and accumulation of nanoparticles depending on the nature of plant species as well as their shape, size, type, chemical composition, functionalization, and stability in the nano-fertilizers.

In agricultural-based countries like India, any kind of positive strategy for agricultural purposes will no doubt be helpful to farmers. Under these circumstances, incorporating nanoparticles in the nano-fertilizer and its application in the crop fields will open a new window in agricultural sectors which will help to fight against the huge food demand of the ever-growing population.

Keywords: bio-compatibility, bio-fertilizer, conventional fertilizer, crop yield, inorganic fertilizer, Nano-fertilizer, nanoparticle, Nutrient use efficiency, organic fertilizer, plant growth

Seminars Attended

"आत्मनिर्भरभारताय विज्ञानस्वास्थ्याय च विज्ञानम्"
Science for Self-Reliant India and Global Welfare

MINISTRY OF SCIENCE AND TECHNOLOGY
MINISTRY OF EARTH SCIENCES
MINISTRY OF HEALTH & FAMILY WELFARE
GOVERNMENT OF INDIA

SCIENCE FOR SELF-RELIANT INDIA AND GLOBAL WELFARE

INDIA INTERNATIONAL SCIENCE FESTIVAL 2020

Certificate of Participation

This is to certify that

MRS SANGHITA DAS

from - has successfully participated in

Young Scientists Conference (YSC) conducted from 22-12-2020 to 25-12-2020, as part of

INDIA INTERNATIONAL SCIENCE FESTIVAL 2020 (IISF 2020)

organised by Ministry of Science and Technology; Ministry of Earth Sciences,

and Ministry of Health and Family Welfare, Govt. of India

in collaboration with Vijnana Bharati (VIBHA)

by Council of Scientific & Industrial Research (CSIR).

Dr. Shekhar C. Mande
Director General, CSIR

Dr. Vijay P. Bhatkar
President, Vijnana Bharati

National Symposium
on
Strategies for Improving Agricultural Productivity and Farmer's Income in the Context of Climate Change

Organised by

THE AGRICULTURAL SOCIETY OF INDIA

In Collaboration with

INSTITUTE OF AGRICULTURAL SCIENCE, UNIVERSITY OF CALCUTTA

Certificate

This is to certify that

SANGHITA DAS, JADAVPUR UNIVERSITY

has participated and presented paper in poster / oral in the National Symposium held at Institute of Agricultural Science, University of Calcutta, Kolkata, West Bengal on December, 16 - 18, 2023

Kolkata
December 18, 2023

(Prof. R. K. Sarkar)
Secretary

EuroSciCon

40 Bloomsbury Way Lower Ground Floor London, United Kingdom WC1A 2SE

Certificate OF RECOGNITION

EuroSciCon and the Editors of Journal of Single cell Biology
wish to thank

Ms. Sanghita Das

Jadavpur University, India

for her phenomenal and worthy oral presentation on

"Guar gum micro-vehicle mediated delivery strategy of thymoquinone and piperine: An in vitro study of synergistic antibacterial and anticancer activity"

at the "6th Annual Congress on Plant Science and Biology

held during November 09-10, 2020 in Webinar

The award has been attributed in recognition of research paper quality, novelty and significance.

Andrea Wilson
Andrea Wilson
Program Manager

A one-day seminar in

"COMMEMORATION OF CENTENARY BIRTH ANNIVERSARY OF PROF. SHYAMAL SENGUPTA"

Condensed Matter Physics Research Centre
Estd. 1990

Organised by

Condensed Matter Physics Research Centre & Department of Physics, Jadavpur University

CERTIFICATE OF PARTICIPATION

This certificate has been awarded to ***Sanghita Das*** *of Dept. Of Physics, Jadavpur University in appreciation of her oral presentation titled* ***Gaur gum-psyllium husk derived phytochemical incorporated nanocomposite: A comparative antibacterial and anticancer profile*** *at the one day seminar in "Commemoration Of Centenary Birth Anniversary Of Prof. Shyamal Sengupta" held at Jadavpur University, Kolkata, India on 7th February 2024.*

07.02.2024

H.O.D. Dept. Of Physics, JU

7/02/2024

Co-Ordinator CMPRC, JU

SPRINGER NATURE

CERTIFICATE OF PARTICIPATION

presented to

Prof./Dr./Mr./Ms. **Sanghita Das**

for attending an international webinar on

The Challenges and Scientific Advances of SARS – COV 2

organized by

Department of Microbiology

ASSAM UNIVERSITY

in collaboration with

SPRINGER NATURE

and

SOCIETY FOR ENVIRONMENTAL SUSTAINABILITY

on August 27, 2020

Prof. Piyush Pandey
Head, Dept of Microbiology,
Assam University, Silchar

Dr. Mamta Kapila
Executive Editor,
Springer Nature

One day workshop on Artificial Intelligence in Drug Discovery

Organized by
CSIR-North East Institute of Science & Technology

Sl. No. AIDD3099

Certificate of Participation

This is to certify that

Sanghita Das

---

has participated in the
one day workshop on "Artificial Intelligence in Drug Discovery" organized by
CSIR-North East Institute of Science and Technology, Jorhat on 01-09-2020.

Debabrata Das

Mr. Debabrata Das
Coordinator
CSIR-NEIST, Jorhat

Dr. G. Narahari Sastry
Director, CSIR-NEIST
Jorhat, Assam

Ministry of Environment, Forest & Climate Change

सत्यमेव जयते

GOVERNMENT OF INDIA

MINISTRY OF ENVIRONMENT, FORESTS AND CLIMATE CHANGE

ZOOLOGICAL SURVEY OF INDIA, MARINE AQUARIUM & REGIONAL CENTRE

DIGHA – 721428, WEST BENGAL, INDIA

E-Certificate of Participation

This is to certify that ***Mrs. Sanghita Das, Jadavpur University*** *has participated in* ***Unique Marine Fauna Webinar Series (04)*** *on "Marine Ornamental Aquaculture: Measure towards Conservation of Biodiversity" conducted by Marine Aquarium and Regional Centre, Zoological Survey of India, Ministry of Environment, Forests & Climate Change, Govt. of India, Digha, West Bengal, on 24th August 2020.*

Ms. Debashree Dam
Scientist-B & In-Charge, Outreach Program

Dr. S. Balakrishnan
Scientist-D & Officer-in-Charge

One day National Webinar on

"Aquatic Faunal Diversity of Arunachal Pradesh"

This is to certify that ***Sanghita Das,*** Research Scholar of Jadavpur University has attended one day National Webinar on "Aquatic Faunal Diversity of Arunachal Pradesh" organized by Zoological Survey of India, Arunachal Pradesh Regional Centre, Itanagar on 20th August 2020

(Dr. Narender Sharma)
Officer-in-Charge, APRC, Zoological Survey of India
Itanagar, Arunachal Pradesh

DINABANDHU ANDREWS COLLEGE
KOLKATA, WEST BENGAL, INDIA
(NAAC ACCREDITED)

DAC/IQAC/BOT/
IW10671

CERTIFICATE OF PARTICIPATION

This is to certify that

Mrs. Mrs. Sanghita Das, Research Scholar, Jadavpur University

has actively participated in the one day International Webinar on "Science, Biology and the World's Future" organised by the Department of Botany in collaboration with Internal Quality Assurance Cell (IQAC), Dinabandhu Andrews College on 25th August, 2020.

Dr. Somnath Mukhopadhyay	Dr. Amitabha Roy	Dr. Mithun Maji	Dr. Joy Sarkar	Prof. Bruce Alberts
Principal	Coordinator, IQAC	Head, Dept. of Botany	Convenor	(Speaker)